NMR of Solid Phosphorus-containing Compounds

by

Lindsey Alexandra Crowe B.Sc. (Hons. Dunelm)
Trevelyan College
University of Durham

A thesis submitted in partial fulfilment of the requirements for the degree of Doctor of Philosophy

Department of Chemistry
University of Durham

1999

NMR of Solid Phosphorus-containing Compounds

Lindsey A. Crowe B.Sc. (Hons. Dunelm)
Submitted for the degree of Doctor of Philosophy
1999

ABSTRACT

Solid-state NMR techniques have been applied to the structure and dynamic characterisation of a range of phosphorus-containing compounds. Comparisons have been made within several series of compounds as well as studies of individual molecules with interesting NMR properties, whether dynamic, structural or magnetic.

Spectral features such as shielding anisotropy, the high sensitivity of phosphorus and its large chemical shift range are extensively utilised in this work. Triple-channel, fluorine-observe and variable-temperature spectrometer facilities at different magnetic field strengths have been explored to give as much complementary information as possible.

For both chlorinated and fluorinated diazadiphosphetidines, motional properties have been examined and the indirect spin-spin and dipolar interactions, together with shielding have been studied. Spectra from the NMR-active nuclei in these cyclic dimers have been used to compare effects of differing substituents on NMR properties. The 'bowl-shaped' molecules, calix[4]resorcinols with phosphorus functionality modifying the upper rim, constitute the other major group of compounds studied. These are of interest in inclusion chemistry. As well as simple one-dimensional NMR characterisation of solid-state calix[4]resorcinol compounds, interesting two-dimensional correlation results have helped with the assignment and conformational conclusions.

A qualitative and quantitative study of a co-crystal of triphenylphosphine oxide and phenol was made to establish the nature of the disorder observed, but undefined, in an X-ray structural investigation of the hydrogen-bonded network. Complementary NMR techniques were used to extend the temperature range over which the rate of any motion can be characterised. Bandshape analysis, $T_{1\rho}$ measurement and selective polarisation inversion experiments have proved to be accurate in different regions of a variable temperature study.

Other compounds explored were those which showed interesting solid-state NMR results, for example, the complexities of cross-polarisation dynamics between two abundant spins in inorganic phosphates, and compounds with potential solid-state applications. These include (i) phosphorus-containing compounds with chlorine and fluorinated aromatic substituents and (ii) complexes with transition metals. Comparison with single-crystal and powder X-ray diffraction has also been exploited. In some cases, data have been produced, and in others the applicability of a theoretical approach has led to other conclusions.

Memorandum

The research presented in this thesis has been carried out in the Department of Chemistry, University of Durham, between October 1996 and September 1999. Unless otherwise stated it is the original work of the author. None of this work has been submitted for any other degree.

Acknowledgements

There are many people, in many places, that I would like to thank for their help and support over the last three years.

Firstly, many thanks go to my supervisor, Prof. Robin K. Harris, for his constant help and encouragement. The occupants of room 'CG22' have provided entertaining and informative discussions, and, of course, lab lunches! - thanks to Alison, Susan, Stefan, Julian, Jon, Naser, Alessia, Paolo, Ian and Helen !!! To all our visitors, staff and post-docs: Lucy, Minoru, Gustavo, Philippe, Jerome, Philippe, Philip, Bruno, Pierre, Ulrich and Peter. To Shinji, David, Nicola, Barry, Paul, Eric H, Eric B and Claudia - thanks for all the help with spectrometers, NMR and stuff!

Huge hugs to Suzi, Kath, Kate, Helen, Terry, Anna, Roberto and Kevin for being great friends, along with all the others who have helped make my 6 years in Durham so enjoyable! Roberto also deserves a special mention for his sense of humour and computer know-how! To Mark, 1999 has been the best year ever! Thanks for everything. Special thanks to Mum and Dad for all their love and support.

On a more formal note, for a most generous supply of compounds, crystal structure data and access to spectrometers, acknowledgement goes to several groups:
Prof. Reinhard Schmutzler, Dr. Alex Vollbrecht, Holger Thönnessen and Dr. Peter Jones in Braunschweig, Germany for all the synthetic chemistry expertise (also to the other members of the Inorganic Chemistry groups for an interesting visit!);
Acknowledgements to Dr. Keith Dillon, Dr. John Evans, and Dr. A. Batsanov (Durham), Dr. P. Challoner, Dr. R. Harrison (Sussex) and Prof. N. Shankland (Strathclyde);
Prof. Ray Dupree, Dr. Mark Smith and Dr. Andy Howes for all the help with the 600 MHz spectrometer at Warwick University Physics Department.

Many Thanks

Lindsey

To Mum and Dad.

Abbreviations, symbols and notation

The following acronyms and symbols have been use in this thesis. In general, these are in standard notation and are included here for reference purposes.

α, β	Euler angles
ad	acquisition delay
χ	quadrupolar coupling constant
CP	cross-polarisation
CRAMPS	combined rotation and multiple pulse spectroscopy
δ_X	chemical shift (of nucleus X)
$\Delta H^{\#}$	enthalpy change (transition state)
ΔJ	anisotropy in indirect (spin-spin) coupling
$\Delta S^{\#}$	entropy change (transition state)
D	dipolar coupling constant
D'	effective dipolar coupling constant
ε	ratio of nuclei (CP dynamics study)
E_a	activation energy
η	asymmetry
EFG	electric field gradient
FID	free induction decay
FT	fourier transform
fwhh	full width at half-height
γ	gyromagnetic ratio
h	Planck's constant = 6.626×10^{-34} J s. ($\hbar=h/2\pi$)
HETCOR	heteronuclear correlation
HF	proton-fluorine probe
HFX	proton-fluorine-X nucleus probe
HX	proton-X nucleus probe
HXY	proton-X nucleus-Y nucleus probe
J	indirect scalar (spin-spin) coupling
κ	transmission coefficient
k	rate constant
k_b	Boltzmann constant = 1.381×10^{-23} J K^{-1}
Kel-F	$(CF_2CFCl)_n$
M	magnetisation
MAS	magic-angle spinning
MAT	magic-angle turning
ν	frequency
NMR	nuclear magnetic resonance

ω	angular frequency
PAS	principle axis system
PDMSO	polydimethylsiloxane
ppm	parts per million
PXRD	powder X-ray diffraction
r	internuclear distance
R	gas constant = 8.314 J mol^{-1} K^{-1}
rd	receiver delay
RDC	residual dipolar coupling
rf	radio frequency
SA ($\Delta\sigma$)	shielding anisotropy
σ	shielding
SPI	selective polarisation inversion
ssb	spinning sideband
T_1	spin-lattice relaxation time
$T_{1\rho}$	spin-lattice relaxation time in the rotating frame ($T_{1\rho}$*, effective value)
T_2	spin-spin relaxation time
T_{HP}	cross-polarisation time (T_{HP}*, effective value)
tau	delay time
τ_c	correlation time
t_{cp}	contact time
t_m	mixing time
TTMSS	tetrakis trimethyl silyl silane
VACP	variable amplitude cross-polarisation
Vespel	fluorine-free polymer
VT	variable temperature
ZDP	zinc(II)bis(O,O'-diethyldithiophosphate)

Standard symbols comply with IUPAC conventions.
(R.K. Harris, J. Kowalewski, S.C. de Menezes, *Pure & Appl. Chem.*, 1997, **12**, 2489.)

Contents

1 Introduction....1
1.1 Solid-state NMR....1
1.2 Phosphorus....2
1.3 Overview of compounds studies....3
Phosphates....3
Diazadiphosphetidines and Calix[4]resorcinols....3
TPPO-Phenol....3
ArP compounds and Carbonyl(dihydrido) tris(triphenylphosphine)ruthenium(II)....4
1.4 General Overview....4
Introduction....4
Magnetic interactions....5
Magic-angle spinning....7
Spinning sideband analysis....8
Cross Polarisation....10
Motion....11
Coupling....12
Residual Dipolar Coupling....12
Fluorine....13
Bloch-Siegert Shift....14
References....16

2 Experimental....17
2.1 Spectrometers....17
CMX 200....17
Varian Unity Plus 300....19
CMX Infinity 600....19
2.2 Sample Handling and Rotors....19
2.3 Probes....20

2.3.1 HX....21
General set-up....21
Magic-angle setting....21
2.3.2 HF....23
Observing Fluorine....23
Magic-angle setting....23
2.3.3 HFX....23
Triple-channel....23
2.3.1 HXY....24
2.4 Spectrometer set-up....24
2.4.1 Setting powers for CP experiments....24
Measuring and calibrating powers....26
2.4.2 Variable Temperature....28
Calibration....28
General VT operation....28
2.5 Acquisition of Spectra....31
2.6 Magic-angle turning....33
PHORMAT results....36
References....39

3 Cross-polarisation Dynamics in Proton-phosphorus Systems....40
3.1 Introduction....40
3.2 Results and Discussion....48
Individual Experiments....49
Simultaneous Fitting....53
References....59

4 One- and Two-dimensional NMR Techniques in the Study of Phosphorus-containing Calix[4]resorcinols....60
4.1 Introduction....60
4.1.1 Applications....60
4.1.2 Synthesis and Structure....60

4.2 Compounds I, Tetrakis-(O-P(-Cl)-O)-bridged Calix[4]resorcinol, and II, Tetrakis-(O-P(-Cl)-O) -bridged Calix[4]resorcinol-Br..... 66
4.2.1 Phosphorus-31 Spectra.....66
4.2.2 Carbon-13 Spectra and Assignments. 68
4.2.3 Correlation..... 72
Introduction.....72
Results and Interpretation..... 74
Conclusions.....78
4.3 Related Compounds Containing F- or N-Substituents on Phosphorus.....79
4.3.1 Compound III.....79
4.3.2 Compound IV..... 82
4.3.3 Compound V..... 87
4.3.4 Compound VI..... 89
4.3.5 Conclusions.....90
References.....93

5 Fluorinated Diazadiphosphetidines.....94
5.1 Introduction.....94
5.2 Experimental Considerations.....99
5.3 Results and Discussion..... 103
Powder XRD.....103
General Features of ^{19}F and ^{31}P Spectra..... 104
^{19}F and ^{31}P Spinning Sideband Analysis.....112
Results for $(Ph_2FPNMe)_2$..... 114
Results for $(PhF_2PNMe)_2$..... 115
Results for $(^tBuF_2PNMe)_2$..... 118
Results for $(F_3PNPh)_2$..... 118
Static ^{19}F and ^{31}P Spectra.....119
Variable Temperature Spectra..... 121
Carbon-13 Spectra..... 124
Nitrogen-15 Spectra.....125
Proton Spectra.....126

Relaxation times....128
5.4 Conclusions....131
References....133

6 Chlorinated Diazadiphosphetidines....135
6.1 Introduction....135
6.2 Results and Discussion....136
6.2.1 Phosphorus-31 Spectra....136
6.2.2 Carbon-13 Spectra....144
6.2.3 Nitrogen-15 Spectra....146
6.2.4 Proton Spectra....147
6.2.5 Cross-polarisation Dynamics....147
6.3 Conclusions....149
References....150

7 Disorder in the TPPO-Phenol Complex....151
7.1 Introduction....151
7.2 X-ray Results....156
7.3 NMR Results....160
7.3.1 Single-crystal experiments....160
7.3.2 Solid-state ^{31}P MAS NMR....162
7.3.3 VT on Powder Samples....164
7.4 Exchange Analysis....166
7.4.1 Bandshape analysis....166
7.4.2 SPI....168
7.4.3 $T_{1\rho}$ measurements....172
7.4.4 Activation Parameters....174
7.5 Conclusions....176
References....178

8 Ruthenium-, Platinum- and Chlorine-containing Compounds....180
Compound I Ar'Ar"PCl....182
Phosphorus-31 NMR....182
Cross-polarisation experiments....190

Fluorine-19 NMR..... 191
Carbon-13 NMR.....195
II Cis-dichloro Pt (PEt_3)(Ar'PCl).....197
Phosphorus-31 NMR.....197
MAT.....200
Carbon-13 NMR.....203
Fluorine-19 NMR spectra and motion.....204
Relaxation times.....207
III Carbonyl(dihydrido) tris(triphenylphosphine) ruthenium(II).....214
Phosphorus-31 Spectra.....215
Carbon-13 NMR.....218
Proton MAS NMR.....219
Conclusions.....219
References.....221

Conclusions and Further Work.....222
Appendix: Conferences, Work Presented etc.....226
Colloquia.....228

1. INTRODUCTION

1.1. Solid-state NMR

Solid-state NMR is used in the elucidation of structure and dynamics of many inorganic and organic compounds. Characterisation of the local electronic environment of a nucleus, in this way, can lead to a thorough understanding of the molecular structure and the interactions in the solid state. It is useful in cases where solution-state NMR and X-ray diffraction are not available or do not give the required information. In the case of many large inorganic molecules, solubility, and therefore sensitivity in solution-state NMR, is very limited. Insolubility will also hinder the growth of single crystals for diffraction studies, therefore limiting structural data obtainable from such methods. Even when these techniques are applicable, there is a wealth of additional information that can be obtained from solid-state NMR. Distinction can be made between static and dynamic disorder and a dynamic rate of motion determined, along with identification of species too disordered to appear accurately represented in X-ray diffraction data. Despite the tethered nature of many of the compounds studied (e.g. cyclic diazadiphosphetidines and bridged calix[4]resorcinol systems), interesting motional effects have been observed in what would seem to be fairly rigid solid-state structures. Conformational differences and interactions in the solid state should be clearly identifiable by NMR. Structure, interactions and dynamics in the solid-state have been of particular interest in this work.

Packing effects and intermolecular interactions can play an important role in the differences between a solid-state structure and that in solution. The NMR spectrum of a microcrystalline powder sample or single crystal will provide substantial information, with spectra relying heavily on the local electronic environment of the nuclei as well as the molecular orientation. The solid-state structure is often vital in understanding the possible applications and behaviour of a compound, for example, in the pharmaceutical industry, when the final usage form will be in the solid-state and a particular active structure must be carefully identified.

1.2. Phosphorus

The chemistry of the group V element, phosphorus, is varied. It has several stable oxidation states: +5, (5-co-ordinate covalent, e.g. PF_5, 6-co-ordinate complexes, e.g. $[PF_6^-]$, 4-co-ordinate tetrahedral, e.g. $[PCl_4]^+$, $[PO_4]^{3-}$) and +3 (3-co-ordinate pyramidal, e.g. PH_3). Compounds under investigation here include a range of interactions of phosphorus centres with halogen, platinum and organic residues in both 3 and 5 co-ordinate species, along with simple phosphate systems. One of the common features of phosphorus compounds (particularly those containing fluorine) is their susceptibility to decomposition, reacting rapidly with oxygen or moisture. Solid powder samples are easily sealed if they would undergo decomposition when in contact with oxygen or moisture. Rotors of outer diameter 5 mm or bigger will take sealed inserts, and tight fitting end-caps will often suffice for very small rotors. Using nitrogen as the spinning gas would also help. Recovery of the samples is also a lot simpler than extraction from solution after a solution-state NMR experiment.

Phosphorus-31 NMR features heavily in this work, although complementary information is also gained from other nuclei, specifically ^{19}F, ^{13}C, ^{1}H and ^{15}N. Having a 100 % natural abundance spin-1/2 isotope, ^{31}P is a useful, and very sensitive, probe of many compounds. It has strong interactions with other nuclei, for example leading to resolved indirect spin-spin coupling. A large ^{31}P chemical shift range means significant separation of different chemical species within the different co-ordination states. Substantial shielding anisotropy and dipolar interactions can be studied to give further information on the environment of a phosphorus centre. With phosphorus, however, we do not generally have severe problems sometimes associated with a large anisotropy (static bandwidth) and chemical shift range, and uniform excitation over the relevant spectral width is possible. With static spectra, it may be necessary to use an echo sequence to ensure the correct shape is obtained from the fast decaying FID. Problems of distortion of the spinning sideband intensities does not seem to be a significant problem. Thus, changing the transmitter position, in general, does not lead to alteration of the pattern of intensities.

1.3. Overview of compounds studied

Each series of compounds will be introduced in the corresponding chapters, but a brief overview is also given here. The different motivation behind the study of each distinct class of compound is described.

Phosphates:
A series of commercially available phosphates was used mainly for development of a study of cross-polarisation dynamics (as well as the use as a standard sample for Hartmann-Hahn matching). The applicability of theory previously applied to the proton-fluorine spin systems is tested for the proton-phosphorus combination.

Diazadiphosphetidines and calix[4]resorcinols:
These compounds were supplied by the group of Prof. R. Schmutzler at the University of Braunschweig, Germany. Several of the diazadiphosphetidines and all the calix[4]resorcinol type compounds were newly synthesised, either on request or because of the group's own research interests. Following interesting solution-state results in previous studies by Schmutzler, Harris et al. (for exact references see the appropriate chapter), a series of dimeric halogenated diazadiphosphetidines was investigated for coupling, structural and dynamic effects. The two relevant chapters cover systems with both fluorine and chlorine, including different substituents on nitrogen.

Structural information for several calix[4]resorcinols is sought. These compounds have modifications to the cavity shape and interactions made by addition of phosphorus functionality. This is particularly important for potential applications in supramolecular or inclusion chemistry.

TPPO-Phenol:
The disorder observed in the X-ray structure of a triphenylphosphine oxide-phenol complex was examined both qualitatively and quantitatively. The aims were to identify the nature of the disorder (spatial or dynamic) - 'half' an oxygen atom had been previously observed, by X-ray crystallography, in two different positions in the unit cell - and, once this was found to be a motional process, to determine activation parameters

from rate constants at different temperatures. As this work follows from the crystal structure studies of a group in Sussex, both the powdered complex and single crystals were supplied by them, although some further samples were prepared from commercially available starting materials (TPPO and phenol) by Dr. Claudia Lagier, who was also involved in this part of the project.

ArP compounds and Carbonyl(dihydrido)tris(triphenylphosphine)ruthenium(II):
Finally, PCl and PPt compounds of possible pharmaceutical interest containing $-C_6H_3(CF_3)_2$ aromatic groups, were characterised, and the transition metal complex, carbonyl(dihydrido)tris(triphenylphosphine)ruthenium(II), was studied. All three of these compounds show an interesting variety of effects in their solid-state spectra.

The two different Ar'P compounds were synthesized in Durham by students of Dr K. B. Dillon as part of a project to investigate novel phosphorus chemistry. They are possible pharmaceutical candidates (as anti-cancer agents).

The interest in carbonyl(dihydrido)tris(triphenylphosphine)ruthenium(II) was inspired by the work of Dr N. Shankland in the Department of Pharmaceutical Sciences at Strathclyde University. Initial studies to provide basic NMR data for use as a precursor to powder X-ray diffraction studies led to the investigations on this compound. The sample is commercially available from Strem Chemicals, Newburyport, MA, USA.

1.4. General overview.

Introduction
Although the chapters in this thesis mainly concentrate on each of the compound types in turn, similar themes are developed throughout because of the characteristics of phosphorus-containing compounds. Some general techniques are covered by different compounds and observed phenomena are compared and contrasted in different cases.

Unusual triple-channel applications have been developed, in particular cross-polarisation and decoupling combinations, to help with understanding structural proximity, indirect spin-spin coupling and dipolar interactions. These include

phosphorus/fluorine/proton and carbon/phosphorus/proton combinations. The HFX probe (X = phosphorus) was used extensively for the fluorinated diazadiphosphetidines and calix[4]resorcinols to produce simpler spectra and investigate the PF interaction. This probe was also used for the ^{1}H-^{19}F-^{13}C combination for some compounds. Although the set-up of this probe in terms of capacitors and power specifications had already been established, it was still necessary to observe some simple spectra from sensitive samples to test the efficiency of the various experiments. All proton/fluorine combinations, because of the close proximity of the resonance frequencies, necessitate specifically designed probes and filters. The decoupling of phosphorus from fluorine spectra has been attempted for the first time on our triple channel HFX probe, although the simultaneous use of the proton channel in this case is not possible with the filters available. This system was also used for carbon spectra with double decoupling. The carbon-phosphorus studies needed initial test work on simple samples. In particular, power levels and capacitor values for the probe had to be optimised.

This chapter will continue with a brief description of some of the basic ideas that are generally applicable to solid-state nuclear magnetic resonance experiments. The theory of solid-state NMR is now well-known, so only a short qualitative summary is appropriate. A few more specific points are discussed in later chapters.

Magnetic interactions.

As already implied, phosphorus is in many ways an ideal nucleus for NMR study. The high gyromagnetic ratio and 100% natural abundance of a spin ½ isotope (and consequent high receptivity) mean that many new experimental techniques, including two-dimensional experiments, are easily exploited in a relatively short space of time. There are now well-established solid-state techniques for obtaining high-resolution spectra, avoiding the limitations placed on the system by shielding anisotropy, dipolar interactions (homo- and hetero-nuclear), lack of sensitivity and long spin-lattice relaxation times. Although information can often be extracted from internuclear interactions, it is advantageous to obtain a simple initial spectrum free of splittings and/or complex lineshapes, to assist interpretation.

The internal interactions of the spin systems, namely shielding, indirect (scalar) coupling, dipolar and quadrupolar coupling, all contribute to the observed NMR

spectrum. The majority of these interactions are anisotropic and, to a first-order approximation, have an orientation dependence which includes the term $(3\cos^2\theta - 1)$, θ being the angle between the molecular fixed direction and the magnetic field B_o. In a powdered sample all orientations of molecules will be present. Every orientation has a different energy and therefore a different transition frequency, leading to the observation of a powder pattern for a static sample. The interactions mentioned affect the width and shape of this pattern.

A typical heteronuclear dipolar powder pattern (Figure 1) for an isolated spin-pair, has two subspectra represented by:

$m_x = + \frac{1}{2}$ and $- \frac{1}{2}$, with $D = (\mu_o/4\pi)(h/4\pi^2)\gamma_A\gamma_X r_{AX}^{-3}$

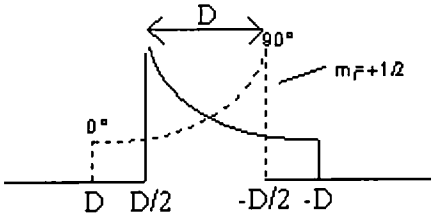

Figure 1. Powder pattern showing dipolar coupling.

Isolation of spin pairs in real chemical systems of interest is rare, and therefore static powder spectra from randomly oriented molecules in powders are, generally, broad and featureless due to overlap of many components. In solution-state nuclear magnetic resonance the rapid molecular tumbling will average many of the anisotropic interactions to zero leaving only the isotropic chemical shift and isotropic indirect scalar coupling to influence the spectrum. In the solid-state there is no such general mechanism. Shielding is orientation dependent, resulting in a powder pattern even for isolated nuclei (this is shown in Figure 2).

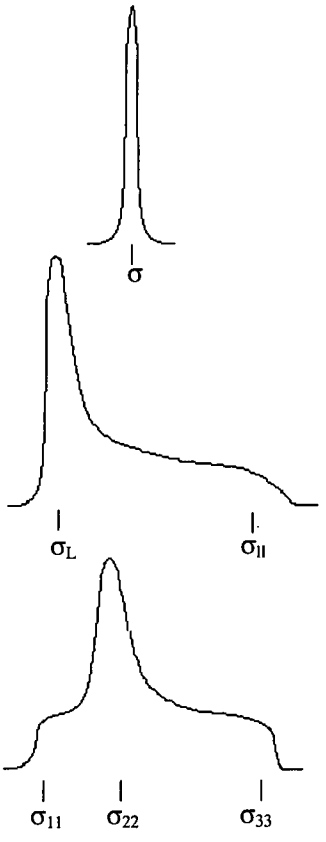

Figure 2. Shielding powder patterns with shapes representing, from top - cubic symmetry, axial symmetry and asymmetry.

In real cases the static pattern for a solid is influenced by both shielding anisotropy and dipolar interactions.[1] Often analysis of the powder lineshape can lead to useful information about the shielding anisotropy and asymmetry of the molecule. However, in complex molecules, severe overlap may occur and all useful information will be lost.

The techniques of magic-angle spinning (MAS), high-power (proton) decoupling (HP(P)D) and cross-polarisation (CP), are often used in combination to produced narrow-line spectra in the shortest possible time.

Magic-angle spinning

Magic-angle spinning (MAS) is the technique used to produce high-resolution spectra by reducing the effects of shielding anisotropy and dipolar interactions on the spectrum. The cylindrical sample rotor spins about an axis at 54°44' (β) to the applied magnetic field (with the individual molecular orientations represented by θ). The average value of $(3\cos^2\theta - 1)$ (which is proportional to $(3\cos^2\beta - 1)$) is therefore brought to zero,

reducing effects of these orientation-dependent interactions. Accurate setting of the 'magic angle' is essential. Also, the spinning speed must be of the same order of magnitude as the interaction in order to effect narrowing and for some interactions, such as proton dipolar interactions, speeds are not sufficient to achieve complete narrowing, so that high power decoupling frequencies also need to be applied to the systems to produce narrow lines. CRAMP (combined rotation and multiple pulse) sequences,[2,3] in addition to high-speed spinning,[4] can be used to reduce strong homonuclear (^{19}F or ^{1}H) dipolar interactions, which would otherwise cause significant line broadening and loss of resolution. Residual Dipolar Coupling (RDC) which is caused by the interaction of a strongly quadrupolar nucleus ($I > ½$) with the observed spin-½ nucleus via a dipolar mechanism, does not have the same geometry dependence and is therefore not removed by MAS. This effect is described in more detail later.

Spinning sideband analysis.

As well as producing well-resolved isotropic chemical shifts, it is sometimes possible to retain anisotropic information with moderate spinning speeds, in the form of spinning sidebands. If the MAS spin rate is slower than the static linewidth in hertz, as is often the case in phosphorus and fluorine NMR, the powder pattern will break up into spinning sidebands - lines separated from the isotropic shift by multiples of the rotor spinning frequency. As the spinning sidebands define the same properties as a static lineshape, but often without overlap, the intensity of these lines can be analysed to extract information on shielding anisotropy and asymmetry similar to that obtained from analysing a static powder lineshape. Sidebands will often result in complex spectra from multiple lines. In these cases a careful choice of spin rate is required in order to separate peaks. The isotropic shifts in a spectrum can be easily identified as the peaks that do not change frequency when the spin rate is changed.

For the analysis of spinning sidebands, to obtain values for anisotropy and asymmetry via the principal shielding tensor components, several programs were used. The first was an "in-house" program,[5] which assumes coaxial tensors, based on the theory described by Maricq and Waugh.[6] This programme was updated to a similar but extended version to include statistical error analysis.[7] This will be referred to as ssb97.[8] It is worth noting here the simple relationship between the σ and δ scales used for

shielding anisotropy (and the principle components) and the isotropic chemical shifts respectively. The shielding constants and shift scales, by convention, are related by $\delta = 10^6 (\sigma_{TMS} - \sigma_{SAMPLE})$ and therefore increase in opposite directions.

There is also a triple-fit program that will simulate and fit anisotropy values simultaneously from three sets of experimental data to obtain $\Delta\sigma$ and D', along with the angles α and β which define the orientation of the tensors (Figure 3). A graphical analysis based on Herzfeld-Berger theory[9] was used for comparison in some of the systems studied early in this work, and in general confirmed results from the iterative fitting 'ssb' programmes. The values from this graphical method are not reported in the thesis.

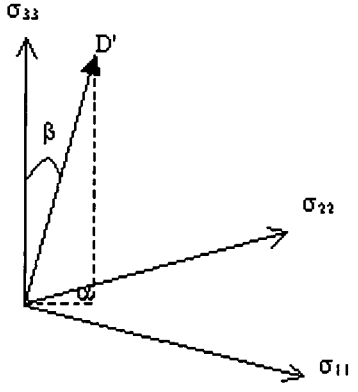

Figure 3. Orientation angles.

In cases where J coupling is visible (e.g. in some of the PF systems studied) the interplay of tensors acts to produce, for example, different sideband manifolds for each of the peaks of a coupled doublet.[1] The effective shielding tensors observed are related to the actual shielding and dipolar tensors by the following equation in cases where the tensors are co-axial;

$$\zeta_{eff} = \zeta - 2\Sigma m_X \frac{D'}{\nu_0}$$

where m_X is the component quantum number of the coupled spin (the summation is only relevant in a case of AX_2 or higher) and $D' = D - \frac{\Delta J}{3}$.

This means that, for each peak of a doublet there is either a 'stretched' or 'compressed' manifold. The assumption is generally made that the tensors (dipolar coupling, shielding and indirect coupling) are coaxial, but in favourable cases three sets of data from the same coupled system (e.g. a coupled doublet and decoupled singlet from an AX system) can be fitted simultaneously to give values of α and β (the angles relating the tensors). In an AX_2 case, a triplet may be observed. The -1 subspectrum for the A spin will have the anisotropy and D' additive, the 0 subspectrum will give the value of the true shielding directly without the influence of the dipolar interaction, and finally for the +1 subspectrum the anisotropy and dipolar interaction subtract. Assuming that D' and $\Delta\sigma$ have the same sign, the first and last subspectra above will be stretched and compressed, respectively. However analysis of this type is only straightforward for a linear X-A-X system.

Definitions of the shielding anisotropy and asymmetry parameters that will be used throughout are:

anisotropy, $\zeta = \sigma_{33} - \sigma_{iso}$;

and asymmetry, $\eta = \dfrac{\sigma_{22} - \sigma_{11}}{\sigma_{33} - \sigma_{iso}}$;

with the shielding component convention $|\sigma_{33} - \sigma_{iso}| \geq |\sigma_{11} - \sigma_{iso}| \geq |\sigma_{22} - \sigma_{iso}|$.

Cross-polarisation

The problems associated with long relaxation times (T_1) and lack of sensitivity can be partially overcome by cross-polarisation (CP) techniques - transfer of magnetisation from protons (or other abundant nuclei, e.g. fluorine) to the 'rare' observed nucleus. Also, in cases of two abundant spins where T_1 relaxation times differ, e.g proton-to-fluorine, fluorine-to-phosphorus or proton-to-phosphorus cross-polarisation experiments, the relaxation time of the first may lead to a more favourable recycle delay. The complexities of the situation for cross-polarisation dynamics between two abundant spins are considered in chapter 3. In a CP experiment the transfer occurs during the contact time, when both radio frequencies are being transmitted, usually with maximum intensity when the Hartmann-Hahn matching condition, $\gamma_S B_{1S} = \gamma_H B_{1H}$, is satisfied. In this situation the component of the magnetisation for each nucleus due to precession around the spin-lock direction (i.e. along the y-axis), has the same time

dependence. The gyromagnetic ratios are fixed for a particular nucleus, and therefore the magnitude of the applied r.f. field on each channel is adjusted to enable transfer of magnetisation. Varying the contact time in any cross-polarisation experiment results in the possibility to analyse cross-polarisation dynamics.

When spinning at some of the faster speeds accessible on current equipment, i.e. up to 16 kHz used with the 3.2 mm probe for some of this work (although the probe specifications allow spinning at 25 kHz), the matching profile will often break down into spinning sidebands. When this occurs, the accuracy of the match setting becomes much more critical and it is possible that matching on a sideband gives greater efficiency (as the matching profile shows a dip at the centreband). There is then a restriction that the same spinning speed must be used in all subsequent experiments with that match condition, and that the samples have similar sideband properties. It may be appropriate to use a pulse sequence incorporating a variable or ramped amplitude cross-polarisation power,[10,11] extending the range of the matching condition. This was tested on the CMX200 in previous work.[12] Ramp CP is also helpful in, for example, ^{15}N spectra and when the matching condition is naturally narrow for a particular sample.

Motion

Disorder in a molecule, visible in an NMR spectrum or crystal structure, can easily be identified, as static disorder within the crystal repetition, or dynamic (molecular motion), by variable temperature solid-state NMR.[13] Molecular motion, hindered rotations and phase transitions can occur in the solid state. Rotations about a C_3 axis, e.g. of t-butyl, methyl, ammonium or trifluoromethyl groups, are frequently fast on the NMR timescale and may only be observed, even in a solid, when rates are slowed by steric restriction of the motion. Line broadening is caused by ineffective decoupling in the case when a rate of a dynamic process is of the same order as the frequency of the decoupling power applied (~ tens of kHz) or by ineffective MAS narrowing when the motional rate is comparable to the spinning rate. Where rates are accessible on the NMR timescale and distinct shifts are seen for the exchanging species, it is possible to see the coalescence point for the bandshape by variation of the probe temperature. Coalescence is not usually followed by an immediate sharpening of the averaged line. The signal-to-noise ratio decreases as resonances broaden before sharpening at much higher temperatures to a single averaged site and polarisation transfer efficiency is

lowered when a chemical exchange process occurs at a rate comparable to the spin-lock frequency. This effect is observed in several systems studied here.

Coupling

Indirect spin-spin coupling, J, causes a splitting of the resonance lines of an A spin due to the spin state (α or β) of adjacent X spins. The interaction is generally a through-bond phenomenon, although cases of through-space spin-spin coupling have been observed. Spectra with resolved J-splittings are not usually obtained from solid-state MAS NMR spectroscopy as the magnitude of J is often smaller than the natural solid-state linewidth. In cases where the coupling constant is large (e.g. PF systems), however, such splittings have been observed. Although J coupling is defined by a tensor, it will also be averaged to its isotropic value by magic-angle spinning. The energy levels for the A spin are then modified depending on whether the X nucleus is spin +½ or -½, leading to a transition frequency that is ±J/2 from the unperturbed value. The separation of the two lines observed for this transition is then J. In solution-state NMR this value is dependent on the solvent[14] and can be used as a probe of solvent-solute interactions. As the value of the splitting changes with changing intermolecular interactions, it is possible that values in solid-state spectra may be significantly different to those in solution due to the nature of the crystal packing.

To simplify spectra, and to determine the identity of any splitting as a J-coupling interaction, heteronuclear decoupling can be applied, in addition to proton decoupling, in a triple-resonance experiment. Any splitting in a phosphorus spectrum due to coupling to fluorine will be removed by high power heteronuclear decoupling. Similarly, the same PF coupling will be evident in the fluorine spectrum. The effect of the strong homonuclear interactions in the fluorine spectrum may also cause further broadening of the multiplet peaks These effects are seen in later chapters describing both fluorinated diazadiphosphetidines and calix[4]resorcinols.

Residual dipolar coupling

Another form of splitting is that caused by residual dipolar coupling to quadrupolar nuclei. For heteronuclear dipolar splittings to a nucleus of spin I > ½, a single-crystal NMR spectrum will show a multiplet with lines corresponding to states -m, -m+1, ... +m. To a first approximation the magnetic moments associated with the states of the

quadrupolar nuclei are aligned with the Zeeman field and have values proportional to m. In this case, a symmetric multiplet will be observed (in the absence of shielding anisotropy) which depends on crystal orientation. For large nuclear quadrupole coupling constants, the quadrupolar spin states are no longer quantized along the Zeeman field. This leads to a change in direction and magnitude of the magnetic moments of the eigenstates. The symmetry of the multiplet and the orientational dependence of its peak positions will also change. In such situations where the quadrupolar coupling constant is active it is not possible to achieve complete narrowing of the dipolar broadening by MAS.

Fluorine

In addition to the study of phosphorus NMR, fluorine has also been an important part of the characterisation of some of the molecules in this thesis. Despite its favourable gyromagnetic ratio there are several problems associated with the acquisition of fluorine spectra.[15] Instrumentally, high speeds are required for the analogue-to-digital converter and wide bandwidths for the amplifier. In a 4.7 T field (200 MHz for protons) the full spectral range for fluorine is about 0.2 MHz (i.e. 1000 ppm), though within a single system the range may be much more restricted than this. Short pulses (~3 μs for a 90° pulse duration) are required to produce a uniform excitation over this complete range, and this means that the probe must be capable of taking high powers. With MAS only, very high resolution spectra have been reported in cases of inorganic systems with few or no protons (e.g. fluoroapatite,[16] $Ca_5(PO_4)_3F$), or molecules where there is significant molecular motion in the solid.[17] Resolution often necessitates 'combined rotation and multiple-pulse spectroscopy', usually abbreviated to CRAMPS, which causes averaging in spin-space by a series of short pulses. This reduces the large homonuclear dipolar interactions that may otherwise broaden lines to give a composite featureless band from all resonances in a sample.

Proton and fluorine resonance frequencies have a difference of only 6% (200.1 and 188.3 MHz for a 4.7 T magnet) and it is rarely possible to achieve sufficient quality spectra without high-power proton decoupling. The specially designed HF probe has two fixed-frequency narrowband channels and high specification filters in order to provide sufficient isolation between the channels to allow the double-resonance experiments. Conventional bandpass filters cannot cope with the high powers and such

close proximity with respect to frequency. A broad probe background ^{19}F signal is sometimes observed in direct polarisation experiments with a long recycle delay, but spectra with a flat baseline were achieved by running with cross-polarisation from proton to fluorine. When quoting fluorine chemical shifts, from spectra acquired under the conditions of proton decoupling, the Bloch-Siegert effect must be corrected for.

Bloch-Siegert shift.

The application of a decoupling frequency has an effect on the apparent chemical shift of the observed nucleus.[18] Referencing can be done after acquisition, by precise calculation for the particular nuclei using the theory described below. However, experimentally, the Bloch-Siegert shift is easy to correct for by running reference spectra with the high-power decoupling frequency applied, as the effect of the shift will still be observed even if the reference sample does not contain the decoupled nucleus (e.g. proton decoupling on C_6F_6).

The extent of the effect on the chemical shift, Δ, can be calculated in ppm according to the equation

$$\Delta = \frac{\left[\nu_1\left(\gamma_0/\gamma\right)\right]^2}{\left(\nu_0^2 - \nu^2\right)} 10^6$$

where ν_0 is the Larmor frequency of the observe nucleus, ν is that of the nucleus being decoupled, ν_1 is the decoupling power (expressed in Hz) and the γ values represent the gyromagnetic ratios of the nuclei. This effect has been found experimentally to be significant for the case of fluorine spectra with proton decoupling. It is also of interest to calculate the possible effect for some other possible combinations (Table 1). The values are based on typical parameters used on the CMX200 spectrometer. It can be seen from Table 1 that, for most combinations observed for this thesis apart from ^1H-^{19}F, the Bloch-Siegert effect is insignificant compared to the accuracy of measurement of chemical shifts. The magnitude of the shift for the case of carbon observed with phosphorus decoupling is not negligible. However, the majority of work for which assignment was based on chemical shift, with ^{31}P and ^{13}C, involved cross-polarisation and decoupling of protons only. Decoupling was used, after shifts had been established to investigate the effect on linewidth, and not for determination of chemical shifts to the

accuracy needed to distinguish the Bloch-Siegert shift. In the case of carbon and nitrogen the calculated Bloch-Siegert shift is very large. The observation/decoupling of these two nuclei in this particular combination does not feature in this thesis, though due to work on setting up this tuning combination on the HXY probe it is perhaps appropriate to compare the shift values calculated.

Observe nucleus	Decouple nucleus	γ / rad T^{-1} s^{-1} (obs)	γ / rad T^{-1} s^{-1} (dec)	decoupling power[a] / Hz	Larmor frequency (obs) / Hz	Larmor frequency (dec) / Hz	Δ / ppm
^{1}H	^{19}F	2.52×10^{8}	2.68×10^{8}	8.33×10^{4}	1.88×10^{8}	2.00×10^{8}	-1.34
^{13}C	^{31}P	6.73×10^{7}	1.08×10^{8}	5.00×10^{4}	5.03×10^{7}	8.10×10^{7}	-0.24
^{13}C	^{14}N	6.73×10^{7}	1.93×10^{7}	5.00×10^{4}	5.03×10^{7}	1.45×10^{7}	13.0
^{13}C	^{15}N	6.73×10^{7}	-2.70×10^{7}	5.00×10^{4}	5.03×10^{7}	2.03×10^{7}	7.32
^{31}P	^{1}H	1.08×10^{8}	2.68×10^{8}	5.00×10^{4}	8.10×10^{7}	2.00×10^{8}	-0.0123
^{13}C	^{1}H	6.73×10^{7}	2.68×10^{8}	5.00×10^{4}	5.03×10^{7}	2.00×10^{8}	-0.00421
^{31}P	^{19}F	1.08×10^{8}	2.52×10^{8}	5.00×10^{4}	8.10×10^{7}	1.88×10^{8}	-0.0160

[a] corresponding to a 3 or 5 μs 90° pulse ($\gamma B_1/2\pi$).

Table 1. Bloch-Siegert shifts

The remaining chapters in this thesis are as follows:

- Experimental, an outline of the spectrometer operation and techniques used,
- A study of cross-polarisation dynamics for ^{1}H-to-^{31}P CP,

followed by results and discussion chapters for

- Calix[4]resorcinols
- Diazadiphosphetidines -
    - PF_n
    - PCl_3
- Other PCl, PPt and PRu compounds.
- Triphenylphosphine oxide

The majority of the conclusions will be made in the separate chapters, but a few specific points and ideas for further work will be summarised at the end.

REFERENCES

[1] R.K. Harris, K.J. Packer, A.M. Thayer, *J. Magn. Reson*, 1985, **62**, 284.

[2] D.P. Burum, W.K. Rhim, *J. Chem. Phys.*, 1979, **71**(2), 944.

[3] U. Scheler, R.K. Harris, *Chem. Phys. Lett.*, 1996, **262**, 137.

[4] S.F. Dec, C.E. Bronniman, R.A. Wind, G.E. Maciel, *J. Magn. Reson.*, 1989, **82**, 454.

[5] J.R. Ascenso, L.H. Merwin, H.-P. Bai, J.C. Cherryman, unpublished

[6] M.M. Maricq, J.S. Waugh, *J.Chem.Phys*, **70**, 3300-3316, (1979)

[7] A.C. Olivieri, *J.Magn.Reson.*A, **123**, 207-210, (1996)

[8] J.C. Cherryman, Personal communication.

[9] J. Herzfeld, A.E. Berger, *J. Chem. Phys.*, 1980, **73**, 6021.

[10] O.B. Peerson, X. Wu, I. Kustanovich, S.O. Smith, *J. Magn. Reson. A*, 1994, **106**, 127.

[11] G. Metz, X. Wu, S.O. Smith, *J. Magn. Reson. A*, 1994, **110**, 209.

[12] A. Nordon, Ph.D. Thesis, Durham 1997.

[13] W. Domalewski, F.G. Riddell, L. Stefaniak, *Bulletin of the Polish Academy of Sciences.*, 1998, **46**, 35.

[14] Encyclopædia of NMR, Ed. R.K. Harris, D.M. Grant (Indirect coupling: intermolecular and solvent effects).

[15] Encyclopædia of NMR, Ed. R.K. Harris, D.M. Grant (Fluorine-19 NMR).

[16] J.P. Yesinowski, M.J. Mobley, *J.Am.Chem.Soc.*, 1983, **105**, 6191.

[17] S. Carss, PhD Thesis, Durham 1995.

[18] S. A. Vierkötter, *J. Magn. Reson. A*, 1996, **118**, 84.

2. EXPERIMENTAL

2.1. Spectrometers

Three solid-state Nuclear Magnetic Resonance (NMR) spectrometers have been used for the work presented here. Working at different field strengths allows additional information to be obtained. At higher field, several effects are observed: line separation in hertz, and therefore resolution, is usually increased (depending on the origin of the linewidths), couplings are reduced on the parts per million, chemical shift scale, and more spinning sidebands are obtained within the same shielding anisotropy manifold. The last-mentioned can be a disadvantage if it causes overlap of sidebands and isotropic peaks, but this can be overcome if faster spin rates are also employed. Often the accuracy of calculations from spinning sideband analysis can be increased by careful choice of field and spin-rate.

The general experimental procedures will be explained in this chapter, but first, an indication of the basic arrangement of, and differences between the three spectrometers will be described.

CMX 200:

A Chemagnetics CMX 200 was used for the majority of this work. It has triple-channel capability with a single pre-amp for the observe channel. There are four possible amplifiers: American Microwave Technology (AMT) broadband 6-220 MHz, AMT low frequency 30-122 MHz, Creative Electronics (CE) narrowband (fluorine or proton; 188.3, 200.1 MHz) and Bruker narrowband which is generally used for fluorine and Combined Rotation and Multiple-Pulse Spectroscopy (CRAMPS) because of the pulse shape, but it can also be tuned to most other frequencies with significant changes in the set-up. The CE amplifier will operate in two modes, class A/B and class C. Class A/B gives a linear output and is the mode for general use. Class C is used for CRAMP experiments as it gives the square pulse shape needed for precision when applying many short pulses in fast succession. Just as when changing frequencies on an amplifier (Bruker or CE), the CE has to be re-tuned between the two modes. This is done by maximising the signal output with both high and low input powers from the frequency

transmitters. The 200 MHz wide-bore (89 mm) Oxford Instruments magnet takes Chemagnetics probes that use the pencil rotor system. More details of the probes are given later in this chapter. The whole system is a Chemagnetics spectrometer with the hardware controlled from a Sun workstation via 'Spinsight' software[1], the digital card cage and pulse programmer. The signal from the amplifiers and that returning from the probe are directed through the electronics by a set of crossed diodes and the appropriate $\lambda/4$ cable, to be mixed with the reference frequency to record the free induction decay in the receiver. Figure 1 shows part of the cabling layout. The applied frequency pulses from the amplifier pass straight through a set of crossed diodes and a filter (with the appropriate frequency range and power capabilities for the probe and nucleus combination). This is then directed straight to the probe. The returning, low-voltage, signal to be recorded passes back through the same filter, but when it reaches the T-junction it can not pass back through the crossed diodes, and is instead directed to the pre-amp and receiver, down a quarter-wavelength cable because of the voltage and impedance difference produced across it. The earthed diodes work as a stop at the end of the quarter-wavelength cable which controls the current flow by setting up a standing wave across it.

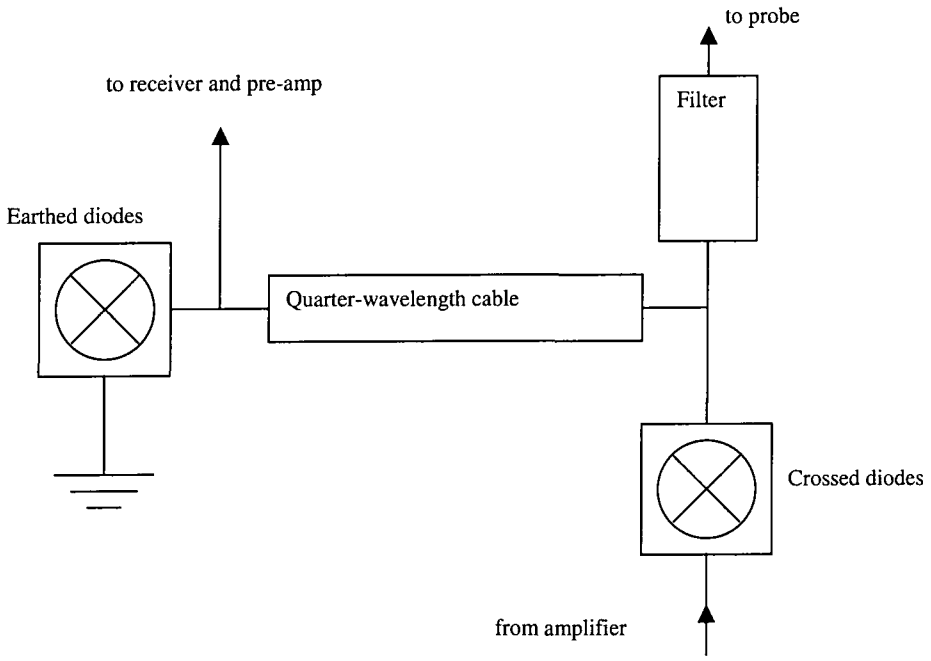

Figure 1. Cabling layout between amplifier, probe and receiver.

Varian Unity Plus 300:

The higher field instrument was used for study of field-dependent effects and for some of the variable temperature (VT) work, in particular the exchange studies on TPPO-Phenol. This system uses Doty probes with a double bearing that is heated/cooled for VT work, and takes 7 mm zirconia rotors. If higher spinning speeds are necessary for ^{13}C or ^{31}P spectra, this system also has a small rotor diameter (5 mm) HX probe. Only two amplifiers/channels are available, i.e X observe (phosphorus, carbon or nitrogen are relevant in this work) with cross-polarisation from, and decoupling of, protons. A Varian console with VNMR software controls the system.

CMX Infinity 600:

Recent access to this spectrometer in the Physics Department at Warwick University has enabled the study of carbon, proton and phosphorus spectra at both higher field and, with the 3.2 mm (rotor diameter) Chemagnetics probe, higher spinning speeds. This system also has triple-channel capability, each with a separate pre-amplifier. The set-up is, otherwise, similar to that at Durham (CMX200). There is a need for variable amplitude cross-polarisation sequences to increase cross polarisation efficiency for the spinning speeds achieved on the 3.2 mm probe. The Hartmann-Hahn matching profile may break down into sidebands at the high spin rates used with the small diameter rotor. Although more sidebands will be evident in each shielding anisotropy manifold with comparable spinning speeds than at a lower field, the smaller rotor of the 3.2 mm probe allows spin rates in excess of 15 kHz. This means that overlap problems are not normally encountered and, in general, similar numbers of sidebands can be obtained from faster spinning at the higher field.

2.2. Sample handling and rotors

As the majority of the compounds studied in this work are moderately oxygen/moisture sensitive, initial sample handling was carried out in a nitrogen atmosphere glove box. Here the powders were packed into small plastic inserts with tight-fitting caps. These inserts fit exactly into the sample space in the rotor (as would a well-packed powder), as is shown in Figure 2. Stable spinning is still possible. Inserts can be used repeatedly without having to unpack the sample and are therefore appropriate for small sample

quantity as well as unstable samples. Also, an improvement in resolution is sometimes possible by the use of inserts to restrict the sample to a smaller volume, and therefore to more homogeneous field. Between experiments, the inserts containing easily decomposed samples are stored in vials in a vacuum desiccator.

The rotors used in both the 200 and 600 MHz spectrometers are of the Chemagnetics 'pencil' design with a zirconia sleeve and fluted drive tip (smooth drive tips are also available for very slow spinning, for example in the case of CRAMPS or MAT). Depending on the nucleus to be observed and whether cross-polarisation is to be used, there are proton- and fluorine-free spacers and end caps (Kel-F, i.e. $(CF_2CFCl)_n$, and teflon or boron nitride and Vespel). A black mark extending half-way around the top of the rotor is used for optical reading of the spinning speed. The Varian spectrometer takes Doty probes, for which the rotors are of similar design, a cylinder, but this time with two flat end caps - one fluted and the other marked half black, half white for optical measurement of speed.

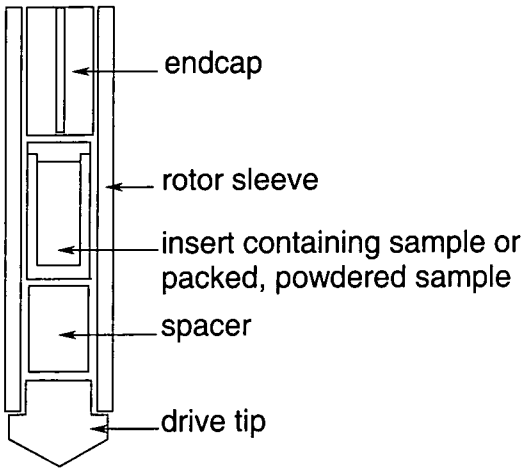

Figure 2. Pencil rotor and insert

2.3. Probes

This section will concentrate on the Chemagnetics probes for the CMX 200 as these were used for the majority of this work. All the probes have MAS capability, but can also be used for static powder or single crystal samples. A single crystal can be held in an insert which is then placed in the rotor. Purge gas (a general cooling system) can still

be used in the body of the probe, but no bearing or drive gas is required. For spinning, the friction is reduced by a circular air bearing, with the drive air catching the flutes on a drive tip. Spin rate is read optically from a black mark extending halfway around the top of the rotor. In order to keep a desired spin rate constant over a long experiment, the speed controller has the facility to lock at a certain speed and will adjust the pressures to compensate for any fluctuations.

2.3.1. HX

General set-up:

The HX has a proton channel and the X channel which tunes to frequencies in the range 19 to 83 MHz via the correct combination of two 'plug-in' capacitors. Samples are packed in 7.5 mm (outer diameter) zirconia rotors capable of spinning up to 6.5 kHz. Smooth drive tips can be used for stable slow spinning experiments (less than 500 Hz).

Magic-angle setting:

Different samples are convenient for setting the magic angle for ^{13}C, ^{31}P and ^{15}N observation. When setting up to acquire carbon spectra on the HX, (and also the HXY or HFX) probe, the ^{79}Br resonance from KBr can be easily observed without re-tuning the probe. The sample can also be mixed with adamantane and the set-up carried out without the need to change rotor. The imperfections in the cubic lattice of KBr mean that the quadrupolar interactions do not vanish producing rotational echoes in the spectrum. The angle is corrected by maximising the number of rotational echoes in the FID.

As the phosphorus frequency is too far from that of carbon to use KBr in a normal set-up, a phosphorus sample was needed to enable the angle to be checked regularly. Zinc (II) Bis(O,O'-diethyldithiophosphate) (ZDP) was prepared according to the literature method[2] by precipitation from a 1:2 mixture of zinc sulphate and ammonium diethyldithiophosphate solutions. Because of the large shielding anisotropy of this sample, it is very sensitive to the magic angle. With spinning at around 3 kHz with a recycle delay of 10 s and a contact time of 5 ms, the lineshape can be used to determine the accuracy of setting of the magic angle. A scaled powder pattern is observed when

the rotor is spinning off angle, but the anisotropy is reduced to zero giving just the isotropic shifts (symmetric lineshape) with the spinning axis at 54 ° 44 " to the magnetic field. By comparing the static linewidth with the scaled powder patterns of the spinning sample the angle can be estimated. A range of spectra at various angles is shown in Figure 3.

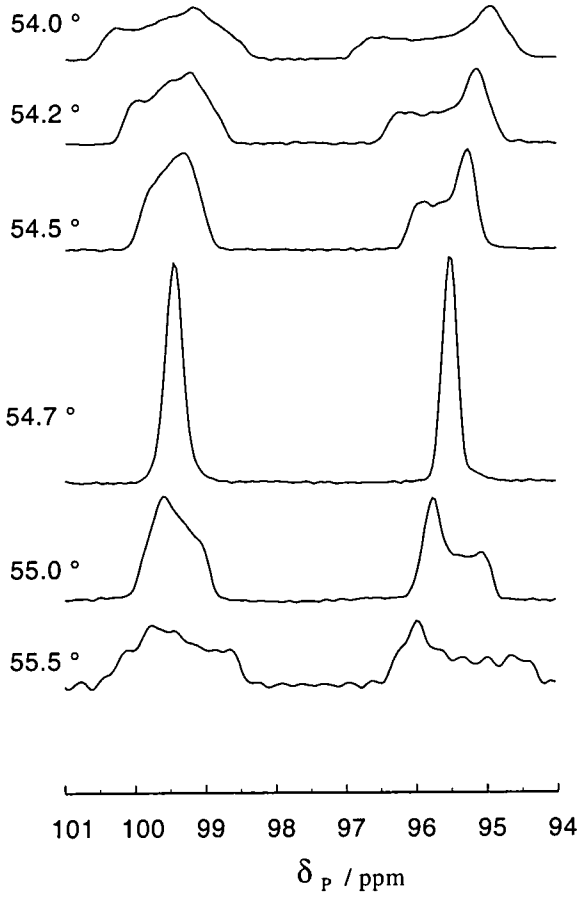

Figure 3. Effect of angle on phosphorus spectrum of Zinc (II) Bis(O,O'-diethyldithiophosphate). Centre-band region only. $^{31}P\{^{1}H\}$ at 81 MHz.

As only a single acquisition was necessary to obtain a spectrum with sufficient signal to noise, the sample is also appropriate for setting the Hartmann-Hahn match (between proton and phosphorus) and can be used as a chemical shift reference. Therefore, once a proton power has been set the rest of the set-up, including checking of the magic angle, can be carried out on this sample, as an alternative to the standard brushite or 85 % phosphoric acid used for Hartmann-Hahn matching.

In the case of ^{15}N observation the shape of the nitrate signal in the ammonium nitrate standard sample can also be used to check the magic angle. This leads to a very similar situation to that described above for phosphorus.

2.3.2. HF

Observing fluorine in the presence of proton:

Because of the close proximity of frequency (the proton and fluorine frequencies have a separation of only 6 %) a specially designed probe and narrowpass filters are needed to separate the r.f. in the two channels. With the use of these high specification filters (which are designed specifically for the power levels of the probe) and the electronics of a trap of appropriate capacitance inside the probe, isolation is sufficient for any combination of cross polarisation, observe, decouple with these two nuclei (i.e. H to F cp, F to H cp, H{F}, F{H}).

Magic-angle setting:

As there is no low-frequency, X, observe channel on this probe, the most commonly used method for setting the magic angle is to observe the lineshape of the ^{1}H CRAMP spectrum of $KHSO_4$.[3] As the set-up for CRAMPS is a complex and lengthy procedure, this means the angle will not be checked regularly. A recent method developed in this group involves the observation of the fluorine signal from a p-tert-butylcalix[4]arene containing α,α,α-trifluorotoluene[4], a method which can be included in any standard HF probe set-up. This shows a similar effect to that observed with the phosphorus sample, ZDP.

2.3.3. HFX

Triple-channel decoupling combinations:

This probe will allow the observation of the X nucleus, together with decoupling of proton and/or fluorine, with cross-polarisation from either of these two. Because the narrowpass filters available will not take the power necessary for this probe, it is not possible to observe fluorine in the presence of irradiation at the proton frequency. However, if resolution of the fluorine spectrum is sufficient without ^{1}H decoupling, a

spectrum such as $^{19}F\{^{31}P\}$ is possible. The probe incorporates a trap to isolate the proton and fluorine frequencies. Identical bandpass 200 MHz filters are used on both high-frequency channels. The low-frequency channel can be tuned to the range of X nuclei studied without need to change capacitors. 'Tune' and 'match' to give minimum reflected power on all three channels will need significant adjustment when altering the X resonant frequency.

2.3.4. HXY

This triple-channel probe can be used to observe nuclei (other than fluorine) in the presence of another nucleus as well as with high-power proton decoupling and/or cross polarisation. For example, experiments with carbon and phosphorus include ^{31}P to ^{13}C cross polarisation and $^{13}C\{^{31}P\}\{^{1}H\}$. To set up this probe, the correct combination of capacitors (front, back and trap) have to be chosen for the particular frequency combination required. Calculations for capacitor combinations to study carbon-13 and phosphorus-31 on this probe were made according to the probe manual. For 50.33 and 81.02 MHz (^{13}C and ^{31}P respectively) for the low and middle frequency channels, a small trap with capacitance, C_T, 39 pF was chosen (a large trap is only needed when the middle frequency is more than twice the low frequency). This gives 33 pF as the choice for the front capacitor, C_f, for this frequency range. As the calculated value for C_b is less than the lowest available, no back capacitor is needed, ($C_b = 1.7 * C_f - C_T$ is the equation appropriate for a combination with a small trap). Once it was confirmed that this capacitor combination allowed tuning, it was tested with standard experiments on simple systems.

2.4. Spectrometer set-up

2.4.1. Setting powers for cross-polarisation experiments

The required probe is placed in the magnet and in all cases the proton pulse durations are calibrated on a sample of polydimethylsiloxane (PDMSO). Reflected power must first be minimised (and subsequently on each sample used) by adjusting the variable capacitors of the 'tune' and 'match' circuits, which adjust the position and depth of the

reflected power minimum, on each channel. With the correct 200 MHz filter in place, the transmitter power can then be adjusted to give a 5 μs π/2 pulse on proton (3 μs π/2 pulse for the HF probe). The static PDMSO sample can also be used for checking the shims, in terms of lineshape and width. All combinations of the shim coil settings can be adjusted individually while repeating a single acquisition of the PDMSO spectrum. The software shim controller adjusts the homogeneity of the magnetic field by changing the current flowing to each of the room-temperature shim coils.

The next sample generally has three purposes,

- to set the X power in order to fulfil the Hartmann-Hahn condition for cross-polarisation $\gamma_X B_{1X} = \gamma_H B_{1H}$
- to check the magic angle (in the case of carbon, these first two steps use a mixed sample of adamantane and KBr)
- to set the reference chemical shift scale for the subsequent spectra (referencing by replacement)

and is spun slowly, i.e. between 1 and 3 kHz.

An exception is the case of fluorine where a static liquid C_6F_6 sample is used to set a fluorine 90° pulse in a similar fashion to the setting of a proton pulse duration. This will give an approximate match condition, and if CP is required this is optimised on the spectrum to be recorded.

With the proton pulse duration already set, the Hartmann-Hahn match can be most easily optimised by applying the appropriate duration of pulse and maximising the FID amplitude by altering the transmitter output power (or amplifier output in the case of the Bruker amplifier).

Table 1 below gives the frequencies and chemical shift references of the standard samples used.

Nucleus	Frequency / MHz	Sample	δ / ppm	Primary standard at 0 ppm
^{1}H	200.13	Polydimethylsiloxane PDMSO	0	TMS
^{31}P	81.02	Brushite ($CaHPO_4$)	1.2	85 % H_3PO_4
^{31}P	81.02	Zinc (II) Bis(O,O'-diethyldithiophosphate)	99.2[a]	85 % H_3PO_4
^{19}F	188.29	Hexafluorobenzene (C_6F_6)	-166.4	$CFCl_3$
^{13}C	50.33	Adamantane ($C_{10}H_{16}$)	38.4[a]	TMS
^{15}N	20.29	Ammonium nitrate	-5.1[b]	CH_3NO_2

Table 1. Standard samples.

[a] High frequency resonance

[b] Nitrate peak

The sample to be studied can then be placed in the probe, the 'tune' and 'match' adjusted on each channel to minimise the reflected power for that particular sample, and parameters such as recycle delay, contact time and resonance frequency optimised.

Measuring and calibrating powers:

As the input values on the power dials can vary dramatically with the amplifier and probe combination, it is important to know the power levels going into the probe. This can be done by taking the output of the cable that takes the rf into the probe and connecting via a 30 dB attenuator to an oscilloscope. With a long pulse duration and short recycle delay a repeated single pulse can be observed on the oscilloscope and its power measured from the peak-to-peak voltage. This is then easily converted to watts using the standard conversion.

If any experiments require different power levels on the same channel throughout the pulse sequence, the method used is to set the 90 ° pulse duration and match as normal and then use the software control to lower the power (from its maximum setting of 255) without altering the set levels on the transmitter or oscilloscope. Spin-lock and decoupling powers, for instance, can then be arrayed in a single experiment. Care must be taken, however, to calibrate the software control, as each amplifier/transmitter combination will give a different, non-linear, output. If the duration of the 90 ° pulse is known (from where the maximum, 90 °, and null, 180 °, signals occur in a direct

polarisation experiment with varying pulse duration) the power in frequency terms can be calculated as 1/(4*duration). A calibration experiment involves changing the software power level, decreasing from 255, and measuring the 90 ° pulse duration.

Figure 4 shows a graph plotted from such a calibration measuring the fluorine 90° pulse duration observing C_6F_6 (HF probe), using the AMT amplifier. The data fits to a power function $y=0.0008x^{2.10}$. Figure 5 is the curve for phosphorus powers on the HX probe ($y = 0.0004x^{2.17}$).

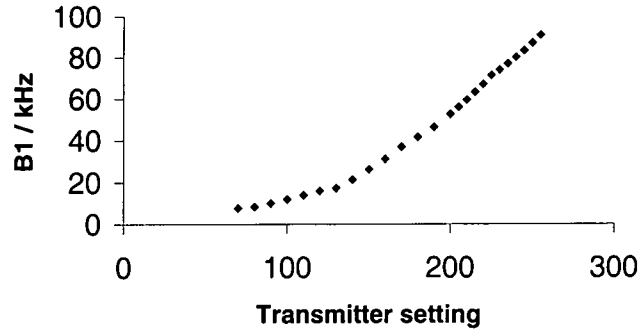

Figure 4. Power calibration (B_1 in frequency units) for fluorine the HF probe (AMT amplifier).

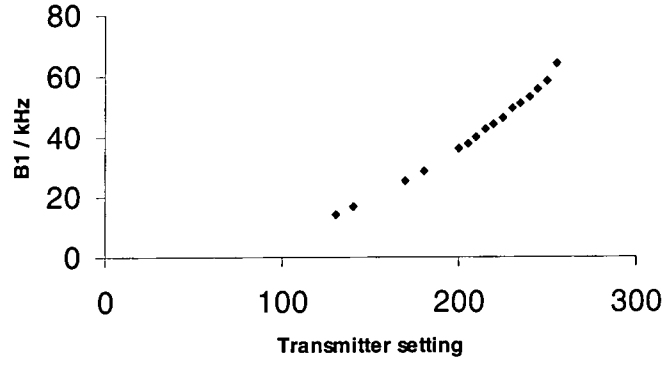

Figure 5. Power calibration (B_1 in frequency units) for phosphorus the HX probe (AMT amplifier).

The curve and exact values in such studies will be dependent on the amplifier, probe and frequency combination as each will produce different pulse and linear/non-linear amplification characteristics. For this method of measurement, an accurate T_1 is needed and sufficient recycle delay must be used. The curve parameters will be accurate if T_1

is properly considered, but it can be noted that measurement of T_1 is only needed at one of the field values used as there should be no effect on this using weaker, longer pulses. It is also assumed that there is significant difference between T_1 and $T_{1\rho}$ which, for the samples studied here, in general, is justified.

2.4.2. VT

Calibration:

An important consideration when studying exchange processes is the calibration of the variable temperature control system. The calibration was carried out by observing the frequency difference between the resonances of the methyl and hydroxy protons of methanol in its spectrum when adsorbed on tetrakis(trimethylsilyl)silane (TTMSS).[5] These samples are sealed in glass before placing in the rotor so as to retain the adsorbate. At higher temperatures the hydrogen bonding is reduced and the hydroxyl proton resonance is shifted towards the lower frequency methyl proton signal. The equation[6]

$$T_{cal}\,(K) = 403.0 - 0.059\,|\,\Delta\nu\,(Hz)\,| - (0.953 \times 10^{-4})\,|\,\Delta\nu\,(Hz)\,|^{2}$$

is used, which relates the actual temperature in the rotor to the frequency difference between the two peaks. Various temperatures and spin rates were investigated for all the probes, from which graphs and calibration equations were derived.[7] The effect of time after reaching set temperature on the methanol/TTMSS spectrum was also investigated, since it is important to wait sufficient time before acquiring at a specific temperature in order to minimize any temperature gradients within the rotor. Several other methods exist for checking temperature gradients in a rotor, including the use of lead nitrate[8,9] or the ^{13}C resonances of samarium acetate.[10] However, from these experiments, it is clear that if sufficient equilibration time is left the 'VT gas', which is directed at the centre of the rotor length, will produce an even heating effect.

General VT operation:

The Chemagnetics probes spin with an air bearing and drive gas supply. When operating at temperatures above and below ambient probe temperature a third gas inlet, with dry nitrogen from a boil-off dewar, is used as the heating/cooling and purge gas. The nitrogen flows through a copper coil submersed in liquid nitrogen (this is not

needed for high temperature work). This cold gas then continues to the temperature control stack, where it is heated to the desired temperature before being directed across a sensor which feeds this value back to the controller unit. As soon as the gas temperature is measured it flows around the rotor. Usually up to 20 minutes is required before the entire sample has reached an equilibrium temperature, that may be taken, with calibration of the set temperature, to be the temperature throughout the experiment. The out-flowing gas, now mixed with the purge, spinning and bearing gases is allowed to escape from the top of the heater unit. As the temperature is measured before it reaches the sample rotor, the reading does not take account of temperature gradients within the rotor or frictional heating due to high speed spinning, which can be considered in careful calibration experiments.

The importance of calibration and the effect of temperature gradients can be illustrated in the spectra of TPPO-phenol shown in Figure 6. At the coalescence temperature the spectrum changes from a single peak to two separate resonances as exchange is slowed. Initial spectra (run by G. McGeorge) showed what appeared to be a complex bandshape of a triplet, but after repeating these experiments with sufficient time to allow equilibration and avoid temperature gradients, the individual spectra showed either a doublet or singlet, and not a superposition of the two. By comparing spectra, it can also be seen that the 'approximate temperatures' given for the earlier spectra are not sufficiently accurate for any quantitative analysis.

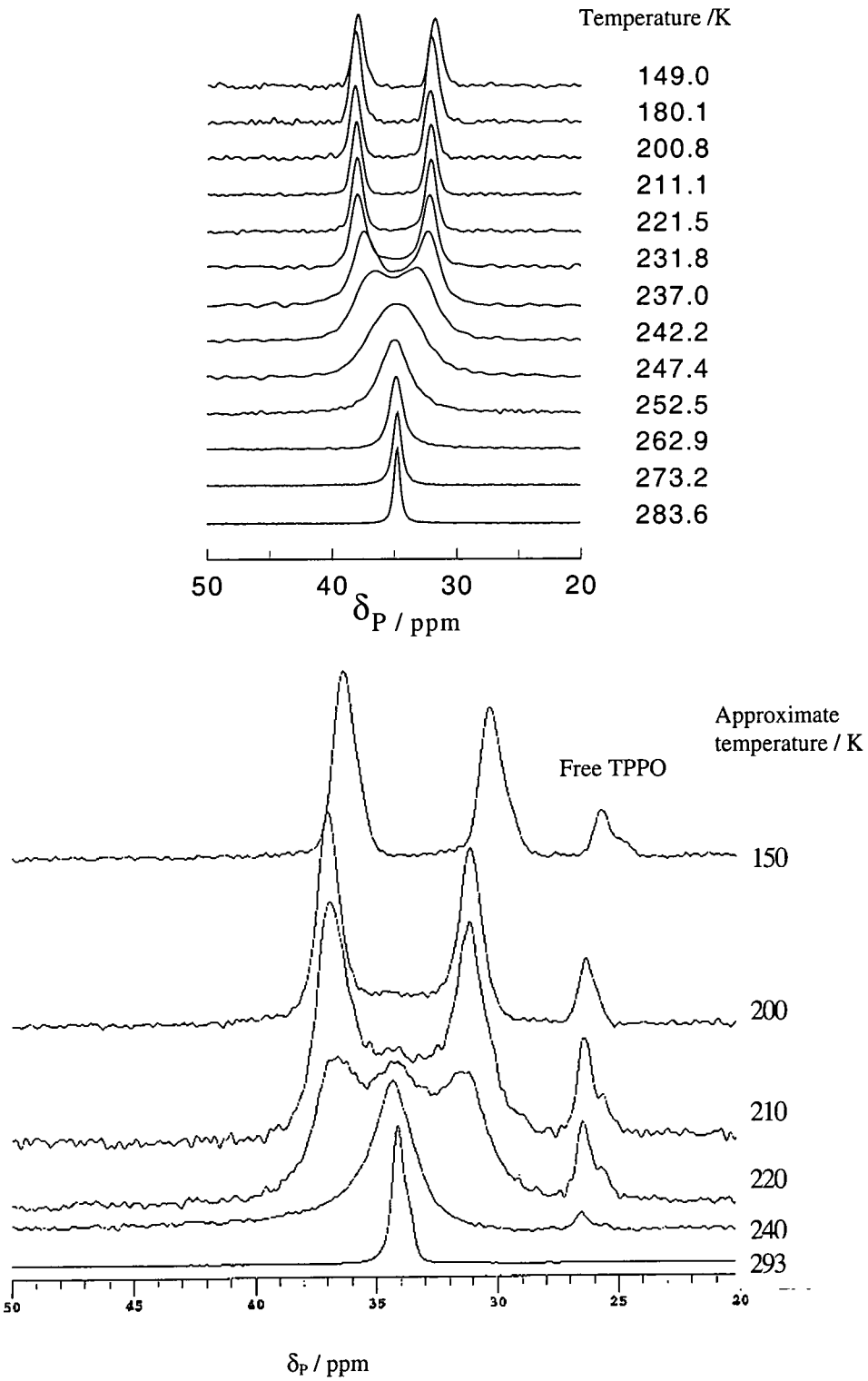

Figure 6. Variable temperate ^{31}P spectra of triphenylphosphine oxide-phenol. Top - spectra from this work. Bottom - spectra pre-1996 (G. McGeorge). $^{31}P\{^{1}H\}$ at 121 MHz.

2.5. ACQUISITION OF SPECTRA

Spinning sideband analysis is described in more detail in the theoretical section of the introduction and for specific applications in later chapters. It is however related to some experimental considerations. For samples with large anisotropy for which such calculations are desired it is necessary to obtain accurate intensities for the small outermost sidebands. In the first instance this will require an excellent signal-to-noise ratio. As well as sufficient repetitions it is also necessary to ensure uniform excitation over the whole manifold. The choice of spectral width is vital, and a method used to check that sideband intensities are not being distorted is to vary the transmitter frequency over the 'static' linewidth, repeating the same experiment.

In the case of broad static spectra for which lineshape can also be analysed it is important to record accurately the first points in the free induction decay (FID), else a distorted pattern will result. As there has to be a short delay before acquisition to cope with the problems of probe ring-down and the FID will also decay very quickly, it is often better to use an echo sequence to record the FID from the top of the echo. In this way it is more certain that an accurate lineshape will be recorded. The Hahn-echo sequence consists of a 90° proton pulse, contact, delay time tau, 180° refocusing pulse, delay time tau and acquisition. Not so much of a problem with the magnitudes of shielding anisotropy observed in these phosphorus compounds, but still an important consideration is, again, ensuring even excitation over the whole width. A distorted intensity could be observed if signals (or part of a static powder pattern) were outside the bandwidth covered by a particular excitation pulse.

The simple Hartmann-Hahn cross-polarisation sequence is described, along with the TORQUE experiment in Chapter 3, which also serves as an introduction to cross polarisation. Other sequences, which are used for specific compounds, such as the HETCOR spectra of the calix[4]resorcinol compounds and the SPI study of exchange, are described in the appropriate chapters.

Relaxation time measurement is important both for checking optimum acquisition parameters and for characterisation of structural and motional properties. The following pulse sequences were used extensively for the measurements carried out in this work.

T_1^H and T_1^X both used cross-polarisation techniques based on the method of Torchia.[11] In the figures (Figure 7 and Figure 8) the arrayed relaxation delay is marked tau and the relaxation and acquisition delays (to avoid probe ring down effects) are rd and ad, respectively. Both sequences contain two blocks which allow a change of phase in the X case, and the production of a difference spectrum, and therefore an exponential decay, in the case of the proton T_1 measurement which would otherwise take the form of an inversion-recovery plot.

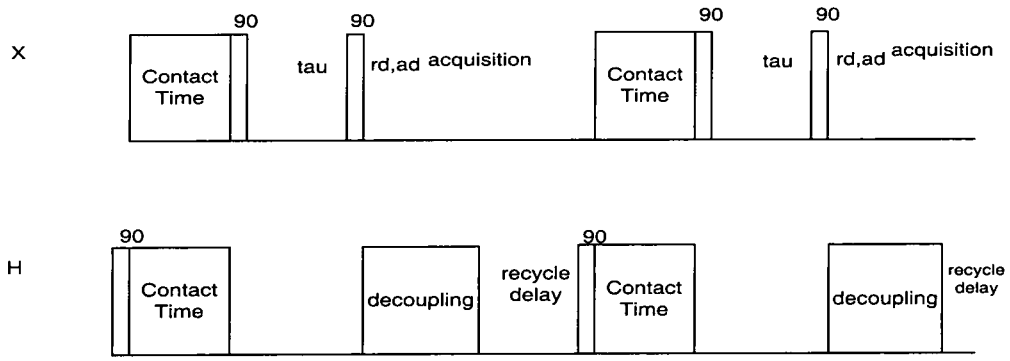

Figure 7. T1XCP, second loop has a change of phase of the proton 90° pulse.

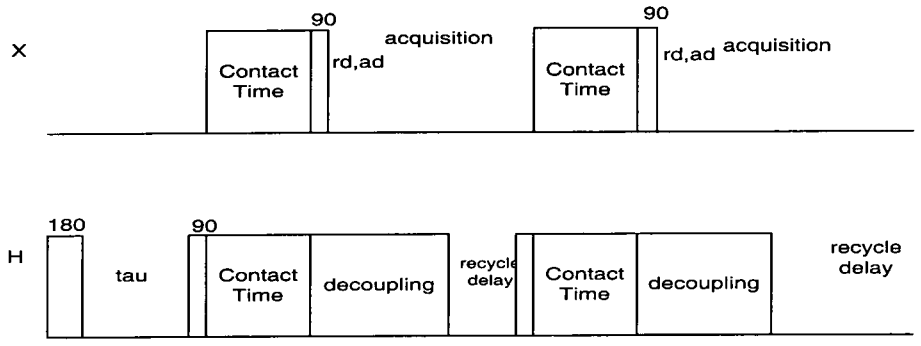

Figure 8. T1HCP, second loop does not contain the inversion and time tau.

$T_{1\rho}$ is generally measured directly via a variable spin-lock time experiment, with or without cross polarisation depending on which nucleus is being studied. Variable

contact time cross-polarisation experiments were used to find optimum conditions for general acquisition, but can also be used to extract cross-polarisation rate, T_{IS}^* and $T_{I\rho}^*$ from the exponential rise and decay of the magnetisation.

Modification of several 'system' and 'in-house' pulse programmes has been required for the triple-channel work in this thesis. Double-decoupling combinations and programmes with 'transmitter blanking' added to allow use of the required amplifier combinations were devised from some of the existing sequences. Also, for measurement of B_1 fields, a cross-polarisation experiment was needed with software amplitude control for each separate pulse in the sequence.

2.6 Magic-angle turning, and its application to phosphorus systems.

Shielding anisotropy (SA) gives information about the local structural and dynamic environment of molecules in the solid state. Overlap of the typically broad powder patterns often obscures this information for multiple site systems. Two-dimensional experiments such as magic-angle turning (MAT) have been effective in resolving this difficulty by separating the anisotropy and the isotropic chemical shift.[12,13] MAT experiments have previously been used for ^{13}C and ^{15}N systems which have very long total accumulation times due to low sensitivity. This particular, recently developed technique had not been previously applied to the study of phosphorus. In many cases these experiments will be extremely useful in separating the complex anisotropy patterns often observed in spectra with multiple phosphorus sites. In comparison to the rare spin nuclei previously observed, with ^{31}P, the time for the 2-D experiment is significantly reduced.

For Magic Angle Turning, stable turning (at 30-40 Hz) is needed. One method involves placing twelve equally spaced marks on the rotor (instead of the usual one) so that 30 Hz rotor spinning would be controlled by the MAS unit optically reading at 360 Hz. A flow constrictor can be placed in the line supplying the drive gas to reduce pressure and improve spinning speed control. It was found in this study that the Chemagnetics speed controller was capable of stable slow speeds (to ±1 Hz) with use of the air line

constriction and smooth drive tip. There was, however, found to be a slight upward drift in spinning speed with time, and the maximum experimental time was limited.

The shielding anisotropy shown in a static or moderate spinning spectrum (frequency less than the static linewidth) is very useful in obtaining information about local structure and dynamics. But in complicated cases where large shielding anisotropy causes the close chemical shifts to overlap, analysing these to give quantitative information can be difficult. MAT is a technique that produces spectra that correlate a high resolution isotropic chemical shift (evolution dimension) with the chemical shielding anisotropy (directly detected) for solid samples preserving the static bandshape for analysis to find the tensor principle components. It involves stable spinning at speeds as low as 30 Hz and special pulse sequences, of which there have been several modifications, timed so that the evolution period corresponds to specific rotor positions (multiples of 1/3 of the rotor period).

Two pulse sequences exist for the MAT experiment in Durham:[14] TRIPLE ECHO and PHORMAT (PHase cORrected MAT). Set-up of these pulse sequences and the accompanying acquisition and processing macros was done in collaboration with Dr. Eric Brouwer. Both sequences collect two data sets and are processed using the hypercomplex method. Processed data from the triple-echo experiments also require shearing to correct a twist of the frequency dimensions.

The absence of spinning sidebands and the low spin rate enables the use of a large volume rotor and high field, reducing the experiment time. Phase corrected MAT (PHORMAT) gives the isotropic shift in the evolution dimension and does not require shearing because of the incorporated echo pulses that give the exact refocusing. Triple echo and MAT sequences are simpler to run, but require more complex processing including shearing. The pulse sequence for the PHORMAT experiment is shown in Figure 9. The pulses are applied over increments allowing the sample to turn through 120°. This is the same principle as the magic-angle hopping experiment,[15] but involves slow spinning (producing a pseudo-static pattern in one dimension) and accurately timed pulses, as opposed to mechanical turning of the sample through 120° steps. The isotropic shift is obtained from these 120° steps as, in the molecular frame, the static

field is rotated by 90°, and the average of the three tensor components of the anisotropy becomes the trace of the tensor.

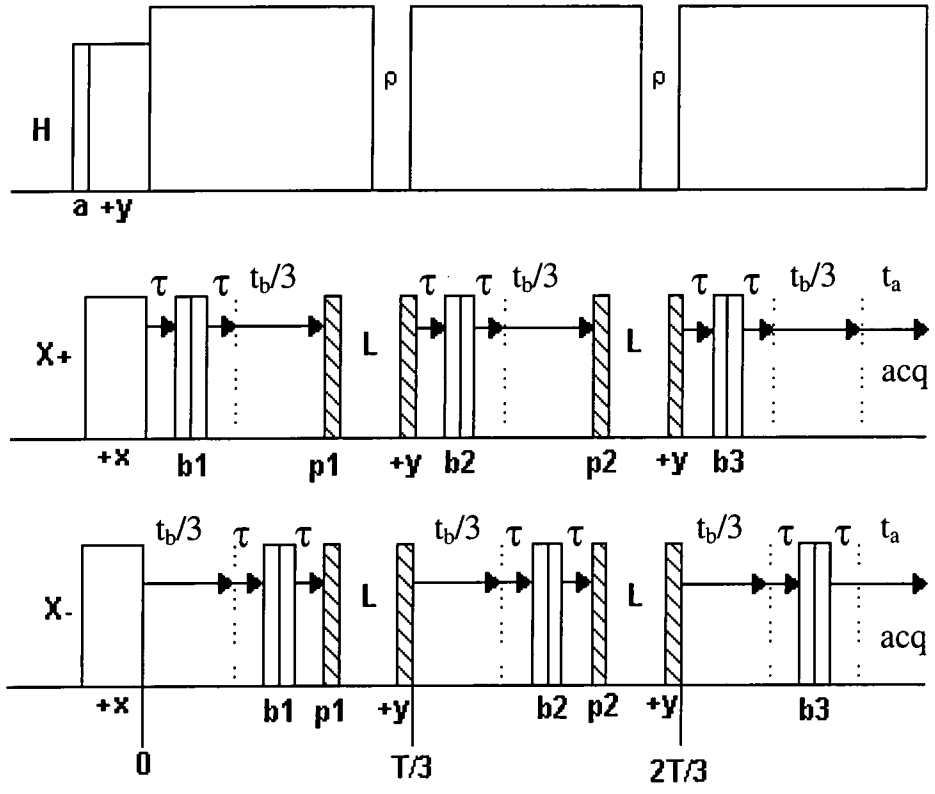

Figure 9. Pulse sequence for collecting the + and - data sets in a PHORMAT experiment. T = rotor period, τ defines a refocusing echo time around pulses b, x and y are pulse phases and p indicates a read pulse.

The magnetisation is created by standard Hartmann-Hahn CP. After a time $t_b/3$, a component of the magnetisation is stored in the z direction for a time L, and then recorded in the transverse plane after $^1/_3$ of a rotor period. The phase corrected experiment is slightly more complicated than the simpler MAT experiment, as it also includes refocusing periods indicated by the times τ and the 180° pulses. It is also necessary to acquire 'plus' and 'minus' subspectra (usually in two separate data sets) to allow phase correction in two dimensions.

A complication with an abundant nucleus such as phosphorus is the contribution to the static lineshape by homonuclear coupling. As the sample spinning is very slow, dipolar couplings are not removed from the anisotropic shielding pattern. Brushite ($CaHPO_4$)

contains one fairly isolated ^{31}P centre. The static spectrum of brushite consists of a single powder lineshape. Although the brushite spectrum is simple, not containing any overlapping manifolds (so that MAT will not yield additional information), it was found to be a good sample to test the experiments (Figure 10). Initial work on this technique to test the stability spinning, synchronisation and the various pulse programs was carried out on brushite (commonly used as a solid standard for ^{31}P NMR). This is a simple system with only one phosphorus environment and was useful for modifying conditions and checking processing without the complication of multiple peaks. In theory, peaks separated by as little as 5 ppm will be distinguishable. Other suitable phosphorus systems with multiple environments require certain criteria in order to make MAT a viable experiment. A MAS spectra showing overlapping sideband manifolds is more difficult to interpret than under MAT conditions, but the phosphorus nuclei must be sufficiently far apart in space (greater than about 3 Å) so that the dipolar interactions are not significant. The molecule studied in Chapter 8 has two phosphorus nuclei separated by a distance of 3.3 Å, just above this limit.

PHORMAT Results

The PHORMAT sequence performed better in the initial tests and proved to give a superior signal-to-noise ratio and has the advantage of requiring less processing (no shearing is needed). This was the sequence chosen to explore the experiments. The pulse duration needs to be carefully calibrated for both sequences in order to obtain accurate 2-D spectra, particularly for the triple-echo sequence. A PHORMAT spectrum of brushite is shown in contour form in Figure 10, with slices through this two-dimensional spectrum shown in Figure 11. There is some distortion of the isotropic lineshape and a fairly high noise level in the slices, but the experiment was successful.

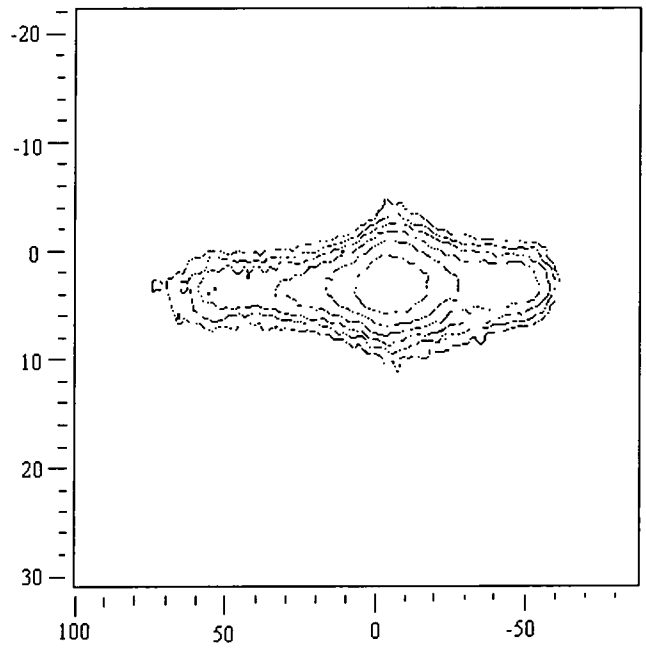

Figure 10. PHORMAT spectrum of brushite. 81 MHz phosphorus frequency, number of acquisitions 96, no. of increments 112, spinning speed 30 Hz, contact time 2.5 μs, recycle delay 2 s.

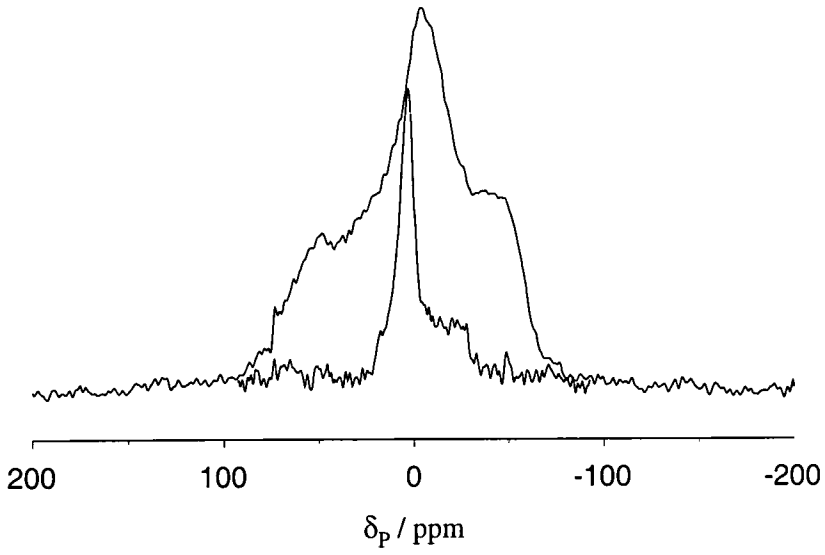

Figure 11. Slices through dimensions of brushite PHORMAT spectrum, showing the isotropic and anisotropic dimensions.

Spinning sideband analysis of a brushite MAS spectrum gave ζ = -60 ppm and η = 0.8. The pseudo-static pattern from the PHORMAT experiment was fitted using a simplex

fitting routine in a programme, 'fitstatic', provided by P. Hodgkinson.[16] The fit is shown in Figure 12. The results from this are ζ = -68 ppm and η = 0.8. The static lineshape is not as good as could be expected, there is some distortion of intensity between the shoulders representing the principal components. Despite this, the general shape of the fit is good, and the agreement between the fast-spinning and 'turning' methods is reasonable. Another result for a multiple site system is given in Chapter 8. This later experiment shows better representation of the static lineshapes and agreement with spinning sideband analysis results is excellent.

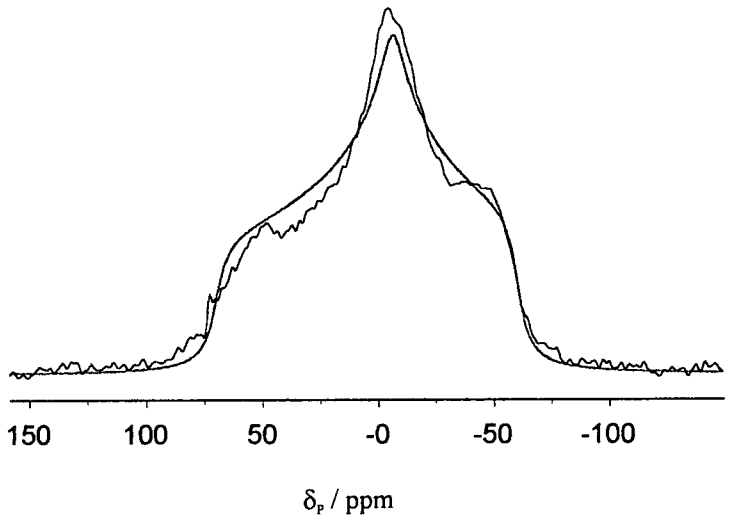

Figure 12. Fit of pseudo-static pattern from PHORMAT experiment on Brushite. $^{31}P\{^1H\}$ at 81 MHz.

REFERENCES

[1] Chemagnetics Spinsight. Version 3.5.2. © Otsuka Electronics (U.S.A.) Inc.

[2] A. Kubo, C.A. McDowell, *J. Magn. Reson.*, 1991, **92**, 409.

[3] P.Jackson, R.K.Harris, *Magn.Reson.Chem.*, 1988, **26**, 1003.

[4] E.B.Brouwer, R.K. Harris, submitted to *J.Magn.Reson.*

[5] AE Aliev, KDM Harris, *Mag.Res.Chem.*,1994, **32**, 366.

[6] AL van Geet, *Anal.Chem.*, 1970, **42**, 679.

[7] H E Birkett, S C Campbell, J C Cherryman, L A Crowe, A Nordon, J A Shaw, Nov '96 and Feb '99. unpublished.

[8] A. Bielecki, D.P. Burum, *J.Magn.Reson.*,1995, **116**, 215.

[9] L.C.M. van Gorkom, J.M Hook, M.B. Logan, J.V. Hanna, R.E. Wasylichen, *Magn.Reson.Chem.*, 1995, **33**, 791.

[10] J.F. Haw, G.C. Campbell, R.C. Crosby, *Anal. Chem.*,1986, **58**b, 3173.

[11] DA Torchia, *J.Mag.Res.* 1978, **30**, 613.

[12] Z. Gan, *J. Am. Chem. Soc.* 1992, **114**, 8307.

[13] J.Z. Hu, W. Wang, R.J. Pugmire, "Magic Angle Turning and Hopping" in *Encyclopedia of NMR*, R.K. Harris, D.M. Grant, Eds. 1996.

[14] D. M. Grant, Utah. Personal communication.

[15] N.M. Szeverenyi, A. Bax, G.E. Maciel, *J. Magn. Reson.*, 1983, **51**, 400.

[16] P. Hodgkinson, Durham University. Personal communication.

3. Cross-polarisation dynamics in proton-phosphorus systems

3.1 Introduction.

Two effects in solid-state NMR - that of low sensitivity for rare nuclei such as carbon and nitrogen, and the long spin-lattice, T_1, relaxation times of nuclei other than protons, can both be overcome by cross-polarisation techniques. Transfer of magnetisation from protons to the X spins to be observed will increase sensitivity (in abundant to rare spin cases) and may reduce the time required between repeated acquisitions (for almost all sensible cases - abundant-to-rare and transfer between two abundant spins where T_1 relaxation times differ e.g. H-to-F, F-to-P or H-to-P cross polarisation). Here, cross-polarisation dynamics for transfer between two abundant spins (H-to-P) are discussed.

The samples that will be described here are three simple inorganic phosphates: $K_3PO_4.2H_2O$, $(NH_4)_3PO_4$, $CaHPO_4$ and a molecule related to the study of structure and dynamics in this thesis, $(C_6H_5)_3PO$ (i.e. TPPO). The compounds investigated represent varying natures of directly bonded and remote protons, inorganic and organic environments, and values of relaxation times and CP rate (obtained from initial individual measurements). The phosphates are the simple test systems initially selected because of their availability. Similar data for $(Cl_3PNCH_2CH_2Cl)_2$ are discussed in the chapter on chlorinated diazadiphosphetidines, as it was found to be a case where the experimental data did not allow a successful fit using this approach.

Cross-polarisation is a three-stage process. In the conventional experiment, the spin-temperature of the abundant spins in the rotating frame is lowered by a 90° pulse to rotate the magnetisation into the y-direction. Polarisation transfer between the two spin baths is most often effected by spin-locking both abundant (I) and rare (S) spin magnetisations in the same direction. Thermal contact is thus established and the temperature of the rare spins will drop. The abundant spins have a much greater heat capacity and, as the population difference of the rare spins is dramatically increased during cross-polarisation compared with direct-polarisation experiments, sensitivity is increased. The Hartmann-Hahn condition, $\gamma_I B_{1I} = \gamma_S B_{1S}$, relating the gyromagnetic ratios and applied radio frequency magnetic fields for the two nuclei (I represents the 'abundant' spin, and S, the 'rare' spin), serves to bring the energy of the two spin baths to

equivalent levels in the rotating frame, so that efficient polarisation transfer can occur. The spin-lock on the S spins is stopped at a time to give maximum intensity, the build up of magnetisation being characterised by cross-polarisation time, T_{IS}. The rotating-frame spin-lattice relaxation will work against the increase in magnetisation and will result in a reduced signal intensity if the 'contact time' is too long. The I spin-lock can be, and usually is, maintained to give decoupling during acquisition. This acquisition of the resulting S-spin magnetisation under the desired decoupling conditions is the final stage.

In this work, a series of simple phosphorus compounds, mainly phosphates, are analysed in terms of their cross-polarisation dynamics. Phosphorus-31 is an abundant spin (100% natural abundance spin-1/2 isotope) and there may be comparable numbers of phosphorus nuclei and protons, particularly in inorganic molecules. Therefore, the actual cross-polarisation time, T_{HP}, and the spin-lattice relaxation times in the rotating frame, $T_{1\rho}$ can not always be determined separately from simple fitting of the variable contact time behaviour of the magnetisation (i.e. signal intensity). When the numbers of ^{1}H and ^{31}P atoms are approximately equal and both are abundant spin systems, the observed, effective values of $T_{1\rho}^{*}$ and T_{HP}^{*} will not be the true time constants for the process. It is expected, from theoretical considerations, that the observed cross-polarisation rate will be faster than the actual rate. More complex expressions are required and values can be extracted from a simultaneous fit of the contact time curve and that from the modified TORQUE experiment, which quenches the $T_{1\rho}$ dependence in the latter portion of the CP curve. This has been done using a modified version of a fitting programme originally written by S. Ando,[1] which has been altered for use with ^{1}H-^{31}P systems (the programme was initially written for analysis of proton-fluorine systems) and to run using the qbasic software available.[2]

In a similar fashion to the HF systems studied previously[3,4] we may have, for proton-to-phosphorus cross-polarisation, comparable values for the ^{1}H and ^{31}P spin-lattice relaxation times in the rotating frame, and similar heat capacities for the spin baths of the two nuclei. However, phosphorus and protons do not have the same valency (unlike proton and fluorine) and will therefore not have a similar chemical position within a molecule (as is often the case for the univalent proton and fluorine nuclei).

Varying the contact time results in the possibility of analysing effective cross-polarisation dynamics. During the contact time when the ^{31}P magnetisation is spin locked, the initial increase in signal intensity (magnetisation) will be governed by the effective cross-polarisation time T_{HP}^{*} whereas at longer times, the subsequent decay is characteristic of an effective spin-lattice relaxation time in the rotating frame, $T_{1\rho}^{*}$ (which is assumed to be, and generally is, longer than T_{HP}^{*}). The signal intensity in an array experiment in which the contact time is varied can be fitted to extract these two time constants. The parameters can also be measured directly by arraying the spin-lock time on a single channel, observing the decay due to $T_{1\rho}$, or by the TORQUE experiment ('$T_{1\rho}$ quenched')[5] which, in favourable circumstances, will measure T_{HP} independently of any relaxation decay. In a TORQUE experiment the contact time is varied, but within a constant duration spin-lock on the protons (i.e. tau1 and ct are varied within a constant proton spin-lock time, tau, as illustrated in Figure 1).

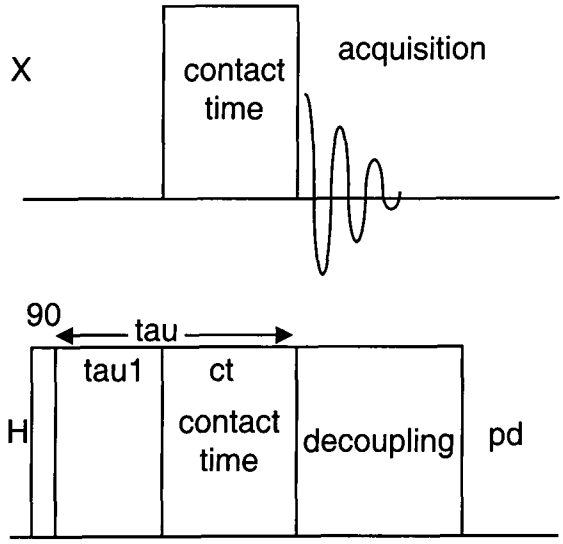

Figure 1. TORQUE pulse sequence.

At long contact times the TORQUE curve should reach a constant maximum value after the initial exponential rise. However, depending on the relative magnitude of the rotating-frame relaxation times of the two abundant spin systems, the slope of the long time, 'plateau' region may be modified with the slopes as indicated:

negative slope: $T_{1\rho}^{H} > T_{1\rho}^{P}$

zero slope: $T_{1\rho}^{H} = T_{1\rho}^{P}$

positive slope: $T_{1\rho}^{H} < T_{1\rho}^{P}$

These three cases can not be readily distinguished by the standard cross-polarisation curve (Hartmann-Hahn cross-polarisation with arrayed values of contact time) where only an effective, overall rotating-frame relaxation time is obtained, but can be easily identified by simple inspection of a TORQUE curve, giving an instant indication of the relative magnitude of the $T_{1\rho}$ of the two nuclei. These relationships only apply if $(1+\varepsilon)/T_{HX}$ is greater than $(1/T_{1\rho}^{H} - 1/T_{1\rho}^{P})$. For all the systems studied here, the last of the three situations is applicable. A positive slope is observed at long contact time and is also predicted by the direct measurements of $T_{1\rho}$.

The following pair of coupled differential equations for the two nuclei give the change in the inverse spin temperatures, β_X and β_H (in this case X = P), with cross-polarisation time, t_{CP}, under cross-relaxation conditions.[6] The modifications to this system of equations for an abundant-abundant spin system have been explored by S. Ando.[3]

$$\frac{d}{dt_{CP}}\beta_X = -\frac{1}{T_{HX}}(\beta_X - \beta_H) - \frac{1}{T_{1\rho}^{X}}\beta_X$$

$$\frac{d}{dt_{CP}}\beta_H = -\frac{\varepsilon}{T_{HX}}(\beta_H - \beta_X) - \frac{1}{T_{1\rho}^{H}}\beta_H$$

Here the rotating-frame spin-lattice relaxation times and CP rate are defined as normal, and ε is given by

$$\varepsilon = \frac{N_X(\gamma_X B_{1X})^2}{N_H(\gamma_H B_{1H})^2}.$$

When the Hartmann-Hahn condition for cross-polarisation is satisfied, i.e. $\gamma_H B_{1H} = \gamma_X B_{1X}$ (as is the case in these experiments), the squared terms are equal and cancel, so ε becomes the ratio of the numbers of each type of spin (N_X/N_H). In these experiments the ε values were calculated from the molecular formulae. In order that ε can be assumed to be this simple ratio of the number of atoms, the system must be such that there are only two spin baths (one for X and one for H). For instance, this will occur if the atoms are chemically equivalent, or are strongly coupled by homonuclear dipolar interactions. This is unlikely to be an exact model in a situation in which the spectrum shows resolved peaks for more than one distinct type of protons. The value of ε is also, obviously, sensitive to the accuracy of the match condition. Care was taken to obtain an

accurate match condition, which will be particularly important in these systems where the proton spectrum may be narrow.

It is assumed throughout that thermal equilibrium is established within each spin system. It should be noted that, particularly for a directly bonded isolated spin pair, it is possible that coherent transfer would occur, causing oscillations in the CP curve. This situation has not been observed here. We also have to rely on the validity of the spin temperature approach, but have no proof that this will not be the case.

In a standard cross-polarisation experiment the evolution of X magnetisation (via the inverse spin temperatures) is given by the following expression: [3]

$$\left(\frac{\beta_X(t)}{\beta_{H0}}\right)_{CP} = \frac{1}{a_+ - a_-}\left\{-\exp\left(-\frac{a_+}{T_{HX}}t_{CP}\right)+\exp\left(-\frac{a_-}{T_{HX}}t_{CP}\right)\right\}$$

where

$$a_\pm = a_0 \pm \sqrt{a_0^2 - b}$$

with

$$a_0 = \frac{1}{2}\left(1+\varepsilon+\frac{T_{HX}}{T_{1\rho}^H}+\frac{T_{HX}}{T_{1\rho}^X}\right)$$

and

$$b = \frac{T_{HX}}{T_{1\rho}^H}\left(1+\frac{T_{HX}}{T_{1\rho}^X}\right)+\varepsilon\frac{T_{HX}}{T_{1\rho}^X}$$

When ε approaches unity (i.e. there are comparable numbers of the two nuclei and the heat capacity of the spin baths becomes comparable) and $1/T^X_{1\rho}$ is not negligibly small (i.e. $T^X_{1\rho} \sim T^H_{1\rho}$), the decaying slope of the standard cross-polarisation curve is governed by a function of $1/T^H_{1\rho}$ and $1/T^X_{1\rho}$, not just $1/T^H_{1\rho}$. For the decay to be clearly dominated by $1/T^H_{1\rho}$, this value must be a lot larger than $1/T^X_{1\rho}$, as in the case of carbon. This will occur when the number of X spins is a lot smaller than the number of protons.

The curve produced from the TORQUE experiment is of the form:

$$\left(\frac{\beta_X(t)}{\beta_{H0}}\right)_{TOR} = \exp\left(-\frac{t_{SL}}{T_{1\rho}^H}\right) * \left(\frac{\beta_X(t)}{\beta_{H0}}\right)_{CP}$$

This equation, along with that for the CP curve, is used in the simultaneous fitting programme.

The effect of non-negligible ε and differing relative magnitudes of relaxation times can be investigated, theoretically, by observing the value of the partial derivative of the torque curve.[3]

$$\frac{\partial\left(\beta_X(t)/\beta_{H0}\right)_{TOR}}{\partial t_{CP}} =$$

$$\frac{1}{a_+ - a_-}\exp\left(-\frac{t_{SL}}{T_{1\rho}^H}\right) * \left[\left(\frac{1}{T_{1\rho}^H} - \frac{a_-}{T_{HX}}\right) * \exp\left(-\frac{a_-}{T_{HX}}t_{CP}\right) - \left(\frac{1}{T_{1\rho}^H} - \frac{a_+}{T_{HX}}\right) * \exp\left(-\frac{a_-}{T_{HX}}t_{CP}\right)\right]$$

This will indicate when the slope is positive, negative or zero. With a non-negligible ε, and a difference in $T_{1\rho}$ of 20 % between the relaxation times of the two nuclei (if T_{HP} is around one tenth of this value), the slopes are clearly non-zero. This is similar to the data observed in the experimental situation described here.

This whole analysis will also rely on the fact that the spin-lattice relaxation times, T_1, are a lot longer than the rotating-frame values, so that there are not T_1 effects in the decay. This is normally the case in the solid state where T_1 ~ s and $T_{1\rho}$ ~ ms.

There are two functions, f_1 and f_2, which describe the deviation from the standard CP condition, as their values become further from unity. These can be plotted as contour graphs, for a particular value of ε and for different combinations of $T_{HX}/T_{1\rho}^H$ and $T_{HX}/T_{1\rho}^H$ (the graphs here, Figure 2 and Figure 3, illustrate ε = 0.25, which is the case for $K_3PO_4.2H_2O$). They relate the observed and actual values of the time constants under investigation according to the equations given.

$$T_{HX}^* = \frac{T_{HX}}{a_0 + \sqrt{a_0^2 - b}} = f_1 . T_{HX}$$

$$T_{1\varrho}^{*} = \frac{1}{a_0 + \sqrt{a_0^2 - b}} \cdot \frac{T_{HX}}{T_{1\varrho}^{H}} \cdot T_{1\varrho}^{H} = f_2 \cdot T_{1\varrho}^{H}$$

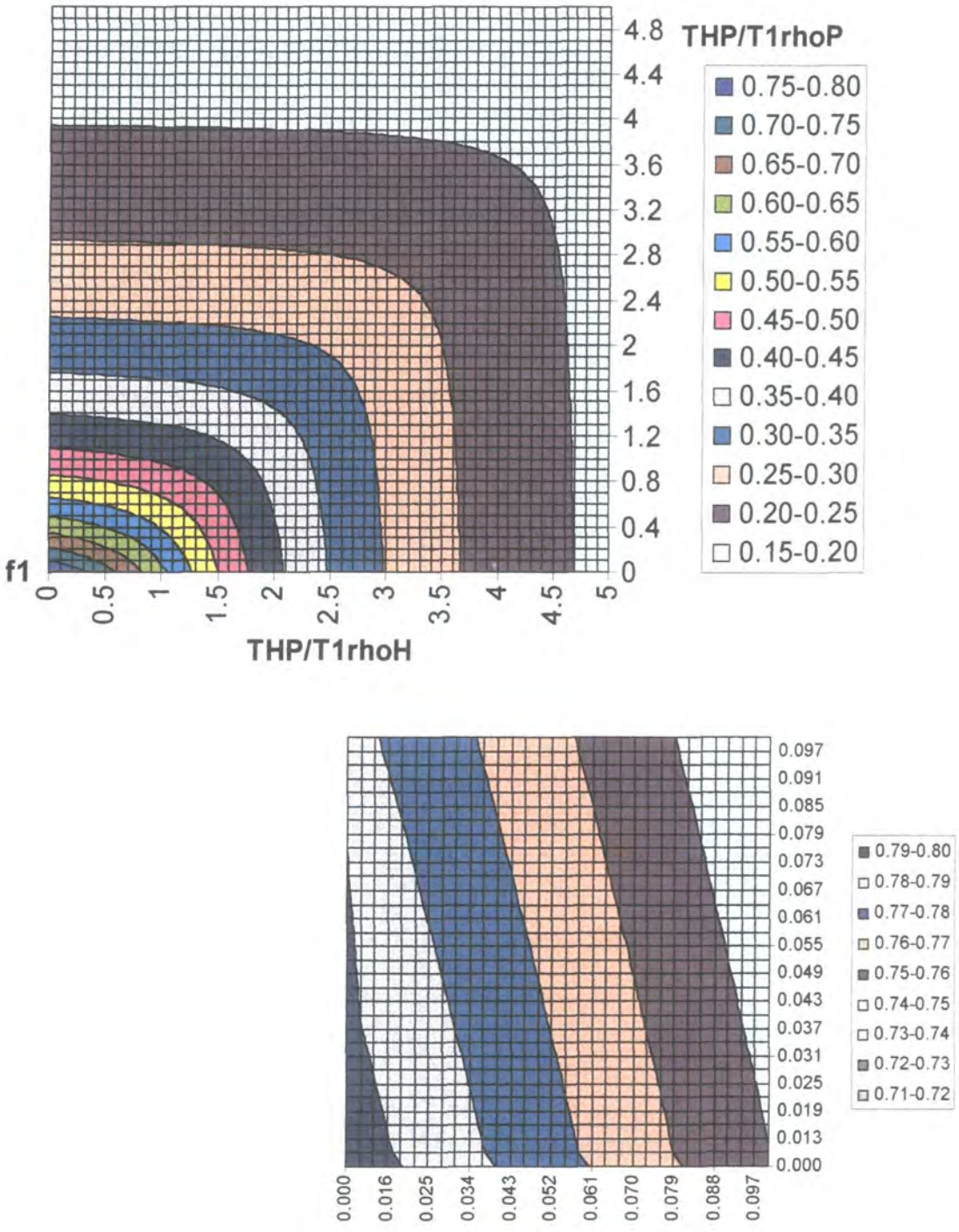

Figure 2. f_1 variation with ratio of time constants for $\varepsilon = 0.25$. The smaller inset shows an expansion for small values of T_{HP} (a key to colours is given beside each individual plot).

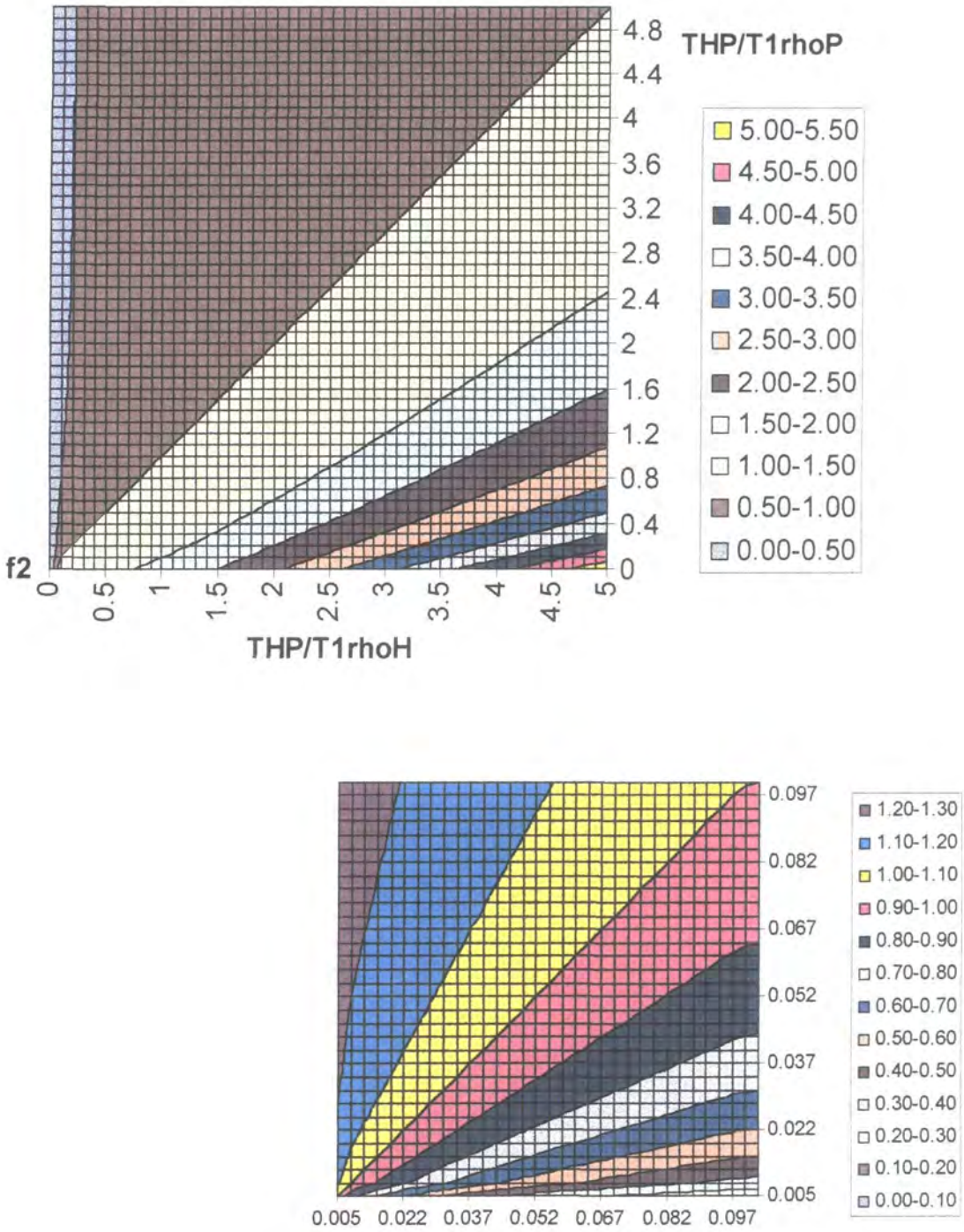

Figure 3. f_2 variation with ratio of time constants for $\varepsilon = 0.25$. The smaller inset shows an expansion for small values of T_{HP}.

Figure 2 shows an example of the variation of the value of f_1 for the case where we have a ratio of four protons to one phosphorus. In fact, in the systems studied here, we are interested only in the region where $T_{HP} < T_{1\rho}$. As T_{HP} increases, the value of f_1 decreases. By definition, at the standard CP condition, f_1 is unity, and it can be seen

that as ε becomes this large, the standard value of f_1 is not obtained, even in the case where T_{HP} is very much smaller than $T_{1\rho}{}^{H}$ and $T_{1\rho}{}^{P}$. For the case where $T_{HP} < T_{1\rho}{}^{H}$ and $T_{1\rho}{}^{P}$, the value of f_1 is between ~0.5 and 0.8. When ε is non-negligible the value of f_1 will not reach unity. This means that the observed value will never be exactly the same as the true value for such values of ε, which was also found to be the case in similar calculations for HF.[3] For the other cases studied here the maximum possible value of f_1 is over 0.9 for the ammonium phosphate and TPPO compounds, but for an ε of 1 ($CaHPO_4$), f_1 can only reach 0.5. This can be compared favourably with the directly measured values and simultaneous fit results discussed below. There is a slightly steeper slope, and therefore more dramatic deviation from standard conditions, when considering the effects of values of $T_{1\rho}{}^{P}$ as opposed to $T_{1\rho}{}^{H}$.

For f_2, the dependence on the relative magnitude of the time constants is illustrated in Figure 3. The value of f_2 remains at unity when $T_{HX}/T_{1\rho}{}^{H} = T_{HX}/T_{1\rho}{}^{X}$, i.e. if the rotating-frame relaxation times are equal, then the situation approaches that of the standard condition with respect to $T_{1\rho}{}^{H}$. However, f_2 increases dramatically as the situation where $T_{HP} > T_{1\rho}{}^{H}$ is reached. This value also drops to zero above the line representing 'unity' (i.e. when $T_{1\rho}{}^{H} > T_{1\rho}{}^{X}$, again, this situation is not relevant to these studies).

3.2 Results and discussion.

In order to see the difference between effective and actual time constants, both the results from individual experiments and simultaneous fitting will be discussed.

Compound (ε)	CP curve			individual $T_{1\rho}$ (spin-lock experiments)			simultaneous fit of CP and TORQUE curves				
	T_{HP}^{*} /ms	$T_{1\rho}^{*}$ /ms	no. of points[a]	$T_{1\rho}^{H}$ /ms	$T_{1\rho}^{P}$ /ms	no. of points[a]	T_{HP} /ms	$T_{1\rho}^{H}$ /ms	$T_{1\rho}^{P}$ /ms fixed	$T_{1\rho}^{P}$ /ms opt	no. of iterations
$K_3PO_4.2H_2O$ (0.25) [b]	0.40	5.0	40 (0.001)	2.1	8.2	20 (1.5e-4/ 3.4e-4)	0.90	3.2	8.2	-----	14
[c]	0.40	5.0	40	2.1	8.2	20	0.88	3.1	----	9.6	21
[d]	0.40	5.0	40	2.1	8.2	20	1.2	2.1	8.2		11
$(NH_4)_3 PO_4$ (0.083) [b]	0.14	7.0	38 (0.002)	2.9	16	19/22 (9.5e-4/ 0.0016)	0.18	5.4	16	-----	11
$CaHPO_4$ (1.0) [b]	0.31	5.9	40 (0.03)	3.2	75	17/21 (0.0088/ 0.19)	0.60	3.4	75	-----	14
$(C_6H_5)_3PO$ (0.067)	0.33	2.1	15 (3.9e-5)	2.0	12	15 (3.9e-5/ 4.6e-5)	-----	-----	-----	-----	

[a] χ^2 given in brackets. In order to compare χ^2 values, because of the differing (but arbitrary) intensity scales recorded, they have been normalised, in terms of intensity and no. of points. Where two values are given for the $T_{1\rho}$ measurements these apply to proton and phosphorus respectively.

[b] T_{HP} and $T_{1\rho}^{H}$ optimised for simultaneous CP and TORQUE fit.

[c] all three time parameters optimised for simultaneous CP and TORQUE fit.

[d] only T_{HP} varied for simultaneous CP and TORQUE fit.

Table 1. Directly measured values and simultaneous fit results for CP dynamics.

Individual Experiments.

The figures below (4-7) show the curves for independent experiments. The intensities were measured within the Spinsight software, with integrals of the single phosphorus peaks being used to create each data set. Because of the way the xy files are created in the different experiments there is not a normalised maximum intensity. Therefore, the intensity scales on the plots are arbitrary and the absolute intensities in the experiments are not directly related. The lines are an optimised fit to the exponential functions available in Spinsight and represent the fitted values given the first columns of Table 1. Due to the plotting method there appears to be a slight 'background' intensity in some of the relaxation time measurements. This was not visible in the actual fit on the computer screen. The data accurately represent an exponential decay to zero intensity.

Data in the TORQUE curves are difficult to fit as a single parameter in a simple function due to the dependence on the relative magnitude of the relaxation constants at

long contact times. As described, all these cases have a further rise in the latter portion of the curve which will result in a longer T_{HP} and a severely inaccurate result in attempts to fit to a single exponential. These data were therefore only used to determine the relative magnitude of the rotating-frame relaxation times. Experiments were recorded with the maximum TORQUE spin-lock time equal to the maximum contact time in the CP curve experiment. In this case we do get comparable intensities, as the same number of acquisitions and other conditions were used.

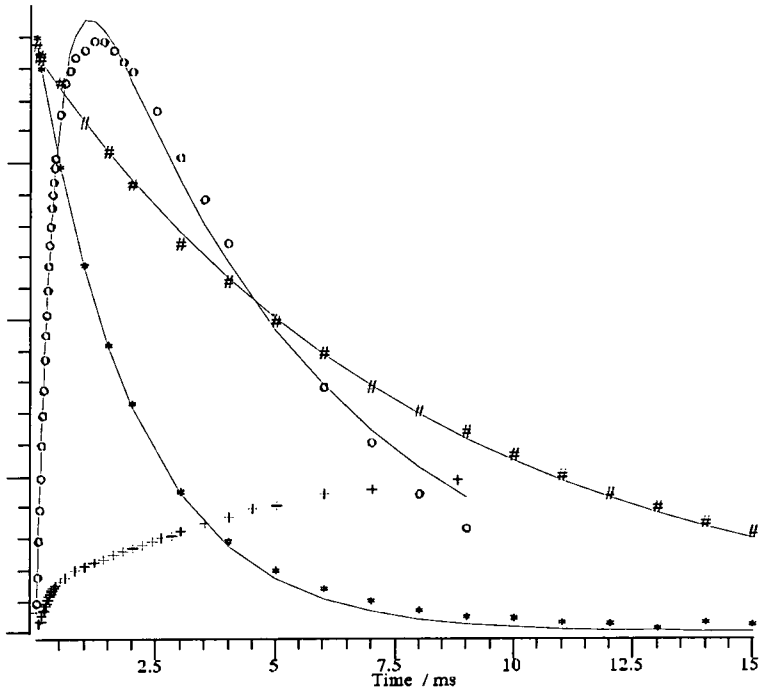

*Figure 4. $K_3PO_4.2H_2O$. # $T_{1\rho}^{P}$, * $T_{1\rho}^{H}$, o CP curve, + TORQUE curve.*

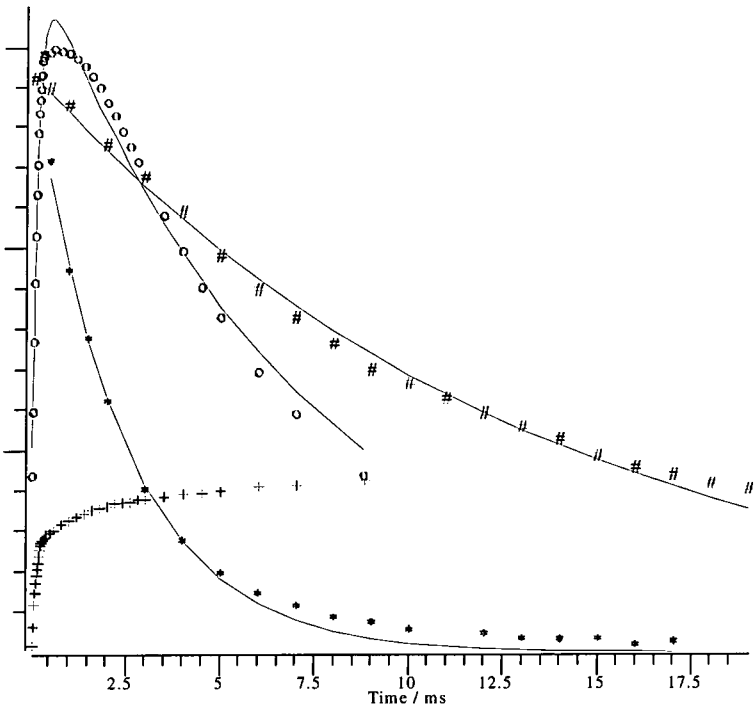

Figure 5. $(NH_4)_3PO_4$. # $T_{1\rho}^{P}$, * $T_{1\rho}^{H}$, o *CP curve, + TORQUE curve.*

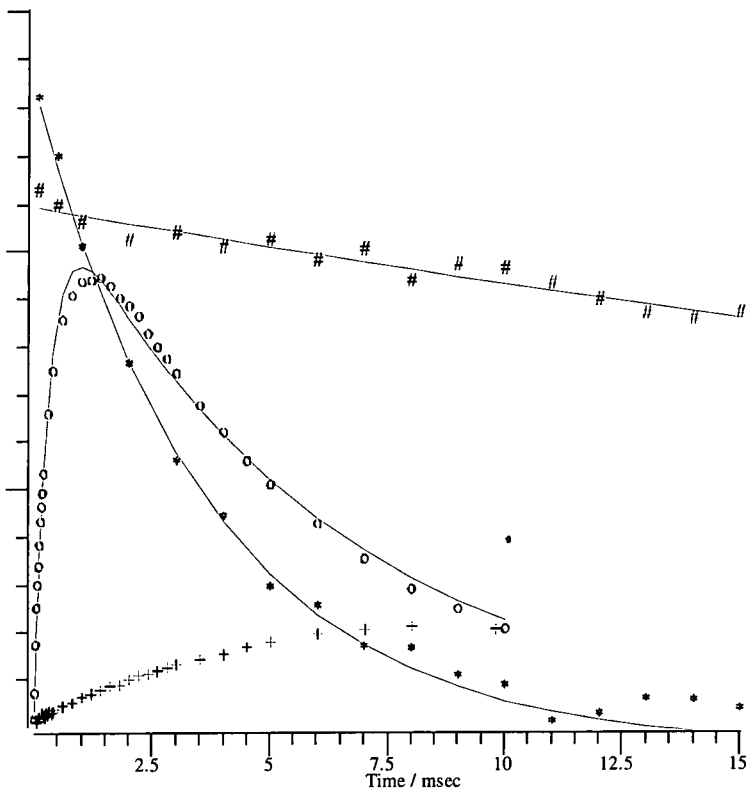

Figure 6. $CaHPO_4$. # $T_{1\rho}^{P}$, * $T_{1\rho}^{H}$, o *CP curve, + TORQUE curve.*

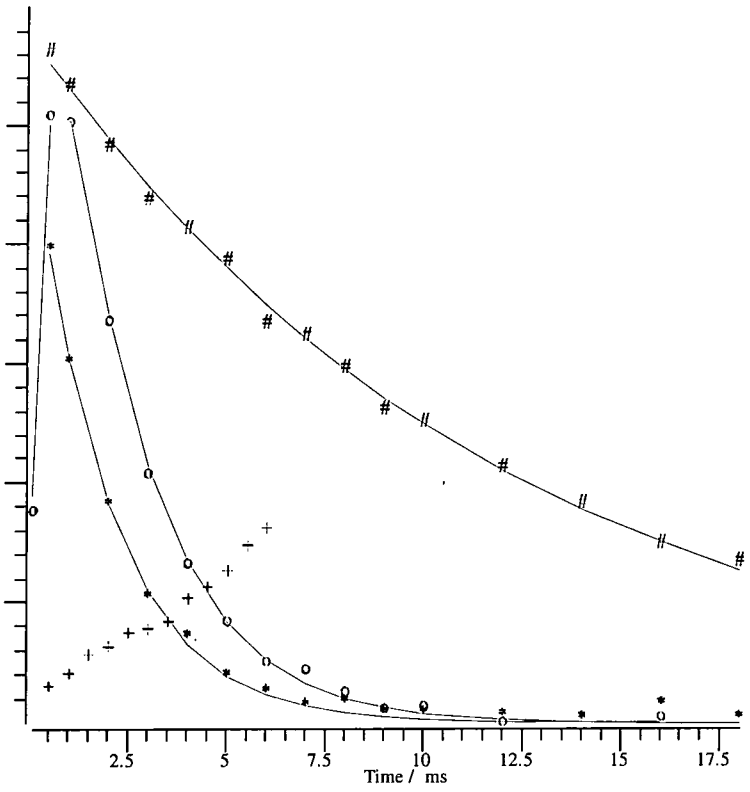

*Figure 7. TPPO. # $T_{1\rho}^{P}$, * $T_{1\rho}^{H}$, o CP curve, + TORQUE curve.*

Over the whole range of compounds, when looking at the individual measurements only, the extent of the effect that each rotating-frame relaxation time has on the CP curve decay is not clear. Both proton and phosphorus $T_{1\rho}$ values seem to dominate the CP curve intensity decay in different cases.

It can be seen that the $T_{1\rho}^{P}$ data for $(NH_4)_3PO_4$ show an apparent weak oscillation of unknown origin that is not truly represented by a single exponential. A high accuracy result will not be obtained by fitting to one parameter. At long spin-lock time the $T_{1\rho}^{H}$ data may also be a poorer representation of a single exponential decay, but this will be mainly due to the larger uncertainties in intensity measurement with the high noise level in these later slices of the decay experiment.

Despite several repetitions of the experiment, there seem to be significant problems with the TORQUE curve for TPPO. Unlike the other cases there is no evidence of a 'plateau' region. With the contact times used and the obvious decay of the $T_{1\rho}$ and CP curves, it seems unlikely that the TORQUE curve is still on its initial rise. This will, of course,

contribute to the failure of the simultaneous fit for this compound. Problems were encountered on trying to increase the total spin-lock time in the TORQUE experiment, and no satisfactory signal was obtained.

Simultaneous Fitting of CP and TORQUE curves.

The values in the later columns of Table 1 are derived from the experiments and plots described here. Initial input parameters for T_{HP}, $T_{1\rho}^{H}$ and $T_{1\rho}^{P}$ for the simulation programme were those obtained from the individual experiments. The values of ε were not optimised, but calculated from the molecular formulae. The capability of the simultaneous fit programme to run to completion depends, to some extent, on the accuracy of these initial parameters. It was also tried to use input parameters of the correct order of magnitude only. The same output was obtained from the fit, but in more iterations. In most cases the simultaneous fitting programme failed if an optimisation of $T_{1\rho}^{P}$ was included, and this limits the results obtained. During the initial iterations, the value of $T_{1\rho}^{P}$ would diverge, or become negative, leading to an error in the programme. Due to the small number of iterations possible for $T_{1\rho}^{P}$ optimisation, it is not felt appropriate in most cases to quote the values obtained since the errors are outside acceptable limits; a satisfactory termination in the programme had not been reached. The values from individual $T_{1\rho}^{P}$ should not be significantly altered in the fitting, as they are, in most cases, large compared to the other parameters defining the curve, and so this time constant was generally fixed. A check was made that altering the fixed value by a significant increment had the expected effect on the CP curve. The simulations for $K_3PO_4.2H_2O$, however, allowed all parameters to be optimised. It was also attempted, with varying success to fit both curves with all parameters except T_{HP} fixed.

If a successful fit is obtained, the programme will reach a natural stop when the fractional change in the fitted parameters for the curve is less than 0.0001. The number of iterations that the programme carried out before coming to this conclusion is given in Table 1. This depended on the accuracy of the input parameters. The better the agreement between initial and fitted results, the fewer iterations required. In each case the programme reached a satisfactory result well below its maximum number of iterations. Variable contact time (CP curves) and the TORQUE curves are shown

(figures 8-12) with the lines representing data from a simultaneous fit. The x-axis scales represent contact time and, again, the vertical intensity scale is arbitrary (but here it is consistent for the two experiments in each figure).

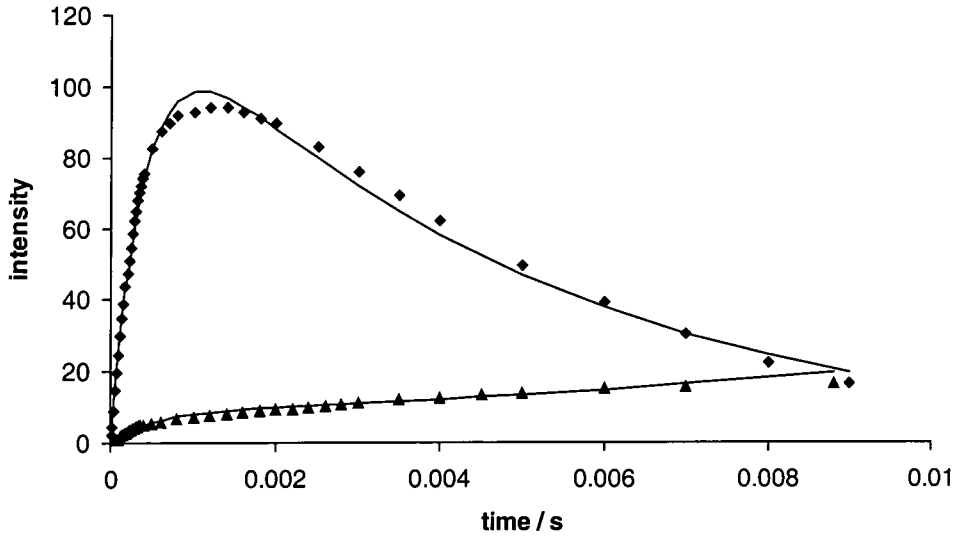

Figure 8. CP and TORQUE curve from simultaneous fit, $K_3PO_4.2H_2O$, $T_{1\rho}^{P}$ fixed.

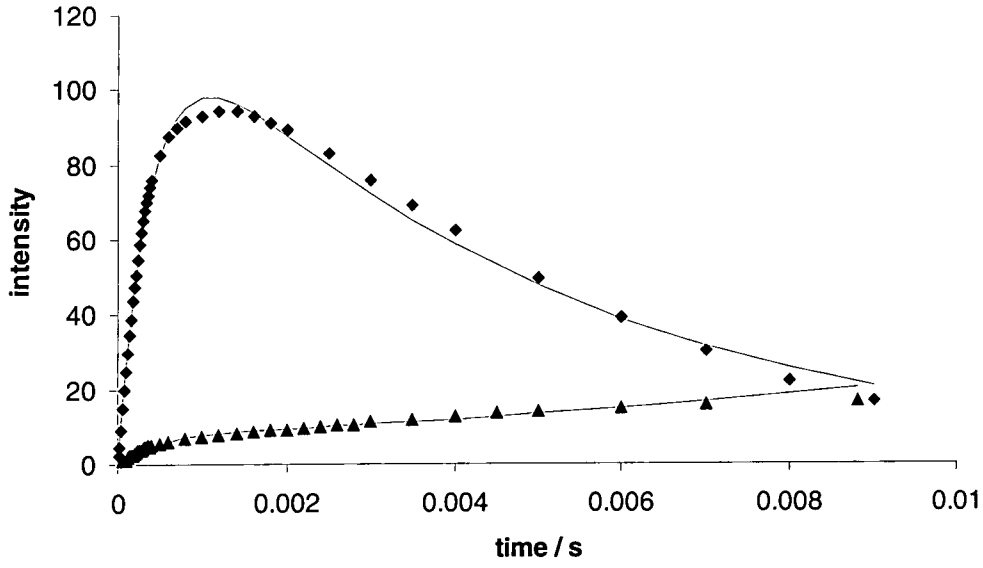

Figure 9. CP and TORQUE curve from simultaneous fit, $K_3PO_4.2H_2O$, varying all three time parameters.

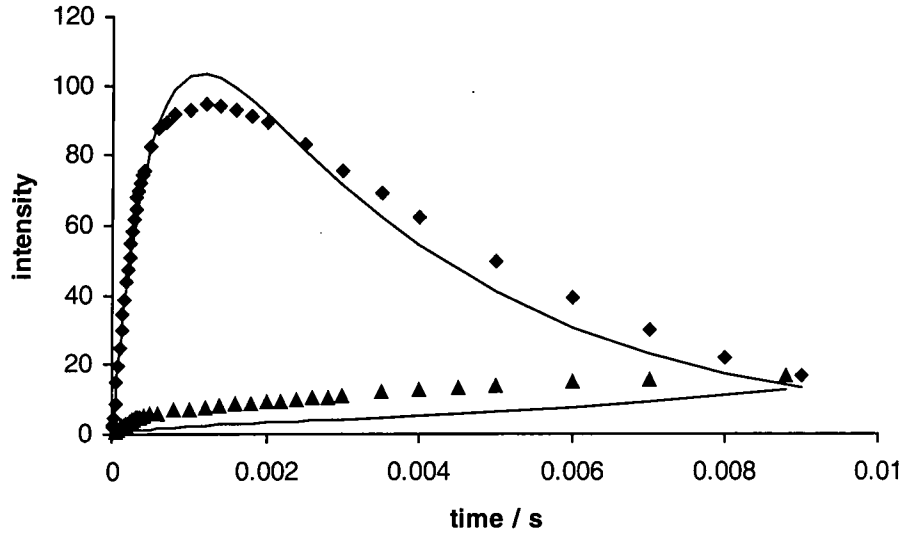

Figure 10. CP and TORQUE curve from simultaneous fit, $K_3PO_4.2H_2O$, $T_{1\rho}^{P}$ and $T_{1\rho}^{H}$ fixed.

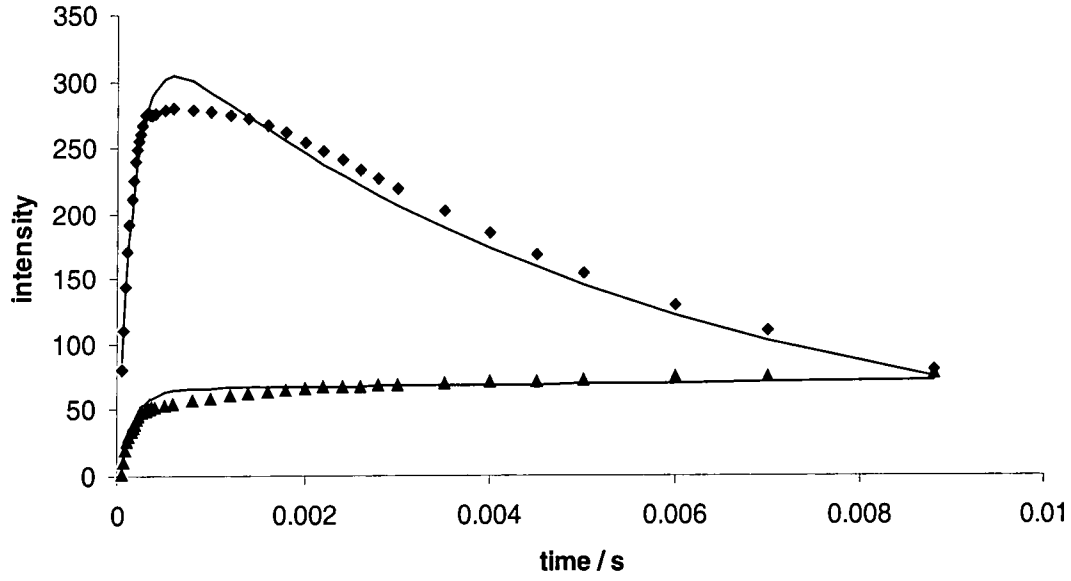

Figure 11. CP and TORQUE curve from simultaneous fit, $(NH_4)_3PO_4$.

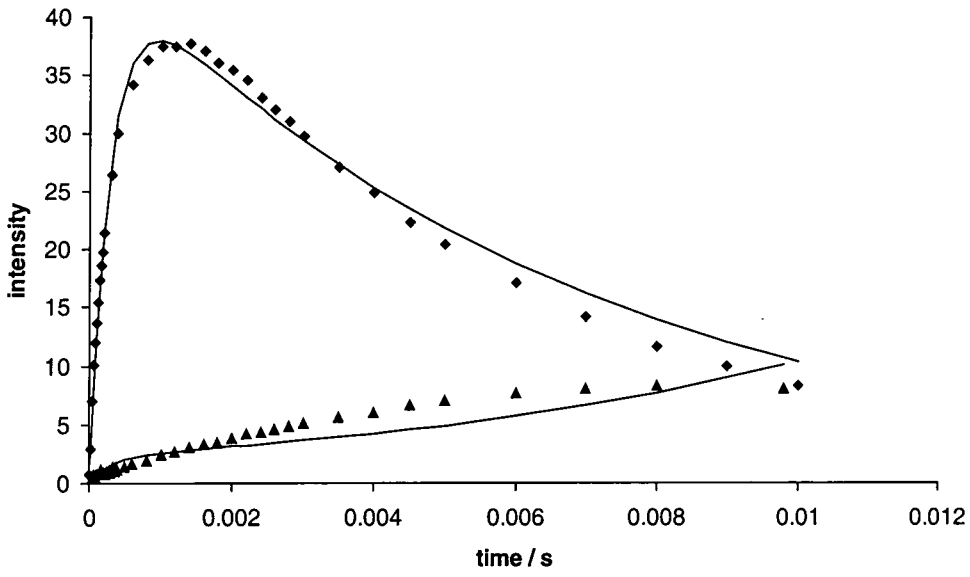

Figure 12. CP and TORQUE curves from simultaneous fit, $CaHPO_4$.

The time constants illustrated in all the above figures are summarised in Table 1.

For $(C_6H_5)_3PO$ the parameters did not fit easily to the proposed model due to problems with the TORQUE data. Therefore no data are available from the simultaneous fit of CP and TORQUE curves. Problems will likely be due to the small ratio of spins, ε, and the rapid cross-polarisation rate, T_{HP}. Here, we are approaching a situation with relative magnitudes of time constants similar to those of, for instance, proton-to-carbon cross-polarisation, where the observed values are a good representation of the system.

The actual line fits for the CP curve do not seem to be a dramatic improvement on the single fits, but we have been able to obtain the individual parameters for the rotating-frame relaxation times for the individual nuclei and have been able to obtain quantitative results from the TORQUE experiments. In all cases, however, there is still some discrepancy at the highest intensity point of the CP curve, though the initial rise and subsequent decay seem to be well defined. At this stage this effect is not easily explained. In general, however, an improvement over the single CP curve fit is obtained and parameters are modified as expected.

As expected from theoretical considerations, it is true in general that the observed value for the cross-polarisation time constant, T_{HP}^{*}, in the case of the individual calculations is faster than the actual rate, T_{HP}, derived from the simultaneous fit. The first case, $K_3PO_4.2H_2O$, shows only slight modification of the parameters using the different options within the simulation programme. Both the CP and TORQUE curves (Figure 8 to Figure 10) show the simultaneous fitting. For $K_3PO_4.2H_2O$, with $T_{1\rho}^{P}$ fixed or optimised there is only a small effect on the other parameters derived. This initially suggests that T_{HP} is fairly insensitive to $T_{1\rho}^{P}$. However, when the simulation is repeated with both $T_{1\rho}^{H}$ and $T_{1\rho}^{P}$ fixed at the individually measured values, T_{HP} is modified, to an even higher (slower) value and the fit of the TORQUE curve is less successful.

The reason for discrepancies in the results and also for the modification of parameters on going from individual to simultaneous fitting, could be the errors in the individual $T_{1\rho}$ measurements (especially for the long $T_{1\rho}^{P}$ values, which are limited in accuracy by the feasible maximum spin-lock times).

For $(NH_4)_3PO_4$, the CP curve is in fair agreement, and in order to extract estimates for the other parameters the TORQUE curve shows a slight distortion. It should be noted that, for the ammonium case, the slope of the torque curve fit approaches zero. This case has the lowest value of ε of the three phosphates studied. The higher ε value for the potassium compound compensates for the closer values of the rotating-frame relaxation times, and the slope of the TORQUE curve is positive. This ammonium compound is perhaps the poorest example. The torque fit shows an almost horizontal plateau (indicating equal $T_{1\rho}$ values, in the 'non-negligible ε' case) however, we know from the individual measurements that this is not the case. This compound can be analysed by the standard method (where CP is considered to be fitted to a combination of an exponential rise and decay). This is justified by the fact that the value of ε is small (the proton spin bath is large) and the rate of cross polarisation is very fast. These factors define the applicability of the standard condition.

For $CaHPO_4$ it was not possible to fit all three parameters, and any attempt to alter $T_{1\rho}^{P}$, did not give a successful simulation. It was however possible to fix $T_{1\rho}^{P}$ and obtain a reasonable fit of the TORQUE and CP curves, though the former is not as good as

hoped. One of the problems with the third case, $CaHPO_4$, as with many other situations is most likely due to the very large value of $T_{1\rho}^{P}$ and the consequent inaccuracies in its measurement.

In all three phosphate cases it has proved to be possible to use the TORQUE data, not only to decide the relative magnitude of the rotating-frame relaxation times, but to calculate the parameters governing CP. This method takes account of these individual values and checks the modification of the effective values obtained from simple standard experiments.

Although it is an abundant spin, unlike carbon, the rotating-frame relaxation times can still be very much longer than those for the proton system. In the fluorine cases studied previously this is less likely.[3,4] These phosphate compounds have provided good model systems that were very successful in testing the simultaneous CP/TORQUE fitting programme and its relevance to this particular spin system. A variety of situations have been investigated - equal vs. unequal numbers of protons to phosphorus and directly bonded vs. 'remote' protons. All three have provided interesting and satisfactory results.

REFERENCES

[1] Shinji Ando, Durham University/Department of Polymer Chemistry, Tokyo Institute of Technology, Japan. Personal communication.

[2] MS-DOS QBasic, Version 1.0, Copyright © Microsoft Corporation, 1987-1991.

[3] S. Ando, R.K. Harris, S. A. Reinsberg, Submitted to *J. Magn. Reson.*

[4] S. Ando, R.K. Harris, G. A. Monti, S. A. Reinsberg, Submitted to *Magn. Reson. Chem.*

[5] P. Tekeley, V. Gerardy, P. Palmas, D. Canet, A. Retournard, *Solid State Nucl. Magn. Reson.*, **4**, 1995, 361-367

[6] M. Mehring, *Principles of High Resolution NMR in Solids.* 2nd Ed. Springer-Verlag, Berlin, Heidelberg, New York. 1983

4. One- and Two-Dimensional NMR Techniques in the Study of Phosphorus-containing Calix[4]resorcinols.

4.1. Introduction

4.1.1. Applications

A recent review of general calixarene chemistry[1] describes the host-guest properties and supramolecular chemistry of the family of chemical species that were first named calixarenes by Gutsche.[2] The basic structural unit (illustrated in Figure 1) forms complexes with neutral molecules.[3] Molecules containing bridging units between the hydroxyl groups, such as those containing phosphorus, are more rigid structures.[4] The solubility of such molecules in organic solvents can be limited and is dependent on the presence of potential guests in solution. Functionality on the 'upper rim' of the bowl-shaped calixarene-type molecule will modify the properties of the molecule as a whole, but also the size, shape and binding capacity of the cavity (the upper rim is the outer functionality in the two-dimensional molecular schemes, e.g. OH, P etc.). In relation to the possibility of host-guest compounds incorporating calix[4]resorcinols, there are several points that can be made. Modifying the properties in this way will lead to a wider variety of possible guest molecules because of the differing electronic and steric properties. Cage or channel structures are common in this type of system, with no direct bond formation between guest and host molecules, the whole structure relying on intermolecular (host-host, or host-guest) interactions. Applications of potential host systems include separation techniques and molecule delivery systems, non-linear optics and inclusion polymerisation.

4.1.2. Synthesis and Structure

The calix[4]resorcinol starting material is commercially available. Phosphorus halides are used to provide the upper-rim functionality. Synthesis of the compounds studied was carried out in Braunschweig, Germany and Cambridge, UK, by Dr A. Vollbrecht. An example of the synthesis route can be found in the literature.[5] Calixresorcinols[6] are prepared from $4C_6H_4(OH)_2 + 4R'CHO$ with the loss of two equivalents of water. This is the basic structural building block (shown in Figure 1) for many of the functionalised molecules, including those described here.

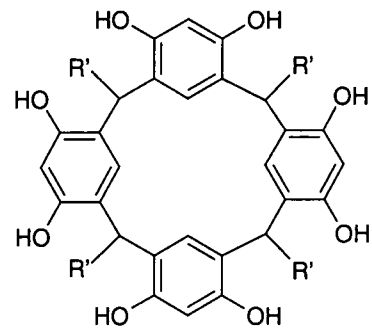

Figure 1.

Substitution can take place around the upper rim ortho to the OH groups,[7] replacing the aromatic proton with, for example, Br. To create the phosphorus linkages, this product is then reacted with phosphorus trichloride[7] in THF reflux to give the 'tethered' structure, with loss of HCl from the PCl_3 and OH groups (Figure 2). This will give, for example,

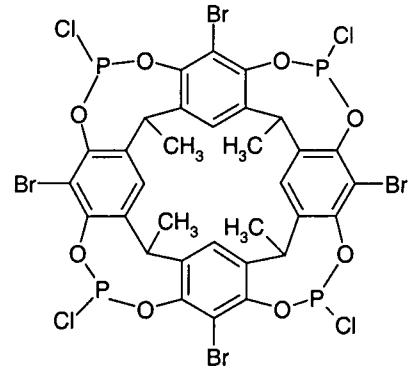

Figure 2.

The compounds are white solids which will darken on decomposition. The impurities that may be observed are, in general, the decomposition products and can be identified in favourable circumstances where there is no overlap with the desired spectrum. This statement refers in particular to phosphorus spectra, where a careful choice of the spin rate will allow the spinning sideband manifolds of the compound and impurity to be separately resolved. On exposure to air/moisture, the phosphorus-halogen (e.g. P-Cl) groups will be hydrolysed and produce a group related to phosphorous acid. 85% H_3PO_4 is a reference sample for ^{31}P NMR, with the single resonance at zero ppm and the chemical shift of phosphorous acid is 5 ppm.[8] Therefore, the decomposition can be

monitored by the emergence of a resonance centred around this shift value. The decomposition mechanism can be thought of as follows (Figure 3):

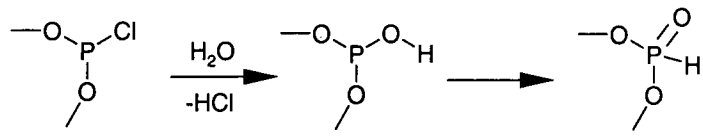

Figure 3.

The rearrangement in the second stage illustrated above is more likely than the oxidation of the intermediate species. Another possible mechanism which could produce a phosphoric acid derivative would be oxidation of the initial species followed by hydrolysis. In spite of the presence of decomposition products it was decided to complete the study of this series of compounds because of interest in their synthesis and application. It proved difficult to purify the compounds and every effort was made to preserve the samples by sealing rotor inserts. As will be seen from the details in this chapter it is, however, easy to identify the NMR spectra of the desired compound and these can be analysed as would those for a pure sample.

Due to the complexity of the synthetic route, and the host-guest nature of the molecule, there are several different solvents which could be retained in the solid crystal and are therefore observable in the MAS spectrum. The spectra of these can be interesting as they depend highly on the position of the solvent molecules within the 'lattice', as will be discussed later in this chapter.

There are various combinations of phosphorus groups that can be incorporated into the molecule, and a series of calix[4]resorcinol derivatives have been studied in terms of their structure, chemical shifts and couplings. Resolution of the splitting arising from $^1J_{PF}$ is observed in the coupling patterns in both the phosphorus and fluorine spectra of PF- and PF_2-containing molecules. For the simple resorcinol systems (with OH groups, and also compounds V and VI - see below) there are many possible isomers as there is considerable intramolecular mobility around the methylene bridges because of the lack of linking around the upper rim. However, once the phosphorus links are in place, the flexibility of the molecule is restricted, so that, apart from slight distortions of the bowl-shaped cavity, the system is fairly rigid with respect to phenyl ring positions. However, depending on the substituents on phosphorus and the carbon of the 'upper

rim', there is still some possibility of isomerism, and subsequently lack of symmetry, in the phosphorus-bridged systems.

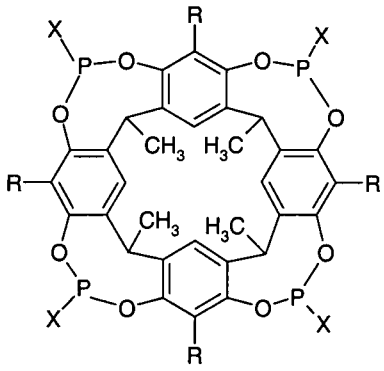

Figure 4.

In addition to a general distortion of the cavity, or even a dynamic twisting/breathing motion of the bowl shape, the atom or group X (Figure 4) can be orientated in or out of the cavity, especially when R is small (e.g. H). This also leads to the possibility of the formation of isomers. The isomerisation would manifest itself in multiple sites observed in a spectrum of either X or ^{31}P, with the chemical shift distinguishable according to the orientation of X. Such isomerisation may be static, but variable temperature solid-state NMR experiments allow the investigation of the possible dynamic nature of the molecule. In the cases studied here, in the solid-state, no positive changes were seen in variable temperature experiments, and there is therefore no evidence for dynamic isomerism. When R = Br (or alkyl), X will be forced into the centre of the ring by steric interactions and other isomers are unlikely. In many cases this would imply four-fold symmetry of the molecule (as observed in solution-state studies of some of the chlorinated molecules).[9] The multiplicity of the solid-state ^{31}P NMR data will indicate the existence of any isomerism - a single peak indicating that the asymmetric unit is one quarter of the molecule.

For ease of discussion a scheme is provided showing all the compounds that will be described (Figure 5), together with an indication of the numbering of carbon atoms (Figure 6) used in the discussion of assignment of chemical shifts.

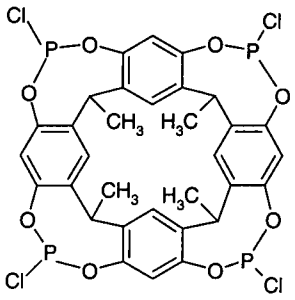

I

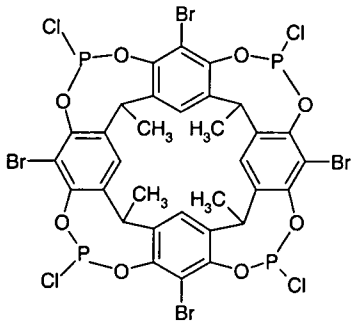

II

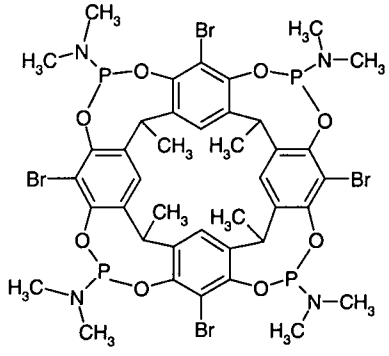

III

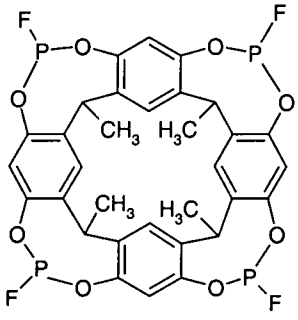

IV

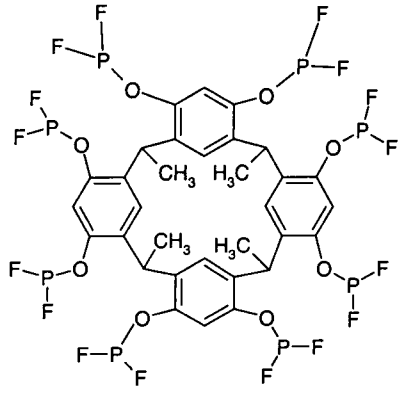

8AuCl

V

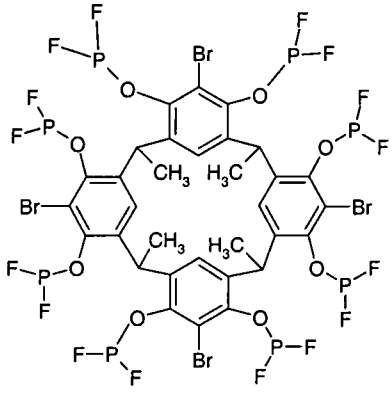

VI

Figure 5.

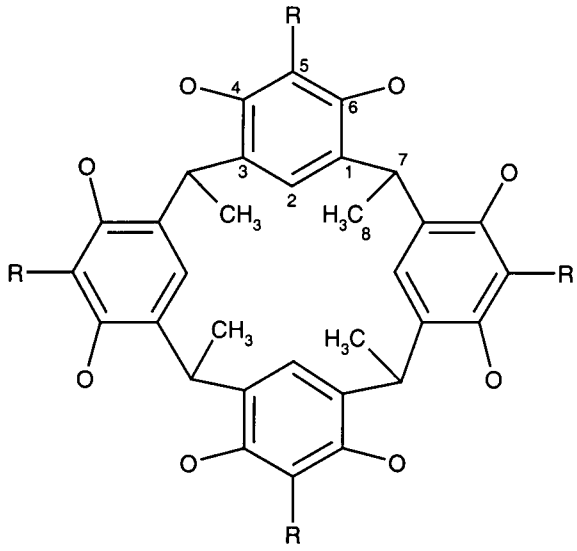

Figure 6.

In the case of compound II, the crystal structure is known.[5] Comparison of NMR data from this compound with other similar results enables conclusions to be drawn about compounds for which a crystal structure is not available and therefore structural information from NMR is very important.

4.2. Compounds I, Tetrakis-(O-P(Cl)-O)-Bridged Calix[4]resorcinol and II, Tetrakis-(O-P(Cl)-O)-Bridged Calix[4]resorcinol-Br

A more detailed study was made of these two compounds in comparison to the other related structures, and so that analogies can easily be drawn, each topic of discussion will cover both compounds.

4.2.1. Phosphorus-31 spectra

The ^{31}P chemical shifts are 121 and 129 ppm for compounds I and II respectively (Figure 8 and Figure 9), the bromine causing deshielding. Spinning sidebands are observed and a further splitting is evident when compound I is run at the lower field (81 MHz for phosphorus compared with 121 MHz) suggesting possible residual dipolar coupling effects to the adjacent quadrupolar chlorine. The splitting is not sufficiently defined for detailed quantitative analysis and is not resolved at the higher field. Because of the absence of the bromine substituent it is possible that the orientation on the PCl bond is different in the two molecules, causing this difference in the magnitude of the effect of residual dipolar coupling, which relies heavily on angular criteria. Spinning sideband manifolds evident with an isotropic shift around 0 ppm result from the decomposition product.

Using an 'in-house' program[10] based on the methods of Maricq and Waugh, lineshape parameters were calculated from the spinning sideband intensities. The values are defined as throughout this thesis, i.e. anisotropy, $\zeta = \sigma_{33} - \sigma_{iso}$; asymmetry, $\eta = (\sigma_{22} - \sigma_{11})/\zeta$; where σ_{11}, σ_{22} and σ_{33} are the shielding tensor components ordered according to the convention $|\sigma_{33} - \sigma_{iso}| > |\sigma_{11} - \sigma_{iso}| \geq |\sigma_{22} - \sigma_{iso}|$

Similarity between the results from the two compounds I and II is due to the almost identical environments of the phosphorus. Where a splitting is observed in compound I, separate values have not been calculated as resolution was not sufficient. Results for compound I with a spin rate of 4.0 kHz are (the data and simulation results, with a 'sum of differences squared error' of about 1.5 are illustrated in Figure 7):

ζ = 134 (1) ppm

η = 0.26 (0.01)

σ_{11} = -206 (1) ppm

σ_{22} = -171 (1) ppm

σ_{33} =12 (1) ppm

Similarly, results for compound II at 4.2 kHz spin rate are:

ζ = 139 (7) ppm

η = 0.38 (0.06)

σ_{11} = -225 (7) ppm

σ_{22} = -172 (5) ppm

σ_{33} = 9 (7) ppm

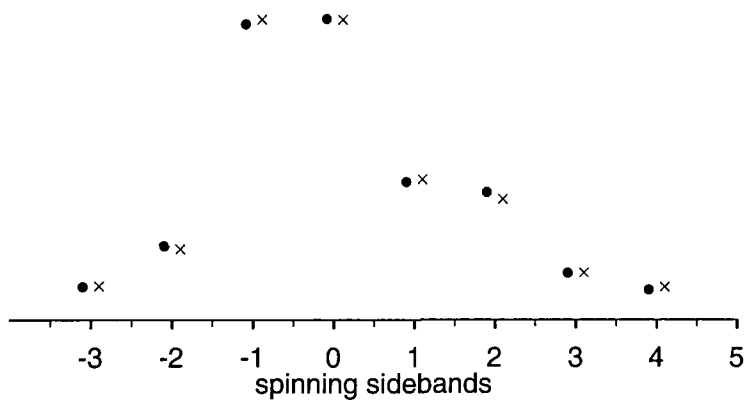

Figure 7. *Comparison of sideband intensities for the phosphorus spectrum of Compound I. Spin rate 4 kHz. Filled circles indicate experimental (integrated) intensity and crosses represent the simulated data.*

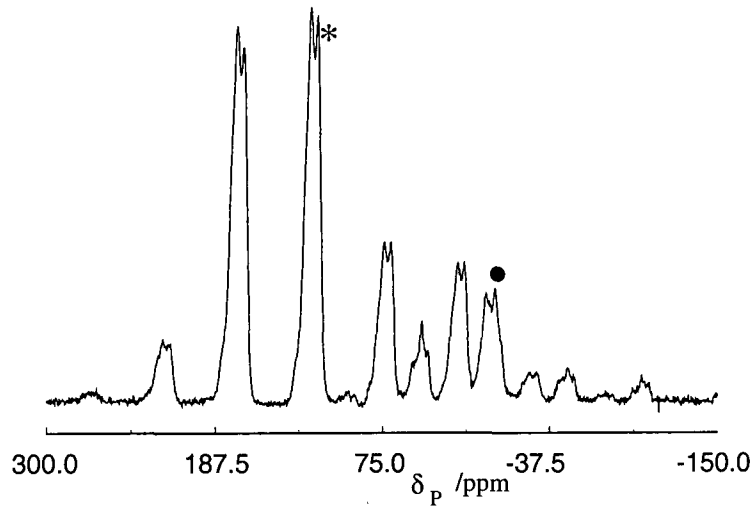

*Figure 8. Phosphorus spectrum (81.02 MHz) of compound I, spin rate 4 kHz, contact time 6 ms, recycle delay 2 s, 600 acquisitions. * = centre band, • = impurity centre band.*

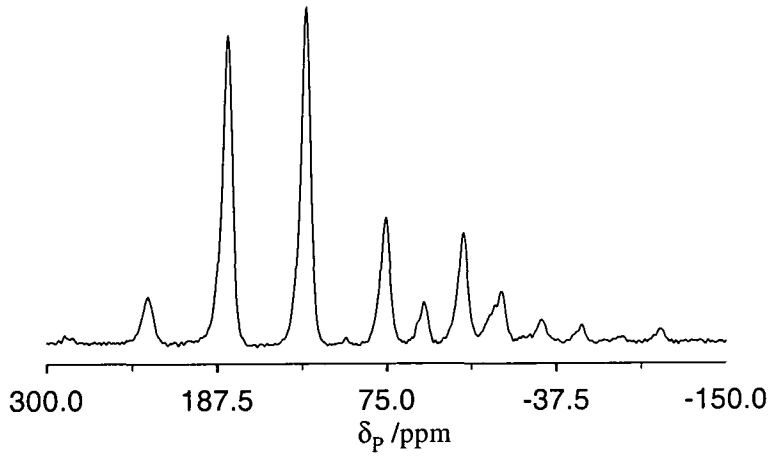

Figure 9. Phosphorus spectrum (81.02 MHz) of compound II (spin rate 4.2 kHz).

Solution-state data are also known for compound II,[5] δ_H = 1.89, 4.34, 6.62 ppm, δ_P = 129.8 ppm. The value of δ_P shows good agreement with the solid-state result from this work considering the differences in intermolecular interactions in the solid- and solution-state. The insolubility of compound I, one of the reasons for the solid-state NMR characterisation, means that there are no comparable data for this compound.

4.2.2. Carbon-13 spectra and assignments.

From the 1-dimensional carbon-13 spectra (Figure 10 and Figure 11) initial assignments can be made considering the effect of substitution on the aromatic carbon shifts. Dipolar dephasing was used to assist assignment of the carbon chemical shifts, with

only the quaternary and methyl signals remaining after a 50 μs dephasing time. These are given in Table 1. Further conclusions will be drawn later in this chapter when considering heteronuclear correlation experiments. Second-order effects from the interaction with bromine will cause the directly bonded carbon (in compound II) to produce a very broad resonance. This effect is often so great that the signals are not observed.

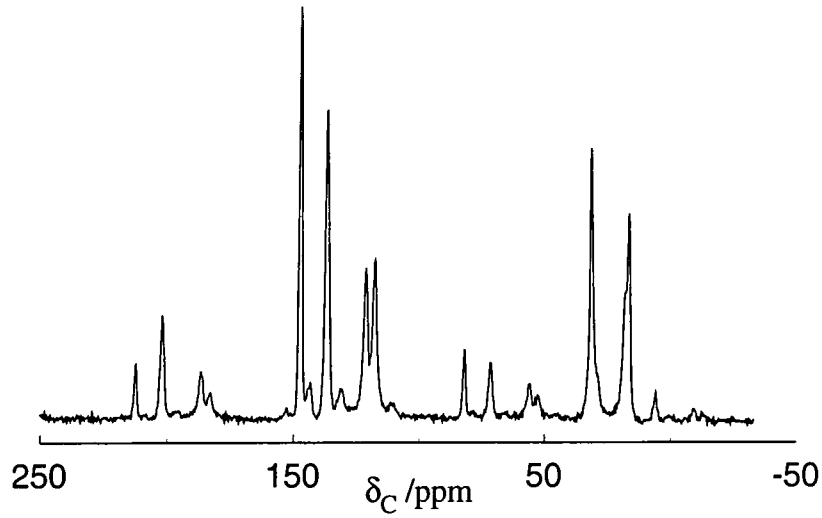

Figure 10. Carbon spectrum (75.43 MHz) of compound I, spin rate 5 kHz, contact time 6 ms, recycle delay 2 s, 1800 acquisitions.

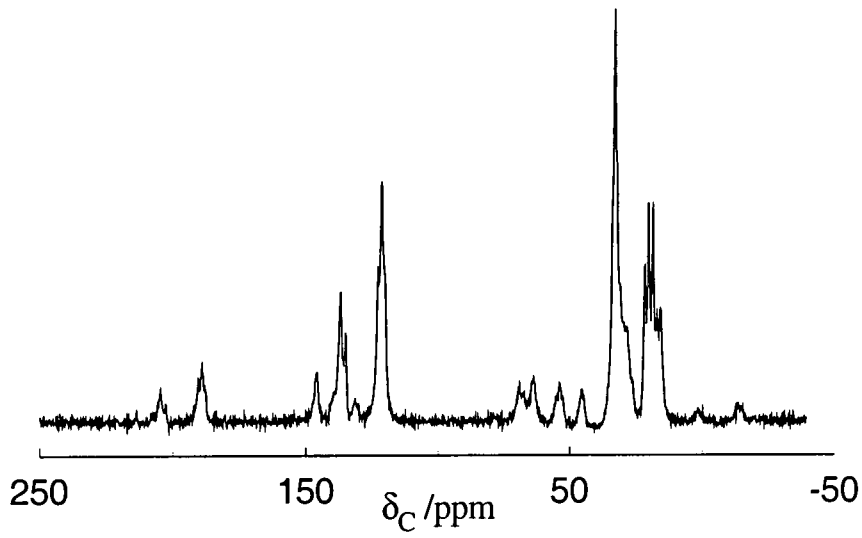

Figure 11. Carbon spectrum of compound II. Acquisition parameters as for compound I.

compound I	*Assignment*	*carbon number* [a]	**compound II**
17	*Methyl*	*8*	16-22
32	*CH aliphatic*	*7*	33
not observed	*Solvent*	CH_2Cl_2	46/64[b]
118	*CH aromatic*	*5*	not observed (C-Br)
121	*CH aromatic*	*2*	121
131	*Impurity*		131
137	*Aromatic quaternary*	*1,3*	137
143	*Impurity*		not observed
147	*Aromatic quaternary*	*4,6*	146

Table 1. Carbon-13 chemical shifts (δ) and assignments for compounds I and II.

[a] The third column gives the carbon numbers as illustrated in Figure 6.

[b] See text for CH_2Cl_2 value and explanation.

Solvent can exist as 'guest molecules' in spaces in the crystal structure, within the calixarene cavity and also in the hexagonal channels between stacked molecules, leading to two very different guest environments as illustrated below (Figure 12). In the solid-state structure channels can be formed by the calixarene/resorcinol molecules. Because of the inclusion compound nature of these systems, there will almost always be solvent molecules contained within the crystal as guests. In these cases the most likely possibilities are THF and CH_2Cl_2. Such molecules appear disordered in the crystal structure and must therefore be identified by NMR. The 'solvent' shifts observed for compound II are indicated in Table 1.

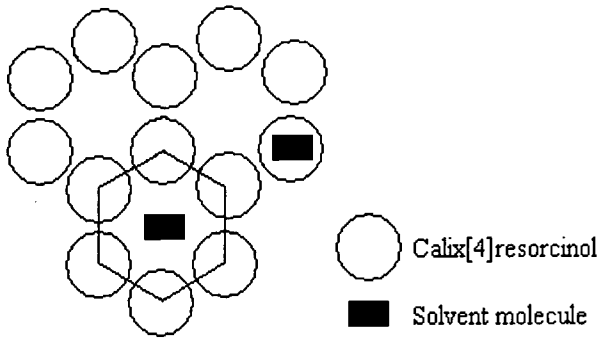

Figure 12. Possible solvent environments within the crystal structure.

Two solvent peaks are observed in the ^{13}C NMR spectrum of compound II, both not far from that of free liquid CH_2Cl_2 (δ_C = 53.73; δ_H = 5.31).[11] The two possible environments will be very different due to the proximity of the aromatic systems and also the halogen centres around the upper ring of each molecule. Comparing compounds I and II, the cavity in I is likely to be more open due to the lower functionality around the upper rim and possible different orientations of the PCl bond, meaning that the trapping of solvent on crystallisation may not be such a significant factor.

The decomposition product is likely to have a very similar ^{13}C spectrum as the difference at the phosphorus centre is fairly remote. Indeed, it has been seen in spectra of compounds where a significant proportion of the decomposition product is observed (in a ^{31}P spectrum) that the carbon shifts are not significantly altered by this particular substitution.

Finally in this section, T_1^C relaxation times were measured via the Torchia pulse sequence incorporating cross-polarisation from protons before the variable relaxation delay.[12] Fitting to exponential decays gave the following time constants (Table 2).

Compound I			Compound II	
δ_C /ppm	T_1^C /s ± 0.5s	Assignment	δ_C /ppm	T_1^C /s ± 0.5s
17	0.5	Me	18	0.3
32	14.2	CH of aliphatic bridge	33	8.3
118	25.5	Protonated aromatic		
121	20.5	Protonated aromatic	121	5.6
131	6.9	impurity	131	5.9
137	19.7	Aromatic bonded to C	137	7.8
143	11.4	impurity		
147	23.0	Aromatic bonded to O	146	9.5

Table 2. Carbon-13 spin-lattice relaxation times for compound II.

The assignments given are those derived from the 1-dimensional spectra (these will be confirmed in the following sections describing heteronuclear correlation), but

conclusions can also be made from these results alone. The methyl relaxation is very fast due to the rapid group reorientation, whereas the aromatic carbon bonded to oxygen has the slowest relaxation time in compound II, with the upper CH aromatic slowest to relax in compound I. This can be explained by considering the effect of rapid internal rotation about the C-CH_3 bond on the dipolar relaxation mechanism. Since ^{13}C is a dilute spin, the effects of spin diffusion are expected to be minimal.

Resolved T_1^C values are seen for both compounds, with each individual carbon resonance having its own characteristic decay. It can also be seen that the values for compound I are generally larger than those for compound II. This could be a result of several effects and suggests that the effect of the bromine substituent is significant: differing dipolar interactions will occur because of replacement of a proton, or the extent of motion within the molecule may vary. However the correlation results described below show that crystal packing effects are similar. Methyl group rotation is still occurring in compound I, giving a fast T_1^C. The most significant effect is seen for the carbons ortho and para to the bromine substituent.

The short proton T_1 relaxation times for these compounds were measured as being around 0.3 s, and the phosphorus T_1 = 19 s for compound I, is substantially longer than the 5 s calculated for compound II (in an analogous fashion to the carbon results). Here we can see that the bromine substituent is having a significant effect in reducing the relaxation times of the surrounding nuclei (^{13}C and ^{31}P), as well as having the deshielding effect on phosphorus.

4.2.3. Correlation

Introduction

There are structural similarities between compounds I and II, and therefore heteronuclear correlation experiments were explored in order to elucidate further structural information. The main aim of these experiments when applied to the resorcinol systems was threefold: to obtain, indirectly, by separation into two dimensions, a resolved proton spectrum which can then be assigned; to use the combination of information to definitively assign the carbon spectrum; and to provide indirect correlation of ^{31}P and ^{13}C via combination of information from ^{13}C-^{1}H and ^{31}P-

^{1}H correlation experiments. Although, in theory, ^{31}P-^{13}C correlation would be possible on a triple-channel probe, still allowing proton decoupling, the efficiency of cross-polarisation is not sufficient to allow such experiments to be carried out in the time available.

The pulse sequence for heteronuclear correlation (HETCOR) in solids is described below.[13] This two-dimensional technique correlates ^{1}H and ^{n}X resonances via a dipolar coupling interaction. A series of 90° pulses is applied simultaneously on the two channels during the evolution time. Multiple-pulses provide decoupling of homonuclear and heteronuclear interactions during the proton chemical shift evolution time, BB-12 on the ^{13}C or ^{31}P channel for decoupling H-X dipolar interactions[14] and BLEW-24 as a windowless H-H dipolar decoupling technique.[15] WIM ('windowless isotropic mixing') of the magnetisation after the proton 90° preparation pulse allows polarisation transfer (cross polarisation) over a short contact time. Effects of spin diffusion will be minimised by using the shortest overall contact time possible. If this was not the case, extensive spin-diffusion would result in correlation to all protons in the molecule and therefore no useful information would be obtained. Reduction of the spin-diffusion effect means that any long-range correlations could be due to the effect of intermolecular interactions arising from crystal packing. In theory, a reduced contact time would lead to a reduction in these long-range correlations, but, in practice, the minimum contact time is limited by the pulse duration and switching capabilities of the spectrometer.

In order to obtain the scaling factor needed to reference the proton chemical shifts (the indirectly detected dimension) a sample with a known HETCOR spectrum is run initially and parameters transferred to the experimental spectrum. Here poly(methyl methacrylate) (Figure 13) was chosen as the reference material as it gives a known and well-defined proton spectrum and gives a good HETCOR spectrum in a relatively short amount of time. The scaling factor is subject to a certain degree of uncertainty and errors may occur, especially when transferring scaling information into a phosphorus-proton experiment. An accuracy of about ± 1 ppm is reasonable for this method.

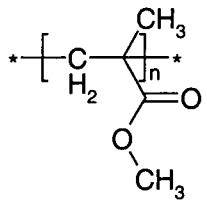

Figure 13. Poly(methyl methacrylate).

Direct comparison with ^{1}H CRAMPS and ^{n}X (^{13}C or ^{31}P) CP-MAS spectra can be obtained, with a resolved spectrum in both the directly and indirectly detected dimensions. As the crystal structure of compound I is not known, it is important to make careful comparisons with compound II before making any conclusions about the nature of the complex CH and PH correlations observed.

Results and interpretation.

The HETCOR experiments can be interpreted by comparing the two compounds in terms of structural similarity. The spectra show both strong, directly-bonded, correlations and weaker, long-range correlations, through space. As carbon-13 assignments have been postulated, they can be confirmed and proton assignments made. The three figures (Figure 14 - Figure 16) show the carbon and phosphorus spectra obtained. The chemical shift assignments are marked with the usual numbering. Spinning sidebands are visible in both carbon and phosphorus experiments and are also indicated in the figures. The spinning speed in all cases was set, and controlled at 5 kHz, to allow multiple-pulse components of the sequence to be rotor synchronised. Spectral parameters for these experiments on the Varian Unity Plus 300 are as follows:

Carbon spectral frequency, 75.43 MHz; contact time, 0.1008 ms; recycle delay, 1 s; number of acquisitions, 600; number of increments (t_1), 64.

Phosphorus spectral frequency, 121.42 MHz; contact time, 0.1008 ms; recycle delay, 1 s; number of acquisitions, 460; number of increments (t_1), 64.

The number of increments will determine the resolution in the indirectly-detected (proton) dimension, with the spectral width in the proton dimension being around 10 kHz. The contact time is restricted by other spectral parameters, e.g. the number of pulses in the multiple pulse sequence and the spinning speed. The contact time is 24* no. of wim cycles * 90° pulse duration (the contact step is a "windowless isotropic mixing" sequence consisting of 24 pulses).

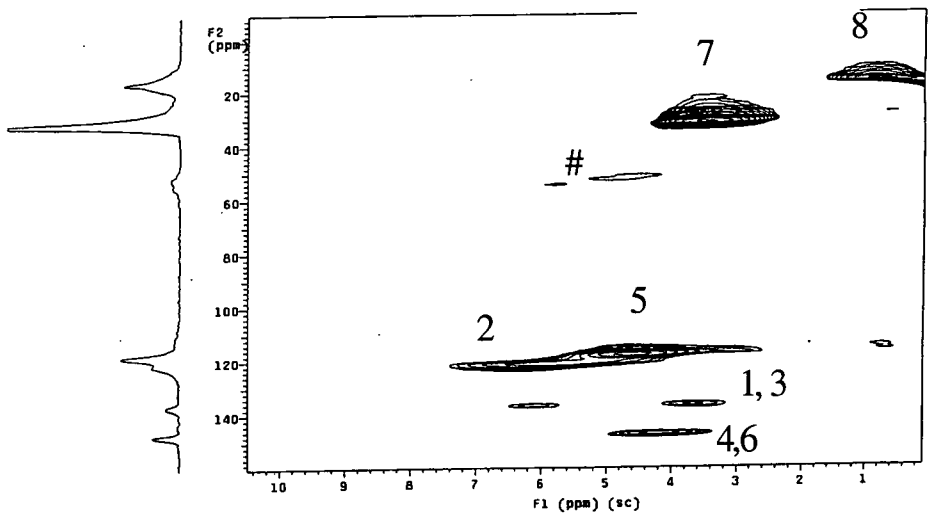

Figure 14. C-H HETCOR compound I. # Spinning sidebands. See text for acquisition parameters.

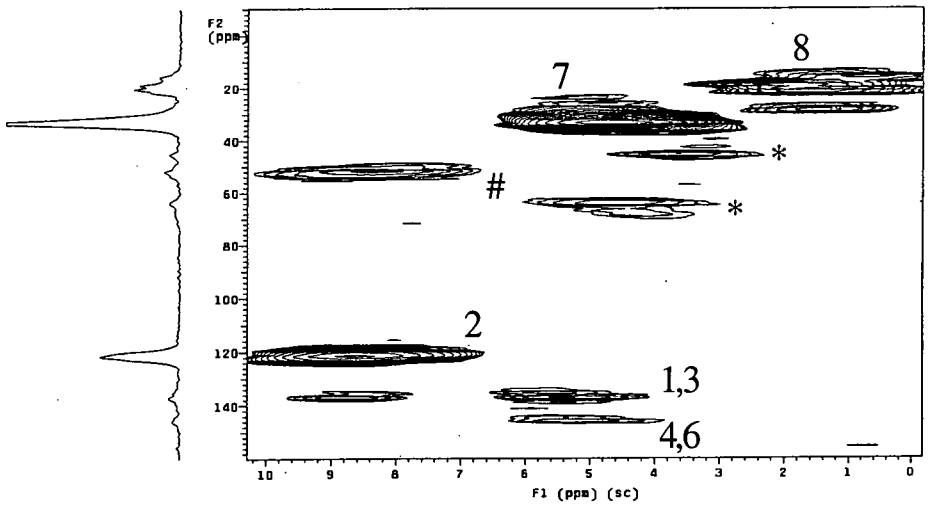

*Figure 15. C-H HETCOR compound II. # Spinning sideband, * solvent.*

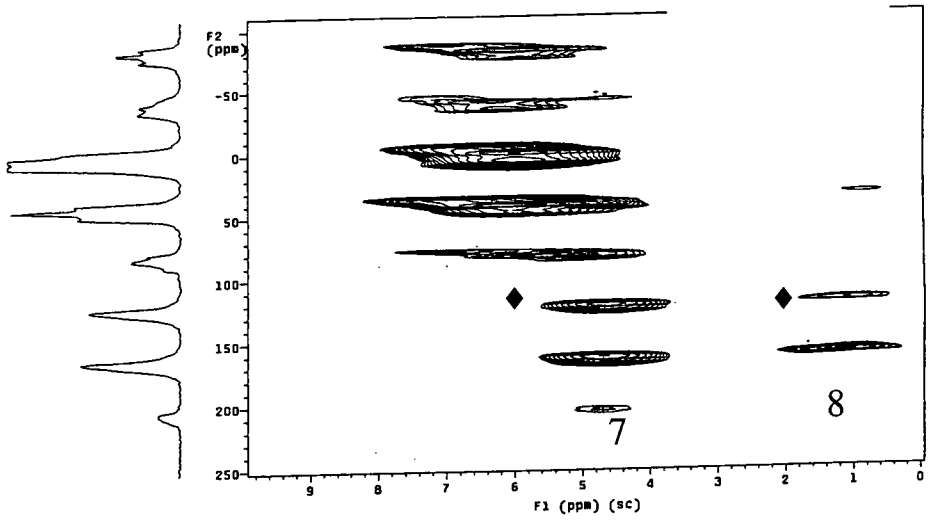

Figure 16. P-H HETCOR compound I. ♦ Centreband peaks.

In the carbon-proton HETCOR of compound I (Figure 14), the protons on carbons 5,2,7 and 8 have been separated and can be assigned according to the attached carbon assignments (Table 3).

Proton on carbon number:	δ_H / ppm (approx.)	Assignment
2	6.0	inner CH aromatic
5	4.5	outer CH aromatic
7	3.5	CH (aliphatic)
8	1.5	methyl

Table 3. Compound I. Proton shifts from HETCOR experiment.

The errors in proton chemical shifts will be a lot larger than in a resolved one-dimensional experiment as the scaling factor is determined in another experiment and therefore relies on there being exactly the same set up in both experiments over the duration of the 2-dimensional acquisition. The proton shifts agree with the expected values for this compound (from known solution-state data and substituent effects). Those for compound II follow a similar pattern, but the scaling factor has led to a slight over-expansion of the range and, therefore, the aromatic chemical shift values are large.

Long-range correlations are seen to the quaternary aromatic carbons 4 and 6 from the aromatic proton on carbon 5, and for 1 and 3 from the aromatic proton on carbon 2 and the aliphatic CH, 7 (for numbering see Figure 6). These long-range correlations also

confirm the quaternary aromatic carbon assignments calculated from the effects of the oxygen, as the magnetisation will come from the proton closest to the carbon. There is a very small long-range correlation from carbon 5 to the methyl group, which is consistent with the phosphorus experiment described below.

In the case of the carbon-proton HETCOR of compound II (Figure 15), there are also correlation peaks (*) from the 'solvent' resonances in this compound. The carbon-13 chemical shifts for the solvent have been described. From this experiment we can extract proton chemical shift data in a range around 3 to 4 ppm. Considering the discussions of accuracy (with proton shifts accurate to about 1 ppm) these seem reasonable for the CH_2Cl_2 proton shift (free liquid 5.3 ppm, with a dependence on environment when in mixed solutions). Considering the significant effects on the carbon shifts, these values seem reasonable. Due to the absence of a proton on carbon 5, the quaternary aromatics 4 and 6 now only have a very weak correlation to the aliphatic CH proton on carbon 7. The methyl region is slightly more complicated in the one-dimensional spectrum for this compound (possible due to impurity peaks) and some correlation between all the low frequency aliphatic peaks is seen.

The signal from the phosphorus impurity is favoured by the short contact time conditions used in the phosphorus-proton HETCOR of compound I (Figure 16) and appears at large intensity. It is, however, well separated from the isotropic shift correlations of the compound under examination in these experiments and does not therefore cause significant interpretation problems. The correlations are marked 7 and 8, which refers to the protons on the corresponding carbons in the methyl/CH bridge. These were identified by comparison with the carbon-proton experiment. The phosphorus-proton HETCOR for compound II is almost identical to that of compound I, and therefore the correlations observed can be compared directly with the known crystal structure. Unlike the carbon spectra where only low order spinning sidebands are observed, in the phosphorus spectra (as in the one-dimensional case) the sideband manifolds are extensive. The centre band of the desired spectrum is marked on the figure and the spread of sidebands can be seen in the phosphorus dimension.

Phosphorus correlating to both the Me and CH protons of the lower rim aliphatic link can be explained by several mechanisms. As we know the individual molecular

geometry for compound II and its identical P-H correlation experiment to that for I, we can rule out the possibility of the methyl pointing up inside the calixarene bowl, rather than straight down from the lower rim. There are two other possible reasons for such a correlation: (i) packing of molecules bringing close intermolecular interactions, or (ii) spin diffusion occurring between protons. There is some separation of shifts in the proton spectrum, inhibiting the effects of spin diffusion, and channel formation from hexagonal layers of calixarene molecules is in evidence in the crystal structure, suggesting intermolecular interactions are the more likely cause of the correlations.

Conclusions.

We can conclude from the results for these two compounds several points of general interest. It is possible to obtain indirect observation of a resolved proton spectrum as well as further assignment conclusions for carbon and assignment of proton shifts (the latter of which is difficult from the broad MAS proton spectra) from correlation experiments. Some molecules cannot be characterised by X-ray structure or solution-state NMR as they are poorly soluble, easily decomposed compounds or will not grow acceptable crystals. With the two-dimensional NMR techniques available such compounds are more appropriate for structural studies via solid-state NMR. Solid-state NMR also allows the observation and identification of disordered solvent molecules. Information on solid-state packing and solvent incorporation may be vital knowledge for the use of such systems for inclusion or molecular recognition applications.

4.3. Related compounds containing F- or N-substituents on phosphorus

Although much of the work with the correlation experiments and the related preliminary discussion of 1-dimensional spectra is appropriate to compounds I and II, it is also of interest to investigate the spectra from other similar compounds with more complex substituent groups than a single chlorine bonded to the phosphorus. These remaining compounds will be considered in turn, and their carbon-13, phosphorus-31 and, where appropriate, fluorine-19 spectra will be discussed. Results are summarised at the end of this chapter.

4.3.1 Compound III, Tetrakis-(O-P(N(CH_3)$_2$)-O)-Bridged Calix[4]resorcinol-Br

Carbon-13 and phosphorus-31 NMR studies of this molecule have been carried out.
In the case of carbon-13, a broad background signal under the aromatic region of the spectrum is evident. Acquisition under the same experimental conditions (short contact time of 1 ms observing carbon with cross polarisation from protons) was performed with an empty insert in the rotor. The resulting spectrum subtracts from the sample spectrum flattening the baseline and so gives confirmation that the broad peak does not result from the sample. The rotor insert material is Kel-F, (i.e. chlorotrifluoroethylene), which is a proton-free plastic. Therefore, the broad carbon background signal from within the probe or rotor set-up, which is observed under these conditions, is perhaps emphasised in intensity when using inserts because of the restriction on actual sample volume. Assignments are given in Table 4. Comparisons with other systems were made and results from computer predictions (acdlabs online service[16]) are also shown as they were used in making assignments. Quaternary and methyl carbons were identified by a dipolar-dephasing or 'non-quaternary suppression' experiment with a window of 50 μs.
The peak at 34.6 ppm is observed in both the cross-polarisation experiment and with dipolar dephasing with a 50 μs dephasing time (where methyl and quaternary carbons remain). Even though, due to chemical shift comparisons, this would be expected to be the aliphatic CH, it is clear from the dipolar dephasing experiment that it is, in fact, the N-Me group. The methyl and that at 139 ppm also remain distinguishable from the

noise after 80 μs dephasing (being at full intensity after 50 μs), but even these have decreased in intensity after the longer dephasing time.

δ_C / ppm	assignment	prediction (minimum error)
147	aromatic (>C-O)	149 (5)
139	aromatic (>C-C)	135 (8)
121.5	non-quaternary aromatic	133 (1)
	[a] C-Br	108 (7)
68.5	impurity	
34.6	N-Me (large intensity)	35 (2)
22.6	CH bridge	38 (3) c.f. other systems ~30
16.9	Me	15 (8) c.f. other systems ~20

Table 4. Carbon-13 chemical shifts for compound III.

[a] Probably not observed because of second-order quadrupolar effects.

There is no clear evidence from this to suggest anything lower than four-fold symmetry of the molecule, for example, a single ^{13}C peak is observed for the 4 methyl groups. The broad N-Me peak has large intensity and an asymmetric lineshape consistent with residual dipolar coupling to directly-bonded nitrogen.

A ^{13}C-^{1}H HETCOR experiment was also attempted in this case, in order to try and separate the C-methyl and N-methyl proton resonances, the latter of which should be at higher frequency. Parameters include a spectral frequency of 75.43 MHz, spinning speed of 4340 Hz, 24 increments in the t_1 dimension, recycle delay 2 s and contact time 115 μs. The short contact time means that spin-diffusion is minimised. The ^{13}C assignments give a methyl (of the lower-rim bridge) at 17 ppm and a ^{13}C resonance at 35 ppm. Few peaks were observed, but included a low intensity peak defining the aliphatic methyl and a very large intensity peak for the N-Me groups at higher proton and carbon frequencies. The N-Me carbon also showed low intensity correlations to the aliphatic methyl protons and to an aromatic proton. The non-quaternary aromatic also

shows a correlation. It appears that none of the quaternary aromatic or the bridging CH signals are visible under the conditions used. The N-Me proton chemical shift is confirmed as being around 2 ppm higher than that of the aliphatic methyl. As there is only one protonated aromatic carbon environment in this compound, the higher frequency region of the HETCOR experiment is easily explained.

The N-Me carbon signal was also of high intensity in the one-dimensional spectrum, and this effect will be emphasised by the short contact time. This is perhaps why the long range correlations to quaternary carbons are not observed, in contrast to compounds I and II. They will be very small in comparison to the N-Me resonance and will not be distinguishable from the noise.

When observing phosphorus, as with other comparable compounds, the shielding anisotropy is such that a clear spinning sideband manifold can be seen at the spin rates generally used (3-5 kHz). Two sets of peaks are evident, but because of their dissimilarity in terms of shielding anisotropy and chemical shift it is likely that the smaller of the two signals (with a shift of 2.4 ppm) results from an impurity rather than molecular asymmetry and chemical shift differences for the calix[4]resorcinol molecule. The low intensity peak does not have a chemical shift consistent with the expected phosphorus environment of the molecule (bonded to two oxygens and a nitrogen). Each spinning sideband contains a single resonance from the four equivalent phosphorus centres around the upper rim. For the main peak an anisotropy of 180 ppm (±3 ppm, σ_{33} - σ_{iso}) was calculated and an asymmetry parameter of 0.5 (to within 0.03) around an isotropic chemical shift of 139 ppm. This is highly deshielded in comparison to the other calix[4]resorcinols studied. A variable contact time experiment was also used to estimate proton $T_{1\rho}$ from the decay of intensity of two of the signals (for comparison, the isotropic and the largest intensity spinning sideband were used). An average value of 9.3 ms was calculated with little variation when fitting the two different peaks.

4.3.2 Compound IV, Tetrakis-(O-P(F)-O)-Bridged Calix[4]resorcinol.

Carbon-13 spectra were recorded using cross-polarisation (from protons), and dipolar-dephasing experiments, with a 50 μs dephasing window in the proton radio frequency (Figure 17). Background signal from the inserts was observed, giving a broad signal under the sharp sample peaks. This is corrected by running a spectrum of the empty insert and subtracting this from the results. That shown in the figure is without subtraction of the background. The effect of dipolar dephasing, in terms of suppression of the non-quaternary carbon signals (but not methyl carbons) is seen. In addition to proton decoupling, high power fluorine decoupling was also applied. This resulted in only a slight narrowing of signals in the aromatic region, and therefore those shown in the figure are with only proton decoupling.

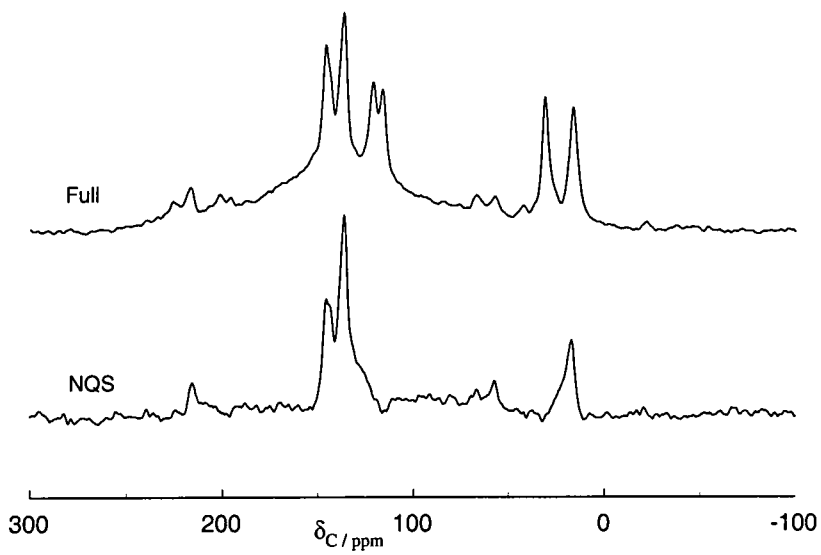

Figure 17 $^{13}C\{^{1}H\}$. Frequency 50.33 MHz, spin rate 4 kHz, contact time 4 ms, recycle delay 2 s, 6296 acquisitions, dephasing time 50 μs. NQS indicates the dipolar-dephasing experiment.

The chemical shifts can be assigned as follows (Table 5):

Chemical Shift / ppm	Assignment	NQS
146.1	Aromatic (>C-O)	quaternary
136.9	Aromatic (>C-C)	quaternary
121.4	Aromatic (C2-H)	protonated
116.5	Aromatic (C5-H)	protonated
31.1	CH	protonated
16.5	Methyl	methyl

Table 5. Carbon-13 chemical shifts for compound IV.

The aromatic region shows four peaks (two quaternary, two non-quaternary) in both the proton and double (HF) decoupled spectra. It can be noted that in the similar compound I, this resolution of the inner and outer non-quaternary carbons was also observed as well as the distinction between the two types of quaternary aromatic.

The ^{31}P spectrum (Figure 18) shows two sites at 92 ppm (sharp) and -1.1/12 ppm, the apparent structure in this broader region at lower ppm is not removed or resolved by fluorine decoupling. Isotropic shifts were identified by changing the spin rate, and sideband manifolds of each were determined by their separation of 5 kHz from the isotropic peak in the relevant spectrum. The broader signal is a complex lineshape, consisting of multiple peaks. From observation of the whole sideband manifold by deconvolution, it can be postulated that the region is consistent with a broad peak and a shoulder. The 'two peaks' from deconvolution of the broader signal at lower ppm do not sum to a 1:1 intensity ratio over the sideband manifolds, but their relative intensities remain the same over the whole region, the higher frequency peak being approximately 0.2 times the intensity of the other. Shoulders are still observed in the double decoupled spectra even though resolution is slightly reduced (this effect cannot, at present, be definitively explained). This band is consistent with decomposition products. The fine structure of the sharp peaks at 92 ppm (marked * on Figure 18) is removed in the double decoupled spectra giving a singlet peak, so this is believed to arise from the compound of interest. From the experiment with just proton decoupling the PF coupling constants can be calculated. For the sharp peaks a value of 1.2 kHz is clearly observed and is consistent throughout the spinning sideband manifold. Integration shows good

agreement of intensities between the H and HF decoupled spectra of both the sharp and broad regions.

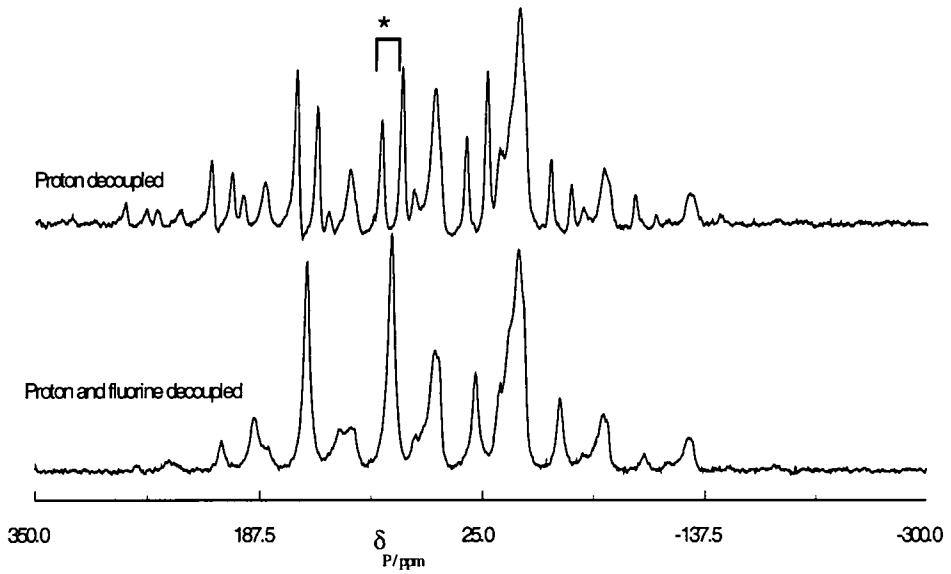

Figure 18. $^{31}P\{^{1}H\}$ spectrum of compound IV. Frequency 81.02 MHz, spin rate 5 kHz, contact time 6 ms, recycle delay 2 s, 3448 acquisitions.

These results may indicate either a lack of symmetry and/or the presence of a phosphorus-containing impurity. However the absence of molecular symmetry is not observed in the carbon-13 measurements or for the equivalent chlorinated compound discussed previously (compound I) for which there was a single isotropic shift at 121 ppm. The sharp fluorine-coupled band at 92 ppm is therefore that of interest.

Comparison of cross-polarisation and single-pulse spectra shows that the intensity of the broad band is significantly increased with respect to the sharp signal centred around 92 ppm when proton magnetisation is transferred. This is consistent with an impurity containing PH rather than PF bonds, in which the phosphorus atoms are closer to a hydrogen centre, or are more rigid, facilitating polarisation transfer. The difference in linewidth is caused by a larger PH heteronuclear interaction causing broadening. Therefore the existence of these peaks is confirmation of the decomposition mechanism described in Figure 3.

The effective shielding anisotropy observed for a PF coupled system can be analysed to provide information on the dipolar interaction. The two spinning sideband manifolds (of a PF doublet) are governed by the effective tensors

$\zeta_{eff} = \zeta - 2\Sigma m_x D'/\nu_o$

where $m_x = \pm$ ½ (the spin component quantum number for the relevant heteronucleus), $D' = D - \Delta J/3$ is the observed pseudo dipolar interaction, with ΔJ the anisotropy in J, and ν_o is the Larmor precession frequency. $\Sigma m_x = \pm 1/2$ for PF and therefore we have two different manifolds, one being expanded and the other compressed. The computed values of the effective anisotropies can then be used to find the true shielding anisotropy (ζ) and the effective dipolar coupling (D') individually. The results obtained from the ssb97 program (which assumes coaxiality of the tensors) and the resulting calculations are shown for the sharp doublet at the chemical shift indicated.

High frequency component (99 ppm)

Anisotropy ($\zeta_{eff} = \sigma_{33} - \sigma_{iso}$) = 204.0 ppm

(σ_{11} = -275, σ_{22} = -132, σ_{33} = 111)

η = 0.7

Low frequency component (84.5 ppm)

Anisotropy (ζ_{eff}) = -167.3 ppm

(σ_{11} = 66, σ_{22} = -67, σ_{33} = -253)

η = 0.7

These data lead to D' = 1.5 kHz and ζ = 186 ppm. The ^{19}F-decoupled spectrum gives ζ = 164 ppm and a triple fit of the ^{19}F coupled and decoupled spectrum, allowing angles to vary gives ζ = 177 ppm, D' = 3.8 kHz, α = 90°, β = 60° with a high value of $\eta(1)$. All these values are in fair agreement, taking into consideration the assumptions made (e.g. colinearity), the 10° accuracy of the Euler angles and the intensity measurement of each spinning sideband. The two broader peaks give values of 139 and 133 ppm for the anisotropy (with statistical errors of 14 and 6 respectively). The agreement between these numbers suggests that this signal is not governed by the PF coupling effect described above so that it is simply from two very similar chemical species.

Fluorine-19 NMR should compare well with these results because of the strong PF coupling. δ_F = -66.6 ppm with a splitting of ~1 kHz for $^1J_{PF}$. Spinning sideband analysis of the doublets by deconvolution leads to effective anisotropy (asymmetry values are given in parentheses) values of 63 (0.2) and –116 (0.8). Using these effective values we get ζ = 89.5 ppm and D' = 5 kHz. The latter of these is of the same order of magnitude as the calculation from the ^{31}P observe spectrum. This may be an over simplified situation, since it assumes colinearity of tensors, and the fact that the two asymmetry values are different for the two effective tensors suggests a degree of uncertainty in the results, even though, for the three co-ordinate phosphorus in this compound, colinearity of tensors would be expected.

4.3.3 Compound V, Tetrakis-(O-PF_2) Calix[4]resorcinol (AuCl)

The ^{13}C spectrum can be assigned as shown in Table 6:

δ_C / ppm	Assignment
20.5	Methyl
32.0	C-H
109.5	Non-quaternary phenyl
113.1	Non-quaternary phenyl
117.7	Non-quaternary phenyl
129.4	Decays only partially during dephasing
145.7	Quaternary Phenyl (bonded to C)
151.0	Quaternary Phenyl (bonded to O)

Table 6. Carbon-13 chemical shifts for compound V.

The signal at 129.4 ppm which displays only partial decay during the 50 μs dephasing time could result from two possibilities. The dephasing time, even at the value generally used to separate out quaternary carbons, may not be sufficient, or more likely, the peak results from the overlap of two carbon resonances. The existence of four non-quaternary aromatics implies that there is not just a simple four-fold symmetric molecule in the sample.

The ^{31}P spectrum was acquired with both H and F decoupling using the HFX probe with the sample spinning at 4 kHz. A sharp peak at 8.1 ppm with a smaller peak at -0.2 ppm were observed as well as a broader peak at 97 ppm (as before, this is the peak of interest), with a sideband manifold covering the region from +200 to -100 ppm. Broadness could be a result of the F decoupling being off resonance, but as this was checked and the best apparent value chosen, it is more likely in this situation due to the AuCl salt present in the crystals.

Two fluorine peaks are observed with isotropic shifts, at -59.8 and -74.8 ppm with PF splittings of 1073 and 904 Hz, respectively. This suggests two fluorine environments in the OPF_2 groups. However, a second peak was observed in the phosphorus spectrum

and it is possible that one of the two signals observed, which are not in an exact 1:1 ratio, results from the same impurity. However, the PF_2 groups in this molecule do not form part of a tethering bridge and there will exist more possibilities for isomerism. Also the phosphorus impurity peak is easily explained according to the decomposition mechanism. The phosphorus centres will be free to take up positions around the upper rim and will not be sterically restricted into pointing in or out of the calix[4]resorcinol cavity.

4.3.4 Compound VI, Tetrakis-(O-PF_2)Calix[4]resorcinol-Br

Similar experiments were attempted for this sample, but, despite packing in a rotor insert, decomposition occurred at some point during the run (the white powder darkened to a brown solid). This calls into question the validity of some of the results, in particular the ^{31}P spectra, which were run after those measuring carbon-13 resonances, although comparisons with the similar compound V for both nuclei do give some encouragement. Because of this problem and the small quantity of this compound originally available, further experiments on this system were difficult. The first experiments were the observation of carbon-13, by cross-polarisation from protons, with double decoupling and with and without dipolar-dephasing (involving an 80 μs dephasing window (Table 7). In this case there appears at first to be only three aromatic peaks. However, there is only partial decay of the peak at 124.8 ppm during NQS, which on closer inspection in the complete spectrum has a slight shoulder. It may be suggested, from this and by comparison with other systems that the peak at 124.8 ppm actually consists of two signals, corresponding to both the non-quaternary carbon and that bonded to Br. The bromine nucleus will reduce the chemical shift of the directly bonded carbon so that where two separate peaks were observed for the inner and outer non-quaternary aromatics in the previously studied compounds these now become superimposed. The higher-frequency carbon in other systems (which may now be assigned to the outer edge of the system) is shifted down to become almost exactly coincident with the inner unsubstituted aromatic carbon. This is an alternative to the previous explanation that the C-Br peak is broadened to the extent that it is not observed. However, in rigid systems containing bromine directly bonded to carbon, complex second order (quadrupolar) effects would be expected, causing broadening or lack of resolution. This is not entirely consistent with the relatively sharp peak obtained in this spectrum.

δ_C / ppm	Assignment
149.7	Aromatic Quaternary
137.2	Aromatic Quaternary
124.8	Aromatics CH (non-quat.)
	[a] CBr (quaternary)
32.4	Aliphatic CH(R)
16.9	R = Methyl

Table 7. Carbon-13 chemical shifts of compound VI.

[a] Unlikely to be observed due to second-order broadening effects.

Direct-polarisation experiments and those with cross-polarisation (from protons) were acquired, observing ^{31}P. The small sample of this compound which remained after the decomposition was used without further problems. The sample did not change colour and spectra at the beginning and end of the run showed identical results. In contrast with the above compound V, which is also a PF_2 system only one signal is observed, δ_F = -63.8 ppm $^1J_{PF}$ = 1730 Hz. The presence of the bromine will mean that there are limited possibilities for isomerism and therefore the PF_2 positions will be fixed.

4.3.5 Conclusions

In addition to the specific conclusions already given in the section describing compounds I and II, it is also appropriate to bring together some general conclusions. Structural information has been obtained for a series of calix[4]resorcinols with varying upper ring substituents. All contain 4 phosphorus atoms per molecule, with 3 co-ordinating atoms, either bridging the upper rim or un-tethered, and the molecular symmetry has been confirmed. Further investigations of molecular packing have been possible using two-dimensional NMR spectra and comparisons with X-ray crystal structures, for an insoluble, air/moisture sensitive microcrystalline solid. The coupling patterns and shielding effects of the different substituents are clearly seen in one-dimensional spectra, and assignments of chemical shifts are determined from such spectra and known data, but are reinforced by information from more complex experiments. Although it has not been possible to obtain distance information, a

qualitative packing description and quantitative data on PF interactions have been obtained.

It is worth, at this stage, combining all the chemical shift data from the whole range of compounds in order to draw some general conclusions about any trends observed. The phosphorus data (Table 8) are summarised for all compounds below.

Compound	Group[a]	δ_P / ppm
I	PCl	121
II	PCl CBr	129
III	$PN(CH_3)_2$ CBr	139
IV	PF	92
V	PF_2 (AuCl)	97

Table 8. Summary of phosphorus chemical shifts.

[a] All phosphorus is three co-ordinate, the other positions being occupied by oxygen.

Comparing compounds I and II, it is obvious that the bromine substituent on the aromatic ring is causing deshielding. This is also seen in case III where the phosphorus chemical shift is higher than expected for the P-N combination. The oxygen will tend to have the opposite effect, lowering the chemical shift, and this is illustrated by the shifts being a lot lower than the fully halogenated three co-ordinate phosphorus compounds.

For comparison of the carbon chemical shifts the following table has been derived (Table 9). The similarities can clearly be seen, as can the absence of a visible resonance from carbon 2 when it is directly bonded to bromine. The only major discrepancy is in the aliphatic region of compound III. By comparing chemical shifts alone one would suspect that the resonance at 35 ppm compares favourably with the CH shifts, but from the dipolar dephasing results it is assigned to N-Me.

	Chemical shift of carbon number /ppm								
	1	2	3	4	5	6	7	8	N-Me
I	137	121	137	147	118	147	32	17	
II	137	121	137	146	-	146	33	16-22	
III	138	122	139	147	-	147	23	17	35
IV	137	121	137	146	117	146	31	17	
V	146	109-129	146	151	118	151	32	21	
VI	137	124	137	150	-	150	32	17	

Table 9. Summary of carbon chemical shifts for compounds I to VI.

REFERENCES

[1] V. Böhmer, *Angew. Chem. Int. Ed. Engl.*, 1995, **34**, 713.

[2] C.D. Gutsche, *Calixarenes*, The Royal Society of Chemistry, Cambridge, England. 1989.

[3] H.-J. Schneider, D. Göttes, U. Schneider, *J. Am. Chem. Soc.*, 1988, **110**, 6449; P.D. Beer, E.L. Tite, *Tetrahedron Letters* 1988, **29**, 2349; Y. Aoyama, Y. Tanaka, S. Sugahara, . *J. Am. Chem. Soc.*, 1989, **111**, 5397; K Kurihara, K. Ohto, Y. Tanaka, Y. Aoyama, T. Kunitake, *J. Am. Chem. Soc.* 1991, **113**, 444; Y. Kikuchi, Y. Kato, Y. Tanaka, H. Toi, Y. Aoyama, *J. Am. Chem. Soc.* 1991, **113**, 1349; Y. Kikuchi, K. Kobayashi, Y. Aoyama, *J. Am. Chem. Soc.* 1992, **114**, 1351; Y. Kikuchi, Y. Tanaka, S. Sutarto, K. Kobayashi, H. Toi, Y. Aoyama, *ibid,* 1992, **114**, 10302; K. Kobayashi, Y. Asakawa, Y. Kato, Y. Aoyama, *ibid,* 1992, **114**, 10307; K. Kobayashi, Y. Asakawa, Y. Kikuchi, H. Toi, Y. Aoyama, *ibid,* 1993, **115**, 2648; E.U. Thoden van Vetzen, J.F.J. Engbersen, D.N. Reinboudt, *J. Am. Chem. Soc.* 1994, **116**, 3597; M. Inouye, K. Hashimoto, K. Isagawa, *J. Am. Chem. Soc.* 1994, **116**, 5517.

[4] P. Delangle, J.P. Dutasta, *Tetrahedron Letters,* 1995, **36**, 9325.

[5] A. Vollbrecht, I. Neda, H. Thönnessen, P.G. Jones, R.K. Harris, L.A. Crowe, R. Schmutzler, *Chem. Ber. / Recueil,* 1997, **130**, 1715.

[6] J.B. Niederl, H.J. Vogel, *J. Am. Chem. Soc.*, 1940, **62**, 2512.

[7] D.J. Cram, S. Karbach, H.-E. Kim, C.B. Knobler, E.F. Maverick, J.L. Ericson, R.C. Helgeson, *J. Am. Chem. Soc.*, 1988, **110**, 2229.

[8] E. Fluck, *Die kernmagnetische Resonanz und ihre Anwendung in der anorganishen Chemie*, Springer Verlag, Berlin. 1963.

[9] A. Vollbrecht, personal communication.

[10] J.R. Ascenso, L.H. Merwin, H.-P. Bai, J.C. Cherryman, unpublished.

[11] University of Potsdam, Am Neuen Palais 10, 14469 Potsdam, GERMANY. Webpage for NMR solvent data.

[12] DA Torchia, *J. Magn. Reson.* 1978, **30**, 613.

[13] C.E. Bronnimann, C.F. Ridenour, D.R. Kinney, G.E. Maciel, *J. Magn. Reson.*, 1992, **97**, 522.

[14] D.P. Burum, *Concepts Magn. Reson.*, 1990, **2**, 213.

[15] D.P. Burum, M. Linder, R.R. Ernst, *J. Magn. Reson.*, 1981, **44**, 173.

[16] Advanced Chemistry Development Inc., Ontario, Canada. www.acdlabs.com

5. Fluorinated Diazadiphosphetidines

5.1. Introduction

A solid-state NMR study of a series of diazadiphosphetidines with fluorine substituents has been carried out in order to obtain information on structural and dynamic properties. Triple-resonance techniques have been used to investigate the effects of indirect (scalar) coupling, and the observed (effective) shielding anisotropies, obtained by analysis of spinning sideband manifolds. The results have been combined with crystallographic data to obtain information on the effective dipolar coupling strength in the hope that estimates can be made of the anisotropy of the indirect coupling.

Phosphorus pentafluoride, and its organic derivatives, when reacted with N-substituted hexamethyldisilanes, give cyclic fluorophosphoranes (diazadiphosphetidines) which are of stereochemical interest. To produce substituted compounds, for example, t-butyl lithium will replace one F of a fully fluorinated compound with ^{t}Bu.[1] The synthesis route below has been published previously[2] as has that for unsymmetrical diazadiphosphetidines.[3]

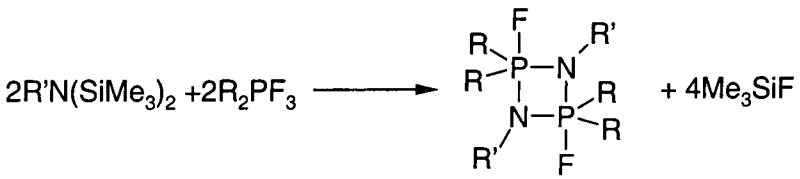

Electron-impact,[4] electron diffraction[5] and X-ray diffraction studies have been carried out on several of these compounds and similar systems. For example, full crystal structures have been reported for $(Ph_2FPNMe)_2$,[6] and other fluorinated diazadiphosphetidines including $(PhF_2PNMe)_2$.[7] The compounds studied in the present investigation are of the form $(X_nY_{3-n}PNR)_2$ where R and X = alkyl or aryl and Y = F. Geometry and intramolecular motion are of particular interest. NMR parameters (derived from solution-state studies) have been shown to depend heavily on the nature of substituents and rates of intramolecular motion.

The dimeric structures consist of penta-coordinate phosphorus within a 4-membered ring. As one axial position and one equatorial position are occupied by the nitrogens in the ring, the remaining substituents on a given phosphorus can only occupy the trigonal bipyramidal positions still available. In the symmetrical fluorinated compounds, one fluorine on each phosphorus will preferentially go axial, any other groups being forced into equatorial positions. These locations can generally be distinguished by (fluorine) chemical shifts and isotropic (J_{PF}) coupling constants. The magnitude of $J_{PF(axial)}$ is generally smaller than that of $J_{PF(equatorial)}$, and axial fluorines are deshielded relative to equatorial fluorines, because axial bonds have less s character than equatorial. The trends in magnitudes of J_{PF} and δ_F can be illustrated by the following values from the literature:

$(Et_2N)_2PF_3$	$\lvert J_{PF(ax)}\rvert$ 750 Hz, $\lvert J_{PF(eq)}\rvert$ 875 Hz[8]
Et_2NPEtF_3	$\lvert J_{PF(ax)}\rvert$ 830 Hz, $\lvert J_{PF(eq)}\rvert$ 984 Hz [8]
$MePF_3NMe_2$	$\lvert J_{PF(ax)}\rvert$ 803 Hz, $\lvert J_{PF(eq)}\rvert$ 964 Hz
	$\delta_{F(ax)}$ -27.6 ppm, $\delta_{F(eq)}$ -69.0 ppm[9]

Isotropic scalar coupling constants, $^1J_{PF}$, are known to be negative.[10] This fact will be used later when discussing the effect on the shape of spinning sideband manifolds in coupled systems.

When there are two fluorines on each phosphorus, there is the possibility of trans/gauche isomerism across the planar ring (Figure 1).[7,11] Values of $^1J_{PF}$ in the range -807 to -922 ppm were reported for trans and gauche isomers of a series of PF_2 diazadiphosphetidines, the trans isomers having values at the lower end of this range and the gauche isomer values generally having a magnitude over 900 Hz.[11] In such cases separate axial and equatorial values are not observed in these solution-state studies, only an average $^1J_{PF}$. The crystal structure of $(PhF_2PNMe)_2$ shows it to be in the trans form,[11] whereas in solution trans↔gauche exchange is rapid on the NMR timescale above room temperature. Therefore when comparing results with the previous solution-state work it is important to consider this conformation. The crystal-structure data will enable us to distinguish which of the two isomers is present in the solid-state structure.

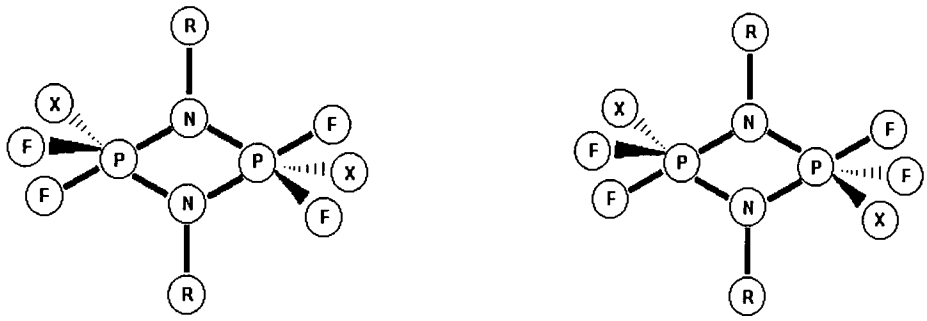

GAUCHE TRANS

Figure 1. Trans/gauche isomerism of di-substituted diazadiphosphetidines.

Despite the bonding around the PN ring tethering two co-ordination sites of each trigonal bipyramidal phosphorus, it has been found[11,12] that a form of motion can occur involving the other three ligands. This is related to Berry pseudo-rotation.[13] The mechanism for this process can be thought of as follows. On transforming from one conformation to another the molecule will pass through an intermediate with a phosphorus centre of approximately tetragonal pyramidal geometry. The three non-bridging groups on phosphorus (axial and equatorial ligands) exchange through 120° about the plane of the 4-membered ring.[11,12] The energy barrier for this process depends on the substituents on phosphorus, which will restrict such a process, and also on the rest of the molecule (the substituents on nitrogen) as will be shown in the variable temperature, solid-state experiments described below. Careful choice of R and X groups must be made to observe this exchange process on the NMR timescale. If the groups are small, motion will be rapid, and an average will be seen at room temperature. If R and X are very large, motion will be slowed and, on the NMR timescale, the spectrum representing the rigid molecule will be observed at ambient probe temperatures. The ideal case will have a coalescence temperature for the motion within the accessible temperature range of the probe specifications. Harris et al.[12,14] have described pseudo-rotation processes in the solution state for diazadiphosphetidines involving the possible pseudo-rotamers in several similar compounds. The mechanisms described, to interconvert between all possible isomers, are axial-equatorial fluorine exchange, gauche-trans exchange and P-N bond equilibration.

All previous NMR studies on these, and closely similar, systems have been made in the solution state.[14] The aim of this work was to see how crystal packing and other

solid-state effects influence the structure and symmetry of the systems, and also to test whether pseudo-rotation effects can be observed in the solid state, and, if so, over what temperature range.

In general, solution-state data have been used for comparison with newly acquired solid-state data for confirmation of shifts and couplings, and also to distinguish any motional differences. These solution-state values are, in general, averages (although trans/gauche isomers have been observed), where for rigid solids one can expect to distinguish axial and equatorial arrangements and to obtain information on anisotropic interactions. It proved possible, in the present study, to gain control over the rate of motion both by varying the experimental temperature and by controlling the substituents.

As fluorine NMR features heavily in this chapter it is worth reiterating the points made previously. Magic-angle spinning and proton decoupling are normally essential for obtaining high-resolution spectra for solids. In the cases of proton and fluorine solid-state NMR, homonuclear interactions have sometimes necessitated the use of multiple-pulse sequences[15,16] or high-speed spinning[17] to produce acceptable resolution. High-power proton decoupling is applied as in other heteronuclear cases, but problems can arise as there is only 6% difference between the proton and fluorine resonance frequencies.[18-20] At 200 MHz the Bloch-Siegert shift is around 2 ppm and has been corrected for experimentally.

Although spinning sidebands are sometimes removed from solid-state MAS spectra for simplicity, in many cases (such as coupled systems) a careful choice of spinning speed can lead to extraction of additional information (when no overlap of resonances occurs). In favourable cases the sideband manifolds in coupled systems can be simulated to obtain shielding anisotropy, shielding asymmetry and D' (a term which includes both D, the dipolar interaction which can be calculated from a known internuclear distance, and the anisotropic indirect coupling, ΔJ). For example, in the simplest case of an isolated two-spin system such as a PF doublet, the two spinning sideband manifolds in either ^{19}F or ^{31}P spectra will differ from each other, with one stretched and the other compressed. This effect has been described previously for both the PC and PF cases.[21,22] Published data for monofluorophosphates[23] includes the following (see Table 1), the first system

having an asymmetry of zero, and the two phosphorus environments in the second compound showing similar, but distinguishable, parameters:

	K_2PO_3F	$K_2P_2O_5F_2$	
		P(a)	P(b)
σ / ppm	-5.7	29.4	26.4
$\Delta\sigma$ / ppm[a]	-140	239	230
η	0.0	0.4	0.4
J_{PF} / Hz	-830	-784	-800
ΔJ_{PF} / Hz	2500	3660	3660

Table 1. NMR parameters previously published for monofluorophosphates.

[a] The definition of $\Delta\sigma$ is different to that of ζ used in this work, by a factor of 3/2.

$\Delta\sigma = \sigma_{33} - (\sigma_{11} + \sigma_{22})/2$.

An observable scalar (isotropic) splitting is essential to distinguish the two manifolds needed to observe the effect of the shielding anisotropy and dipolar coupling. The effective anisotropy, ζ_{eff}, for a given spinning sideband manifold can be found in terms of the following equation, which assumes co-axiality of the true shielding anisotropy, ζ, and D.

$\zeta_{eff} = \zeta - 2\Sigma m_x D'/\nu_o$

where $m_x = \pm ½$ (the spin component quantum number for the relevant heteronucleus), $D' = D - \Delta J/3$ is the observed pseudodipolar interaction and ν_o is the precession frequency. It is assumed that the J and D tensors are co-axial, and asymmetry in J is ignored. D is defined in frequency units by:

$$D = \frac{\mu_o}{4\pi}\gamma_P\gamma_F\frac{\hbar}{2\pi}r_{PF}^{-3}$$

which may be readily calculated if r_{PF} is known from diffraction experiments. Detailed equations for the effective tensor components in cases where ζ and D' are not coaxial have been given.[21,24] These can be used to derive the Euler angles linking σ and D' as well as the values of the tensor components, but only if experimental information is available over and above (for a two-spin case) the two spinning sideband manifolds from a coupled spectrum. In the cases considered here, it is in principle possible to

simultaneously fit[25,26] two spinning sideband manifolds from coupled spectra together with one manifold from a decoupled spectrum (at least for ^{31}P spectra). However, to derive all five parameters requires very high quality spectra, which were difficult to obtain in the present investigation. Moreover no triple-fit procedure can be carried out for ^{19}F work, since probe limitations mean phosphorus-decoupled fluorine spectra can only be recorded without proton decoupling and hence good quality spectra cannot be obtained. In the case described below where the effect of phosphorus decoupling was observed, spinning sideband analysis was still not possible due to a significant background signal obscuring some of the sideband manifold. The HFX probe used is not designed for fluorine observation, and does therefore not have the same 'fluorine-free' specifications as the HF probe.

In the work reported here, a series of diazadiphosphetidines has been investigated to determine their structural and dynamic properties in the solid-state. The number of fluorines and the nature of the other substituents have been altered to investigate rates of motion, symmetry and coupling patterns (references for solution-state NMR and crystal structures are: $(Ph_2FPNMe)_2$,[6] $(PhF_2PNMe)_2$,[7,11,27] $(^tBuF_2PNMe)_2$,[1] $(F_3PNMe)_2$[12]). Solid-state NMR spectra have been recorded for ^{31}P, ^{19}F, ^{13}C, ^{15}N and ^{1}H with various decoupling and cross-polarisation combinations. The first two nuclei listed are particularly useful because of their high sensitivity and 100 % natural abundance, and because the strong interactions between them give two routes to complementary information. Study of the remaining nuclei in a molecule helps to complete the structural information.

5.2. Experimental considerations.

All the diazadiphosphetidines were provided by Prof. R. Schmutzler and H. Thönnessen, Braunschweig University. Because the samples are subject to possible decomposition if exposed to moist air, they were initially handled in a glove box and sealed in small plastic inserts, which then fit tightly into the rotors used. Recrystallisation of some of the compounds was attempted using toluene to remove observed impurities. Even though complete purification was not obtained, significant improvement was found in the case of $(Ph_2FPNMe)_2$, bringing the impurity NMR signals down to acceptably low intensity.

A powder XRD experiment was carried out using the Bruker D8 Advance high resolution powder diffractometer facility at Durham University.[28] This was to help to confirm the identity of $(Ph_2FPNMe)_2$ which is known to have two crystal forms. The general principles behind such an experiment are given. Bombardment of a metal with electrons will provide the source of the X-ray beam used. Vacancies left by K-shell electrons will be filled by L- and M-shell electrons, emitting energy, with the different electrons giving rise to K_α and K_β lines. These X-rays are directed towards the sample. A thin layer of sample is placed on a circular silicon plate (cut along a crystal axis with a systematic absence so no background diffraction is seen) and this is rotated (from the horizontal position, to give angles θ) at half the speed of the detector (which scanned, in this case from 5 to 50° for 2θ) with the incident X-ray beam fixed. Diffraction can sometimes be seen at larger values of 2θ, but for a molecule such as this it will be of very low intensity and all identification can be made from the small angle region. The sample disc is also spun slowly (about the normal to the centre of the plate). A thin layer of the finally ground sample is used to create a random orientation and the rotation of the sample plate is used to increase this effect. Diffraction is caused because the wavelength of X-rays is of the same order of magnitude as interatomic distances. Signal intensity (maxima) will occur when the condition $\lambda = 2d\sin\theta$ is satisfied (i.e. Bragg's Law). The detector will then collect the constructive interference reflections from the different planes within the crystal. Data from the two known crystal structures were used to simulate powder diffraction intensities[28] using Cerius 2 software.[29]

For the solid-state NMR work, the spectrometers used in this work were Chemagnetics CMX200 and Varian Unity Plus 300. The majority of the study was done on the lower field spectrometer. Four probes have been used. These allow almost any combination of observation, cross polarisation and decoupling, with the use of appropriate filters. The only obvious limitation is the inability to decouple proton while observing fluorine, and also decoupling phosphorus, with the HFX probe. Recycle delays were initially determined by variable delay-time experiments and checked by measurement of appropriate relaxation times. For cross-polarisation experiments (nitrogen, carbon, phosphorus and some fluorine spectra), optimum contact times were found by arraying this parameter and choosing that with the greatest signal intensity.

Fluorine-{^{1}H} CRAMPS gave slightly better resolution than fast spinning direct/cross polarisation (with proton decoupling) for $(PhF_2PNMe)_2$. In all cases, however, the standard MAS experiments gave good ^{19}F spectra with sufficient resolution to be able to use deconvolution to extract shift, intensity and linewidth parameters, so that CRAMPS operation was not necessary.

The temperatures have been calibrated using data obtained from the proton spectra of methanol on TTMSS,[30] as described in the experimental chapter. In fast-spinning cases the calibrated temperature is significantly higher than the set temperature.

Spin rates were chosen so as to have an optimum number of spinning sidebands for analysis. The theory behind the choice of spinning speed has been described using the Cramér–Rao lower bounds, minimising this measure of the error as a function of spinning speed.[31] For shielding anisotropy, more reliable data are given from the optimum experiment which contains approximately five sidebands. However, the asymmetry parameter is more accurately determined from static experiments. The reliability of data for dipolar and first-order quadrupolar tensors was described as being best with slightly more data (up to 9 spinning sidebands).

Spinning sideband analysis was done using an in-house program, ssb97,[32] based on the theory of Maricq and Waugh,[33] which includes the error analysis of Olivieri.[34] The tensor components derived are defined according to the convention

$|\sigma_{33} - \sigma_{iso}| \geq |\sigma_{11} - \sigma_{iso}| \geq |\sigma_{22} - \sigma_{iso}|$,

with anisotropy, $\zeta = \sigma_{33} - \sigma_{iso}$

and asymmetry, $\eta = (\sigma_{22} - \sigma_{11})/\zeta$.

Between 5 and 11 peaks were fitted for the sideband manifolds analysed with spin rates of 4-9 kHz for fluorine and 2-5 kHz for phosphorus. The number of spinning sidebands observed depends on the choice of spinning speed, and, in the coupled cases, whether it is the 'stretched' or 'compressed' manifolds that are being measured. For these coupled cases, the ssb97m5 program will give the five parameters required; anisotropy, asymmetry, D', α and β; and an estimate of the error from an input of three sets of spinning sideband intensity data. The program uses the simplex fitting routine to get the first three parameters and will then optimise α and β for this combination. The R^2 value

is minimised for each individual spinning sideband intensity. However, the effective tensor values are initially calculated by simulating the static spectrum (as this is computationally faster and easier than complex numerical simulation of the MAS case) in order to obtain the shielding tensor components.

For the following reported results, α and β are the polar angles defining the internuclear vector (i.e. the direction of the D' tensor axis) in the principal axis system of the shielding tensor. Thus, β is the angle between D' and σ_{33}, and α is the angle from σ_{22} of the projection of $\mathbf{r}_{PF}$ in the σ_{11}-σ_{22} plane. Figure 2 can be used to illustrate the angles α and β quoted above. In fact, if β is 0°, α cannot be defined, as there will be no projection into the σ_{11}-σ_{22} plane (as the vector is along σ_{33}). However, the method used to calculate the angles means they are only accurate to within about 10° and therefore a value of zero simply indicates that the tensor lies close to the σ_{33} axis.

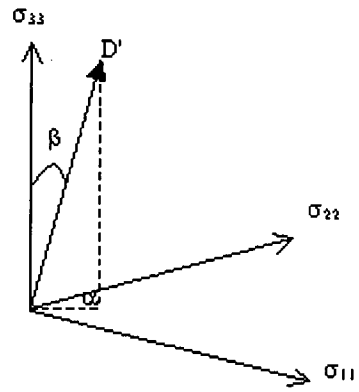

Figure 2. Orientation angles.

The simulation of experimental static bandshapes used a program RZX NMR analysis package with a visual interface 'd8'.[35]

Fluorine-19 spin-lattice relaxation times have been measured using the Torchia sequence,[36] i.e. via $^{1}H \rightarrow {}^{19}F$ CP followed by a 90° ^{19}F pulse, a variable delay and a 90° ^{19}F read pulse. Proton decoupling was applied during acquisition but not during the relaxation delay. In general, coupled spin systems will not yield single exponential plots for relaxation times. However, the present measurements generally showed reasonably single-exponential decay. Considering any random scatter in intensity measurements, the errors in the exponential fits do not indicate that the equations are

inappropriate for these cases. For proton spin-lattice relaxation times the pulse sequence consists of a 180 ° pulse on the proton channel followed by a variable delay, then a 90° ^{1}H pulse and contact to observe ^{31}P spectra. Spin-lattice relaxation in the rotating frame can be measured directly, via spin-lock on a single observe channel, or indirectly via cross-polarisation experiments with variable contact time or a pre-contact spin-lock. Measurements generally have statistical errors of ~2-8 %, with the larger values being for longer relaxation times, where the final points of the decay curve are not observed due to, for instance, limits on spin-lock time.

5.3. RESULTS AND DISCUSSION.

The published diffraction results[6] include both a monoclinic crystal (for the monomer) and a dimeric, triclinic crystal. In the triclinic case there are two independent molecules in the unit cell, but both have an inversion centre relating the two halves. This means that the asymmetric unit is essentially two half molecules. As will be discussed when interpreting the molecular symmetry implied by the solid-state NMR results, significant differences in bond lengths and angles are not observed even between the two molecules. Earlier publications describe the synthesis and crystal structure of the monomer in more detail.[37,38]

Powder XRD.

In order to confirm the identity of the sample of $(Ph_2FPNMe)_2$ (triclinic dimer or monoclinic monomer), a powder X-ray diffraction experiment was carried out and compared with the published single-crystal data in which the two different crystal forms are described (Figure 3).[6] When the patterns simulated from the published single-crystal data are compared with the experimental diffraction pattern it can be concluded that there is good agreement with the expected triclinic form, with all peaks present in the correct positions in the plot of intensity vs. 2θ. None of the calculated monoclinic peaks are present in the experimental pattern. Due to the method used (reflection off a thin layer of sample on a plate, rather than a capillary tube full of powder, through which an X-ray beam would be directed), the intensities are not expected to be exact for an organic molecule such as this, but this is the simplest method for identification of a known structure. As with the NMR spectra a small proportion of the powder XRD

peaks results from an impurity with considerably lower intensity (agreeing with neither of the structures of $(Ph_2FPNMe)_2$). Therefore, from acquisition of an X-ray powder diffraction pattern, it is possible to conclude (from comparison with the powder pattern predicted from the published single crystal results) that the sample used in this work is definitely the triclinic (dimeric) structure.

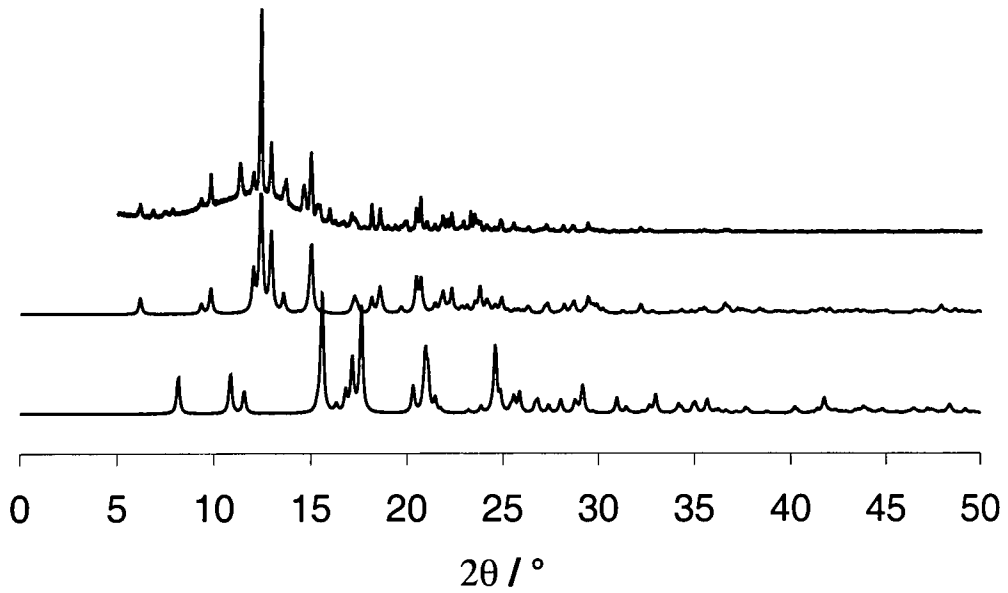

Figure 3. Powder XRD of $(Ph_2FPNMe)_2$ (Upper: experimental, middle: triclinic dimer, lower: monoclinic monomer),

General Features of ^{19}F and ^{31}P Spectra

Isotropic chemical shifts were established by variable spin-rate experiments. In all systems containing one or more fluorine atoms bonded to each phosphorus, the splittings arising from the directly bonded (P, F) coupling constant, $^1J_{PF}$, are clearly resolved. The identity and magnitude of the J splittings were confirmed by comparison of coupled spectra from each nucleus, together with P{F,H} and F{P} spectra. Table 2 gives a summary of chemical shift data for all the compounds studied, including comparisons with solution-state results from the literature. Several general observations can be illustrated by the simplest P-F case, $(Ph_2FPNMe)_2$. The phosphorus and fluorine spectra are shown in Figure 4 and Figure 5 respectively. It is clear that in each case only a single type of site exists for the relevant nucleus. The ^{15}N spectrum also seems to contain a single isotropic peak. Thus the crystallographic asymmetric unit appears to contain a single PF group. The published diffraction results[6] include both a monoclinic crystal (for the monomer) and a dimeric, triclinic crystal. In the latter case there are two

non-equivalent but centrosymmetric molecules in the unit cell. However, even with this case, significant differences in bond lengths and angles are not observed between the two molecules, which explains why we do not see separate NMR signals from them.

Compound	Chemical shift, δ / ppm				Observe ^{31}P $\lvert^1J_{PF}\rvert^b$ / Hz ± 20	Observe ^{19}F $\lvert^1J_{PF}\rvert^b$ / Hz ± 30
	^{31}P	^{19}F	^{13}C	^{15}N		
$(Ph_2FPNMe)_2$	-67.4 (-64.3)	-25.6 (-23.6)	31 ~132	-302	700 (689)	700 (689)
$(PhF_2PNMe)_2$ (trans)	-55.3 (-55.1)	-43.1 (ax) -78.2 (eq) (-63.6)[c]	27.8 128.4 132.6	-287	890[d] (865[d])	623 (ax), 1237 (eq)
$(^tBuF_2PNMe)_2$ (trans)	-39.3 (-39.5)		28.9 33.4 35.7 39.0		930[d] (925[d])	
$(F_3PNPh)_2$	-73.4 (-71.5[e])	-74.2 (-80.7[e]) low temp ca. -50[f] ca. -90[f]		-266	890[g] (922[e])	947 (922[e])

Table 2. Chemical shifts and coupling constants.[a]

[a] Solution-state data are given in brackets (from refs. 1, 7, 12 and 30).

[b] For the solid state the value quoted is derived from the splitting between the intense outer lines and may therefore involve $^3J_{PF}$ as well.

[c] Average for axial and equatorial fluorines.

[d] This is the average, $\frac{1}{2}|^1J_{PF}(ax) + {}^1J_{PF}(eq)|$.

[e] For $(F_3PNMe)_2$, from refs. 13 and 47.

[f] Separate values for axial and equatorial fluorines, from low-temperature spectra.

[g] Average value (from ambient temperature measurement; separate low temperature values cannot be resolved).

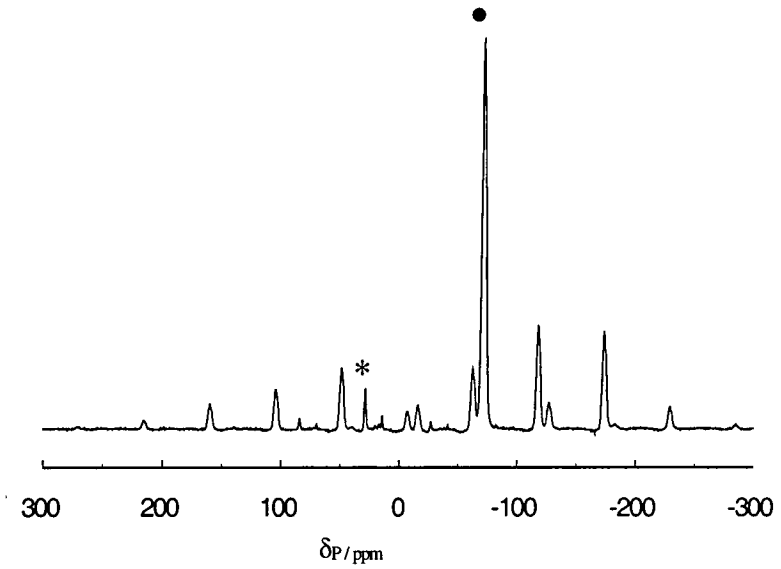

*Figure 4. ^{31}P Spectrum of $(Ph_2FPNMe)_2$ at 81 MHz. Cross-polarisation from protons and high-power proton decoupling were employed. The isotropic doublet is marked • and a phosphorus-containing impurity indicated by *. Contact time 5 ms, number of acquisitions 36, spin rate 4.5 kHz, recycle delay 30 s.*

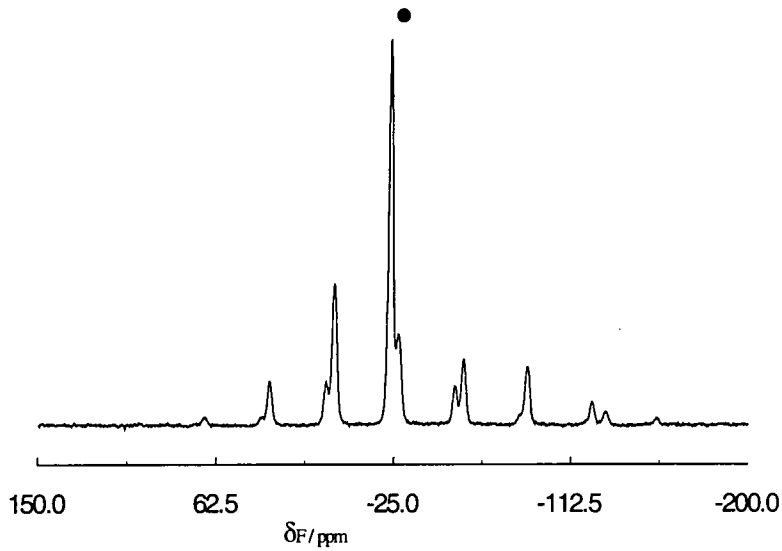

Figure 5. ^{19}F Spectrum of $(Ph_2FPNMe)_2$ at 188 MHz. Cross-polarisation from protons and high-power proton decoupling were employed. Contact time 1 ms, number of acquisitions 100, spin rate 6 kHz, recycle delay 30 s.

The spinning sideband manifolds are extensive in range, but isotropic shifts can be easily identified. The isotropic shifts are measured as δ_P = -67.4 ppm and δ_F = -25.6 ppm for $(Ph_2FPNMe)_2$, close to those reported for solutions. The coupling constant J_{PF} is 700 Hz (within experimental error of the solution-state value). This value of δ_F is low compared to those observed for the other compounds studied here and can therefore be assigned to an axial fluorine. This is consistent with the expected position of a single axial fluorine attached to trigonal bipyramidal phosphorus due to substituent electronegativity considerations, as well as with the solution-state value of -23.61 ppm.[6] In both ^{19}F and ^{31}P spectra there is an observable splitting arising from $^1J_{PF}$, though the intensities of the doublet components differ widely in each case. The long-range (P, F) isotropic coupling is not large enough (being 5.8 Hz in magnitude in the solution state[6]) to be observed within the resolution of these MAS NMR spectra. However, because the spin system involved is symmetrical,[39] the observed splitting may not be precisely $|^1J_{PF}|$ but may involve $|^3J_{PF}|$. Moreover, complications can arise from other couplings in the system.[39] Values of $^2J_{PP}$ for diazadiphosphetidines are significant, being in the range 20 to 140 Hz in magnitude in most cases[1,40] (and as high as 210 Hz for $(F_3PNMe)_2$)[12], but it is not feasible to take such couplings into account in analysis of the spectra. Further complexities occur in principle for centreband and spinning sideband shapes in MAS spectra arising from homonuclear dipolar coupling[41-45] but again these have been necessarily ignored given the linewidths observed, which are ca. 320 Hz for ^{31}P and ca. 480 Hz for ^{19}F. It may be noted that values for D_{PP} for diazadiphosphetidines are around 1 kHz and D_{FF} for the geminal fluorines in, for example, $(RF_2PNMe)_2$ is approximately 10 kHz. However, no splittings are visible in the spectrum arising from $^2J_{PP}$ or $^2J_{FF}$. Therefore, the effects of these dipolar interactions on spinning sideband intensities will be averaged away very effectively for D_{PP} and for cross-ring D_{FF}, which are much less than ζ. This means that the case of $(Ph_2FPNMe)_2$ is relatively straightforward, whereas complications arising from geminal D_{FF} may be significant for $(RF_2PNMe)_2$ and $(F_3PNPh)_2$.

When a second fluorine is introduced around the phosphorus there then exists the possibility of axial and equatorial differences. From the centreband peaks in the ^{19}F spectrum of $(PhF_2PNMe)_2$ it is clear that there are distinct axial and equatorial environments (Figure 6), though the crystallographic asymmetric unit evidently contains

a single PF_2 group. This is the first time separate data for axial and equatorial fluorines have been obtained for a symmetrical diazadiphosphetidine. The solution-state chemical shift is approximately midway between the two values found for the solid, as expected. The crystal structure[7] describes a trans configuration with a crystallographic centre of symmetry and the molecule contains a planar P_2N_2 ring. The NMR data are in agreement with this crystal structure. The J_{PF} coupling constants differ markedly in magnitude (by approximately a factor of two), depending on the position of the fluorine (the s character of the bond changes between equatorial and axial sites in a trigonal bipyramid), as can be seen from both ^{31}P and ^{19}F spectra. No additional splittings arising from $^2J_{FF}$ could be resolved in the ^{19}F spectrum. For distinct fluorine sites to be observable, the system must be towards the slow exchange limit, i.e. 'low temperature', at least below coalescence. For temperatures at which the available energy is sufficient to overcome the pseudo-rotation barrier, then average values for both chemical shift and indirect coupling constant would be observed. The single phosphorus isotropic shift shows a complex pattern arising from different couplings to axial and equatorial fluorine nuclei.

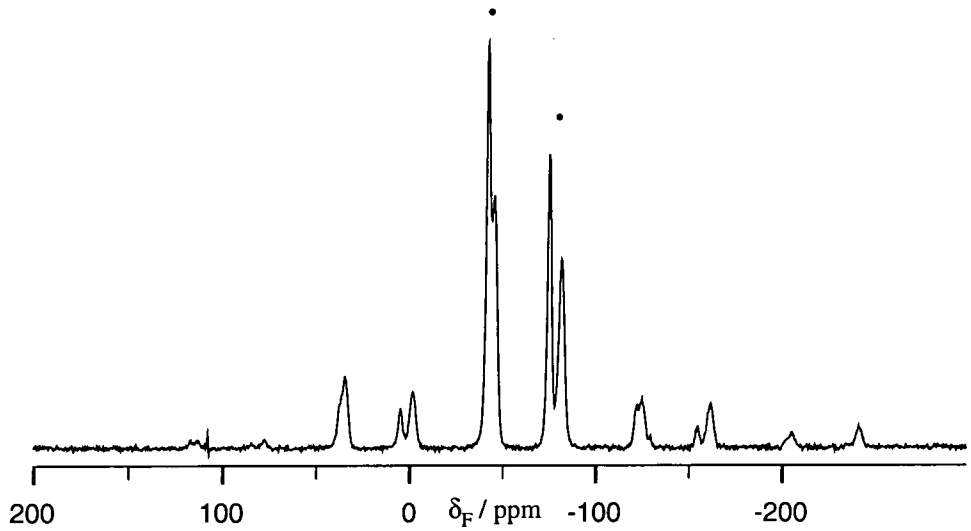

Figure 6. ^{19}F-{^1H} spectrum of $(PhF_2PNMe)_2$ at 188 MHz with cross-polarisation from protons. Centrebands marked • represent axial (high frequency) and equatorial (low frequency) fluorine signals.

Contact time 5 ms, number of acquisitions 64, spin rate 15 kHz, recycle delay 60 s.

For $(RF_2PNMe)_2$, R=Ph or Bu^t the spectral pattern for each nucleus is influenced by the state of the other. The coupling patterns are particularly complex in the phosphorus

region at the slow motion limit. The separation of the outer lines of the centreband is a sum of (P, F) coupling constants (see below). The mixing of states with the same Σm_F will cause the inner ^{31}P peaks, for example, to become unresolved. Both of these effects can be seen in the spectrum, of $(PhF_2PNMe)_2$ (Figure 7).

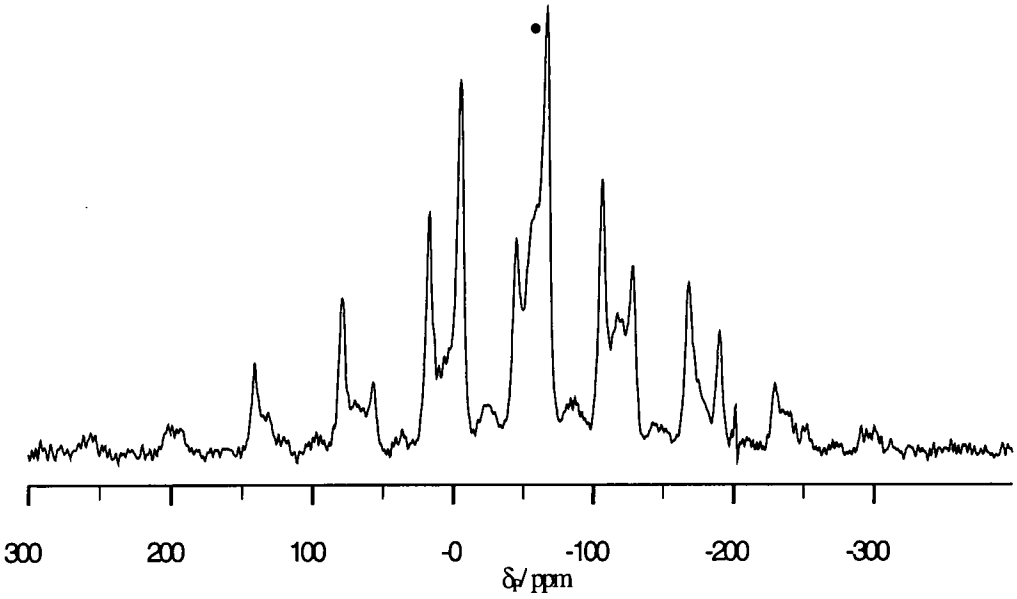

Figure 7. ^{31}P-{^1H} spectrum of $(PhF_2PNMe)_2$ at 81 MHz with cross-polarisation from protons each band showing complex coupling patterns.
Contact time 1 ms, number of acquisitions 180, spin rate 5 kHz, recycle delay 60 s.

Complete study of PF_2 systems will be much more reliable from the $(PhF_2PNMe)_2$ results. Although the phosphorus spectrum of $(^tBuF_2PNMe)_2$ is in obvious agreement with solution-state results, the fluorine spectrum is obscured by a decomposition product, such that extraction of any useful information is impossible. Attempts were made to carry out similar experiments to those for the other compounds and to recrystallise $(^tBuF_2PNMe)_2$ but neither was particularly successful with the quantity of sample available.

To represent the mixing of states more clearly we will take the general case of a PF_2 dimer. In principle, the spin system is of the type $[ABX]_2$. There are four F atoms which can each exist in either α or β states, and the sum of these spin states will determine whether any P transition is unique. With $\alpha\alpha\alpha\alpha$ and $\beta\beta\beta\beta$ the values of Σm_F are +2 and -2 respectively. No other combination gives this value, and these states

therefore give rise to the two intense outer ^{31}P transitions. There is no unique state representing Σm_F = -1, 0, +1, and therefore transitions involving these will form the mixed, unresolved central portion of the band. The total splitting of the outer lines can be seen to be $|^1J_{PFa} + {}^1J_{PFb} + {}^3J_{PFa} + {}^3J_{PFb}|$. In practice $|^3J_{PF}| << |^1J_{PF}|$, so the effect of cross-ring (P,F) coupling is likely to be small, as will the more complicated influence of $^2J_{PP}$ and $^2J_{FF}$. These two bond couplings can give rise to further complications for symmetrical spin systems such as are studied here.[46] Values of $^2J_{PP}$ are significant, being in the range 20-140 Hz in magnitude for diazadiphosphetidines.[1,40,47]

For $(F_3PNPh)_2$, we have obtained chemical shift values of δ_P = -73.4 and δ_F = -74.2 ppm. Observations suggest there is probably only one PF_3 group (half a molecule) in the crystallographic asymmetric unit. $|^1J_{PF}|$ measured from the fluorine spectrum (doublet at ambient probe temperature) is 947 Hz and an average value extracted from the phosphorus quartet is 890 Hz. The difference here will result in considerable part from the accuracy of separation measurement for the fairly broad lines. Solution-state data for comparison[12,48] are only available for $(F_3PNMe)_2$. Figure 8 and Figure 9 illustrate the effects of decoupling for $(F_3PNPh)_2$. The first shows the collapse of the phosphorus quartet (1:3:3:1 intensities over the complete manifold) to a singlet on application of fluorine decoupling. The effects of varying the frequency and power of the decoupling rf can also be monitored. In the case of $(F_3PNPh)_2$, the fluorine decoupling is efficient over a range of ± 5 kHz around the on-resonance fluorine frequency. Away from this the ^{31}P lines broaden, and at an offset of 40 kHz from the ideal frequency a distorted coupling pattern begins to be seen. The F{P} experiment is a novel one for the HFX probe, which is not normally used for fluorine observation. The close proximity of the proton and fluorine frequencies does not allow one to be observed while the other is being decoupled (in contrast to the situation with the specific HF probe) so that in many cases the fluorine spectrum would be broadened by proton interactions and would become featureless. However, in this case, we retain some resolution of $^1J_{PF}$ even in the absence of proton decoupling. Unfortunately there is also a significant fluorine background signal for this probe, but this does not interfere with the centreband region of the spectrum (which was already clearly identified in F{H} experiments).

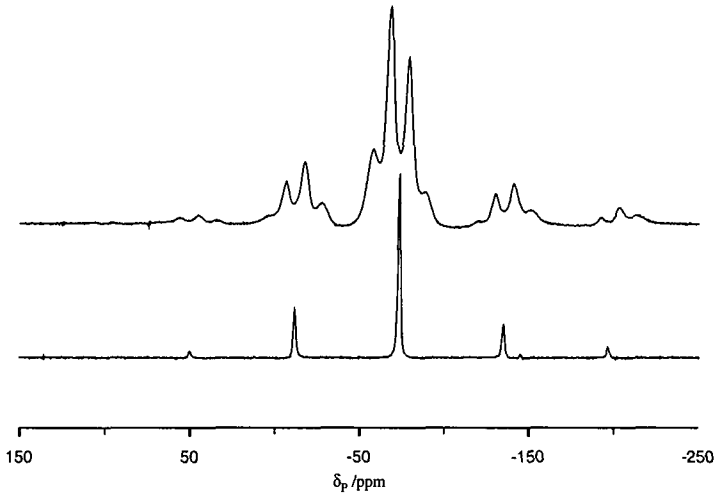

Figure 8. ^{31}P *spectrum of* $(F_3PNPh)_2$ *at 81 MHz: Upper spectrum {H}, lower spectrum {H,F}. Contact time 10 ms, number of acquisitions 360, spin rate 5 kHz, recycle delay 30 s.*

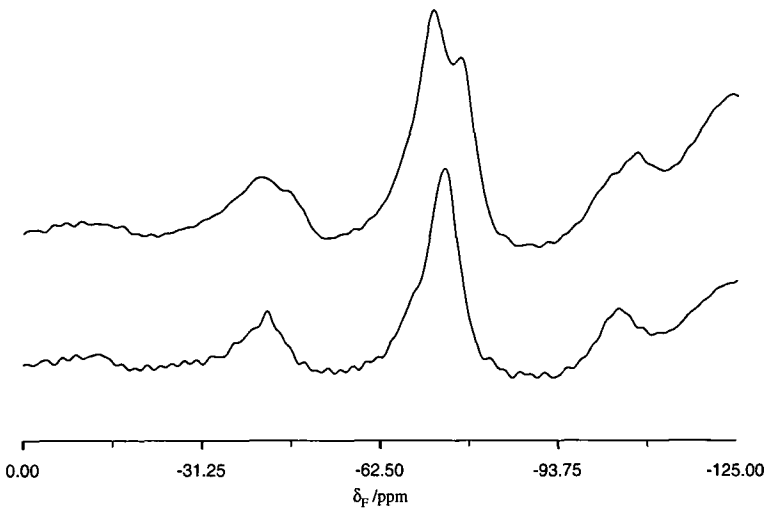

Figure 9. ^{19}F *spectrum of* $(F_3PNPh)_2$ *at 188 MHz: Upper spectrum (single resonance), lower spectrum {P} (to low frequency of -100 ppm, on the edge of the figure, is the broad probe background). Number of acquisitions 200, spin rate 4.1 kHz, recycle delay 5 s.*

Significant chemical shift differences are observed within the range of these molecules. Fluorine would be expected to have a deshielding effect on a phosphorus chemical shift, but in fact the reverse of this is seen when comparing the PF_2 and PF_3 cases. It is possible that axial and equatorial differences in the fluorine are complicating the effect, but it is also probable that the R groups on nitrogen are influencing the phosphorus shift.

Fluorine-19 and Phosphorus-31 Spinning Sideband Analysis.

Spinning sideband analysis has been carried out to determine shielding anisotropies and shielding asymmetries for both ^{31}P and ^{19}F. From the multiplet peaks there is the possibility to determine D' and thence ΔJ. The protocol used initially assumed colinearity of tensors. Use of just the two spinning sideband manifolds from the J_{PF} doublets is unable to deal fully with cases lacking colinearity since there are only 6 measurable effective tensor components in a doublet manifold, and 7 unknown variables (3 principal components of σ, D', $|J_{iso}|$ and two Euler angles relating D' to σ). However, ^{19}F decoupling gives a ^{31}P spinning sideband pattern that yields the principal components of σ immediately, so that the coupled spectrum can then be used to determine the remaining variables. In order to optimise the analysis the $^{31}P\text{-}\{^{19}F\}$ decoupled spectrum and the two spinning sideband manifolds of the coupled spectrum have been fitted simultaneously.[25,26] The computer program ssb97m5, developed in house,[32] was used for this 'triple fit' analysis. A complete set of single-fit anisotropy ($\zeta = \sigma_{33} - \sigma_{iso}$) and asymmetry ($\eta$) values is given in Table 3 and the following results can be used to illustrate the use of stretched and compressed manifolds[21] in determining dipolar interactions.

Compound	ζ_{eff} (η_{eff}) [σ_{11} - σ_{iso}, σ_{22} - σ_{iso}, σ_{33} - σ_{iso}][a]		
	Single fit of multiplet sidebands[b]		Single fit of decoupled spectra[c]
	^{31}P	^{19}F	^{31}P
$(Ph_2FPNMe)_2$	-265 (0.3) [231, 158, -202] -50 (0.8) [117, 77, 22]	-33 (0.8) [54, 26, -10] +108 (0.5) [-54, 2, 135]	-158 (0.7) [158, 143, -88]
$(PhF_2PNMe)_2$	-213 (0.9) [251, 50, -169] +160 (0.4) [-44, 16, 227]	+97 (0) [-6, -6, 138] (ax) -120 (1) [163, 46, -74] +96 (0) [26, 26, 172] (eq) +139 (0.6) [-32, 56, 221]	-156 (0.4) [169, 96, -100]
$(^tBuF_2PNMe)_2$	+119 (0.3) [-29, 10, 169] +229 (0.3) [-120, -57, 226]		+130 (0.6) [-61, 10, 169]
$(F_3PNPh)_2$ [d]	-50 (0) [82, 82, 7] +84 (0.7) [4, 55, 154] +120 (0.4) [-7, 44, 198] +163 (0.3) [-17, 31, 251]	-23 (0) [82, 82, 46] +34 (0.5) [49, 66, 110]	+100 (0.5) [-3, 49, 173]

Table 3. Tensor information.

[a] Data for ζ_{eff} and the (effective) tensor components are given in ppm. Note that the definitions (see text) imply switching of the effective components σ_{11} and σ_{33} depending on the position of σ_{22}, leading to a change of sign in ζ_{eff}. The statistical errors are ± 5 ppm in ζ_{eff} and ±0.1 in η_{eff}, but these are likely to be underestimates of the true errors.

[b] Effective anisotropies and asymmetries.

[c] True shielding anisotropies and asymmetries.

[d] Data for ambient probe temperature (fast axial ↔ equatorial exchange).

As well as the anisotropy values, is it also important to give the three principal components that define the anisotropic shielding. These are shown in the table, and it should be noted that slight changes in these values can give rise to a change in order with respect to the isotropic shielding, according to the convention defined. This will cause a change in the sign of ζ.

Crystal structures are known for these molecules, and, thus D can be calculated and, in principle, a value for the anisotropy in J can be extracted from D'. From the internuclear distances r_{PF}, the values of the dipolar interaction, D are known to be:

$(Ph_2FPNMe)_2$	r_{PF}	1.686 Å	D = 9560 Hz
$(PhF_2PNMe)_2$	axial r_{PF}	1.638 Å	D = 10430 Hz
	equatorial r_{PF}	1.578 Å	D = 11660 Hz

Results for $(Ph_2FPNMe)_2$:

For ^{31}P, effective anisotropies of the two separate spinning sideband manifolds are ζ_{eff} = -50 and -265 ppm (with η = 0.8 and 0.3 respectively). Analysis of the spinning sideband manifold of the decoupled spectrum shows that σ is asymmetric, indicating that colinearity of σ and **D'** is unlikely. A triple fit of the phosphorus spectra (two sideband manifolds for the coupled case and one for the ^{19}F-decoupled situation) gives ζ = -148 ppm, η = 0.4, D' = 10 kHz and β = 0° (within experimental error, leaving α essentially undetermined) . From D', the value of ΔJ = -1.2 kHz may be derived by using r_{PF} = 1.686 Å[6] (D = 9.6 kHz < D'). The estimated uncertainties in this result are mentioned below. The two values of ζ_{eff} show the stretching and compressing of the spinning sideband manifolds.[21] In the 'triple-fit' case, the error calculations show a significant improvement with the variation of α and β in comparison to calculations with the angles fixed at zero (at least an order of magnitude increase in R^2 is seen with angles fixed to zero). Therefore, although there is uncertainty in the actual values of D' calculated, the deviation from colinearity and the actual shielding anisotropy from the 'triple-fit' can be quoted with some confidence. However, the error in ΔJ will be significant, because of the method by which it is calculated. D' is often close to D, but in many of the calculations attempted it varied between values greater than or less than the value of D determined from r_{PF}, giving substantial differences in ΔJ. It must be concluded that significantly better quality data are required to obtain reasonable values of ΔJ, α and β. Triple-fit analysis can not be reported for the fluorine spectra, but single-fit results are given in Table 3. It may be noted here, as mentioned earlier, that for two fluorophosphates Grimmer and co-workers derived[22,49] values of +2500 and +3660 Hz for ΔJ.

The sense of tensor distortions of the stretched and compressed subspectra described above shows[21,22] the relative sign of D' and J. The logic can be followed with the case of the PF spin pair in $(Ph_2FPNMe)_2$. From the static phosphorus spectrum with both proton and fluorine high-power decoupling, one can determine that the shielding anisotropy is negative (in agreement with the triple fit to the spinning sidebands). This is opposite to the two-spin case discussed in the literature,[21] and as σ_{33} is the least shielded component, it will be the 'plus' subspectrum (relating to the $m_F = +½$ state) that is stretched. The spinning sideband manifolds of the fluorine-coupled spectrum show that this state constitutes the high-frequency transition of the doublet caused by (P,F) scalar coupling. Thus, J_{PF} is found to be negative, in agreement with the known sign, obtained from solution-state spectra. As is obvious from Figure 4 and Figure 5, the ^{19}F case (which clearly has the low-frequency sideband manifold stretched) is the reverse of the ^{31}P situation, which immediately suggests the true shielding anisotropy is positive as is in fact suggested by the single-fit analyses.

As an estimate of uncertainty in all these results, the measurement of intensity is subject to an error of around 5 % (depending on the signal to noise ratio) and where error calculation has been made, ζ is accurate to within ± 5 ppm. This error will be compounded for a calculation of D' to give a statistical uncertainty of up to 1 or 2 kHz (depending on which nucleus is being observed.) This will also apply to the other compounds studied, but is a minimum statistical error if all assumptions made are valid. This means that the determination of ΔJ as described above is very difficult.

Results for $(PhF_2PNMe)_2$:

Separate single fits of the fluorine-coupled phosphorus subspectra yield ζ_{eff} = -213 and 160 ppm with η_{eff} = 0.9 and 0.4 for the outer lines. These calculations relate to the sum of the influences of the two fluorines as explained above. Separate data sets are available for the axial and equatorial fluorines. The decoupled ^{31}P spectrum yields a value for the anisotropy of -156 ppm (≡ 12.6 kHz), which is similar to that for $(Ph_2FPNMe)_2$ and is of the same order as D_{PF}, thus explaining the significant intensity variations of the doublet components over the spinning sidebands. As for $(Ph_2FPNMe)_2$, the shielding tensor is asymmetric, underlining the fact that σ and **D** are not colinear. Unfortunately, a triple fit of the fluorine-coupled and decoupled

phosphorus spectra was not feasible. The two PF bonds are approximately 90° apart, introducing extra angular variables and so the true values cannot be extracted from the amount of experimental data measurable. Although in principle, the intensities of the outer lines of the coupled spectrum could be combined with the decoupled values, the triple-fit calculation includes the assumption that there is a single value of D' relating to the two fluorines, but given their axial and equatorial positions this is unlikely. This means that the triple-fit procedure is very much an oversimplification. There are two different dipolar directions for the axial and equatorial fluorines and in order to relate these values we would either need a second set of Euler angles or a direct angular relationship between the two D tensors.

As well as the chemical shift and J_{iso} values for the ^{19}F spectrum, we also have individual single fits of the four peaks. These values also indicate that the environments for the axial and equatorial fluorines are different. Again, because of the non-zero (and varying) asymmetry, the angles of the tensors with respect to the PF bonds are affected, as would be expected, by the nature of the bond.

The data and simulations for the single fits of the coupled and decoupled phosphorus spectra are shown in Figure 10.

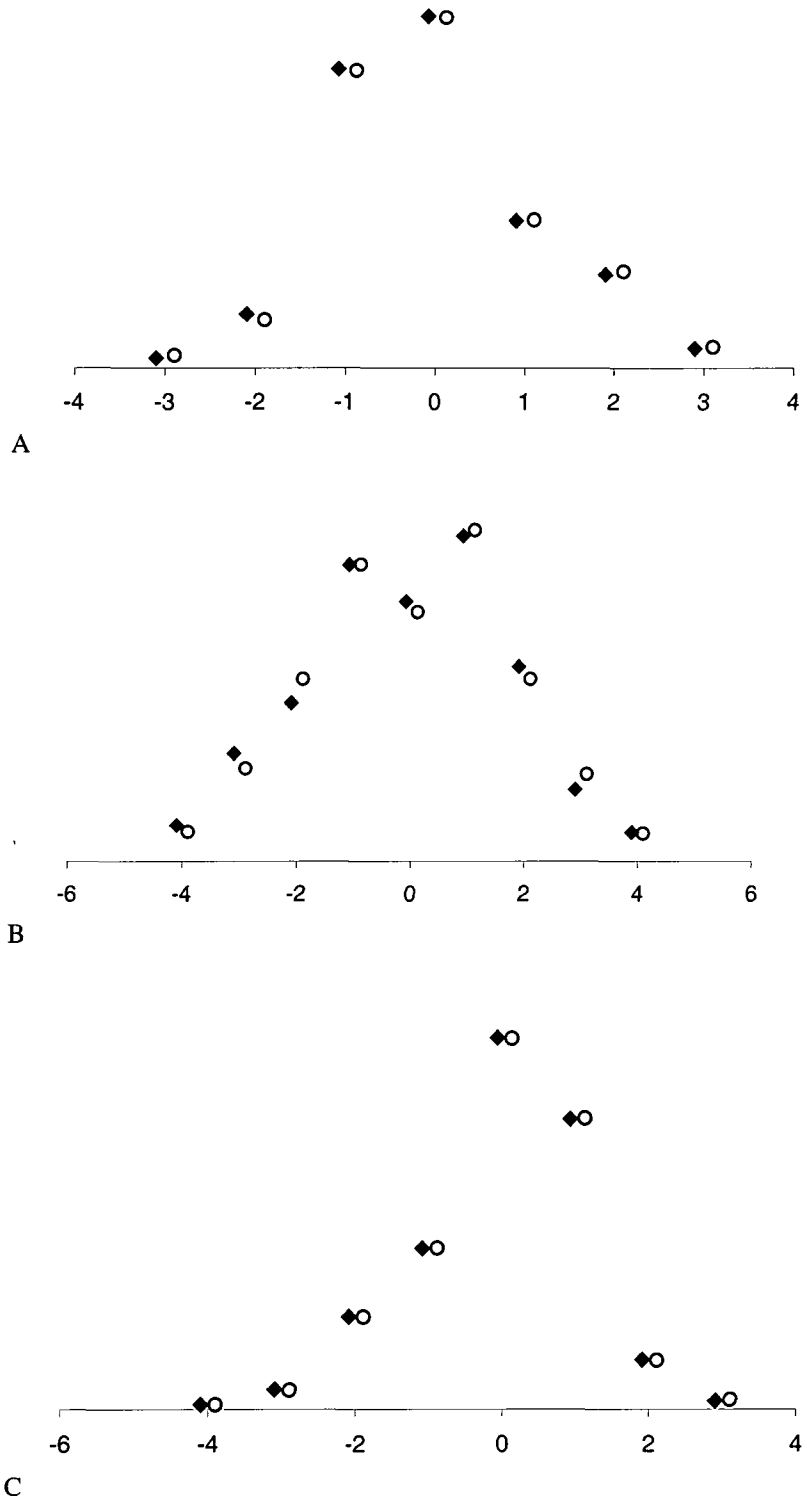

Figure 10. Spinning sideband analysis results for $(PhF_2PNMe)_2$: closed diamond - measured experimental intensity, open circle - simulated intensity. A, B - coupled doublet, C: decoupled singlet.

Results for (^{t}BuF$_2$PNMe)$_2$:

Individual single fits of three sideband manifolds (outer lines of the multiplet in the coupled phosphorus spectrum and the decoupled singlet), assuming colinearity of **D** and σ, give the two 'effective' and the 'actual' (central) anisotropy values, ζ = 119, 229 and 130ppm respectively. This is again a case where the D tensors will not have the same axis system as would be assumed in any triple-fit calculation.

The fluorine spectrum has proved too complicated to extract similar information from as there is an overlapping impurity which cannot be distinguished from the desired isotropic peaks and sidebands. None of the peaks observed is in exact agreement with the solution-state values. This is probably due to differing extents of averaging (as above) with no axial/equatorial distinction in the solution state, compared with separate resonances in the solid-state spectra. Therefore, comparison does not assist in selecting the appropriate frequencies and sideband manifolds.

Although there is no fluorine data for the ^{t}Bu compound, it is useful to compare the phosphorus results available for the two PF_2 compounds. There is a significant difference between the phosphorus chemical shifts, -55.3 and -39.3 ppm for Ph and ^{t}Bu respectively (this is also true for the solution-state values as indicated in Table 2). With regard to tensor values derived, anisotropy values are smaller in magnitude for the ^{t}Bu compound, and it appears that there is a change of sign of the actual anisotropy, which occurs when the order of components is reversed due to their position relative to the isotropic shielding. The separate shielding components for these two compounds show quite different patterns in both the coupled and decoupled spectra (particularly for the 'stretched' manifold). The different shielding properties of the ^{t}Bu and Ph groups are therefore having a dramatic effect on the spectra. It is also possible, due to steric and electronic considerations that the conformations of the two molecules are different.

Results for (F_3PNPh)$_2$:

For (F_3PNPh)$_2$ effective anisotropies from the manifolds of both the ^{31}P and ^{19}F spectra are given in Table 3. These results differ significantly from those of the other compounds but cannot be more fully analysed. This system proved too complex for the multiple fitting programme and therefore no results allowing non-colinearity were

derived. However, it would appear to be likely that both the ^{31}P and ^{19}F shielding anisotropies are smaller in magnitude than those for the other compounds.

Due to the non-axial symmetry found in the single fit results for these compounds it was decided to try to obtain the tensor orientations, and therefore values of D' so that ΔJ could be calculated from crystallographic distance measurements. However, it can be seen that the discrepancies in the calculations from the triple fit results are outside the expected accuracy and are therefore not reliable. There are several factors which could take account of this, including the complexities introduced because of the dimer system, subsequent cross ring interactions and the geminal coupling $^2J_{FF}$, and the extra variables introduced by a PF_2 system. The triple-fit was a natural progression from the results obtained for the simple single fits of effective anisotropy, but in these cases the earlier results appeared to be a more accurate representation of the systems.

Static ^{19}F and ^{31}P Spectra.

Static phosphorus spectra have been recorded (Figure 11, $(Ph_2FPNMe)_2$). Use of a Hahn echo sequence (with a delay times of 20 μs between the excitation, π and read pulses) produces an acceptable lineshape as it results in accurate recording of the start of the fast-decaying broad signals.

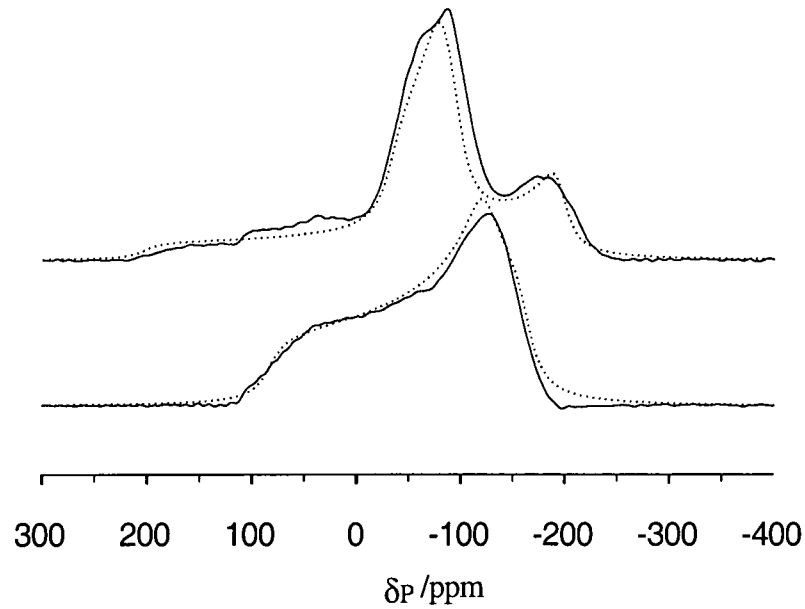

Figure 11. Static phosphorus spectra of $(Ph_2FPNMe)_2$ at 81 MHz. Upper - P{H}, Lower - P{H,F}. Solid line - experimental spectra; dotted line - simulated spectra.
Contact time 5 ms, number of acquisitions 360, recycle delay 30 s.

For $(Ph_2FPNMe)_2$ the ^{31}P-{H} spectrum shows the effects of $^{31}P,^{19}F$ dipolar coupling, with the overall shape consisting of two overlapping static subspectra. An impurity present in this sample was reduced in quantity by recrystallisation from toluene, but its signals are still visible, with isotropic shifts around 19 and 30 ppm. The discrepancy between 0 and 100 ppm in the coupled spectrum results from this remaining low-intensity impurity. A single band is obtained when fluorine decoupling is applied (in addition to proton decoupling). Shielding tensor results from static spectra are compared to those from spinning sideband analysis in Table 4. Since triple fitting was not computationally feasible for these static spectra (and therefore information on the mutual orientation of **D'** and σ was not obtained), Table 4 lists effective tensor parameters for the coupled case. However, comparison of the turning points for the coupled and decoupled spectra helps to link the components of the effective tensors. The simulated spectra are the best fits by eye to the observed spectra. Errors in the resulting parameters will therefore be larger than for iterative fitting of the MAS experiments. It was also mentioned above that, generally, shielding anisotropy is more accurately determined from spinning sideband analysis. A line broadening parameter of 800 Hz in the computation was needed to give a similar shape to the experimental results. This gives some idea of the magnitudes of broadening effects (e.g. dipolar interactions other than $^1D_{PF}$) for the compound.

	MAS	MAS, F decoupled [a]	Static	Static, F decoupled [a]
ζ_{eff}	-265 -50	-158	-265 -36	-150
η_{eff}	0.3 0.8	0.7	0 0.5	0.3

Table 4. Values of ^{31}P anisotropy $\zeta_{eff} = \sigma_{33} - \sigma_{iso}$ (asymmetry, η_{eff}) for $(Ph_2FPNMe)_2$. Errors from the MAS experiment are $\zeta \pm 5$ ppm, $\eta \pm 0.1$. Errors in the static simulation will be larger than for the spinning sideband analysis as the latter is a mathematical fit. Effective anisotropy is given when fitting outer lines of a coupled spectrum.

[a] True shielding anisotropy and asymmetry

The corresponding fluorine spectrum for this compound clearly consists of multiple lineshapes. The quality is not sufficient to provide accurate data for simulation.

As discussed above, the fluorine MAS spectrum of $(PhF_2PNMe)_2$ consists of two doublets (for axial and equatorial environments). The static lineshape consists of 4 overlapping static bands, with a stretched and compressed anisotropy, from $J_{P,F}$-split components for each of the fluorines (axial and equatorial). Approximate fitting by eye suggests the four static lineshapes have effective shielding anisotropy values of 97, 160, 97 and -140, in reasonable agreement with the MAS results, though those of -140 and 160 are about 20 ppm larger in magnitude than their counterparts from fitting of the spinning sideband manifolds. It is important to note that the spinning sideband analyses include an iterative fitting procedure, unlike the 'by-eye' simulation of the static lineshapes, for which the spinning results were used as an initial estimate. The individual values were altered from the MAS derived results by small increments until the sum of the 4 calculated lineshapes most accurately represented the observed spectrum.

Variable Temperature Spectra.

Changes with temperature are clearly illustrated (Figure 12) in the ^{31}P spectra of $(F_3PNPh)_2$. At ambient probe temperature all fluorines are equivalent and, on summing intensities of the multiplet peaks over the spinning sidebands of the phosphorus spectrum, one obtains a quartet of the expected ratio from coupling to three fluorines. Fast reorientation of the fluorine sites means that only the average shift and coupling constant are observed, as in solution. The splitting, $|^1J_{PF}|$, is one third of the remaining doublet splitting observed at low temperature, when the fluorines have become inequivalent (Figure 12). Because of the slower pseudo-rotation at low temperature, the axial and equatorial fluorine sites will show their individual chemical shifts, and coupling constants will no longer be averaged. The ^{31}P spectrum will then be significantly more complex, resulting in broadening of the central two lines of the quartet. However, the outer quartet lines, arising from $\Sigma m_F = \pm 3/2$, are unaffected and remain relatively sharp at all temperatures. The corresponding variable-temperature fluorine spectra show the equivalence at room temperature, then a broadening and separation into two broad bands for axial and equatorial sites in a 1:2 intensity ratio below ca. -80°C (Figure 13). The resolved doublet at the lowest temperature which

does not change significantly with temperature, is that of an impurity. On an absolute scale it stays at constant intensity and shape, becoming more prominent as the diazadiphosphetidine peaks broaden. Lower temperatures might be required to see any narrowing of the separated bands and resolution of the coupling patterns, although deconvolution of the two broad bands into doublets is possible. The coalescence temperature of the fluorine sites (ca. -40 °C) in $(F_3PNPh)_2$ provides an estimate of the rate constant for the axial-equatorial exchange process via Berry pseudo-rotation, namely 12000 s^{-1} from[50]

$k = \pi \delta\nu / \sqrt{2}$.

However, this assumes the low-temperature limit has been reached so that $\delta\nu$ (5400 Hz), the chemical shift separation at the lowest temperature studied, is the true value applicable for -40 °C (i.e. is temperature independent).

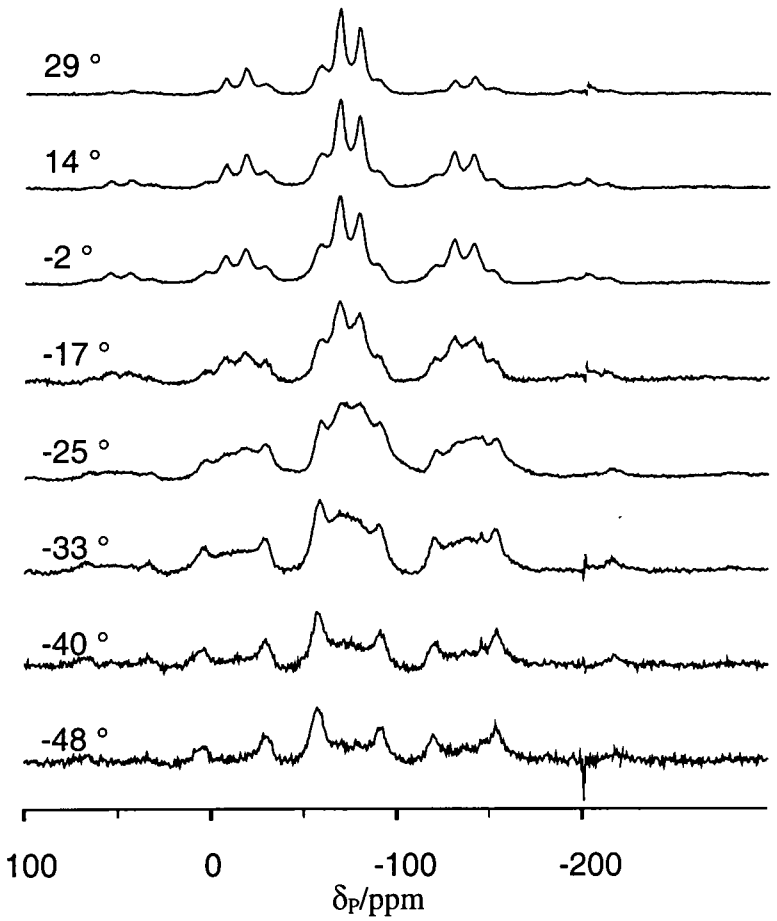

Figure 12. Variable-temperature ^{31}P spectra of $(F_3PNPh)_2$ at 81 MHz. Number of acquisitions 128, spin rate 5 kHz, recycle delay 20 s.

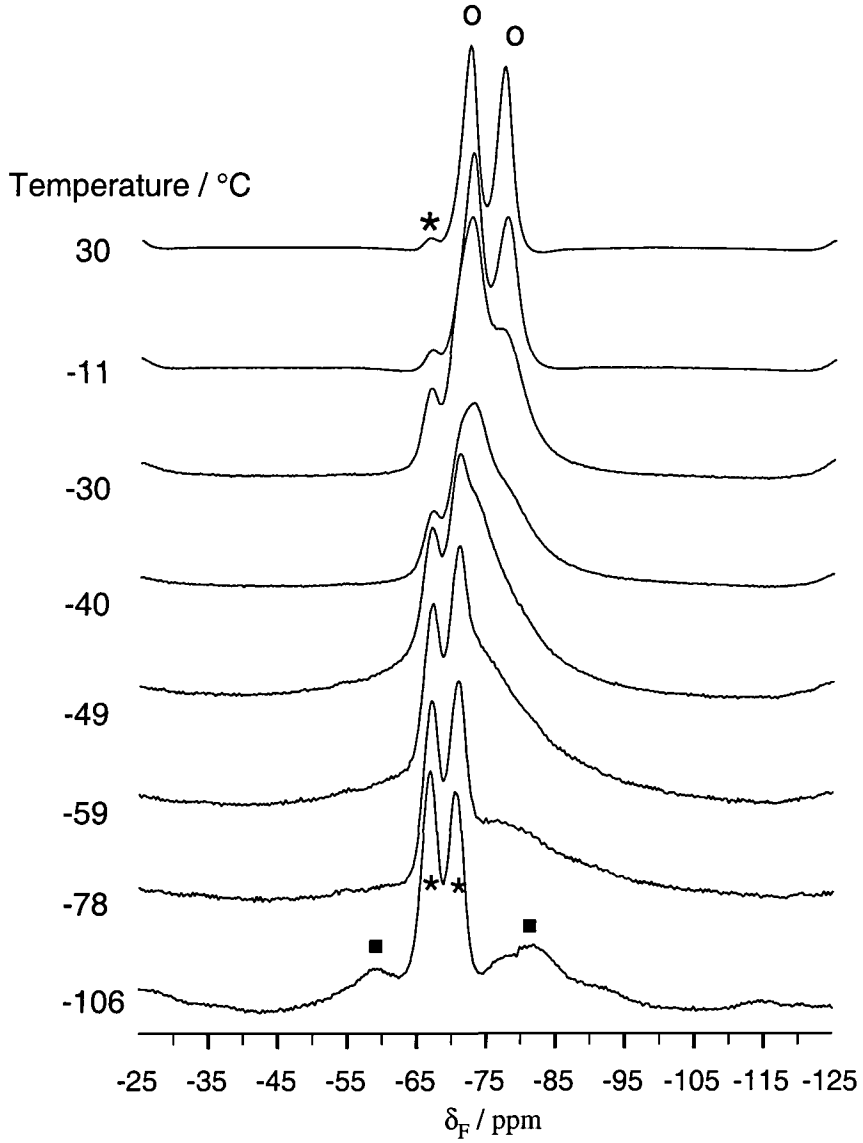

Figure 13. Direct-polarisation ^{19}F-{^{1}H} spectra of $(F_3PNPh)_2$ as a function of temperature. The vertical scales are plotted to equal maximum peak height. The doublet at -68 ppm is a constant-intensity impurity.
Number of acquisitions 16, spin rate 10 kHz, recycle delay 60 s, frequency 188 MHz. High-temperature doublet 'o', low-temperature bands '■', impurity doublet (where visible) ''.*

The variable-temperature experiments, and comparison of the different compounds at ambient temperature, show that different ranges of motion are accessed depending

highly on the substituents. The fully fluorinated compound has less restriction to F exchange via pseudo-rotation, which is also the case for small R groups on nitrogen. However, for $(PhF_2PNMe)_2$ the motion is already sufficiently slow at room temperature to enable the separate fluorine environments to be seen. The barrier is lower for PF_3 compounds because of the symmetry involved in the pseudo-rotation process in such cases. Table 5 summarises the information as to which compounds exhibit observable motional effects relative to the NMR timescale over the temperature range ambient to -120 °C .

Compound	Motion at ambient temperature	Motion at low temp (~-100 °C)
$(Ph_2FPNMe)_2$	-[a]	-[a]
$(PhF_2PNMe)_2$	Slow	Slow
[b] $(^tBuF_2PNMe)_2$	Slow (^{31}P)	^{19}F complex, slight broadening
$(F_3PNPh)_2$	Fast	Medium (two broad resonances)

[a] No information available since only a single ^{19}F site is observed.

[b] only the fluorine spectrum of this compound shows any broadening, and it has already been concluded that spectra observing this nucleus are not reliable.

Table 5. Motional effects relative to the NMR timescale.

Carbon-13 NMR Spectra.

Figure 14 shows the full and dipolar-dephased ^{13}C spectra of $(PhF_2PNMe)_2$, in the latter of which only the quaternary phenyl carbon and methyl signals remain. In order to help assignment and understanding of the carbon spectra, triple-channel techniques, including phosphorus-to-carbon cross-polarisation (with high-power proton decoupling), have been implemented. A variable amplitude (ramped) cross-polarisation sequence[51,52] was found to give a more intense signal than simple CP in a given amount of time because it does not rely so heavily on an accurate Hartmann-Hahn match condition. A contact time of 2 ms was sufficient, and the recycle delay of 360s took into account the long T_1 relaxation time of the phosphorus. Within the complex phenyl carbon region for $(PhF_2PNMe)_2$ a signal from carbon bonded to phosphorus appears as the single peak in the P-to-C cross-polarisation experiment. This peak has a chemical shift of 133 ppm, in agreement with the dipolar-dephasing spectrum. The carbon-13 chemical shifts are summarised in Table 2.

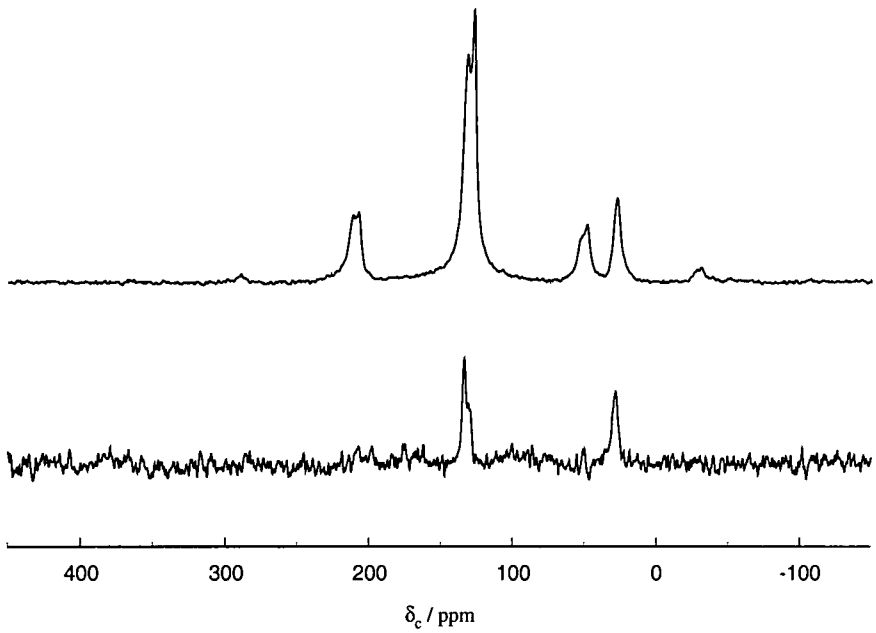

Figure 14. $(PhF_2PNMe)_2$ ^{13}C spectra - Upper - full; Lower - quaternary and methyl carbons.
Contact time 2 ms, number of acquisitions 180, spin rate 4 kHz, recycle delay 60 s, frequency 50 MHz.

Nitrogen-15 NMR Spectra.

The ^{15}N spectra proved to be difficult to acquire, and in some cases it has only been possible to obtain data using the variable-amplitude cross-polarisation sequence. The results and the spectral parameters are summarised in Table 6. The single peaks observed in all cases suggest the asymmetric crystallographic units contain a single N, though it is known not to be the case for $(Ph_2FPNMe)_2$. The Varian 300 spectrometer was used for $(Ph_2FPNMe)_2$ (see Figure 15), whereas the other ^{15}N spectra were run on the Chemagnetics CMX 200. Nitrogen-15 chemical shifts observed over the series of fluorodiazadiphosphetidines show variations depending both on the nature of the adjacent R group attached to nitrogen and on the number of fluorine substituents at phosphorus, increase in the latter causing deshielding. This can be compared to similar, general trends in the literature (for example, see reference 47) derived from solution-state measurements of other fluorinated and partially fluorinated nitrogen-containing compounds. Due to the problems with the sample described above, and further decomposition, it was not possible to record a nitrogen spectrum of $(^tBuF_2PNMe)_2$.

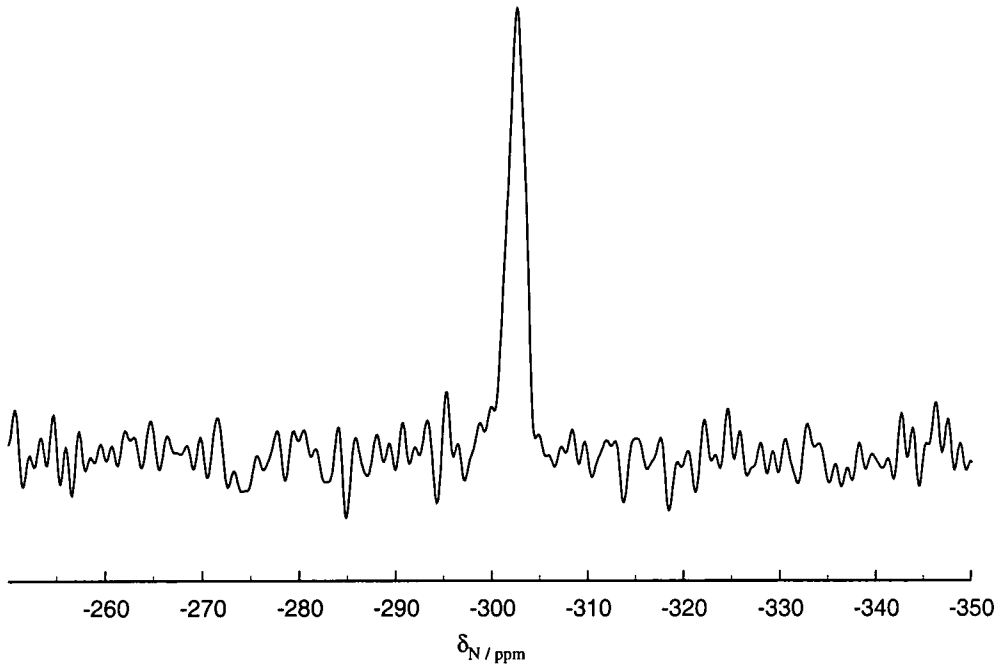

Figure 15. Nitrogen-15 spectrum of $(Ph_2FPNMe)_2$. Contact time 5 ms, number of acquisitions 2000, spin rate 4.4 kHz, recycle delay 30 s, frequency 30 MHz.

Compound	Pulse sequence	Contact time / ms	Number of acquisitions	Linewidth / Hz	$\delta\ 15_N$ / ppm
$(Ph_2FPNMe)_2$	CP	5	2000	66	-302
$(PhF_2PNMe)_2$	Ramp CP[a]	8	2000	200	-287
$(F_3PNPh)_2$	Ramp CP[a]	5	3300	80	-266

Table 6. ^{15}N chemical shift and spectral parameters.

[a]48 increments in proton CP power

Proton NMR Spectra.

In general, solid-state proton spectra are broad and featureless due to strong homonuclear broadening interactions. However, in favourable cases some resolution is observed and this can also be augmented by the use of multiple pulse sequences and/or rapid sample spinning.

$(Ph_2FPNMe)_2$ has a CRAMP spectrum with four broad resonances for the methyl and phenyl protons (highest frequency) at 1.3, 2.4, 5.3 and 7.6 ppm (Figure 16). The NMe signal is expected to be around 2.4 ppm. This rest of this spectrum is not entirely understood. The peak at 1.3 is not expected, and it is possible that the 5.3 ppm resonance is due the presence of the phosphorus shifting down an aromatic proton from the expected value of around 6 or 7 ppm. Comparing this with the solution-state data for the aromatic region, this seems unlikely.[6] However, comparison with solid-state results for the compound below suggests the 5.3 ppm peak could be 'real'. This sample was recrystallised from toluene, but as the impurity is still observed, at low intensity, in the phosphorus spectrum, it is possible that the four proton resonances are not purely from the expected compound.

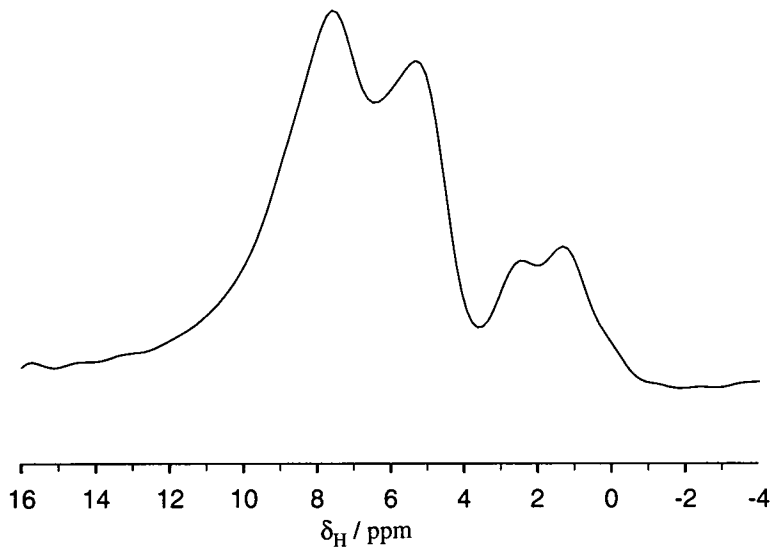

Figure 16. Proton CRAMP spectrum of $(Ph_2FPNMe)_2$.

Number of acquisitions 8, spin rate 1.47 kHz, recycle delay 30 s, frequency 200 MHz.

The broad single band observed in $(F_3PNPh)_2$ (for a simple MAS experiment) is centred around 5.6 ppm. No further resolution was observed with a multiple pulse sequence, which give a single peak at the same chemical shift (to within ± 0.2 ppm: good agreement considering the difficulties involved in peak picking exactly the broad resonances.)

Relaxation Times.

The techniques used to measure relaxation times are given in the experimental section. For T_1 measurements the X-spectrum was observed, with proton decoupling during acquisition. Plots of the decay of intensity characterised by the relaxation time included between 10 and 20 data points. The data discussed below are summarised in Table 7. The method of intensity measurement used to calculate the magnetisation decay will be a significant source of error in relaxation times. Depending on the observed spectrum, either peak height (if there is no overlap) or deconvolution to provide an integrated intensity is used. Intensities measured by both these methods are accurate to within about 2-8 %, the higher the noise level, the greater the inaccuracy. This statistical uncertainty of about 8 % will be the minimum error assuming stability of the spectrometer, negligible pulse imperfections and accurate representation of the lineshape over the whole experimental time. For $(Ph_2FPNMe)_2$, T_1^F is longer (64 s) than T_1^H (26 s) and hence cross polarisation from protons to fluorine gives a good signal in a shorter experiment time than direct polarisation, when observing the ^{19}F spectrum. The value of T_1^F was therefore measured via cross polarisation from protons, as described elsewhere, with proton decoupling during acquisition. For the variable contact time experiment, (H to P CP) the exponential rise gives T_{CP} = 0.33 ms. The decay would generally give $T_{1\rho}^H$, in this case, ~50 ms. However, when abundant nuclei are being observed, the decay with contact time may be a complex combination of parameters.[53] Observation of the spin-lock characteristics of the broad proton MAS spectrum directly also gives values for $T_{1\rho}^H$. The broad band is a combination of Me and Ph proton resonances and those for the latter decay much faster (have shorter $T_{1\rho}^H$) than those for the former. Deconvolution of the band into two broad resonances gave intensities fitting to values of 68 and 20 ms (for methyl and phenyl respectively). These values can only be taken as completely independent if spin diffusion is not effective. If spin diffusion is occurring efficiently it will cause an averaging of these values. However, presumably because MAS results in resolution in the ^1H spectrum, spin diffusion is not fully effective. In the solid state, overall molecular motion will be slow, but there may be fast reorientation of certain groups within a molecule. Figure 17 shows an example of the exponential fit to proton T_1 experiment intensity data for $(Ph_2FPNMe)_2$.

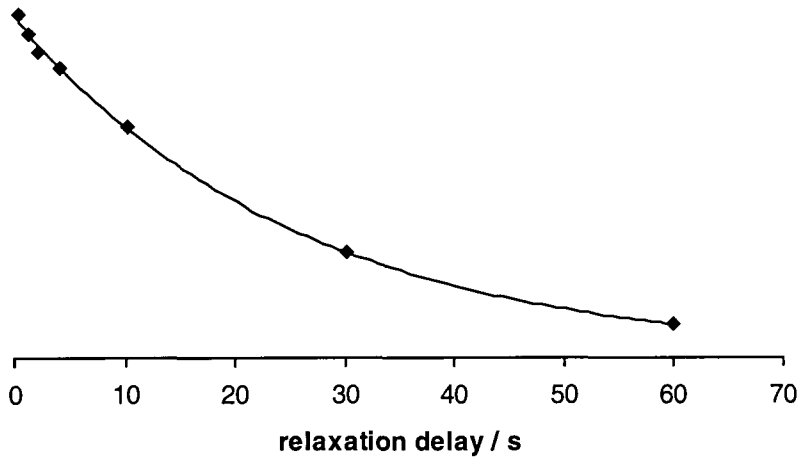

Figure 17. Proton T_1 data and exponential fit for $(Ph_2FPNMe)_2$.

In the $(PhF_2PNMe)_2$ case the two doublets for the axial and equatorial fluorines can be observed separately. For the proton T_1 similar values are obtained from the two fluorine resonances via ^1H inversion followed by CP, and an average time is appropriate. The error in the measured integrals and the similarity of the two plots (intensity vs. time) show that this is valid. The results for this compound are, fluorine T_1 156 s (axial) / 169 s (equatorial), proton T_1 24 s, proton $T_{1\rho}$ about 0.7 s. The accuracy of this last value is limited as the longest spin-lock time used was limited to around 50 ms.

Results for $(^tBuF_2PNMe)_2$ are a T_1^H of 1.5 s and a T_1^F of 13.5 s (both measured via cross polarisation to phosphorus using a pre-contact inversion stage). The exponential rise of the variable contact time experiment (H to P) shows a time constant of 2.4 ms, with a better fit being obtained by incorporating a second, smaller amplitude component of 0.2 ms. The lack of any signal decay after a 5 ms contact time indicates a long proton $T_{1\rho}$. The obvious fluorine impurity must however be remembered when interpreting this set of data.

The F_3 compound, which exhibits fast Berry pseudo-rotation around phosphorus on the NMR timescale at room temperature, has a short proton (NPh) spin-lattice relaxation time (2.5 s) and a very short T_1^F of 0.3 s. Other relaxation values for this compound are: a large value of $T_{1\rho}^H$ and a $^1H \rightarrow {}^{31}P$ CP rate constant of 1.3 ms.

There is close similarity between the T_1^H values for the two fluorinated compounds containing both PPh and NMe groups. This implies the effect of the NMe protons dominates due to their fast internal rotation. Somewhat surprisingly, the T_1^F values for the difluoro case are significantly longer than that for $(Ph_2FPNMe)_2$. However, that for $(F_3PNMe)_2$ is very short. The proton relaxation time for the ^{t}Bu compound is, however, very much shorter, probably because the ^{t}Bu protons are the most significant factor causing the relaxation. That for the PF_2Ph case is the largest. It can be seen that the relaxation times are not merely dependent on the number of fluorines in the molecule. All these measurements are at ambient probe temperature and therefore relate to mobility at ca. 26 °C. As relaxation times are dependent on the rate of any motion within a molecule, it is quite possible that with the differing dynamic effects the values are not directly comparable. At ambient temperature the measured data may represent the minimum or maximum values for a particular compound. The F_3 compound, which exhibits fast Berry pseudo-rotation around phosphorus on the NMR timescale at ambient probe room temperature, has a short proton (NPh) spin-lattice relaxation time.

Compound	T_1^H /s [a]	T_1^F /s	$T_{1\rho}^H$ /ms	T_{CP} /ms
$(Ph_2FPNMe)_2$	26	64	~ 50 [b] 68,[c] 20 [c]	0.33 [b]
$(PhF_2PNMe)_2$	24	156 (ax) 169 (eq)	ca. 700 [d]	
$(^tBuF_2PNMe)_2$	1.5	13.5 [e]	large	2.4 [b]
$(F_3PNPh)_2$	2.5	0.3	large	1.3 [b]

Table 7. Relaxation times.

[a] From $^1H \rightarrow {}^{31}P$ CP following ^1H spin inversion.

[b] From $^1H \rightarrow {}^{31}P$ CP variable contact time experiment.

[c] From proton-observe measurements.

[d] Estimate from a variable contact time $^1H \rightarrow {}^{19}F$ experiment.

[e] Although there are doubts in the fluorine spectrum, the phosphorus spectrum is sensible and therefore T_1^F derived from ^{19}F to ^{31}P cross polarisation should be reliable.

5.4. CONCLUSIONS

It has been found that the NMR data depend on the substituents at both the phosphorus and nitrogen positions, and that motional properties observed in solution-state NMR are slowed in the solid state, but can still be investigated. Axial and equatorial fluorine positions have been distinguished by (fluorine) chemical shift, effective shielding anisotropies and isotropic (J_{PF}) coupling for $(PhF_2PNMe)_2$ at ambient probe temperature.

The number of resonances observed in a solid-state NMR spectrum is related to the asymmetric unit of a structure. The spectra recorded for these compounds indicate that, despite being dimeric structures, only single ^{19}F, ^{31}P and ^{15}N environments are observed. Any multiplicity of lines can be explained by coupling or the loss of averaging of multiple fluorine sites. This is consistent with the reported crystal structure[6] of $(PhF_2PNMe)_2$. However, separate peaks are not seen for the two closely related, but independent molecules in the crystal structure[7] of $(Ph_2FPNMe)_2$.

Rates of motion within the molecule are affected by both substituents on the phosphorus and nitrogen in the ring. In the case of $(PhF_2PNMe)_2$ pseudo-rotation is shown to be slow on the NMR timescale in the solid-state since separate signals are seen for axial and equatorial fluorines. Motion, at the fast limit at ambient probe temperature, makes all three fluorine sites equivalent in the PF_3 compound. As motion is slowed by lowering the temperature, complex patterns are observed in the phosphorus spectrum because of coupling to non-equivalent fluorines (the fluorine situation is simpler as each fluorine is coupled to a single phosphorus and chemical shifts separate the individual environments as exchange is slowed). In this case only the sum of the coupling constants is measurable, as the separation of the outermost lines. Phosphorus-fluorine coupling has been removed in spectra of both nuclei by high-power heteronuclear decoupling and has confirmed that PF indirect coupling is the cause of the splitting.

Although linewidths are substantially larger than for solutions, the solid-state chemical shifts are in agreement with the previous solution-state experiments. This is true of the averaged chemical shifts when there are separate peaks, i.e. in the slow exchange limit,

for the solid state. Thus there appear to be no chemically significant intermolecular interactions in the solid compounds.

Valuable information can be obtained from anisotropies, as measured from spinning sideband manifolds or static spectra, in terms of the effective dipolar interaction. In general, D and ΔJ are not readily mathematically separable, but in cases where crystal structure information is available D can be determined, giving a route to the anisotropy in J (though not to high accuracy).

The ^{13}C and ^{15}N spectra give additional information. Interpretation of carbon spectra has been aided by the use of unusual experiments (^{31}P to ^{13}C cross polarisation) and by calculations of predicted chemical shifts from previous studies and databases.

Measurements of proton relaxation times have provided information on molecular mobility of the compounds in the solid state.

REFERENCES

[1] R.K. Harris, M.I.M. Wazeer, O. Schlak, R. Schmutzler, *J. Chem. Soc. Dalton*, 1976, 17.

[2] R.K. Harris, M.I.M. Wazeer, O. Schlak, R. Schmutzler, *J. Chem. Soc. Dalton*, 1974, 1912.

[3] O. Schlak, R. Schmutzler, R.K. Harris, M. Murray, *J. Chem. Soc. Chem. Comm.*, 1973, 23.

[4] O. Schlak, R. Schmutzler, I.K. Gregor, *Org. Mass Spect.*, 1974, **9**, 582.

[5] A. Almenningen, B. Andersen, E.E. Astrup, *Acta Chem. Scand.*, 1969, **6**, 2179.

[6] R.K. Harris, M.I.M. Wazeer, O. Schlak, R. Schmutzler, W.S. Sheldrick. *J. Chem. Soc. Dalton*, 1977, 517.

[7] P.G. Jones, R. Schmutzler, *Phosphorus, Sulfur, and Silicon,* 1991, **56**, 173.

[8] R. Schmutzler, G.S. Reddy, *Inorg. Chem.*, 1965, **4**, 191.

[9] R. Schmutzler, in *Halogen Chemistry*, ed. V. Gutmann, Academic Press, London 1967, **2**, 31.

[10] C.Shumann, H. Dreeskamp, O. Stelzer, *Chem. Comm.*, 1970, 619.

[11] R.K. Harris, J.R. Woplin, R.E. Dunmur, M. Murray, R Schmutzler, *Ber. Bunsen-Gesell*, 1972, **76**, 44.

[12] R.K. Harris, C.M. Woodman, *Mol. Phys.*, 1966, **10** (5), 437.

[13] R. S. Berry, *J. Chem. Physics*, 1960, **32**, 933

[14] R.K. Harris, M.I.M Wazeer, O. Schlak, R. Schmutzler, *Phosphorus, Sulfur and Silicon,* 1981, **11**, 221.

[15] D.P. Burum, W.K. Rhim, *J. Chem. Phys.*, 1979, **71**(2), 944.

[16] U. Scheler, R.K. Harris, *Chem. Phys. Lett.*, 1996, **262**, 137.

[17] S.F. Dec, C.E. Bronniman, R.A. Wind, G.E. Maciel, *J. Magn. Reson.*, 1989, **82**, 454.

[18] S.A. Carss, U. Scheler, R.K. Harris, P. Holstein, R.A. Fletton, *Magn. Reson. Chem.*, 1996, **34**, 63.

[19] R.K. Harris, S.A. Carss, R. D. Chambers, P. Holstein, A.P. Minoja, U. Scheler, *Bull. Magn. Reson. A,* 1995, **17**, 37.

[20] S. A. Vierkötter, *J. Magn. Reson. A,* 1996, **118**, 84.

[21] R.K. Harris, K.J. Packer, A.M. Thayer, *J. Magn. Reson.*, 1985, **62**, 284.

[22] U. Haubenreisser, U. Sternberg, A.R. Grimmer, *Mol. Phys.*, 1987, **60**,151.

[23] A.R. Grimmer, U. Haubenreisser, *J.Fluo. Chem,*, 1985, **29**, 244.

[24] K.W. Zilm, D.M. Grant, *J. Am. Chem. Soc.*, 1981,**103**, 2913.

[25] J.C. Cherryman, R.K. Harris, *J. Magn. Reson.*, 1997, **128**, 21.

[26] J.C. Cherryman, R.K. Harris, M.G. Davidson, R.D. Price, *J .Brazilian Chem. Soc.*, in press.

[27] R. Schmutzler, *J. Chem. Soc. Dalton*, 1973, 2687.

[28] J.S.O. Evans, Personal communication.

[29] Cerius 2 Software MSI Ltd.

[30] A. E. Aliev, K. D. M. Harris, *Magn. Reson. Chem.*, 1994, **32**, 366.

[31] P. Hodgkinson, L. Emsley, *J. Chem. Phys*, 1997, **107**, 4808.

[32] J.R. Ascenso, L.H. Merwin, H.-P. Bai, J.C. Cherryman. Unpublished work.

[33] M.M. Maricq, J.S. Waugh, *J. Chem. Phys.*, 1979, **70**, 3300.

[34] A.C. Olivieri, *J. Magn. Reson A.*,1996, **123**, 207.

[35] Provided by E. Hughes

[36] D.A. Torchia, *J. Magn. Reson.*, 1978, **30**, 613.

[37] G.W. Adamson, J.C.J. Bart, *Chem. Comm.*, 1969, 1036.

[38] G.W. Adamson, J.C.J. Bart, *J. Chem. Soc. (A),* 1970, 1452.

[39] R.K. Harris, M.I.M. Wazeer, *Ber. Bunsenges. Phys. Chem.,* 1979, **83**, 697.

[40] R.K. Harris, M. Lewellyn, M.I.M. Wazeer, J.R. Woplin, R.E. Dunmur, M.J.C. Hewson, R Schmutzler, *J. Chem. Soc. Dalton*, 1975, 61.

[41] S. Hayashi, K. Hayamizu, *Chem. Phys. Lett.,* 1989, **161**, 158.

[42] G. Wu, R.E. Wasylishen, *J. Chem. Phys.*, 1993, **98**, 6138.

[43] R. Challoner, T. Nakai, C.A. McDowell, *J. Magn. Reson.*, 1991, **94**, 433.

[44] S. Dusold, A. Sebald, *Mol. Phys.,* 1998, **95**, 1237.

[45] E. Klaus, A. Sebald, *Angew. Chem.* 1995, **34**, 667.

[46] R.K. Harris, M.I.M. Wazeer, *Ber. Bunsenges. Phys. Chem.,* 1979, **83**, 697.

[47] S. Berger, S. Braun, H.-O. Kalinowski. *NMR Spectroscopy of the Non-metallic Elements.* Wiley, 1997.

[48] R Schmutzler, *Chem. Comm,* 1965, 19.

[49] A.R. Grimmer, U. Haubenreisser, *J.Fluo. Chem,,* 1985, **29**, 244.

[50] J. Sandstrom. *Dynamic NMR spectroscopy.* Academic Press, 1982.

[51] O.B. Peerson, X. Wu, I. Kustanovich, S.O. Smith, *J. Magn. Reson. A.* 1994, **106**, 127.

[52] G. Metz, X. Wu, S.O. Smith, *J. Magn. Reson. A*, 1994, **110**, 209.

[53] S. Ando, R.K. Harris, S.A. Reinsberg, *J. Magn. Reson.* In press.

6. Chlorinated diazadiphosphetidines

6.1 Introduction

The previous chapter consisted of a discussion of a series of fluorinated diazadiphosphetidine compounds. Complementary information is gained, for example phosphorus chemical shifts, and other interesting effects are also observed in compounds with chlorine substituents. As the change of halogen substituent means that many different effects are observed it is appropriate to discuss these systems separately. Two fully chlorinated diazadiphosphetidines, with the postulated formulae $(Cl_3PNCH_2CH_2Cl)_2$ and $(Cl_3PNMe)_2$, have been studied. There is slightly less scope in terms of the number of nuclei that can be easily observed, to obtain structural information directly, as we no longer have ^{19}F NMR available. The interaction between the phosphorus and chlorine is more complex than that with fluorine, because of the high natural abundance quadrupolar isotopes (^{35}Cl - 75.53% abundance and ^{37}Cl - 24.47%), both spin-3/2. Simple multiplets from isotropic indirect spin-spin coupling are not observed, but line distortion effects can result from residual dipolar coupling. This can cause splitting into multiplets which are often unsymmetrical. These effects may also be unresolved depending on the ratio of the strength of the field and/or efficiency of self-decoupling, in which case a broad, asymmetric lineshape may be observed. The origin of splittings or complex lineshapes can be identified by running spectra at different field strengths.

Similarly to the fluorinated compounds, the effect of temperature on the motion in the molecule, i.e. Berry pseudo-rotation of the chlorine, is of interest. In this case, there may be inequivalence of the chlorine nuclei at low temperature, or improved self-decoupling (of the P-Cl dipolar interaction) at high temperature where there is fast motion, which will result in changes in the variable temperature spectra. The differing substituents on the nitrogen affect the properties of both the nitrogen and the phosphorus. The carbon spectra of the substituent groups have also been investigated.

6.2. Results and discussion

6.2.1 PHOSPHORUS-31 SPECTRA

The ^{31}P spectra of these compounds consist of a single centreband with the shielding anisotropy observed as a set of spinning sidebands. This implies that the asymmetric unit probably contains a single phosphorus (i.e. half the molecule). The linewidth and lineshape will be discussed later along with variable temperature studies. The larger, chlorine-containing side chains on nitrogen in $(Cl_3PNCH_2CH_2Cl)_2$ (compared with the methyl groups) will have an effect on its magnetic properties, although the phosphorus is too remote to also be affected in terms of shielding by the additional chlorine on the nitrogen. The substituents will also affect the possible motion of the chlorine atoms bonded to phosphorus due to molecular packing effects. Although larger groups may at first imply more restricted motion arising from intramolecular steric interactions, it is possible that the Berry pseudo-rotation around the phosphorus will have lower steric hindrance as the linear side chains force neighbouring molecules into a more open crystal packing arrangement.

When the phosphorus shifts are compared with those from the fluorinated compounds (Table 1), it can be seen that the chlorine compounds are more shielded. The same trend is observed for other five co-ordinate compounds such as $X_3P(C_6H_5)_2$ where δ_P = -65 and -30 ppm for X=Cl and F respectively.[1] More importantly, it is known[2] that increasing the number of chlorines in a symmetrical compound of general formula $(F_mCl_{3-m}PNMe)_2$ causes a shift to higher frequency, with a sudden drop, to a lower frequency than the initial PF_3 value, when PCl_3 is reached. Therefore, the variations in chemical shift for the diazadiphosphetidines reported in this thesis are as expected. The chlorinated compounds discussed in the present chapter are the m=0 case, but with differing substituents on nitrogen. The solution-state phosphorus shift for $(Cl_3PNMe)_2$, after converting values because of the different reference scale, is -78.2 ppm, which is in good agreement with the value observed here, so there are evidently no significant changes in molecular structure with phase. Replacement of Me with CH_2CH_2Cl seems to have no observable effect on the chemical shift, but does alter the lineshape, as will be discussed below.

Compound	δ_P / ppm
$(Cl_3PNMe)_2$	-78.9
$(Cl_3PNCH_2CH_2Cl)_2$	-78.9
$(Ph_2FPNMe)_2$	-67.4
$(PhF_2PNMe)_2$	-55.3
$(^tBuF_2PNMe)_2$	-39.3
$(F_3PNPh)_2$	-73.4

Table 1. Comparison of phosphorus chemical shifts.

Spinning sideband analysis was carried out using the ssb97 programme.[3] The anisotropy is given according to the definition $\zeta = \sigma_{33} - \sigma_{iso}$, and is accurate to within ±3 ppm. The small difference in sideband intensities can be seen when spectra of the two compounds are overlaid (Figure 1 - this figure shows spectra at a slightly slower spinning speed to those used in the calculations as they illustrate the differences more clearly than those used for analysis, where sidebands are more separated), but due to the broad lines of the methyl compound, some overlap of intensities may occur and the outer sidebands, on which the accuracy of the spinning sideband analysis depends, will not be as distinguishable from the noise.

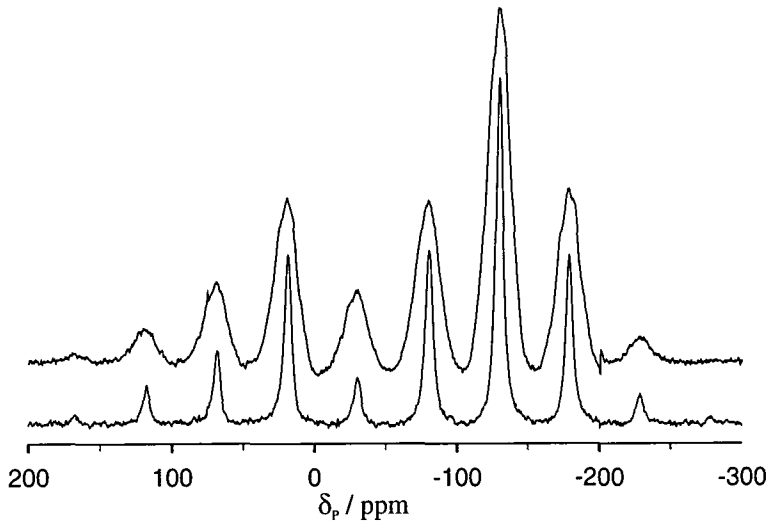

Figure 1. Phosphorus-31 spectra (81 MHz) at 4kHz spin-rate. Upper - $(Cl_3PNMe)_2$, Lower - $(Cl_3PNCH_2CH_2Cl)_2$. Cross polarisation from protons, contact time 5 ms, recycle delay 60 s, 16 acquisitions.

A comparison of the actual (from integration) and simulated spinning sideband intensities for the methyl compound is shown in Figure 2.

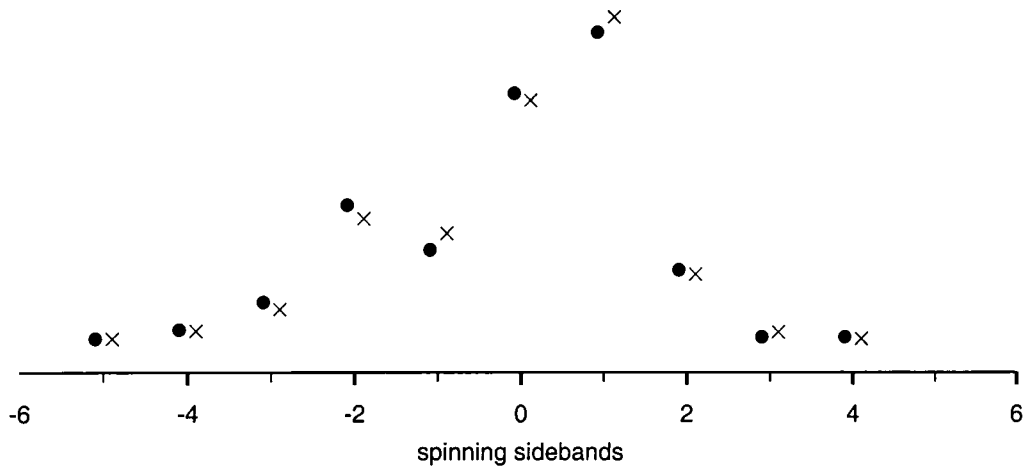

Figure 2. Comparison of sideband intensities for the phosphorus spectrum of $(Cl_3PNMe)_2$. Spin rate 5 kHz. Filled circles indicate experimental (integrated) intensity and crosses represent the simulated data.

These results show anisotropy values (ζ) of -190 and -200 ppm with asymmetry, $\eta = 0$ (errors ± 3 ppm and 0.05 respectively, which implies that axial symmetry can be assumed), (Table 2). The 'sum of difference squared errors' are 7 and 10 for the methyl and CH_2CH_2Cl compound respectively.

Compound	^{31}P		
	δ / ppm	ζ / ppm	η
$(Cl_3PNMe)_2$	-78.9	-190	0
$(Cl_3PNCH_2CH_2Cl)_2$	-78.9	-200	0

Table 2. Results of spinning sideband analyses.

These anisotropy values are larger than those for the fluorinated compounds, indicating a higher orientational dependence. Also, to within experimental error, there is no deviation from axial symmetry.

Comparison of phosphorus static lineshapes and spinning sideband analysis has been made. Results from phosphorus spinning sideband analysis can be used to simulate a static lineshape which compares with the experimental spectrum as shown below (Figure 3). Changing the parameters, from those derived from spinning sideband analysis, did not give any improvement to the fit.

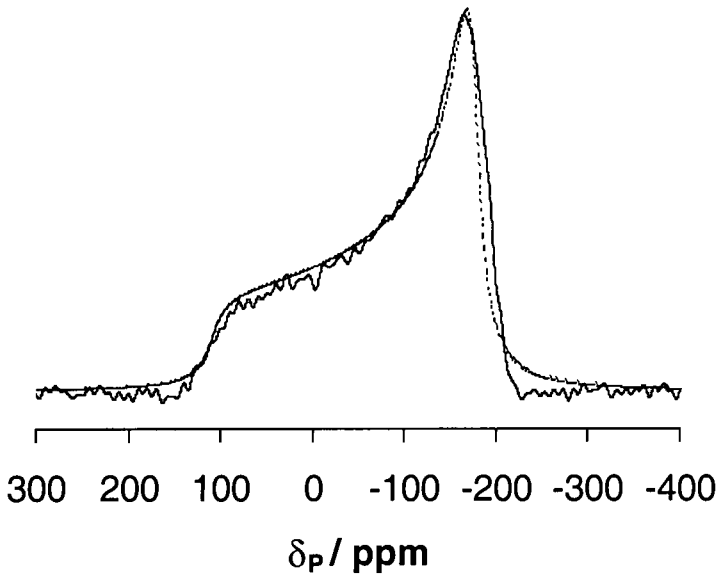

Figure 3. Static phosphorus spectra of $(Cl_3PNCH_2CH_2Cl)_2$ at 81 MHz. Solid-experimental (cross-polarisation from protons, contact time 5ms, recycle delay 100 s, 56 acquisitions), dotted-simulated

An echo sequence was not used, so it is probable that the slight discrepancy is due to lineshape distortion resulting from missing the first data points. In order to fit the experimental data, a 'line broadening' factor of 2000 Hz was applied to the simulated spectrum. This value, which converts the ideal lineshape, showing only effects of shielding anisotropy and asymmetry, into one comparable with the observed spectrum gives an idea of the magnitude of any broadening mechanisms that affect the experimental static lineshape. Although no splittings are observed in the phosphorus spectrum (the static spectrum fits to a single lineshape), heteronuclear interactions with chlorine and nitrogen, and possibly homonuclear P-P interactions, will cause significant broadening. As the effects of nitrogen heteronuclear or phosphorus homonuclear broadening are not particularly evident in the analogous fluorine compounds it seems

highly likely that there is a significant effect from the chlorine. There is little noticeable effect on the static ^{31}P spectra with and without the application of high-power proton decoupling (Figure 4). A very slightly broader line is observed in the absence of proton decoupling, suggesting that more dominant interactions are defining the lineshape.

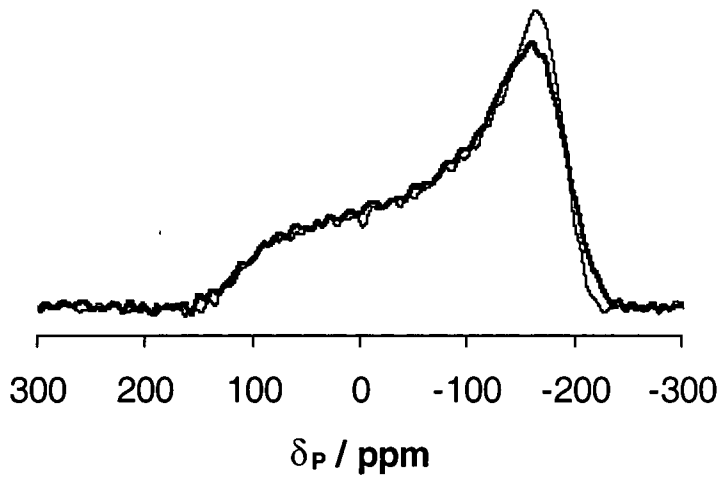

Figure 4. Static spectra of $(Cl_3PNCH_2CH_2Cl)_2$ at 81 MHz. Thin line - $^{31}P\{^1H\}$, thick line - ^{31}P (no proton decoupling).

Despite linewidth differences in MAS spectra of the two chlorinated compounds, at room temperature the static phosphorus spectra appear almost identical.

Quadrupolar effects play an important role in the spectra of the P-Cl compounds. The broadening observed in the phosphorus spectrum is most likely to result from coupling to chlorine, although no splitting or structure is resolved. In the case where motional averaging takes place, for example at high temperature, narrowing of the spectrum can occur.[4] The existence of splittings (residual dipolar, dipolar or indirect spin-spin) depends on the lifetimes of the quadrupolar spin states in comparison to the frequency separations in the spin-½ spectrum. If spin-lattice relaxation times of the quadrupolar nuclei become sufficiently short (for example during the rapid rotation at the high-temperature limit) this will cause the lines to narrow due to self-decoupling. This is illustrated in the ^{31}P spectrum of $(Cl_3PNCH_2CH_2Cl)_2$ by the fact that as temperature is lowered the linewidth increases to that comparable with the ambient temperature spectrum of the methyl compound. As motion slows at low temperature the effect of self-decoupling will be reduced (see Figure 5) because T_1^{Cl} increases. This therefore

implies that, at ambient probe temperature, for the methyl compound motion is relatively slow so as not to give efficient self-decoupling, but with the larger RCl substituted compound, the temperature has to be much lower before the motion is slowed and therefore the self-decoupling is reduced to the same extent. Because of the similarities in phosphorus environment, it is highly unlikely that the extra broadening is due to other factors, such as strength of quadrupolar interaction, with chlorine or nitrogen, which will be very similar. At low temperature, the phosphorus spectrum of the methyl compound shows no further broadening and is therefore already at its slow motion limit at ambient probe temperature.

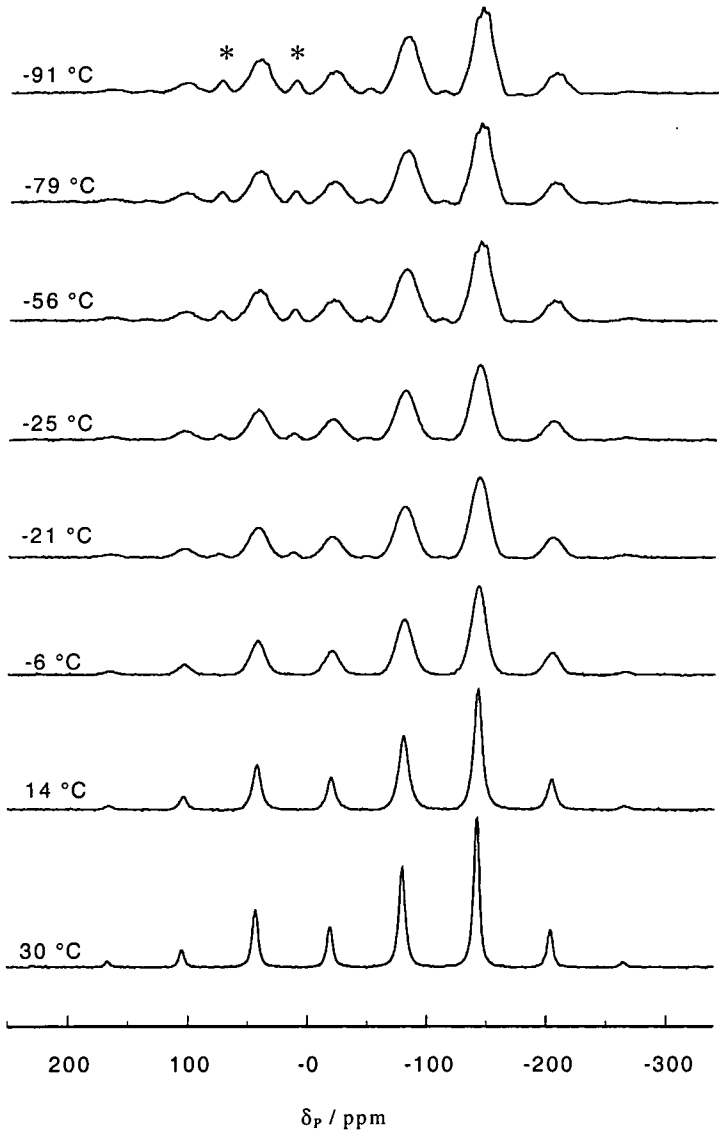

Figure 5. Variable-temperature phosphorus spectra (81 MHz) showing self-decoupling in $(Cl_3PNCH_2CH_2Cl)_2$. Conditions as for ambient temperature spectra.

The extra peak (accompanied by a sideband manifold) appearing at low temperature, between the spinning sidebands of the expected compound, is an impurity (marked * in Figure 5).

From the linewidths (spectra processed with 10 Hz line broadening added) it can be seen that self decoupling for $(Cl_3PNCH_2CH_2Cl)_2$ is only really efficient above 0 °C where the spin-lattice relaxation time must be short (Figure 6). There is quite a dramatic change around this temperature from the broad to narrow lines. Also, it was found that as soon as significant quadrupolar broadening was observed (spectra

acquired at -6 °C or lower), the lineshapes fit reasonably accurately to a Gaussian lineshape (Table 3) although one possible reason for this is that at the lowest temperatures the bandshape is more complex than a single line.

Temperature (calibrated) /°C	Linewidth (fwhh) / Hz	% Gaussian/ Lorentzian
30	460	0
14	587	0
-6	1221	100
-21	1415	100
-25	1424	100
-56	1504	100
-79	1508	100
-91	1512	100

Table 3. Linewidths for $(Cl_3PNCH_2CH_2Cl)_2$ ^{31}P spectra, variable temperature.

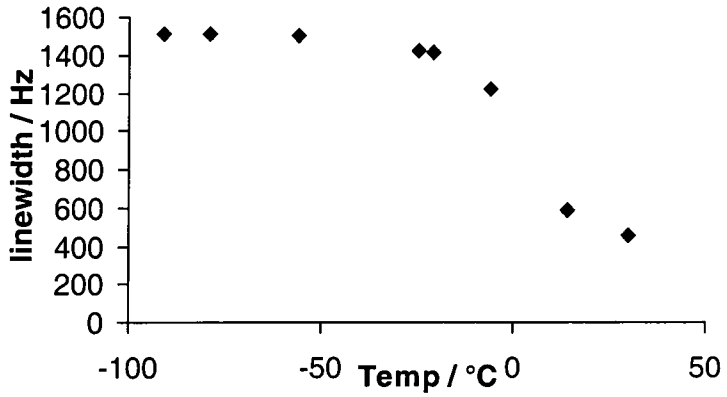

Figure 6. Change of linewidth with temperature

On closer inspection it can be seen at the low temperature limit that some structure is appearing. In addition to some outlying intensity on each band, there are three lines visible, for which deconvolution provides the following shifts for the centreband, 76.4, 81.2, 86.0 ppm (resolution is, however, clearest in the high frequency spinning sidebands). The resolution of this structure is poor and therefore it is not possible to

characterise completely the effect of residual dipolar coupling and/or inequivalence of chlorine substituents.

6.2.2 CARBON-13 SPECTRA

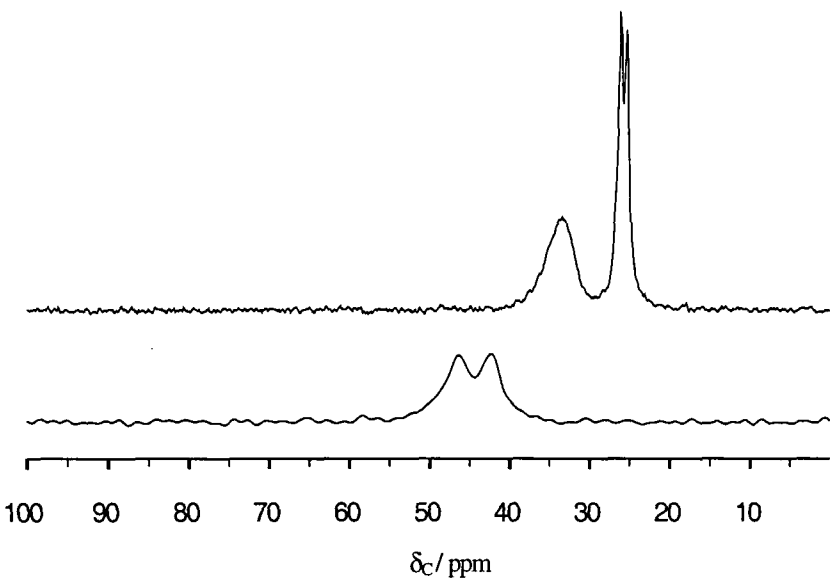

Figure 7. ^{13}C spectra (50 MHz). Upper spectrum, $(Cl_3PNMe)_2$; lower spectrum $(Cl_3PNCH_2CH_2Cl)_2$. Cross polarisation from protons, contact time 8 ms, recycle delay 60 s, 360 acquisitions.

For $(Cl_3PNMe)_2$, two carbon resonance bands are observed (Figure 7). From the results obtained for other nuclei in this and similar compounds, it can be assumed that one of these is an impurity (though no extra peaks were seen in the ^{31}P spectrum). The significant difference in linewidth and chemical shift for the two peaks also means that the appearance of the spectrum is not merely the result of a lack of symmetry within the molecule - the two methyl groups will deviate very little, if at all, from being equivalent in agreement with the single phosphorus shift. A broad ^{13}C peak at 33.5 ppm is believed to be that of interest, the other band being the impurity (doublet peaks at 25.6 and 26.3 ppm). When run at higher field (600 MHz proton) the broad line narrows on the ppm scale as expected, but also the linewidth in hertz (full width at half height) is reduced from 194 to 140 Hz. A similar comparison spectrum run on the 300 MHz spectrometer gives a linewidth of 150 Hz. As narrowing to a larger extent than this would be expected at the highest field if second-order coupling to ^{14}N is involved, these

results suggest that there are other factors affecting the linewidth on the 600 MHz instrument. Perhaps at this stage, this can be attributed to insufficient power for proton decoupling since the 600 MHz spectrometer specifications have not been completely optimised. It is also observed that the resolution is lost in the doublet of the impurity peak, with the reduction in splitting only observable as a decrease in the total width of the doublet. However, although the inefficient proton decoupling may be causing broadening, the linewidth due to quadrupolar interactions is seen to be reduced. There is, therefore, an indication that a large proportion of the linewidth results from quadrupolar interaction with adjacent nitrogen-14 centres and possibly the chlorine in the molecule (separated by only three bonds), and which leads to the broad featureless line.

The carbon spectrum of $(Cl_3PNCH_2CH_2Cl)_2$ shows two very broad signals (fwhh approximately 200 Hz) at 42.3 and 46.4 ppm (Figure 7), resolved to about half height. These can be assigned to the two CH_2 environments. The majority of the additional linewidth, above what is expected for a solid-state ^{13}C spectrum of a simple CH_2 chain, will be from interactions with the quadrupolar nuclei, each carbon having both a nitrogen and chlorine, one in the α position and the other β. The resolution can be slightly improved (linewidths reduced) by working with the HXY probe by applying phosphorus decoupling (though this latter effect results from interaction through at least two bonds). As well as using a smaller rotor and sample volume, the application of phosphorus decoupling seems also to be effective. For other similar compounds for which carbon spectra were acquired on both the HX and HXY probes, there was not a significant change in linewidth with the same conditions (i.e. proton to carbon CP with proton decoupling only). It can therefore be postulated that the reduction in linewidth is due to the phosphorus decoupling and not simply an effect of the change of probe or improved homogeneity due to a reduced sample size. Calculations from known chemical shifts using the online 'Spec Info' software,[5] and published tables of data,[6] suggest the higher frequency carbon is that bonded to N. This will be the carbon closest (through bonds) to phosphorus and it can be seen that on the application of phosphorus decoupling this peak shows more narrowing (Table 4). This also suggests that this is not a probe effect and is true decoupling, as the two peaks are affected to different extents. Values of J_{PC} for similar compounds are around 50 Hz,[1] but, results for exactly analogous C-N-P structures have not been reported in detail.

	Linewidth /Hz C{H}	Linewidth /Hz C{HP}
High frequency (C-N-P)	200	90
Low frequency (C-Cl)	150	130

Table 4. ^{13}C linewidths for $(Cl_3PNCH_2CH_2Cl)_2$.

6.2.3 NITROGEN-15 SPECTRA

For these two chlorine-containing compounds, nitrogen-15 spectra were easily obtained with Hartmann-Hahn cross-polarisation from protons and single chemical shifts have been extracted. Both compounds exhibit increased shielding of the ^{15}N nucleus in comparison to the fluorinated compounds.

Compound	Pulse sequence	Contact time / ms	Number of acquisitions	Linewidth / Hz	δ_N / ppm
R = Me	CP	5	250	70	-232
R= CH_2CH_2Cl	CP	5	1200	30	-224

Table 5. ^{15}N chemical shift and spectral parameters for $(Cl_3PNR)_2$.

As in the phosphorus spectra, the linewidth of the signal from the methyl compound is larger. One would expect the molecule with the most Cl centres to have the broadest lines, although again it could be an effect of the motional restriction in the molecules and the consequent relative efficiency of self-decoupling. The methyl compound also has the lower of the two nitrogen resonance frequencies (more shielded). Both the carbon and nitrogen chemical shifts of the methyl compound indicate a higher shielding.

Table 6 summarises the above chemical shift information for these two compounds.

Compound	Chemical shift δ / ppm		
	^{31}P	^{13}C	^{15}N
R = Me	-78.9	33.5	-232
R= CH_2CH_2Cl	-78.9	42.3 46.4	-224

Table 6. Chemical shifts for $(Cl_3PNR)_2$.

6.2.4 PROTON SPECTRA

The following proton shifts have been determined from simple MAS NMR, although it is known from spectra of other nuclei that the methyl compound contains an impurity and therefore this possibility must be considered before making any firm conclusions. $(Cl_3PNMe)_2$ has broad resonances observable at 7.3 and 5.7 ppm with narrow, equal intensity peaks at 3.3 and 2.8 ppm (a separation of 100 Hz). Both the narrow peaks are consistent with methyl proton resonances. No significant conclusions can be made from this spectrum. For $(Cl_3PNCH_2CH_2Cl)_2$, the main proton resonance is observed at 3.8 ppm. Calculations from known data,[6] considering only the effects of the nearest group, gives 3.6 ppm for Cl-CH_2 protons and 2.5 ppm for N-CH_2. When the effects of the second group (N and Cl are only separated by two CH_2 groups) are considered, it is possible that these two resonances are brought closer together and are consequently not resolved in the experimental spectrum.

6.2.5 CROSS-POLARISATION DYNAMICS

The relaxation times and cross-polarisation dynamics have been measured for the compound $(Cl_3PNCH_2CH_2Cl)_2$ for proton to phosphorus CP. Although a detailed study of abundant spin cross-polarisation dynamics was made for other compounds in chapter 3, the properties of this compound have made it unsuitable for inclusion in that theoretical approach. It is close to the standard CP situation and therefore analysis is simplified. There are two types of proton and relative values of the time constants suggest we are approaching a situation similar to that for normal abundant-to-rare spin CP. From a CP curve (variable contact time experiment) the following effective parameters were obtained (χ^2 error in brackets): $T_{HP}^* = 0.56$ ms, $T_{1\rho}^* = 74$ ms (0.8). As the rotating frame relaxation time is long, the accuracy of the directly measured, individual values (from variable spin-lock time experiments) is limited. Limits on

maximum spin-lock time for the instrumentation available mean that only the first part of the decay curve is well defined. The number of data points recorded was eleven. However, approximate values of $T_{1\rho}^{H}$ = 25 ms (0.4) and $T_{1\rho}^{P}$ = 75 ms (0.3) can be quoted. These values are shown in *Figure 8* (the vertical scale shows only arbitrary intensity).

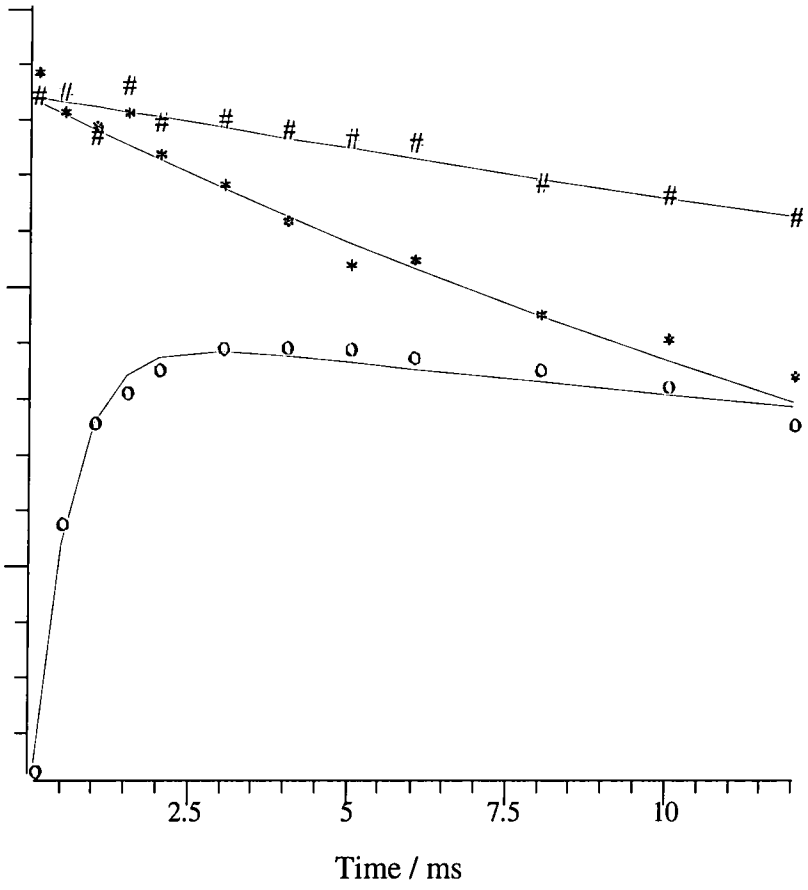

Figure 8. $T_{1\rho}^{H}$ *(*),*$T_{1\rho}^{P}$ *(#) and* T_{HP} *(o) data for* $(Cl_3PNCH_2CH_2Cl)_2$.

A TORQUE curve which measures the value of T_{HP} with quenching of the effect of $T_{1\rho}$ will only fit a single exponential if it is assumed that $T_{1\rho}^{H} = T_{1\rho}^{P}$ which is obviously not true in this case (the derived rate of ~1 ms from the initial slope of the curve is therefore poorly defined). However, this experiment can be used to illustrate the positive slope, at long spin-lock times, representing a case where $T_{1\rho}^{P} > T_{1\rho}^{H}$ (Figure 9). The next stage for abundant-spin systems incorporating a simultaneous fit of torque and CP curves was not appropriate for this case. Despite the abundant phosphorus system, we are approaching the case similar to proton-to-carbon cross-polarisation where the relaxation times in the rotating frame are very different to each other and to T_{IS}.

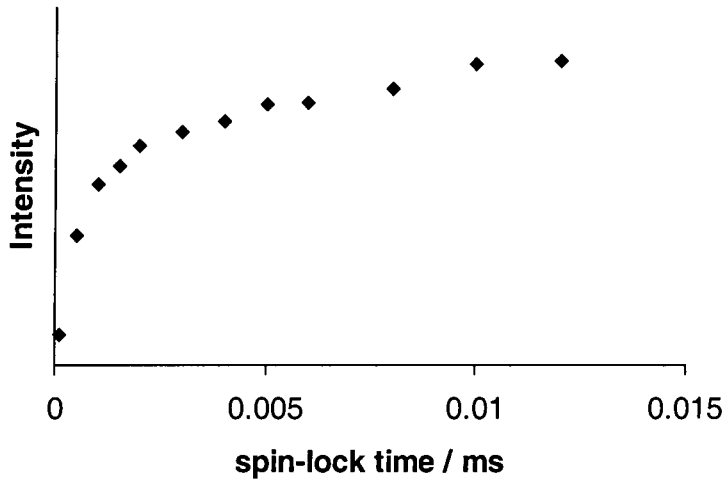

Figure 9. Torque experiment data for $(Cl_3PNCH_2CH_2Cl)_2$.

6.3 Conclusions

Structural and dynamic properties of these molecules have been investigated. From these results there is sufficient evidence to suggest that the postulated structures are correct. Due to the absence of fluorine in these molecules, the exactly analogous methods to those used for the fluorinated compounds could not be used. As direct comparison of two complementary data sets is not possible (e.g. with ^{19}F and ^{31}P NMR), as many conclusions as possible were extracted from the phosphorus data. Substantial changes are seen in altering substituent and sample temperature in terms of the efficiency of quadrupolar self decoupling of chlorine. Other nuclei were observed, with some additional information extracted from carbon-13, proton and nitrogen-15 NMR. The times defining the rate and efficiency of cross-polarisation have been investigated.

REFERENCES

[1] S. Berger, S. Braun, H-O Kalinowski. *NMR Spectroscopy of the Non-metallic elements*. Wiley, Chichester, UK. 1997.

[2] R.K. Harris, M.I.M. Wazeer, *J. Chem. Soc. Dalton,* 1976, 102.

[3] J.R. Ascenso, L.H. Merwin, H.-P. Bai, J.C. Cherryman. Unpublished work.

[4] R.K. Harris, A. Root, *Mol. Phys.*, 1989, **66** (5), 1993.

[5] Daresbury database. Spec Info Version 3.2.3, Jan 1999, Chemical Concepts GmbH, Weinheim.

[6] D.H. Williams, I. Fleming, *Spectroscopic Methods in Organic Chemistry*, 4th Ed. McGraw Hill, Maidenhead, UK. 1989.

7. Disorder in the Triphenylphosphine Oxide-Phenol Complex

7.1. Introduction

A supramolecular assembly (3:2 adduct) of phenol-triphenylphosphine oxide (phenol-TPPO) was studied by means of X-ray diffraction together with high-resolution solid-state ^{31}P NMR spectroscopy. The X-ray results[1] showed a disordered crystal structure belonging to the triclinic $P\bar{1}$ space group. There are two molecules of TPPO and three phenol molecules per unit cell. This is in sharp contrast to most co-crystals of TPPO and substituted phenols, which form with 1:1 stoicheiometry.

A partial molecular structure is shown in Figure 1, and Figure 2 shows a view of the unit cell. The location of one of the phenol molecules is disordered across an apparent inversion centre, with a 50 % occupancy in each orientation (the disorder of the phenol oxygen is indicated in Figure 2 by the shaded atoms). The other phenol residues have a single hydrogen bond to the phosphine oxide. The geometries of the TPPO and phenol moieties are remarkable. The P=O bonds are somewhat lengthened (1.499(3) Å) in comparison with those in various TPPO situations (1.46(1) Å - 1.491(1) Å),[2-7] as would be expected for a H-bonded structure. The hydrogen bond between TPPO and the non-disordered phenol is almost linear, and that from the ordered phenol substantially bent. The hydrogen atoms involved in the H bonds were located on difference maps, but in the case of the disordered phenol this cannot be considered to be highly reliable. Although the TPPO molecules in the unit cell are apparently crystallographically equivalent according to the diffraction results, in each unit cell at a given point in time there must be a TPPO with a single hydrogen bond and a TPPO with two hydrogen bonds. Thus the P=O bond length observed is an average of the two hydrogen-bonded situations.

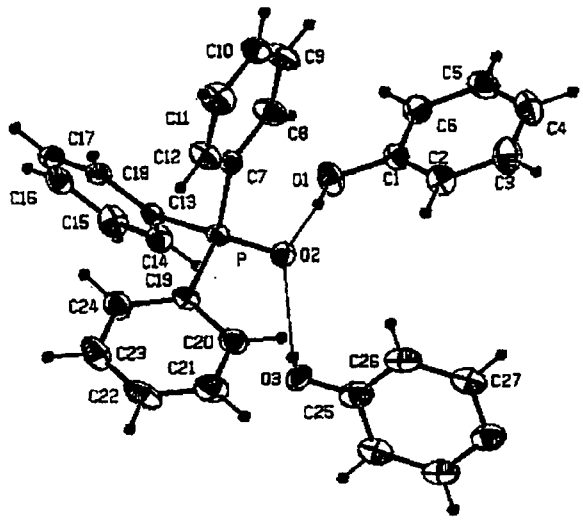

Figure 1. Ortep plot.

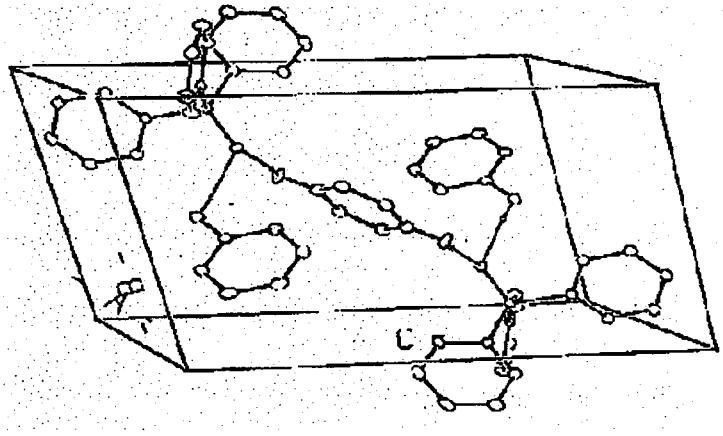

Figure 2. Unit cell.

It is necessary to find out if the structure observed by diffraction studies is a consequence of a static spatially-disordered arrangement of the molecules across the crystal or if, on the other hand, it corresponds to a rapid exchange of the phenol between the two different positions. NMR spectroscopy is the technique chosen to provide evidence to distinguish such static or dynamic disorder.

Initial NMR studies on such systems were to investigate the effect of variation of the co-ordinating acid on hydrogen bond strength (and therefore phosphorus chemical shift).[8] The characterisation of novel compounds containing hydrogen bonds has been pursued in the literature of both diffraction and spectroscopic studies,[9-20] as significant importance is given to research into the hydrogen bond interaction.

Because hydrogen bonding is a weak interaction there is the possibility of being able to overcome the energy barrier and create a dynamic system. X-ray and neutron diffraction techniques allow the determination of positions of the atoms in the compound under study for suitable systems, but it is not often possible to show the extent and nature of disorder. Crystal structure data for this compound are available, and prompted the dynamic study of the system in the solid state via NMR techniques. In cases where such disorder results from an exchange process between different positions, diffraction techniques give an average picture of the crystal structure, since the timescale of the experiment (time of exposure to the radiation) is longer than the rate of the exchange.[21] In these cases, NMR is important in giving additional information to complement diffraction studies.[22,23,24]

A previous NMR study[25] has investigated proton transfer in this and related systems in terms of pKa. Discussion of anisotropy and asymmetry was also made for solid-state spectra at ambient probe temperature. In the present work, for further study of anisotropy, the change in ^{31}P chemical shift for a single crystal of the adduct at different orientations to the magnetic field are observed. Crystals are aligned with one axis at the magic angle and rotated, with a spectrum recorded at each small step. Variable temperature spectra are also studied to investigate the effect of exchange on the anisotropy and asymmetry when the temperature is lower than the coalescence point. NMR parameters such as chemical shifts, relaxation times and coupling constants depend on, among others things, molecular motion Thus, variable-temperature NMR experiments can provide a direct probe of the mobility of a particular system, since temperature will affect the rate constant for the process.

Variable-temperature NMR studies have been used to show that this disorder, previously observed, is dynamic in nature, and have also allowed its characterisation in terms of activation energy parameters. Spectra recorded below the observed coalescence temperature of 247 K showed two phosphorus signals from inequivalence caused by the hydrogen bonding to the phenol. At low temperature one phosphine oxide of the unit cell is involved in hydrogen bonding to one phenol and the other in interacting with two phenol hydroxyl groups, hence the phosphorus resonances are non-equivalent. As the temperature is increased, fast exchange occurs and the two phosphorus resonances become equivalent.

The change in the rate of a chemical exchange will lead to either different relaxation times or distinct bandshapes.[26,27] When slow reversible exchange occurs, separate signals are detected. As temperature increases, broadening of the signals is observed, which continues until the signals coalesce due to fast exchange. On further increase of the temperature a narrowed average spectrum is observed. The bandshape analysis technique is based on the study of linewidths, separations, intensities and shapes of signals arising from changes in temperature, by comparison with spectra theoretically calculated.[27,28] Near the coalescence temperature bandshape analysis gives accurate values of rate constants, whereas at significantly higher or lower temperatures the methods of $T_{1\rho}$ measurement and SPI are more appropriate. At the temperature limits with narrow resonances, accuracy from bandshape fitting is diminished as significant changes in the fitted rate constant cause only negligible changes in linewidth.

However, other available NMR techniques can be used to extend the temperature range covered by bandshape analysis. The approximate rate constants, in s^{-1}, accessible via some of the NMR techniques for solids can be summarised as follows:[29]

Selective Inversion	10^{-1} - 10^{3}
2-D exchange	10^{2} - 10^{3}
$T_{1\rho}$	10^{3} - 10^{5}
MAS	10^{5} - 10^{7}
Quadrupole echo lineshape	10^{4} - 10^{8}
T_2 anisotropy	10^{4} - 10^{12}
T_1 anisotropy	10^{9} - 10^{12}
T_{1Q} anisotropy	10^{9} - 10^{12} and 1 - 10^{3}

The last two of these, in particular, relate to deuterium NMR studies. Both T_{1z} and T_{1Q} vary across a deuteron powder pattern and the detailed lineshape of a spinning sideband manifold will contain considerable dynamic information. The quadrupole coupling is variable with orientation and T_{1z} will be longer at the horns of a deuteron powder pattern than at the shoulders. In addition T_1 and $T_{1\rho}$ are sensitive to motions of the order of 100's MHz and 10's kHz respectively.

Measurements of spin-lattice relaxation in the rotating frame ($T_{1\rho}$), both with variable temperature and variable spin-lock field, can give further rate data at the higher temperature limit. Riddell and co-workers describe in several papers[30] the use of

variable temperature ^{13}C MAS $T_{1\rho}$ experiments. At the temperature where there is a minimum in $T_{1\rho}$, the spin-lock field can be related to the correlation time for motion ($\omega_1\tau_c=1$) and, therefore, to a value of the exchange rate constant. If studies are in a region such that no minimum is reached, the activation energy may be obtained from the average slope of a plot of $\ln(T_{1\rho})$ vs $1/T$.[31] The SPI experiment is one of the best techniques to retrieve accurate data in the slow-exchange regime. For solid-state NMR, this experiment consists of an initial magnetisation transfer (cross polarisation) followed by the "labelling" of one of the exchanging sites via the inversion of the signal (selective inversion of magnetisation).[32-34] The anti-phase situation can be easily achieved following cross-polarisation by giving the magnetisation the appropriate evolution time with a suitable RF reference frequency. However, in a MAS experiment, dephasing of magnetisation not only arises from isotropic chemical shift effects but also as a consequence of the change in the shielding anisotropy (SA) with time.[35] Hence, the period of free precession must coincide with a multiple of the spinning speed. This refocuses the SA effects and, therefore, the evolution is influenced only by the isotropic chemical shifts. Once the exchanging sites are labelled, a period of time t_m is given (the mixing time), during which the chemical exchange produces changes in the signals. Both intensities decrease in magnitude, the change being a function of the exchange rate. The procedure is repeated for several different mixing times and the intensity as a function of t_m yields the rate of exchange if T_1 relaxation effects can be ignored (i.e. if spin-lattice relaxation is negligible during the mixing time). An alternative would be to run a two-dimensional EXSY experiment at difference temperatures and exchange times. Fitting the variation in intensity of the cross peaks would give the same results as SPI, but from significantly longer experimental times.

Bandshape analysis, $T_{1\rho}$ and SPI experiments supply data to calculate the thermodynamic activation parameters by means of the statistical mechanics model proposed by Eyring.[36,37] According to this, the exchange rate, k, is given by equation [1]:

$$k = \kappa \frac{k_b}{h} T.e^{-\Delta G^{\#}/RT} \qquad [1]$$

where κ is the transmission coefficient, k_b is the Boltzmann constant, h is the Planck constant and $\Delta G^{\#}$ is the difference in Gibbs free energy between the activated complex

and the ground state, which can be further evaluated as $\Delta G^{\#} = \Delta H^{\#} - T\Delta S^{\#}$. The transmission coefficient is defined as the fraction of molecules which proceed to the product having reached the transition state. In this case, the transmission coefficient is assumed to be 1/2, as we know from the previous diffraction study that the disorder, if dynamic, consists of 180 ° flips of a phenol molecule, suggesting two minima into which the transition state has an equal probability of proceeding. This assumption can be visualised as a negligible minimum at the transition state or a high energy level from which it is equivalent to fall into either of two minima. From equation [1] activation parameters can be derived by plotting ln k/T vs 1/T (Eyring plot), the slope being equal to $-\Delta H^{\#}/R$, and the intercept ($\Delta S^{\#}/R + \ln \kappa k_b/h$).

7.2 X-ray results

To prepare the co-crystals, 3:2 stoichiometric amounts of phenol and triphenylphosphine oxide were dissolved in chloroform. Crystals suitable for X-ray diffraction can be grown by slow evaporation. The melting point of the co-crystals is 101-103 °C. The preparation of the single crystals, and the X-ray diffraction studies described below were carried out by a group at Sussex University,[1] but because of its link to the studies in this work, it is appropriate to include the details along with the NMR results.

Single-crystal X-ray diffraction studies were carried out using an Enraf Nonius CAD4 diffractometer, operating in the θ-2θ mode with monochromatic Mo Kα radiation, λ = 0.71069 Å. Structures were solved on a MicroVAX computer. Non-H atoms were located by direct methods (SHELXS-86) and refined anisotropically by full matrix least squares using the Enraf-Nonius MolEN program.[38] Data collection and refinement parameters for TPPO/phenol co-crystals were as in Table 1. The atomic positions, bond lengths and angles are in Table 2 and Table 3.

Crystal size (mm)	0.35 x 0.35 x 0.2
Reflections for calculation cell Parameters number, θ_{min}, θ_{max}	25, 7, 10
Data reflection ranges	
H	0→10
K	-11→11
L	-17→17
$\theta_{min,\ max}$ (°)	2→25
Total reflections measured	3883
Unique reflections	3883
Significant reflections $\| F^2 \| > 2\sigma(F^2)$	3252
Max change in standard reflection	-0.8 %
Decay correction	No
Absorption correction, T_{max}, T_{min}	No
H atoms	Freely refined isotropic
R	0.038
R'	0.046
S	1.5
Number of variables	376
Number of observed reflections	3252
$(\Delta/\sigma)_{max}$	0.02
$\Delta\rho_{max,\ min}$ (eÅ^{-3})	+0.26, -0.07

$$\sigma(F^2) = \left\{\sigma^2(I) + (0.041)^2\right\}^{\frac{1}{2}}, w = \sigma^{-2}(F), \Sigma w\left(|F_0| - |F_c|\right)^2 \text{ minimised.}$$

Table 1. Crystal data and structure refinement for the 3:2 phenol-triphenylphosphine oxide complex at 173 K.

Cell dimensions in Å and degrees	a	8.393 (1)	α	104.47 (1)
	b	9.753 (1)	β	101.31 (1)
	c	14.756 (2)	γ	101.42 (1)
Bond lengths (Å)				
P-O2	1.499(1)		P-C7	1.801(2)
P-C13	1.801(2)		P-C19	1.798(1)
O1-C1	1.363(2)		O1-H	0.82(2)
O3[a]-C25	1.204(4)		O3[a]-H	0.52(3)
O1...O2	2.706(1)		O3[a]...O2	2.721(3)
O2...H[b]	1.89(2)		O2...H[c]	2.22(3)
Bond angles (°)				
O2-P-C7	111.46(8)		O2-P-C13	110.95(7)
O2-P-C19	111.40(8)		C7-P-C13	106.11(9)
O7-P-C19	107.43(8)		C13-P-C19	109.40(8)
O1-H10-O2	173(3)		O3[a]-H30-O2	165(3)

Table 2. Cell dimensions, selected bond lengths and angles for the 3:2 phenol-TPPO complex.

[a] O3 is the oxygen in the disordered position

[b] Attached to O1

[c] Attached to O3

	X	Y	z	U_{eq}
P	0.47347(5)	0.11254(5)	0.73031(3)	0.020(1)
O1	0.77580(16)	0.46900(14)	0.85740(9)	0.036(1)
O2	0.55153(15)	0.24996(12)	0.70992(8)	0.026(1)
O3	0.35740(31)	0.39006(27)	0.61553(18)	0.037(1)
C1	0.92922(22)	0.52098(18)	0.84335(13)	0.026(1)
C2	0.96290(24)	0.48575(21)	0.75402(14)	0.033(1)
C3	1.12210(27)	0.54322(23)	0.74557(15)	0.042(1)
C4	1.24620(25)	0.6367(22)	0.82534(16)	0.042(1)
C5	1.21160(25)	0.66948(21)	0.91425(15)	0.037(1)
C6	1.05318(24)	0.61401(20)	0.92394(13)	0.031(1)
C7	0.62365(20)	0.00799(18)	0.75178(11)	0.021(1)
C8	0.78331(25)	0.08484(21)	0.81061(15)	0.035(1)
C9	0.90421(25)	0.01123(22)	0.82899(16)	0.041(1)
C10	0.86847(23)	-0.13839(20)	0.78980(14)	0.034(1)
C11	0.71166(26)	-0.21467(21)	0.73172(15)	0.039(1)
C12	0.58861(23)	-0.14218(20)	0.71214(14)	0.033(1)
C13	0.40006(20)	0.15468(18)	0.83828(11)	0.020(1)
C14	0.37074(23)	0.29244(19)	0.87026(13)	0.029(1)
C15	0.32356(24)	0.33198(2)	0.95560(14)	0.033(1)
C16	0.30349(23)	0.23569(21)	1.00899(13)	0.030(1)
C17	0.32968(22)	0.09785(20)	0.97753(12)	0.028(1)
C18	0.37874(21)	0.05738(18)	0.89266(12)	0.024(1)
C19	0.30122(21)	-0.00405(18)	0.63034(12)	0.023(1)
C20	0.30347(23)	0.00506(21)	0.53781(13)	0.031(1)
C21	0.17653(26)	-0.08530(24)	0.45872(14)	0.040(1)
C22	0.04636(25)	-0.18326(23)	0.47063(15)	0.040(1)
C23	0.04253(26)	-0.19299(24)	0.56199(16)	0.042(1)
C24	0.16963(24)	-0.10392(22)	0.64140(14)	0.034(1)
C25	0.42453(26)	0.43776(21)	0.56077(14)	0.038(1)
C26	0.56891(26)	0.40398(20)	0.53989(14)	0.036(1)
C27	0.64416(25)	0.46661(22)	0.48027(14)	0.037(1)
H10	0.707(3)	0.408(2)	0.810(2)	0.065(7)*
H30	0.385(3)	0.354(3)	0.629(2)	0.013(6)*

U_{eq} is defined as one third of the trace of the orthogonalised U_{ij} tensor

*Uiso

Table 3. Fractional atomic coordinates and equivalent isotropic thermal parameters for 3:2 phenol-TPPO complex.

7.3 NMR Results

7.3.1 Single-crystal experiments:

Spectra used to analyse changes in the ^{31}P chemical shift with the angle between a known crystal axis and the magnetic field, were recorded at ambient probe temperature on the Chemagnetics CMX200 spectrometer, operating at 81.02 MHz for ^{31}P. Cross polarisation (CP) from protons was used to acquire phosphorus-31 spectra for the static sample with high-power proton decoupling. All the spectra were recorded using the following acquisition parameters: ^{1}H pulse duration, 5 μs; contact time, 1 ms; acquisition time, 20 ms; recycle delay, 120 s, and number of acquisitions, 8. The sample, consisting of a single crystal of the TPPO-phenol adduct, was fixed inside a rotor that was placed in the probe at the magic angle. Static spectra were recorded for a range of orientations between 0 and 180°, turning the crystal in ~20° steps. This gives the ^{31}P chemical shift as a function of the orientation (Figure 3). The single crystal was placed in the rotor with the 010 and 100 axes aligned at the magic angle, giving two sets of experimental data. The axes were located by marking the axis parallel to the rotor and submitting the crystals for crystallographic analysis to find the marked axis. The crystals used were several millimetres in all dimensions and it was therefore possible to select the appropriate orientation for mounting in the rotor. Theoretical ^{31}P resonant frequencies corresponding to a single crystal rotated around each of the axes have been calculated,[39] and this produced another two sets of values. The experimental sets have been compared with the theoretical ones and the error in the curve-fit minimised.

The theoretical ^{31}P resonance frequencies were calculated[39] to attempt to explain the pattern of chemical shift vs. orientation obtained for the single-crystal NMR studies. It is assumed that

- the shielding tensor is axially symmetric. The spinning sideband analysis results (see below) suggest that this is reasonable, considering experimental uncertainty.
- $\sigma_{//}$ is along the P=O bond

The angles between the P=O bond and the cell axes along which the single crystal was aligned in the probe (α), were found from the X-ray studies:[40]

α_{010} = 30.9 ° (angle between P=O bond and 010 axis), α_{100} = 72.6 ° (angle between P=O bond and 100 axis)

The shielding tensor was rotated to a new axis system in which $\sigma_{//}$ is along the rotor axis. The theoretical resonance frequency "σ_{lab}" was calculated using two different frames for the shielding tensor (one corresponding to α_{010} and the other one corresponding to α_{100}) for each angle, φ, moved around the rotor axis, taking into account that the rotor was oriented at an angle θ = 54.3°. The equation used was the following:[41,42]

$$\sigma_{lab} = \sigma_{xx}\sin^2\theta\cos^2\varphi + \sigma_{yy}\sin^2\theta\sin^2\varphi + \sigma_{zz}\cos^2\theta + \sigma_{yx}\sin^2\theta\sin 2\varphi + \sigma_{zx}\sin 2\theta\cos\varphi + \sigma_{yz}\sin 2\theta\sin\varphi$$

The fourth and fifth terms of this equations are zero for this tensor, since σ_{yx} and σ_{zx} are zero. Having two experimental sets of data and another two sets of theoretical ones, the experimental (and calculated) values σ_{ii} were referenced to σ_{iso} and σ changed into δ units. Finally, Sigmaplot 2.00 was used to fit the experimental values to the theoretical curves as a function of the angle φ. It was necessary to find the phase between experimental and theoretical values as spectra were recorded starting at an arbitrary angle of rotation. The calculations were made assuming that $\sigma_{//}$ is along the P=O bond, and good agreement was obtained when fitting the experimental data to the theoretical curve (residual standard deviation 5%). Therefore, we can conclude from the analysis of the single-crystal orientation experiments, that $\sigma_{//}$ is along the P=O bond.

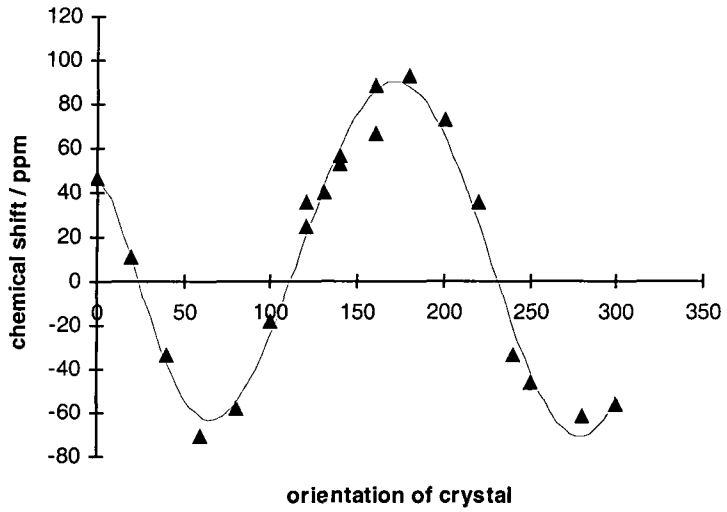

Figure 3. Single-crystal orientation dependence of the phosphorus chemical shift for triphenylphosphine oxide-phenol.

7.3.2 Solid-state phosphorus-31 MAS NMR

The spectrometer involved was a Varian Unity-Plus 300 with a dual-channel Doty probe, operating at a ^{31}P resonance frequency of 121.4 MHz. The sample was packed in a sapphire rotor of 7 mm outer diameter, and confined to the central portion of the rotor using an insert to ensure temperature and field homogeneity; signal intensity was not a problem with this low sample volume.

The crystal structure of phenol-TPPO shows two crystallographically equivalent phosphine oxide molecules in its unit cell. However, due to the disorder, in each unit cell there is one TPPO with a single hydrogen bond, and one with two hydrogen bonds, as mentioned above. Thus, two different ^{31}P signals are predicted from the crystal structure since the phosphorus nuclei are not magnetically equivalent. However, at room temperature, the spectra obtained display only a single signal, suggesting the existence of a rapid exchange between the different positions. If this is the case, a lowering of the temperature should lead to changes in the shape of the signal. This was indeed found to occur (Figure 4 illustrates the separation of resonances and the spinning sideband manifolds), showing that the disorder is the result of an exchange process on a time scale compatible with NMR.

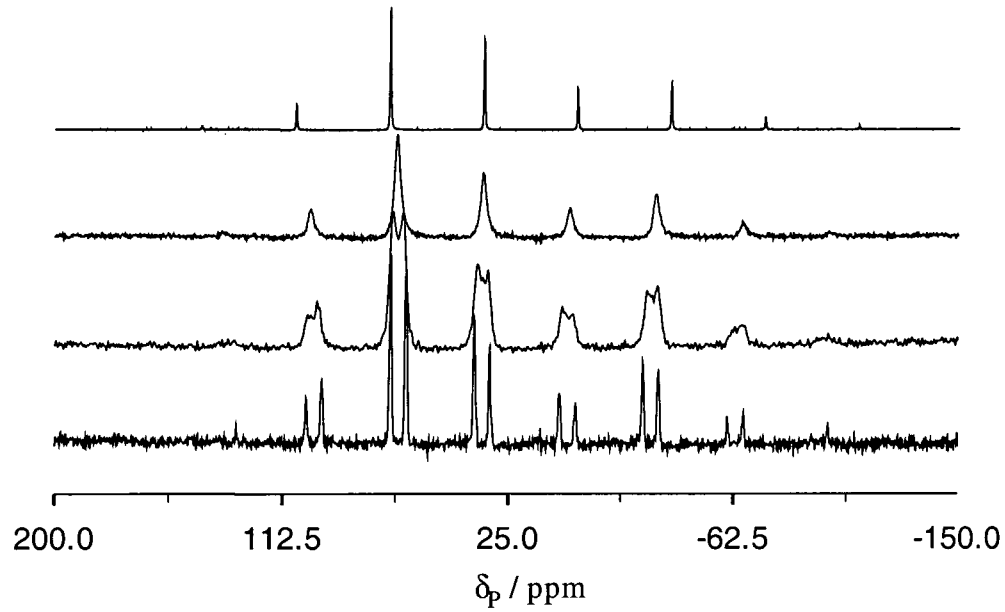

Figure 4. Variable temperature ^{31}P spectra of TPPO-Phenol (121 MHz). From top:284, 240, 230 and 150 K.

In order to understand the quantitative results from this study, it is necessary to consider the exchange mechanism. The difference in phosphorus shift is caused by a change in the hydrogen bonding arrangement in the crystal. This will be the result of a change of orientation of the phenol molecule by 180°. The space swept out by this motion will be restrictively large if it is a head-to-tail flip (Figure 5 A), whereas a 180° rotation in the plane of the phenol molecule would only require the space for the (effective) movement of the OH group around the aromatic ring (Figure 5 B).

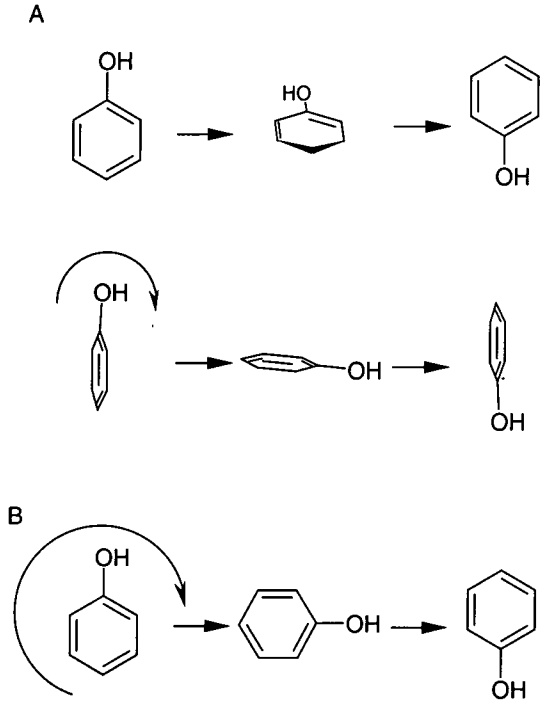

Figure 5. Possible motions of phenol molecule.

There is also the possibility of other motions in this molecule. The well-known phenyl ring flips about the axis of the C-O bond in phenol may also occur, but again requires space in the crystal. The triphenylphosphine molecule may also undergo motional re-orientation of the phenyl rings about the C_3 axis (through the P=O bond).

From spinning sideband analysis it can be seen that both the isotropic chemical shift and shielding anisotropy parameters are averaged at the fast exchange limit. The results for three representative temperatures are shown in Table 4. Spinning sideband analysis was carried out using an iterative fitting method and the experimental spectra are reproduced well. Ambient temperature anisotropy calculations are in agreement with previous results for the single peak and are consistent with the separate values from the two

manifolds at low temperature. Throughout the temperature range, the asymmetry parameter for the powder sample is, within experimental error, zero. This suggests nearly axial symmetry, and within the principal axis system the orientations of σ_{11} and σ_{22} are undefined, apart from being perpendicular to σ_{33}.

Temperature / K	δ_P /ppm		Shielding anisotropy /ppm[a] ($\sigma_{33} - \sigma_{iso}$)		Asymmetry[b] η	
297	34.6		114		0	
211	38.1	32.1	109	126	0	0
180	38.3	32.2	107	121	0	0

[a] From spinning sideband analysis. Statistical errors from computer fitting[33] are ca.±1 ppm, but realistic estimated errors are ±5 ppm.

[b] All values are < 0.1 and errors[33] show η=0 is within the acceptable range. Further calculations from spectra recorded with spin rates between 750 and 2000 Hz suggest a value of 0.05 may be more likely (the increase in number of spinning sidebands increases the accuracy). This value is also within the range of uncertainty for the variable temperature results.

Table 4. Relevant solid-state ^{31}P NMR data for the phenol-TPPO complex, as obtained for different temperatures.

7.3.3 Detailed variable-temperature experiments on powder samples.

For the exchange studies high-resolution phosphorus-31 spectra were acquired using the CP/MAS technique with high-power proton decoupling. For bandshape analysis, spin rates of up to 5 kHz were attained, giving clear separation of the spinning sidebands. The automatic speed controller with feedback from the optical spin-rate sensor was used to keep the rotor spinning speed within an error of less than ± 5 Hz, even at low temperatures. Typical acquisition parameters were: ^1H pulse duration, 5 μs = 90° (5.6 μs = 90° in $T_{1\rho}$ experiments); contact time, 1 ms; recycle delay, 240 s and number of acquisitions, 8-32 (depending on phase cycling of the pulse sequence). Cross polarisation was achieved by optimising the Hartmann-Hahn match condition on the two channels using a sample of brushite. The bearing gas was used to lower the temperature, being cooled in liquid nitrogen and then heated to the required temperature. Significant time (> 25 minutes) was given to allow thermal equilibration both spatially (across the sample) and throughout the experiment time, at each temperature. Calibration of the temperature-control system for the probe was carried

out by observing the separation of the CH_3 and OH proton resonances of methanol absorbed on tetrakistrimethylsilylsilane,[43] as described in the experimental chapter.

As the temperature was lowered, the appearance of the signal changed. The linewidth increased and the single peak broadened until it reached a coalescence point at around -25 °C. At lower temperatures, the signal separated into two broad resonances which then narrowed. This behaviour is typical of a two-site exchange process. Summation over the spinning sidebands gave a ratio of 1:1 intensity overall, indicating equal populations for the two environments, but with different anisotropy behaviour, as indicated by the relative intensities of the two peaks in different sidebands.

The change from one broad signal to two separate peaks (from the two non-equivalent phosphorus sites) occurs over a narrow temperature range. The variable temperature work previously carried out on this system as an initial study, resulted in an unexpectedly complicated lineshape. Around the coalescence region, three peaks made up the band shape. This is shown in Figure 6.[44] There are several possible explanations for this. A distribution of motional correlation times would mean that the transition from the high temperature singlet to low temperature doublet would not be a simple one. The second possible reason involves a physical temperature gradient, either across the spatial dimensions of the rotor or a variation with time throughout the NMR experiment. In order to investigate the origin of this effect, the initial spectra run for this work were to ascertain any time dependence of the bandshape around the coalescence temperature. Once a temperature has been set on the spectrometer, a standard time of 15 minutes was left before acquisition. This produced the 'triplet' structure as observed in the previous experiments. However, after leaving a further 10 to 15 minutes it was found that the spectra simplified to a doublet. It can therefore be concluded that the effects observed were due to a simple temperature gradient. Allowing sufficient time for equilibration before acquisition avoided any problems of complex bandshapes and would eliminate any broadening effects in spectra away from coalescence that were not 'real' exchange phenomena for a single temperature. In the case of temperature gradients, effects can be minimised by confining the sample to the central portion of the rotor by means of an insert as was done for these experiments. The long time delay is still necessary as it will be the centre of the rotor that is last to arrive at the set temperature, but any gradients over space will be reduced. The sample

size will affect the signal-to-noise ratio in that confinement will reduce the filling factor of the coil, but with the strong phosphorus signals resulting from this sample in only a few acquisitions, this is not a significant drawback. The temperatures quoted for the previous studies (as illustrated in Figure 6) are not calibrated, and therefore accurate activation parameters (calculated from rate constant as a function of temperature) could not be derived, even if the coalescence band shape originated from a true exchange effect.

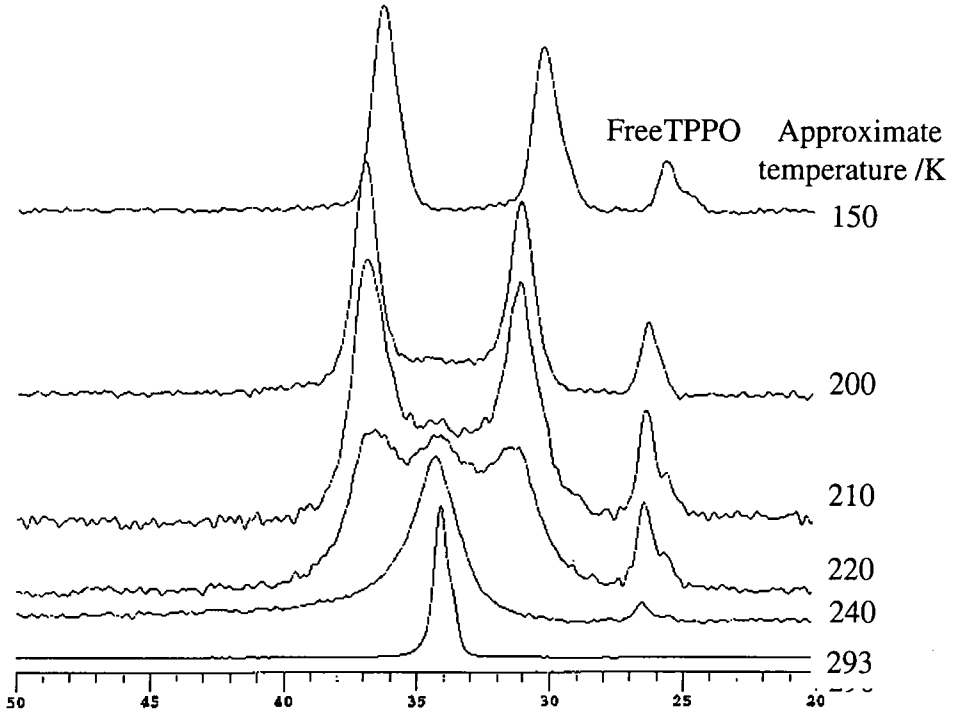

Figure 6. Previously run variable temperature phosphorus spectra (G. McGeorge).

7.4 Exchange Analysis

7.4.1 Bandshape analysis

Exchange rates by the bandshape method were obtained by iterative fitting (least-squares error) with Mathcad software[45] using the standard equations for exchange between two equally-populated sites.[46] Broadening occurs when the exchange rate between two chemically shifted signals is of the order of the separation of the resonances. In the coalescence region bandshape analysis gives accurate values of rate constants. Bandshape analysis used the equations quoted in J. Sandström's Dynamic NMR.[26]

The three equations:

$$P(\nu) = \tau\,(T_{2a}^{-1}\,T_{2b}^{-1} - 4\pi^2\,\mathrm{del}(\nu)^2 + \pi^2\,\Delta^2) + (p_a T_{2a}^{-1} + p_b T_{2b}^{-1})$$

$$Q(\nu) = \tau\,(2\pi\,\mathrm{del}(\nu) - \pi\delta\,(p_a - p_b)$$

$$R(\nu) = 2\pi\,\mathrm{del}(\nu)\,[1 + \tau\,(T_{2a}^{-1} + T_{2b}^{-1})] + \pi\Delta\tau\,(T_{2b}^{-1} - T_{2a}^{-1}) + \pi\Delta\,(p_a - p_b)$$

are used in the final equation

$$J(\nu) = C_o\,\{P(\nu)[1 + \tau\,(p_a T_{2a}^{-1} + p_b T_{2b}^{-1})] + Q(\nu)\,R(\nu)\}/\{P(\nu)^2 + R(\nu)^2\}$$

which simulates the exchanging bandshape. Symbols are defined as:

T_2	natural linewidths without exchange broadening
p	relative populations
del(ν)	average of isotropic frequencies minus frequency ν (calculation range)
Δ	$\nu_a - \nu_b$ (isotropic frequencies at low temperature limit)
τ	p_a/k_a
C_o	normalisation constant (C_A/p_a).

The derivation given is similar to that of McConnell.[47] For a system in equilibrium

$$dG_m/dt = - k_A G_A + k_B G_B.$$

Since the jump rate is a lot faster than the rate of precession of the nuclei ($\sim 10^{-13}$ s cf. $\sim 10^{-7}$ s) we have

$$dG_A/dt = - \alpha_A G_A - iC_A, \text{ where } \alpha_A = T_{2A}^{-1} - 2\pi i\,(\nu_A - \nu).$$

This describes the change in transverse magnetisation in the static and oscillating fields, and combination leads to the modified Bloch equation,

$$dG_A/dt = - \alpha_A G_A - iC_A - k_A G_A + k_B G_B \text{ (and similarly for B)}$$

To incorporate relative populations $C_A = p_A.C_o$ is substituted after solving for G_A and G_B, giving $G = - C_o\,(k_A + k_B + \alpha_A p_B + \alpha_B p_A) / (\alpha_A k_B + \alpha_B k_A + \alpha_A \alpha_B)$. The denominator of this equation contains complex numbers and after a non-trivial separation produces the above expression, J(ν).

It was assumed that the actual chemical shift difference remains essentially constant over the temperature range 297-247 K (for which bandshape is appropriate) and the coalescence of lines is caused by the exchange process. The average shift (exchange averaged single peak and midpoint between peaks in the slow exchange limit) was unchanged, within experimental error in the bandshape analysis over the whole range studied down to 149 K. The value used for the shift difference was the maximum

directly measured at the lowest temperature, 149 K, i.e. 743 Hz. However, the linewidths of the two lines at 149 K, assumed to be in the slow-exchange limit, were 99 Hz, whereas at the fast-exchange limit the linewidth was 43 Hz. Therefore the values used for the iterative fitting were interpolated between these two extremes to account for other broadening effects over the temperature range.

Bandshape analysis was performed for the central region of temperatures. Figure 7 shows the experimental data together with the simulations of the summed spectra: each of the spinning sidebands was added to obtain the illustrated experimental spectra, which are compared with fitted theoretical spectra obtained by ignoring the tensor nature of shielding.

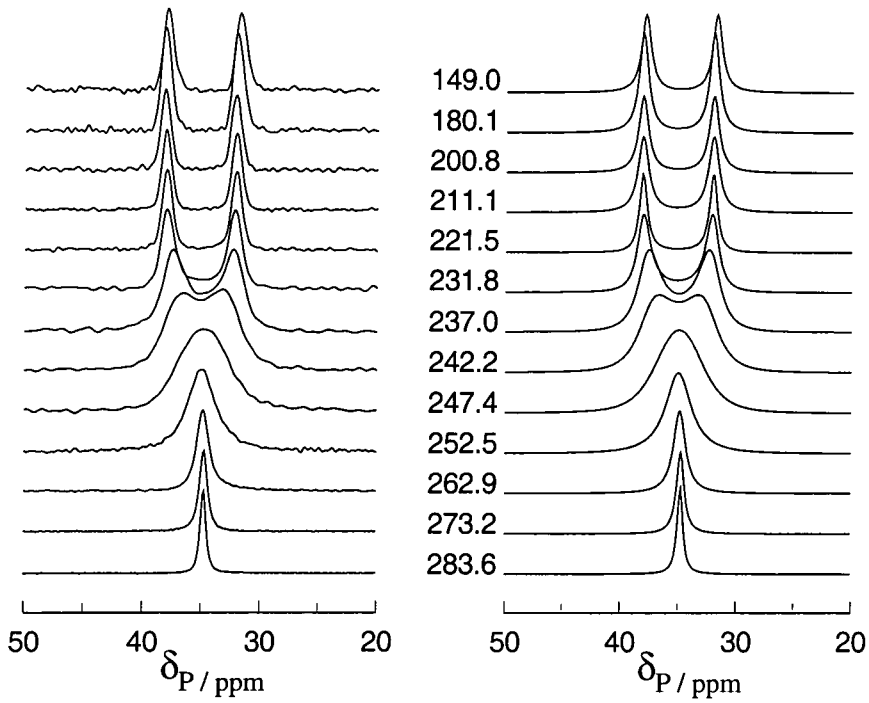

Figure 7. Experimental summed spectra of the phenol-TPPO complex (left), together with those resulting from computer fitting (right), for different temperatures (in K).

7.4.2 SPI

The selective polarisation inversion (SPI) pulse sequence consists of preparation by cross-polarisation, selective inversion of one of the exchanging peaks (by careful selection of the transmitter offset and delay for precession) and a mixing time to allow exchange, and therefore decay of signal intensity, to occur before acquisition. If the carrier frequency is offset from one of the peaks by a frequency equal to the separation

between them, then, after a delay time for precession equal to the reciprocal of the offset, the two peaks will by 180° out of phase. A 90° pulse then places these in the positive and negative z directions for the mixing time, with a final 90° read pulse before acquisition of the spectrum. These experiments were carried out at set temperatures of -50, -65, -80 and -90 °C which calibrate (with conversion to absolute temperature) to 221.5, 206.0, 190.4 and 180.1 K respectively. For the three higher temperatures, a spinning speed of 2856 Hz, transmitter frequency offset (from one of the two exchanging signals) 714 Hz, and delay for precession 0.70 ms, were the appropriate parameters calculated from the peak separation at that particular exchange rate. However, at 180.1 K, a spinning speed of 2972 Hz and delay of 0.67 ms were calculated to be suitable to the increased separation (743 Hz). Mixing times were chosen as appropriate for each temperature so that a significant decay of intensities (due to each different exchange rate) was observed. These were as follows:

Temperature / K	Mixing time / ms
221.5	0.01, 0.5, 1, 2, 4, 8
206.0	0.01, 5, 10, 15, 20, 30, 40
190.4	0.01, 20, 40, 70, 100, 150, 200
180.1	0.01, 20, 40, 70, 100, 150, 300

The procedure used in this work assumes that T_1 of the phosphorus-31 does not have a significant effect on the signal decay during the mixing time. This is valid if the value of the relaxation time is long compared to the relevant exchange lifetimes. In this case the necessary mixing times are of the order of milliseconds, which compare favourably with the estimated T_1 of 500 s at ambient probe temperature, measured via cross polarisation using the Torchia pulse sequence.[48] Due to the relatively small number of data points and long T_1, this value is subject to large errors, but it is clear that it is sufficiently large to be neglected in these calculations. Measurement of T_1 was not made at variable temperature, but no problems were encountered with the assumption that it can be neglected in the calculations from selective polarisation inversion. Figure 8 shows the experimental spectra at -50 °C (221.5 K). The intensities of the positive and inverted peaks were measured for the centreband at each mixing time and the decay of signals was used to determine a rate constant. The decay of intensity of all the spinning sidebands, with increasing mixing time, was the same as that of the centre band, but because of the effects of anisotropy the absolute intensities measured for the pair of exchanging peaks were not in a 1:1 ratio in a single band. Summing over the

complete spinning sideband manifold gave two peaks of equal intensities (opposite sign) at each mixing time, but analysis gave no significant change in the results compared with calculations involving the centreband only.

The equation for the decay of magnetisation, taking the difference between the positive and inverted intensities is:[49]

$$M_{diff} = (M_i^A - M_i^B)\exp\{-(k_f + k_b)t\} + M_f^A - M_f^B \qquad [2]$$

where M^A_i and M^B_i, and M^A_f and M^B_f are the initial and final magnetisations of the positive and inverted peaks, M_{diff} is the difference in magnetisation of 'A' and 'B' at time t, while k_f and k_b are the rate constants for the forward and backward exchange processes. As the forward and reverse processes are identical for an equal-population case, the rate obtained from the exponential term in equation [2] for the signal decay is twice the rate constant for a single direction ($k_f + k_b = 2k$). Graphs plotted using the equation above are shown in Figure 9, and from them the exchange rate at each temperature can be obtained. Table 5 summarises these results as well as those from other methods.

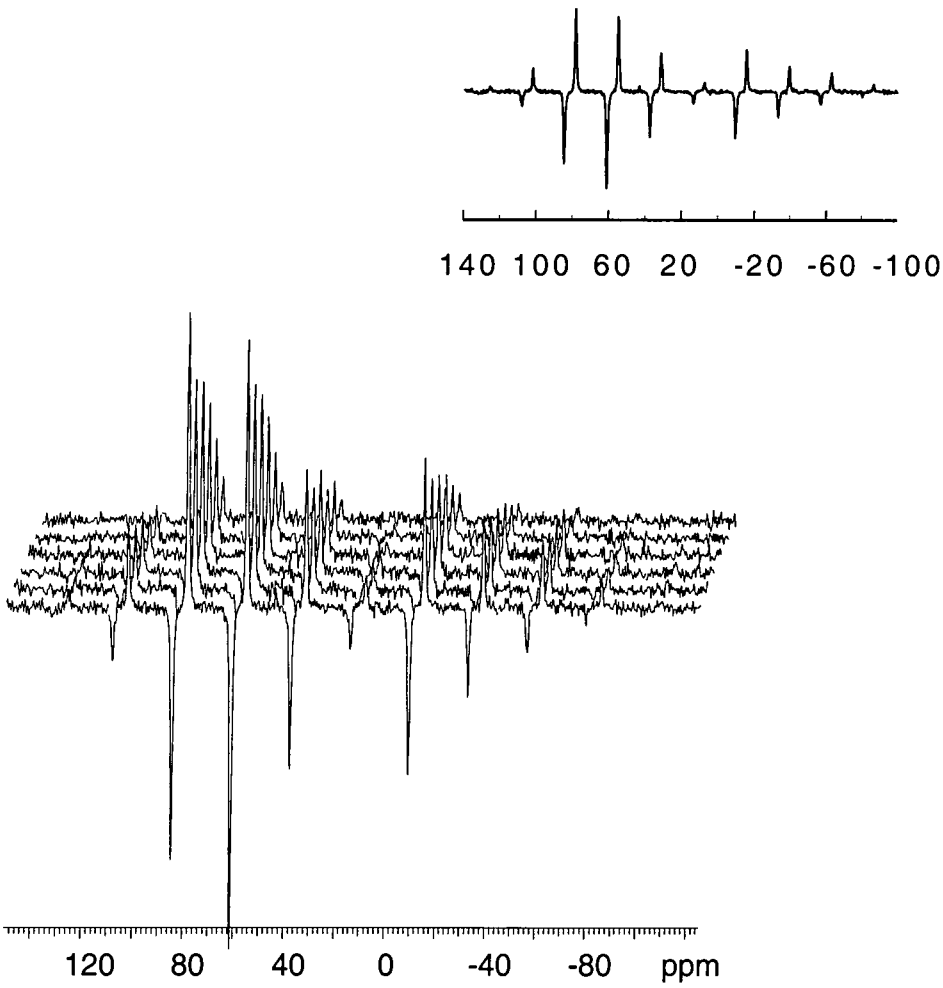

Figure 8. Set of SPI experimental ^{31}P spectra at -50 °C (mixing times 0.01, 0.5, 1, 2, 4, 8 ms). The inset shows the first slice of the experiment at this temperature.

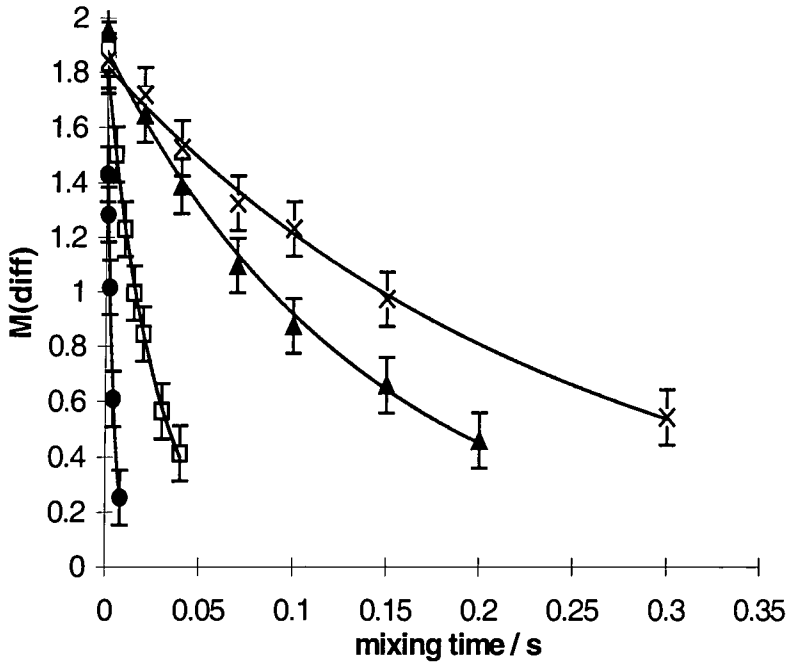

Figure 9. Plot of the decay of magnetisation (see equation [3]), as a function of mixing time for different temperatures (closed circle 221 K, open square 206 K, closed triangle 190 K, cross 180 K).

7.4.3 $T_{1\rho}$ measurements

Measurement of $T_{1\rho}$ (^{31}P) was achieved by a pulse sequence, with cross-polarisation from protons (for signal enhancement and shorter recycle delay), that incorporates a variable ^{31}P spin-lock time. The pulse sequence used does not include high-power heteronuclear (proton) decoupling during the spin locking, but it is applied during acquisition. During the lock time, τ, the decay of the signal characterises the ^{31}P spin-lattice relaxation in the rotating frame.

A rate constant at a temperature well above the coalescence is obtainable from variable temperature $T_{1\rho}$ measurements. The correlation time for 360° motion is equal to the reciprocal of the spin-lock field at the temperature where the minimum $T_{1\rho}$ is reached. The theory used for this correlation time is based on the equation given by Deverell et al.[50] For this case, motion of the phenol molecule is probed via the observation of the phosphorus with which it interacts. An expression of the form:

$$\frac{1}{T_{1\rho}} = C\frac{\tau_c}{1+\omega_1{}^2\tau_c{}^2},$$

where C is a constant and $\omega_1 = \gamma_P B_{1P}$, is applicable and can be differentiated to give a minimum in $T_{1\rho}$ when $\omega_1\tau_c = 1$. Further terms in $\omega_0\tau_c$ can be neglected as these concern motions in the T_1 regime, for which the system can be considered rigid. The ^{31}P 90° pulse duration was measured as being 5.6 μs, representing a radio frequency magnetic field equivalent to 44.6 kHz.

The lowest temperature value (i.e. longest $T_{1\rho}$ measured) is subject to much larger errors than the others in fitting the decay curve, but serves its purpose here in helping to define the minimum. However, the next three points to the low temperature side of the minimum can be used, in conjunction with data derived from that minimum, to obtain further rate constants. If the constant of proportionality, C, can be calculated from the data at the minimum, then the above equation can be used to find the correlation time for different values of $T_{1\rho}$.

In the fast-exchange temperature range, values of $T_{1\rho}$ were measured (Figure 10). The results for the adduct show a minimum in the relaxation time at 303 K. The minimum is broad and therefore an uncertainty of ± 10° is not unreasonable. It can also be seen that another motional process is having an effect at high temperature, as the start of a second minimum is apparent. This cannot be fully characterised as experiments are limited by the sample melting point and spectrometer specifications. However, it can be postulated that this is due to a higher energy motion and could be the propeller-like rotation of the phenyl groups about the P=O bond axis or a different motion of the phenol. The propeller motion will itself be characterised by the nature of the P-O bond, with a restricted rotation in the case of P=O and a relatively free motion if the bond is more ionic in character, i.e. P^+-O^-.

The value of the rate constant at the minimum was calculated from the motional correlation time τ_c, derived from $\omega_1{}^2\tau_c{}^2=1$, where $\omega_1=\gamma B_1$. The desired rate constant is given by $k=1/\tau$ (compare with reference 51). As the exchange process involves 180° flips of the phenol molecule a factor of two would be required to define the rate from the correlation time, as τ represents the full 360 ° motion. This is however equivalent to

saying $\kappa=1/2$ in the final Eyring plot (altering $\Delta S^{\#}$ by ln2). As described above, three of the other $T_{1\rho}$ values were used to calculate further rate constants once C had been calculated from the minimum value. All these points are incorporated into an Eyring plot with rate data from the other methods.

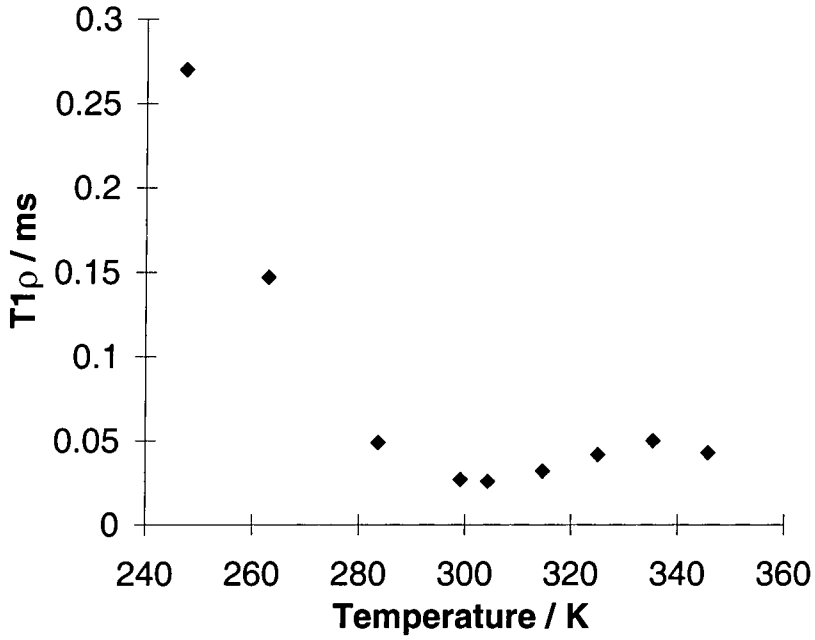

Figure 10. Plot of the ^{31}P spin-lattice relaxation time in the rotating frame, $T_{1\rho}$, as a function of temperature.

7.4.4 Activation parameters

Figure 11 shows the straight-line fit through logarithmic plots of k/T against reciprocal temperature. The results were obtained from the bandshape, $T_{1\rho}$ and SPI results combined. As can be seen, a reasonable fit was obtained through all the data points. Hence, thermodynamic parameters could be obtained. According to equation [1], the estimated activation free energy $\Delta G^{\#}$, at the coalescence temperature (247 K) is 43.9 kJ mol^{-1}; the enthalpy difference between the activated complex and reactants, $\Delta H^{\#}$, is 38 kJ mol^{-1}; and the entropy difference for the same species, $\Delta S^{\#}$, is -23 J mol^{-1} K^{-1}. It is of interest to note that if the points from bandshape fitting alone are used, the resulting values are significantly different, that is, $\Delta H^{\#}$ = 58 kJ mol^{-1} and $\Delta S^{\#}$ = 60 J mol^{-1} K^{-1}. This is due to the inaccuracies described at the temperature extremes of bandshape analysis. The errors shown on the individual points on the Eyring plot were calculated on the basis of temperature measurement ($T_{1\rho}$), intensity measurements (SPI) and shape

of the variation of R^2 (sum of squares error, bandshape). From these it is possible to estimate an error of around 10 % in line fit overall which will give corresponding errors in both the slope (hence $\Delta H^{\#}$) and intercept ($\Delta S^{\#}$) of the best fit line.

temp/ °C	Calibrated	T / K	1000/T	Method	k	error	ln(k/T)
30 (±10)	30	303	3.30	$T_{1\rho\ min}$	89200		5.68
25	26	299	3.34	$T_{1\rho}$	67700		5.42
10	11	284	3.53	$T_{1\rho}$	25600		4.50
-10	-10	263	3.80	$T_{1\rho}$	7950		3.41
-10	-10	263	3.80	Bandshape	11300	(±10%)	3.50
-20	-20	253	3.96	Bandshape	3690	(±8%)	2.60
-25	-26	247	4.04	Bandshape	1840	(±5%)	2.09
-30	-31	242	4.13	Bandshape	1240	(±3%)	1.63
-35	-36	237	4.23	Bandshape	697	(±5%)	1.12
-40	-41	232	4.31	Bandshape	284	(±10%)	0.41
-50	-52	222	4.52	Bandshape	62.5	(±30%)	-0.46
-50	-52	222	4.52	SPI	122	(±10%)	-0.60
-65	-67	206	4.86	SPI	18.9	(±10%)	-2.39
-80	-83	190	5.25	SPI	3.42	(±10%)	-4.02
-90	-93	180	5.55	SPI	1.65	(±10%)	-4.69

Table 5. Exchange rates calculated for the phenol-TPPO complex at each temperature studied using bandshape, SPI and $T_{1\rho}$ methods (estimated errors in parentheses).

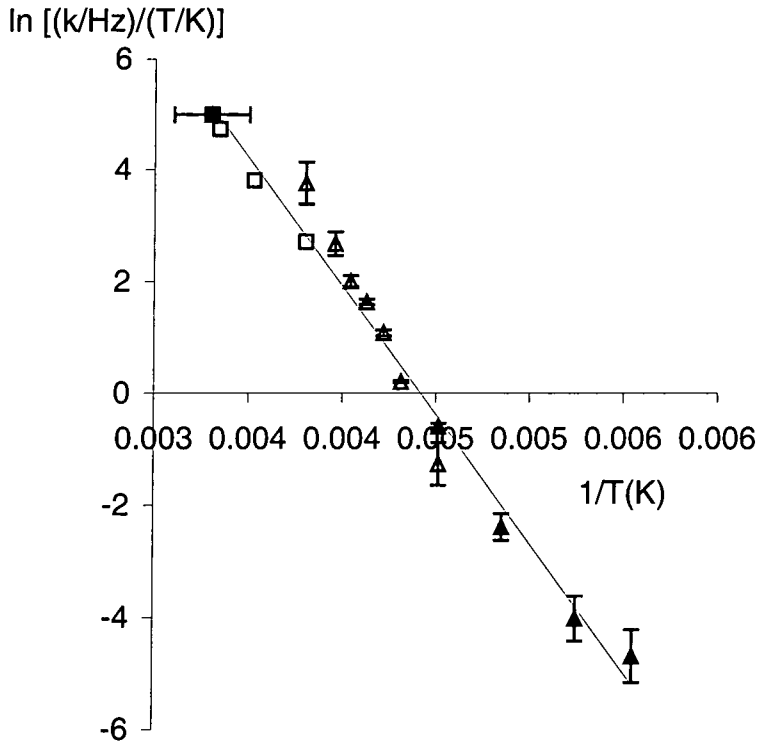

Figure 11. Eyring plot for bandshape analysis, SPI results and $T_{1\rho}$ measurements
(open triangles, bandshape analysis; closed triangles, SPI; open square, $T_{1\rho}$; closed square, $T_{1\rho}$ minimum).

7.5 Conclusions

The crystal structure of the 3:2 phenol-TPPO complex has been obtained by means of X-ray diffraction and shows disorder of one of the phenol molecules across the apparent inversion centre, within the unit cell. Magic-angle spinning NMR spectroscopy elucidates the dynamic nature of this disorder. Phosphorus-31 NMR spectra recorded at low temperature are readily related to the crystal structure, and an exchange process explains the single peak observed at ambient temperature.

Neither X-ray nor NMR experiments throw light on the exact nature of the exchange process, but rotation of the disordered phenol about an axis perpendicular to the aromatic ring would seem to be the most likely motion. The dynamic disorder in this molecule can be described as 180° flips of the phenol molecule so it hydrogen bonds to

different triphenylphosphine oxide molecules. The space for this to occur must be considered. The motion which would require the least space is rotation in the plane about the centre of the ring (as this is, in effect, merely movement of the OH group around the ring. An end to end ring flip would require a lot of free space in the complex.

Bandshape analysis, $T_{1\rho}$ measurements and selective polarisation inversion have been the chosen methodologies to retrieve kinetic information. Reasonable agreement has been observed between the three techniques, when used in the appropriate temperature range, for the calculation of rate constants. This has led to insight into the motion in the crystal in terms of its rate, and allowed the evaluation of the following activation parameters.

The estimated activation free energy $\Delta G^{\#}$, at coalescence (247 K) is 43.9 kJ mol $^{-1}$. The enthalpy difference between the activated complex and reactants, $\Delta H^{\#}$, is 38 kJ mol^{-1} and the entropy difference for the same species, $\Delta S^{\#}$, is -23 J mol^{-1} K^{-1}. The improvement made by using a variety of techniques can be illustrated by the bandshape analysis. Away from the coalescence temperature the logarithm of the rate constants deviates from the straight line fit and, using points from bandshape analysis alone, $\Delta H^{\#}$ = 58 kJ mol^{-1} and $\Delta S^{\#}$ = 60 J mol^{-1} K^{-1} as the whole temperature range is not well defined. As there is no significant change in disorder of the system with the 180° phenol molecule reorientation, the value of $\Delta S^{\#}$ is higher than expected. A value around zero would be expected to be more appropriate. As there is the varying uncertainty in the points that make up the slope it is quite possible that these account for this deviation. It can be seen that $\Delta S^{\#}$ changes from positive to negative depending on whether or not SPI and $T_{1\rho}$ values are included.

REFERENCES

[1] P.A. Chaloner, R.M. Harrison, P.B. Hitchcock, C. Jasieczek. Sussex. Personal communication.

[2] G. Ruban and V. Zabel, *Crys. Struct. Comm.*, 1976, **5**, 671.

[3] C.P. Brock, W.B. Schweizer and J.D. Dunitz, *J.Am.Chem.Soc.*, 1985, **107**, 6964.

[4] A.L. Spek, *Acta Crystallogr.*, 1987, **C43**, 1233.

[5] G. Bandoli, G. Bortolozo, D.A. Clemete, V. Croalto and C. Panattoni, *J. Chem. Soc. (A),* 1970, 2778.

[6] K.A. Al-Farhan, *J. Cryst. Spect. Res.*, 1992, **22**, 687.

[7] J.A. Thomas, T.A. Hamor, *Acta Crystallogr.*, 1993, **C49**, 355.

[8] C. M. Lagier, U. Scheler, G. McGeorge, M. G. Sierra, A. C. Olivieri and R. K. Harris, *J. Chem. Soc., Perkin Trans. 2*, 1996, 1325.

[9] M. Ilczyszyn, Z. Latajka and H. Ratajczak, *Org. Magn. Reson.*, 1980, **13**, 132.

[10] B. Brycki and M. Szafran, *J. Chem. Soc., Perkin Trans. 2*, 1982, 1333.

[11] F. Herbstein, M. Kapon, G.M. Reisner, M.S. Lehman, R.B. Kress, R.B. Wilson, W.I. Shiau, E.N. Duesler, I.C. Paul and D.Y. Curtin, *Proc. R. Soc. London, Ser. A,* 1985, **399**, 295.

[12] M.C. Etter and R.C. Hoye, *Trans. Am. Crystallogr. Assoc.*, 1986, **22**, 31.

[13] J.D. Dunitz, E.F. Maverick and K.N. Trueblood, *Angew. Chem., Int. Ed. Engl.*, 1988, **27**, 880.

[14] M.C. Etter, Z.V. Lipowska, M.Z. Ebrahimi and T.W. Panunto, *J. Am. Chem. Soc.*, 1990, **112**, 8415.

[15] J.A. Zerkowski, C.T. Seto, D.A. Wierda and G.M. Whitesides, *J. Am. Chem. Soc.*, 1990, **112**, 9025.

[16] F.G. Tellado, S.J. Geib, S. Goswami and A.D. Hamilton, *J. Am. Chem. Soc.*, 1991, **113**, 9265.

[17] M.C. Etter, *J.Phys. Chem.*, 1991, **95**, 4601.

[18] A. Vila, C.M. Lagier and A.C. Olivieri, *J. Mol. Struct.*, 1992, **274**, 215.

[19] B. Brycki, B. Brzezinski, G. Zundel and T. Keil, *Magn. Reson. Chem.*, 1992, **30**, 507.

[20] C.M. Lagier, A.C. Olivieri, D.C. Apperley and R.K. Harris, *Solid State NMR*, 1992, **1**, 205.

[21] P. Schuster, G. Zundel and C. Sandorfi, The Hydrogen Bond, Recent Developments in Theory and Experiments, North Holland, Amsterdam, 1976.

[22] A.J. Vila, C.M. Lagier and A.C. Olivieri, *Magn. Reson. Chem.*, 1990, **28**, 529.

[23] J. Emsley, *Struct. Bonding* (Berlin), 1984, **56**, 147.

[24] D. Casarini, R.K. Harris and A.M. Kenwright, *Magn. Reson. Chem.*, 1992, **30**, 434.

[25] C. M. Lagier, U. Scheler, G. McGeorge, M. G. Sierra, A. C. Olivieri and R. K. Harris, *J. Chem. Soc., Perkin Trans. 2*, 1996, 1325.

[26] J. Sandstrom, Dynamic NMR Spectroscopy, Academic Press, London/New York, 1982.

[27] A.N. Lane, *Progr. NMR Spectr.*, 1993, **25**, 481.

[28] R.R. Ernst, G. Bodenhausen and A. Wokaun, Principles of Nuclear Magnetic Resonance in One and Two Dimensions, 2nd Ed., Clarendon Press, Oxford, 1991.

[29] R.L.Vold, 40th ENC, Orlando Florida, March 1999.

[30] a) F.G. Riddell, S. Arumugam, K.D.M. Harris, M. Rogerson, J.H. Strange, *J. Am. Chem. Soc.*, 1993, **115**, 1881. b) F.G. Riddell, P.G. Bruce, P. Lightfoot, M. Rogerson, *J. Chem. Soc., Chem. Comm.*, 1994, **2**, 209. c) F.G. Riddell, M. Bremner, J.H. Strange, *Mag. Reson. Chem.*, 1994, **32**, 118. d) F.G. Riddell, K.S. Cameron, W.B. Turnbull, *Mag. Reson. Chem.*, 1995, **33**, 841. e) F.G. Riddell, M. Rogerson, *J. Chem.*

Soc., Perkin Trans. 2, 1996, **4**, 493. f) F.G. Riddell, M. Rogerson, W.B. Turnbull, F. Fulop, *J. Chem. Soc., Perkin Trans. 2*, 1997, **1**, 95. g) F.G. Riddell, M. Rogerson, *J. Chem. Soc., Perkin Trans. 2*, 1997, **2**, 249. h) F.G. Riddell, M. Rogerson, *Mag. Reson. Chem.*, 1997, **35**, 333.

[31] D.C. Douglass, G.P. Jones, *J. Chem. Phys.*, 1966, **45**, 956.

[32] N.M. Szeverenyi, A. Bax and G.E. Maciel, *J. Am. Chem. Soc.*, 1983, **105**, 2579.

[33] G. McGeorge, R.K. Harris, A.M. Chippendale and J.F. Bullock, *J. Chem. Soc., Perkin Trans.* 2, 1996, **8**, 1733.

[34] A. Nordon, Harris R.K., Yeo L. and Harris K.D.M., *J. Chem. Soc., Chem. Comm.*, 1997, **10**, 961.

[35] M.M. Maricq and J.S. Waugh, *J. Phys. Chem.*, 1979, **70**, 3300.

[36] H. Eyring, *Chem. Revs.* , 1935, **17**, 65.

[37] S. Glasstone, K.J. Laider and H. Eyring, The Theory of Rate Processes, McGraw-Hill, New York, 1941.

[38] G. M. Sheldrick, in Crystallographic Computing 3, Ed G. M. Sheldrick, C. Krüger and R. Goddard, 175, OUP, 1985.

[39] C.M. Lagier. Rosario, Argentina. Personal Communication.

[40] A. Batsanov. Durham. Personal Communication.

[41] J. Facelli and D. M. Grant, "Molecular Structure and Carbon-13 Chemical Shielding Tensors Obtained from Nuclear Magnetic Resonance", Topics in Stereochemistry V19, Ed. Ernst L. Eliel and Samuel H. Wilen, 1989, John Wiley & Sons, Inc.

[42] Veeman, W.S. *Progress in NMR Spectroscopy*, 1984, **16**, 193.

[43]A.E. Aliev and K.D.M. Harris, *Magn. Reson. Chem.*, 1994, **32**, 366.

[44] G. McGeorge, Ph.D Thesis, 1996. University of Durham.

[45]MATHCAD Plus 6, Mathsoft Inc., 1995.

[46] M.T. Rogers and J.C. Woodbrey, *J. Phys. Chem.*, 1962, **28**, 540.

[47] H.M. McConnell, *J. Chem. Phys.*, 1958, **28**, 430.

[48] D. Torchia, *J. Magn. Reson.*, 1978, **30**, 613.

[49] H-H. Limbach, B. Wehrle, M. Schlabach, R. Kendrick and C.S. Yannoni, *J. Magn. Reson.*, 1988, **77**, 84.

[50] C.Deverell, R.E.Morgan, J.H.Strange, Mol.Phys., 1970, **18**, 553.

[51] F.G. Riddell, S. Arumugam, K.D.M. Harris, M. Rogerson, J.H. Strange, *J.Am.Chem.Soc.*,1993, **115**, 1881.

8. Ruthenium-, platinum- and chlorine-containing compounds

This chapter involves the study of two fluoroaromatic phosphorus compounds, I and II, and a triphenylphosphine ruthenium compound, III. Schematic representations of the structures for the three compounds included in this chapter are shown below:

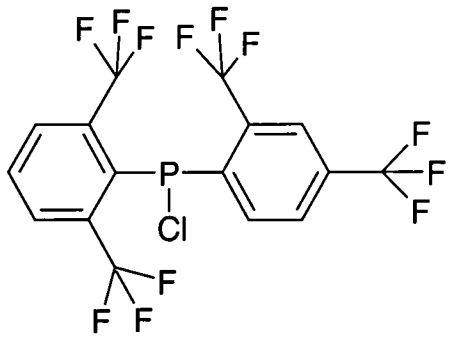

Figure 1. Compound I.

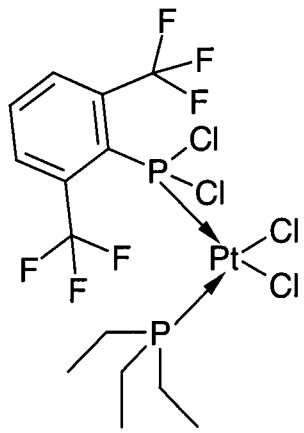

Figure 2. Compound II.

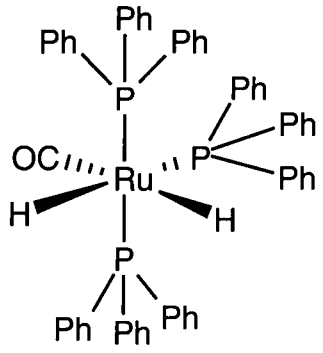

Figure 3. Compound III.

For I and II, crystal structures are known and some solution-state data are available,[1] which will be included in the following discussion. The structure of compound III shown is that derived from the solid-state NMR spectra described in this work.

In the two substituted aromatic phosphorus compounds there are two groups for which the following notation will be used, for simplicity, to distinguish the different CF_3 substitution positions:

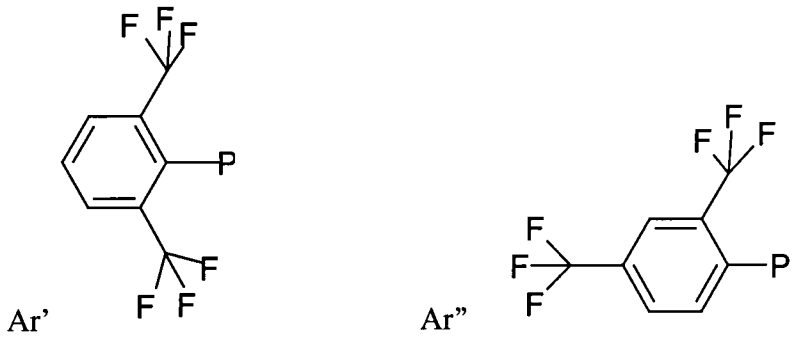

Figure 4. Fluoroaromatic groups.

The aims of the solid-state NMR experiments were to gain structural information about the compounds concerned and to investigate the interactions of phosphorus with other nuclei with spins ≥ ½. For compounds *I* and *II*, it was necessary to obtain a deeper understanding of the structure of molecules of interest in terms of their solid-state interactions. Where compounds have possible pharmaceutical activity it is important to know their solid-state structure (i.e. that in the final dosage form). The bioavailability and activity of a molecule are highly dependent on molecular packing in the crystal, and any impurities or multiple-polymorphs need to be carefully identified. In the case of the

ruthenium compound *III,* the NMR information was required as a starting point for X-ray powder diffraction for this catalytically active compound.

Compound I. Ar'Ar" PCl

(2,6-bis(trifluoromethyl)phenyl-2,4-bis(trifluoromethyl)phenylchlorophosphane

The crystal structure of this compound is known,[1] but it was thought that interesting effects could be observed from the interactions of phosphorus with the halogen centres in the molecule, both directly bonded, quadrupolar chlorine and the more distant CF_3 groups. As well as analysis of spectra from ^{31}P, ^{13}C, ^{19}F and ^{1}H, some cross-polarisation dynamics have been investigated involving phosphorus, in a system containing two abundant nuclei. These can be compared with the standard systems studied in Chapter 3.

Phosphorus-31 NMR Measurements

One phosphorus environment in the molecule is observed, splitting to four lines at the lowest field due to the effect of the adjacent chlorine (Figure 5, lower trace). The shifts of these lines are 75, 72, 66 and 62 ppm on the 200 MHz spectrometer, the last two not being completely resolved, but a shoulder is easily observable. All four shifts can be obtained from deconvolution using the Spinsight software.[2] A recycle delay of 5 s, and a 1 ms contact time were found to be optimum. MAS rates of 4-6 kHz were used for the phosphorus spectra, except at the highest field (600 MHz proton) where the small 3.2 mm diameter rotor meant a speed of 16.5 kHz was easily attained.

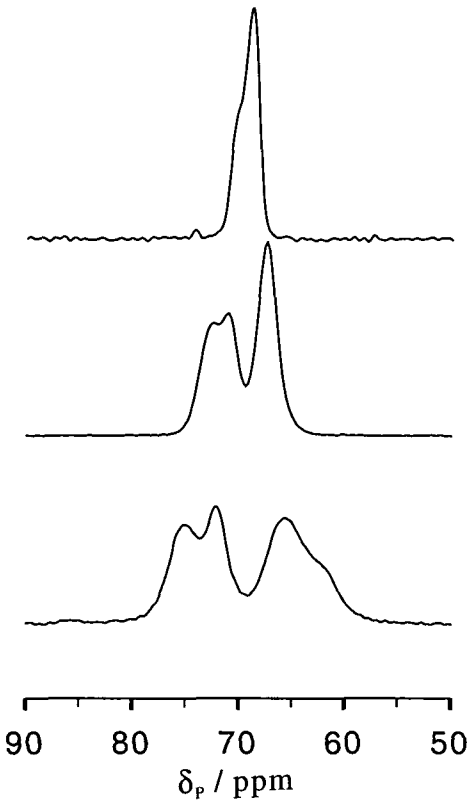

Figure 5. Phosphorus-31 {^{1}H} spectra of Ar'Ar"PCl. Centreband region only. Spectral frequencies (top to bottom) 242.8 MHz, 121.4 MHz, 81.0 MHz. Cross-polarisation from protons. Contact time 9 ms, recycle delay 5 s, number of acquisitions 152-448.

The nature of the splitting is identified by running at different field strengths, 200, 300 and 600 MHz (proton) spectrometers (Figure 5). As the splitting decreases on both a Hz and ppm scale, this confirms that there is a single phosphorus showing the effects of residual dipolar coupling to the adjacent quadrupolar chlorine. For residual dipolar coupling, the spread of frequencies expressed in both Hz and ppm decreases at higher field. This can be contrasted with the cases of isotropic indirect or crystallographic splittings which decrease in ppm and increase in Hz, respectively, on going to higher magnetic field strength, with units of the other scale staying constant. Where all four lines can be seen by deconvolution on the 200 MHz (proton) spectrometer, the separations of the lines are 228, 602 and 287 Hz (from high to low frequency). The first two splittings are still resolved at 300 MHz (proton) and are 188 and 449 Hz, and at 600 MHz (proton) only a single band with a high frequency shoulder is visible. The individual bandshapes do not show any significant changes over the spinning sideband

manifold. Due to the behaviour of these lines we can conclude there is a single phosphorus environment.

The interactions between phosphorus and chlorine may, in principle, be complicated by the two spin-$^3/_2$ isotopes of chlorine. However, due to the differing natural abundance and similar nuclear properties it can be expected that the separate effects will not be resolved within the observed linewidths. In the simulations, both isotopes can, however, be accounted for.

At the highest field there is no splitting observable within the linewidth of 650 Hz (the separation of the shoulder peak is approximately 350 Hz). The expected value of J_{PCl} is likely to be around 100-130 Hz,[3] so it is not surprising that no J splitting is resolved at the higher field. At 121.4 MHz (phosphorus frequency on 300) we seem to be approaching the situation of a doublet (J not effective) whereas at lower field there is perturbation.

The case of PCl_5 has been studied[4] and the effect on phosphorus of such residual dipolar coupling (RDC) to 4 and 6 chlorines of the two counter-ions investigated. At high temperature both phosphorus environments give rise to sharp singlets. The second-order effects collapse due to fast isotropic reorientation and/or short spin-lattice relaxation time of the chlorine nuclei (self decoupling). Isotropic J scalar effects, if these are appropriate, would only be affected by spin-lattice relaxation times.

Under the influence of heteronuclear dipolar splittings, an NMR spectrum will be split into a multiplet with lines corresponding to the states -m, -m+1, ... +m. To a first approximation the magnetic moments associated with the states of the quadrupolar nuclei are aligned with the Zeeman field and have values proportional to m. This leads to a symmetric multiplet. For large nuclear quadrupole coupling constants, the quadrupolar spin states are no longer quantized along the Zeeman field. Therefore, the symmetry of the multiplet is reduced. This also means that complete narrowing of the dipolar broadening by MAS is not possible.

Symmetric splitting, due to incomplete averaging of dipolar coupling, is predicted when first-order perturbation theory is valid. When $\chi >> \nu_s$ 'inverse' first order theory may be

applicable (the quadrupolar Hamiltonian dominates and there is only a small perturbation from the Zeeman term). Outside the limits of perturbation theory the situation is more complex.

Provided ν_Q, the quadrupolar frequency defined as $\nu_Q = \frac{3\chi}{2I(I-1)}$, is small compared to the Larmor frequency of the quadrupolar spin, ν_S, the residual splitting of the MAS peak in the spin-½ spectrum can be evaluated by perturbation theory. This is not necessarily the case for the effect of chlorine on the phosphorus spectrum of Ar'Ar"PCl. The situation with a half-integer spin and large nuclear quadrupole coupling constant (e.g. ^{35}Cl / ^{37}Cl or ^{63}Cu / ^{65}Cu coupled to ^{13}C) has been described by Harris and Olivieri.[4] When residual dipolar coupling to quadrupolar nuclei is observed, a change in value of ratio R (χ/ν_S, quadrupolar coupling constant / Larmor frequency at the appropriate field) will change the appearance of the spectrum. Increasing the applied magnetic field lowers the ratio of quadrupolar to Zeeman interaction and therefore decreases the second order effects (with splitting caused by residual dipolar coupling).

For a spin-$^1/_2$ - spin-$^3/_2$ system, an asymmetric multiplet is predicted when the dipolar and indirect (J) interactions are included. The positions of the lines of the multiplet are illustrated in Figure 6. In the case of a quartet (quadrupolar nucleus of spin-$^3/_2$), as the field decreases the lines will distort, the central two shifting in the opposite direction to the outer lines. Bunching of lines occurs at low frequency if Δ is positive and high frequency if it is negative. Depending on the ratio of all the relevant frequencies and coupling constants, this can often cause lines to cross, and an inner line of the multiplet may be actually observed as an outer line.

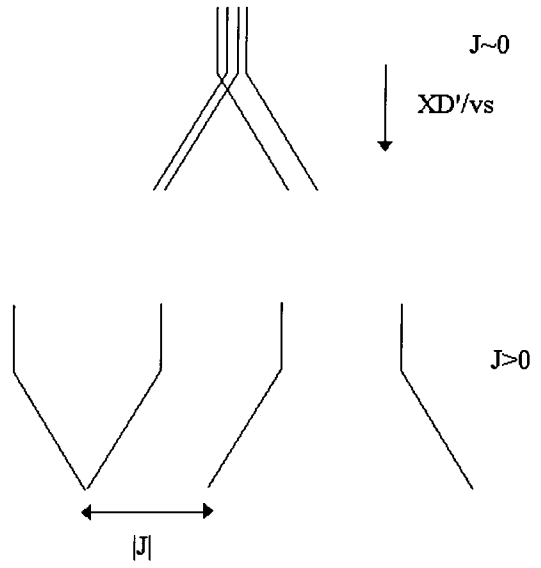

Figure 6. Appearance of a spectrum of a spin-½ nucleus under the influence of a spin-3/2 nucleus. The diagrams show the effect on line separation of J and dipolar interaction, quadrupole coupling constant and Zeeman frequency.

As described elsewhere in this thesis, D' = D - ΔJ/3. This means that residual dipolar coupling to a quadrupolar nucleus can also occur through the anisotropic term, ΔJ, as well as D, as they are mathematically identical. However in many cases the anisotropy in J is negligible and the RDC mechanism is assumed to apply exclusively via the dipolar mechanism.[5] In the simulations carried out below, the anisotropy in J is neglected as the value calculated from the crystal structure is used.

The equation $\Delta = -\frac{3}{10}\frac{\chi D'}{\nu_S}$ describes the deviation from equally spaced lines in the multiplet (the shift of the outer lines).

The signs of D and J depends on γ. If γ_I is negative the sign of the general equation is altered. The sign of γ_S does not affect the situation if D and D' have the same sign. If Δ is positive (bunching of lines is at low frequency), either χ is positive with D and D' same sign or χ is negative with D and D' the opposite sign. If, however, the reduced coupling constant $K_{IS} = J_{IS} / \gamma_I\gamma_S$ is used (as for J, this also has an anisotropy ΔK) the sign situation is simplified. The ambiguities in sign are no longer a problem if the appropriate term (D'/ν_S) is written as:

$$\left|\frac{D}{\nu_S}\right| - \left|\frac{1}{3}\Delta K\right|\left|\frac{\gamma_I\gamma_S}{\nu_S}\right|.$$

The approximate magnitudes of the effects of Δ are shown in Table 1 (assuming D' = D, from the known PCl distance of 2.068 Å, i.e. ignoring the effects of ΔJ, and that this theory is sufficient to describe the multiplet distortions seen in this system). The deviation, Δ, is half the magnitude of the predicted splitting in the observed spectrum and it can be seen from the table that these values are of an approximately correct order of magnitude. However, it is possible that there is also included the effect of a J_{PCl} coupling of the order of 100 Hz.

Isotope	Field (proton frequency) / MHz	r_{PCl} / Å	D' / Hz	χ / MHz	|Δ| /Hz	|2Δ| /Hz	observed splitting / Hz [a]
^{35}Cl	200	2.07	536	-55	557	1114	~860
^{37}Cl			446	-44	446	892	
^{35}Cl	300		536	-55	372	744	~560
^{37}Cl			446	-44	297	594	
^{35}Cl	600		536	-55	186	372	~350
^{37}Cl			446	-44	149	298	

Table 1. Theoretical modifications to the splittings observed.

[a] Doublet splitting at highest field (600), and approximate separation of the midpoints of the pairs of doublets at 200 and 300 MHz.

For the theoretical descriptions, J is assumed to be axially symmetric and coaxial with D. In general, a distorted multiplet from this approach will, in general, appear as a quartet with three lines close to one another, separated from the remaining line. The spectrum observed here is more easily likened to a doublet of doublets, especially at the higher fields.

From ab initio calculations using Gaussian94,[6] the electric field gradient (EFG) of the quadrupolar chlorine nucleus can be estimated. For this simulation the full molecular structure was used, and the calculations to give the NMR parameters also included a structural energy minimisation. Results were converted to an appropriate axis system within a Mathcad worksheet. χ is calculated by multiplying q (in atomic units) by 2.3495×10^{36} C J^{-1} s^{-1} (q is obtained as the largest component of electric field gradient in atomic units from a Hartree-Fock approximation using the 6-31g* basis set). Values

of χ with magnitudes 55 and 44 MHz were calculated for ^{35}Cl and ^{37}Cl respectively. These values were used in the calculations shown above in Table 1 and for the simulation of bandshapes.

Using a programme, kindly provided by A. Olivieri, written in the basic language,[7] the bandshapes at 200 and 300 MHz were simulated. There are several versions of this programme that will account for different situations. The one used here, 'anychi-x', calculates the MAS spectrum of a spin-½ nucleus under the influence of a quadrupolar ($I = {}^3/_2$) spin with assumptions of axially symmetry of the EFG, but allowing the angle β to be altered. A non-zero value of the scalar coupling can also be simulated. The value of χ is not restricted and -55 MHz was used for the ^{35}Cl isotope, -44 MHz for ^{37}Cl. J_{PCl} was set to the literature value of -100 Hz for ^{35}Cl (-83 Hz for ^{37}Cl),[3] and D as calculated from the crystal structure (therefore assuming a negligible value of the anisotropy in J). The exact value of J is not known for this compound, but it would seem that a value of this order of magnitude is likely. It can also be concluded from comparison of simulated and experimental bandshapes that J is negative. As indicated before, such a splitting will not be resolved in the linewidth, but it may, however, contribute to the distortion of the pattern, moving away from a situation which can totally be explained by simple perturbation theory. All bandshapes are initially calculated with the indirect scalar coupling and spectral width expressed in units of D. Altering this value to include a possible anisotropy in J would lead to a slight change in the influence of the scalar coupling and the total width of the whole pattern. Changing the value of D (D') from by ± 60 Hz does not have a very significant effect on the simulated spectrum. A larger value of J leads to an increase in the outer splittings and a smaller value for the largest central splitting. Several different angles, β were attempted (in the range 0 to 180°) and the approximate splittings of the simulated bands compared to the experimental data. The best agreement was found with $\beta = 0°$, with approximate splittings of 290, 530, 280 measuring from the centre of gravity of the simulated powder patterns (experimental values are 228, 602 and 287 Hz). If β is increased to 20°, the splittings move away from the experimental observed values, showing four peaks with more equal separation, although this is not so noticeable once line broadening is applied to the simulation. At higher values of β of around 90° the lines converge and the difference between the experimental simulated curves is obvious. Similarly, the

calculated splittings at 300 MHz are 250 and 430 Hz (compared with measured values 188 and 449, the third splitting being unresolved in this experimental spectrum). These values are in fair agreement with the experimental data, considering the assumptions that the most abundant isotopes dominates, that the perturbation theory is applicable and that the angle is at least close to 0° (a 20° angle gives larger discrepancies). As this system consists of a directly bonded spin pair this last assumption is unlikely to be an oversimplification. At 600 MHz, there is not sufficient resolution in the experimental spectrum to make any meaningful comparison with the simulated lineshapes, however, the overall width of the lines shows reasonable agreement with the width of the unresolved doublet. There are still some slight discrepancies in the exact values in the simulation which result from the oversimplification of the system and the uncertainties in the calculation of χ from an optimised structure, but in general the values of the parameters used are confirmed as a good representation of the actual situation. The contribution from ^{37}Cl does show different lineshapes to ^{35}Cl, but on addition of the two simulated spectra, there is no significant difference in the separations.

In an attempt to try and alter values of χ away from those calculated by ab initio methods, it was found that a slightly lower value around -50 MHz is perhaps more appropriate. In this case the simulated bands are brought slightly more in line with the experimental data. With an even lower value of χ the intensity differences become more inappropriate. In comparison with other systems frequencies of magnitude 25.5, 25.7 and 26.3 MHz are given for $(C_2H_5)_2PCl$, $(Bu)_2PCl$, $(C_6H_5)_2PCl$, respectively.[8] These will represent $\frac{1}{2}e^2Qq$ (i.e. $\frac{1}{2}\chi$) if the asymmetry is zero, and therefore show that the calculated values here are reasonable.

Figure 7 shows a comparison of the lineshapes (χ = -55 MHz and -44 MHz for ^{35}Cl and ^{37}Cl, respectively). There is obviously significantly more broadening on the experimental lineshapes, but for ease of distinguishing the individual lines the simulation linewidth was initially kept low. On first inspection, the peak heights in the simulation are in fair agreement with the experimental lineshapes, and the integrated intensity (larger width for the lower height peaks) may result in better agreement. Once line broadening has been applied the intensities and the values of the splittings show reasonable agreement. Any slight disagreement could be due to the assumptions of

axial symmetry and the limitations of not being able to optimise all the parameters by small increments due to the computational time involved in the calculation of each spectrum. More complex effects outside the capabilities of the simulation may be influencing the experimental spectra.

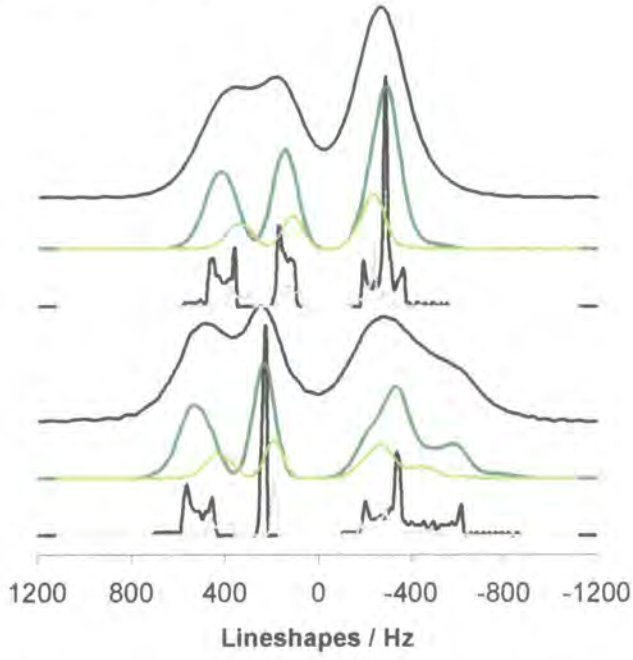

Figure 7. Experimental and simulated centreband shapes for the spectra run at 300 and 200 MHz (upper and lower). The broad black spectrum is the experimental shape at each field. The lower intensity simulated bandshapes (in grey) represent the lower abundance ^{37}Cl isotope. The green lines show the simulated contributions from ^{35}Cl and ^{37}Cl in the relevant proportions, also with the addition of 100 Hz line broadening.

An even lower field spectrometer, from which the splitting would be larger would perhaps help with the resolution of lines, although the asymmetry of the multiplet would be further increased.

Cross-polarisation experiments.

Both ^{19}F and ^{1}H were used for polarisation transfer to phosphorus. In both cases the rise of magnetisation during a variable contact time is a lot faster than the $T_{1\rho}$-dependent decay. For ^{19}F to ^{31}P cross polarisation, both the TORQUE curve (for which the total constant spin-lock time is 10 ms) and standard cross-polarisation experiment show an almost horizontal region at long spin-lock times. This implies that $T_{1\rho}^{F}$ and $T_{1\rho}^{P}$ are both long. The cross-polarisation time T_{FP} is around 0.5 ms and the $T_{1\rho}$ values are a lot longer than the maximum duration of spin-lock pulse available from the amplifiers. It is

therefore difficult to measure these accurately, but a value for $T_{1\rho}^{F}$ from a reasonable fit was obtained with a time constant around 100 ms. This value was obtained for a $^{19}F \rightarrow ^{31}P$ CP experiment, with a variable pre-contact spin-lock time. T_{HP} derived from $^{1}H \rightarrow ^{31}P$ cross polarisation is longer, at 3.5 ms. Here the TORQUE curve has a positive slope at long spin-lock time, suggesting $T_{1\rho}^{H} < T_{1\rho}^{P}$. An advantage of having a small ratio, $\varepsilon = N_S/N_I$, is that the theory used in chapter 3 is simplified as we approach a situation similar to that for $^{1}H \rightarrow ^{13}C$ cross polarisation. In these cases it is 1:12 and 1:6 for P:F and P:H respectively.

Fluorine-19 NMR.

The ^{19}F spectrum (Figure 12) shows four peaks of approximately equal intensity within experimental error (considering the overlap of lines), with chemical shifts at -54, -58, -60, -65 ppm. These observations indicate that there are different environments for all four CF_3 groups, as expected from a lack of molecular symmetry. Rapid internal rotation of these groups will cause averaging of the positions, and therefore chemical shifts, of the three fluorines in each CF_3. A contact time of 7 ms was used for cross polarisation from protons. Cross-polarisation has the advantage of removing the small, broad probe background signal (which is sometimes observed with direct polarisation), but as direct polarisation for fluorine can lead to a better signal-to-noise ratio, in a comparable time, this may be favoured when the background and desired signals are easily identified.

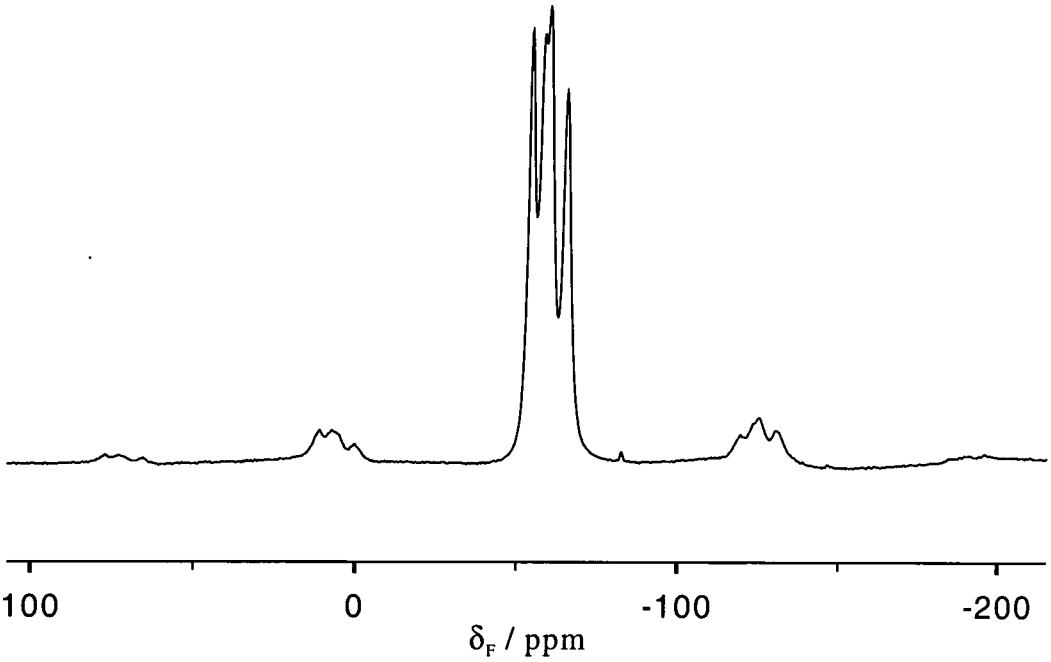

Figure 8. Fluorine-19 direct-polarisation spectrum of Ar'Ar"PCl. Spectral frequency 188.3 MHz, recycle delay 2 s, number of acquisitions 400, spin rate 12 kHz.

Because of the resulting increased averaging of the strong homonuclear interactions spinning at 12 kHz was found to give good resolution. Fluorine shifts are corrected for the Bloch-Siegert effect and referenced by replacement, setting C_6F_6 to -166.4 ppm with respect to $CFCl_3$, with high-power proton decoupling frequency applied.

The solution-state data have been discussed previously.[1] There it is stated that, from high temperature NMR, it can be concluded that rotation of the Ar' group about the P-C bond is fast enough on the NMR timescale to produce averaging. The low-temperature solution-state data suggest that, as well as being inequivalent, one ortho CF_3 group on Ar' is further away from the phosphorus than the other. For the solution state at low temperature there are two doublets and two singlets, with CF_3 fluorines on Ar" giving signals at -59.5 and -64.0 and those on Ar' at -54.5 and -56.6 ppm.

The solid-state fluorine spectra from this work and the previous solution-state results are compared in Table 2 below:

		δ_a /ppm	δ_b / ppm	δ_c / ppm	δ_d / ppm	average linewidth / Hz
	Assignment	Ar'	Ar'	Ar"	Ar" (para)	
Solution	high temp. 100 °C	-55.0 [a]				
	ambient temp.	-55.4 [b]		-59.3 [c]	-64.1 [d]	
	low temp. -78 °C	-54.5 [e]	-56.6	-59.5 [f]	-64.0	
Solid	high temp. 50 °C	-54.1	-57.7	-59.9	-65.3	568
	ambient temp.	-54.3	-58.0	-60.3	-65.5	597
	low temp. -120 °C	-55.1	-57.9, [g] -59.2 [g]	-61.4	-66.6	680

Table 2. Comparison of fluorine chemical shift data.

[a] broad doublet $^4J_{PF}$ = 35.3 Hz
[b] broad, double intensity
[c] doublet $^4J_{PF}$ = 59.1 Hz
[d] sharp
[e] doublet $^4J_{PF}$ = 75.8 Hz
[f] doublet $^4J_{PF}$ = 59.1 Hz
[g] low intensity

The solution-state results describe the following. At room temperature, there are two singlets; one broad, resulting from both groups on the Ar' group and the other from the para CF_3 with a doublet from the remaining Ar" CF_3. At low temperature the doublet and singlet from the Ar" group remain the same and there are two bands (doublet and singlet) from the Ar' group. This implies that, at this temperature, the Ar' CF_3 groups are inequivalent, only one showing $^4J_{PF}$ splitting. Indeed, the X-ray structure shows one ortho CF_3 with fluorine at 2.89 Å from phosphorus (closest distance) and the other at 3.25 Å.

Fluorine-19 spectra of the solid powder sample were obtained over the temperature range -120°C to +50°C. In the case of the solid-state spectra, we see individual resonances for each of the CF_3 groups at all the temperatures recorded (Table 2). $^4J_{PF}$ is not resolved in the solid-state spectra due to linewidths being broader than in solution, but, unlike the solution-state spectrum four peaks are already observed at room temperature, suggesting a crystal packing effect or slowing of motion in the solid-state

making all four CF_3 groups inequivalent. It is also observed that, in contrast to the solution state differences in coupling for each of the CF_3, there are no obvious differences in linewidth from deconvolution of the 4 peaks, so only an average value is quoted here. There is little change in the spectrum as temperature is lowered and the value of T_1^F remains constant at around 0.9 ± 0.1 s, to within experimental error, from -20 down to -80 °C, with a slightly lower value of 0.6 s at ambient temperature (~27 °C). Figure 9 shows the trends in chemical shift with temperature. All four peaks show a similar trend. The equations represent the best fit trend line through the plotted data and show the overall shift. As the slope is very small and approximately the same for all peaks (0.0087 ± 0.0018), it is possible that the change arises from a variation in the referencing procedure, e.g. by a change in the Bloch-Siegert effect as the temperature is lowered. Theoretically, at lower temperatures the Bloch-Siegert shift increased in magnitude. This is because the thermal resistance of the rf coil drops with decreasing temperature. Hence, a given output from the amplifier will generate a larger ^1H decoupling rf field at lower temperatures than it will at higher temperatures. The reference experiment, which corrects for the Bloch-Siegert shift, was not done at low temperature because of the problems with taking the liquid C_6F_6 reference sample down to the low temperatures used. This temperature phenomenon may also explain why, in the case of cross-polarisation, a decrease in the accuracy of the match condition is observed as the probe temperature is altered. As the coil changes temperature (and resistance) the B_1 fields may no longer be at the exact Hartmann-Hahn match. There is also the usual trend of broadening as temperature is decreased (the average values of the widths of each of the four lines were given in Table 2).

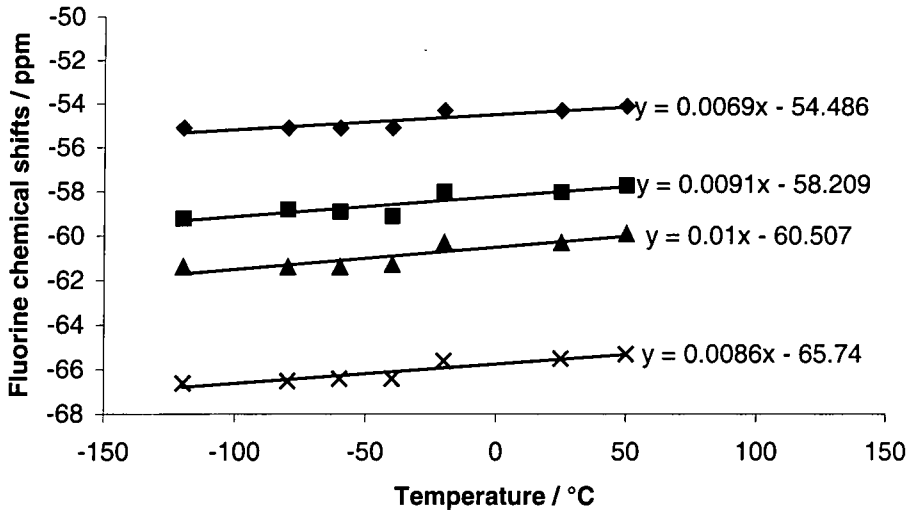

Figure 9. Change of fluorine shifts with temperature.

Carbon-13 NMR.

The carbon-13 spectrum (with cross polarisation from protons, using a recycle delay of 5 s and a contact time of 8 ms) appears to consist of three peaks with chemical shifts 134, 133, 129 ppm (by deconvolution). All these peaks are also observed in a dipolar dephasing experiment in which only quaternary (or methyl) carbons remain. However, with an echo experiment run with identical conditions apart from the presence of the 50 μs dephasing time, a subtraction can be made, resulting in a spectrum of protonated carbons only. In this case we observe a broad underlying peak with a maximum intensity at 134 ppm from the protonated aromatics. Taking advantage of the different cross polarisation and decoupling combinations possible in a fluorinated molecule and the triple-channel HFX probe, further conclusions on the carbon spectrum can be made. The low-frequency peak increases significantly in intensity on application of cross polarisation from fluorine, as does that at the highest frequency, indicating proximity of these carbons to the CF_3 groups. The lowest frequency peak also displays narrowing on application of fluorine decoupling. Although all these peaks appear in the aromatic region of a ^{13}C spectrum, it should also be noted that the shift of a carbon α to a single fluorine will be altered by around 70 ppm. As no peaks are observed in any other region of this spectrum, it is highly likely that the CF_3 resonances are shifted to higher frequency than this and are also contained within the 'aromatic' bands observed.

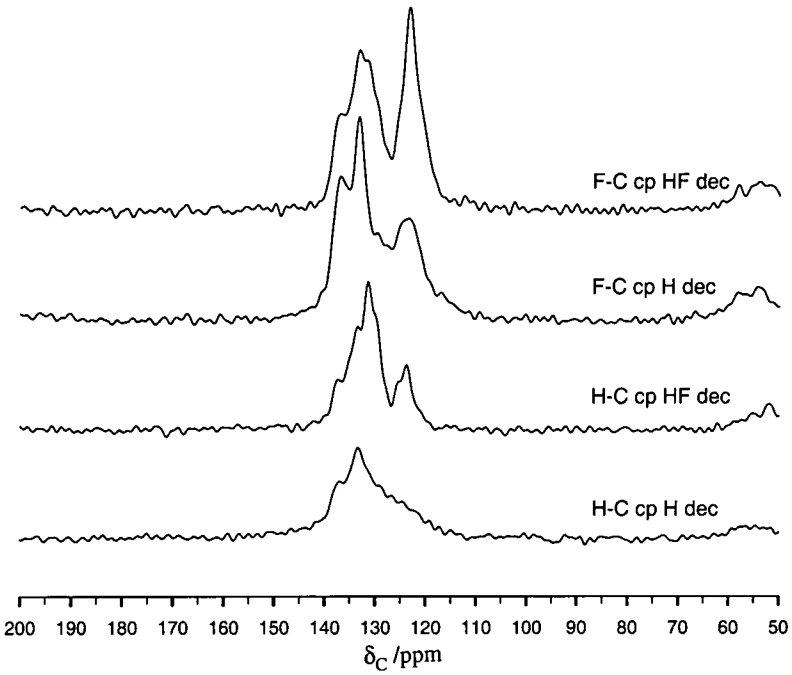

Figure 10. ^{13}C spectra (50 MHz). $^{19}F \rightarrow ^{13}C$ CP - contact time 7 ms, recycle delay 10 s, 280 acquisitions, spin rate 4 kHz. $^{1}H \rightarrow ^{13}C$ CP - contact time 7 ms, recycle delay 10 s, 64 acquisitions, spin rate 4 kHz.

No resolution is observed in the proton MAS spectrum (6 kHz spin rate), with a single, broad resonance seen at δ_H = 7 ppm. This is as expected from the closely related phenyl protons in the molecule and the strong homonuclear interactions.

Compound II.

Cis-dichloro(triethylphosphane)(2,6-bis(trifluoromethyl)phenyldichlorophosphane) platinum (II).

The crystal structure of this compound is illustrated in an 'ortep' plot (Figure 11). Indications are, that with rapid CF_3 re-orientations, the fluorines could all become equivalent. From this diagram there seems to be an approximate mirror plane down the centre of the molecule. The X-ray crystal structure (Figure 11) is described as being not as accurate as hoped.[1] This crystal structure was limited by the possibility of small amounts of the Ar" isomer being a possible product of the reaction. This meant refinement as a single isomer is difficult and the obtained crystal structure may not be truly representative of this system as a whole. The powder sample studied here has undergone purification by re-crystallisation.

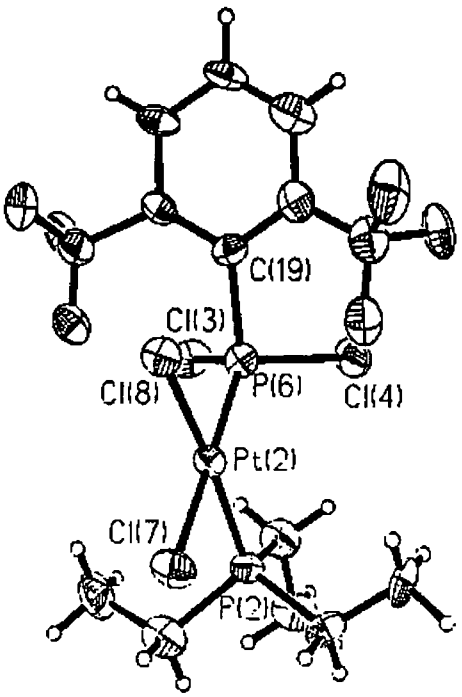

Figure 11. Ortep plot from crystal structure.[1]

Phosphorus-31 NMR results.

Isotropic shifts at 73.6 ppm and 16.9 ppm are consistent with literature, solution-state values of such environments and therefore can be easily assigned to PCl_2Ar' and PEt_3 phosphorus nuclei, respectively. The single shifts suggest that within the limits of the NMR experiments there is one molecule in the asymmetric unit and the two peaks are in

accord with a 1:1 intensity ratio for the two sites. Platinum satellites are observed for both peaks at a proportion of about 19 %, leading to a doublet superimposed on each singlet, with splittings of 5720 and 3410 Hz respectively. At 200 MHz (proton) field satellites from the two centres are exactly coincident making any form of quantitative analysis difficult. Hence these spectra have also been run at higher fields (300 MHz or 600 MHz, proton) to separate peaks with sufficient resolution without losing information. On the 200 MHz instrument, even if the spin rate is chosen such that no other overlap of singlet peaks or spinning sidebands occurs, the sum of half the two satellite splittings is equal to the Hz separation of the singlet peaks when the phosphorus frequency is 81.02 MHz. At higher fields, the Hz separation of the two singlets is increased, but the J coupling for the satellite splitting, obviously, remains the same. Optimum conditions were selected and set as a 5 s recycle delay and a 9 ms contact time for cross polarisation from proton to phosphorus (Figure 12). This was found to be appropriate on both 200 and 300 MHz instruments despite the possible changes in relaxation time at different magnetic field strengths. Including the satellite peaks in the intensity for the centreband and each spinning sideband, shielding anisotropy values of -100 and -60 ppm were calculated (± 2 ppm), with asymmetries of 0.4 and 0.6 (± 0.1) respectively. Two small impurity peaks are observed at either side of the peak at 16.9 ppm, the remaining peaks are all satellite peaks or spinning sidebands.

There is no obvious RDC coupling effect observed (in contrast to compound I). With a PCl_2 group present any effect would be more complex. However, it can be seen that there is a slight broadening of the PCl_2 peak in the lower field spectrum. This peak increases from 185 to 248 Hz in width (300 cf. 200 MHz, proton), with the other showing a change from 114 to 146 Hz. The larger broadening could result from the expected interactions with the directly bonded quadrupolar nuclei. A significant difference in the RDC effect observed in these two PCl compounds could be due to the tensor orientation, or a difference in chlorine relaxation, producing more efficient self decoupling in this second PCl case. This second case can not assume co-axiality of tensors as it is a PCl_2 system, as opposed to having a single direct PCl bond. The presence of two chlorine centres and other atoms in the molecule could easily change the relaxation properties significantly. The proton decoupling power for the spectrum of this compound run at 600 MHz was not sufficient at that stage, and therefore comparison of linewidths is not useful.

It can also be noted that the satellite peaks marked #' on spectra are unequal intensity. This could be an effect of D vs. σ tensor interactions, as discussed previously in this thesis, with interplay of the tensors distorting the sideband manifold. Close inspection shows that there is change of relative intensities over the manifold, that the intensity is constant over the complete manifold and that it is such a tensor effect distorting the spread of intensities over the anisotropic pattern.

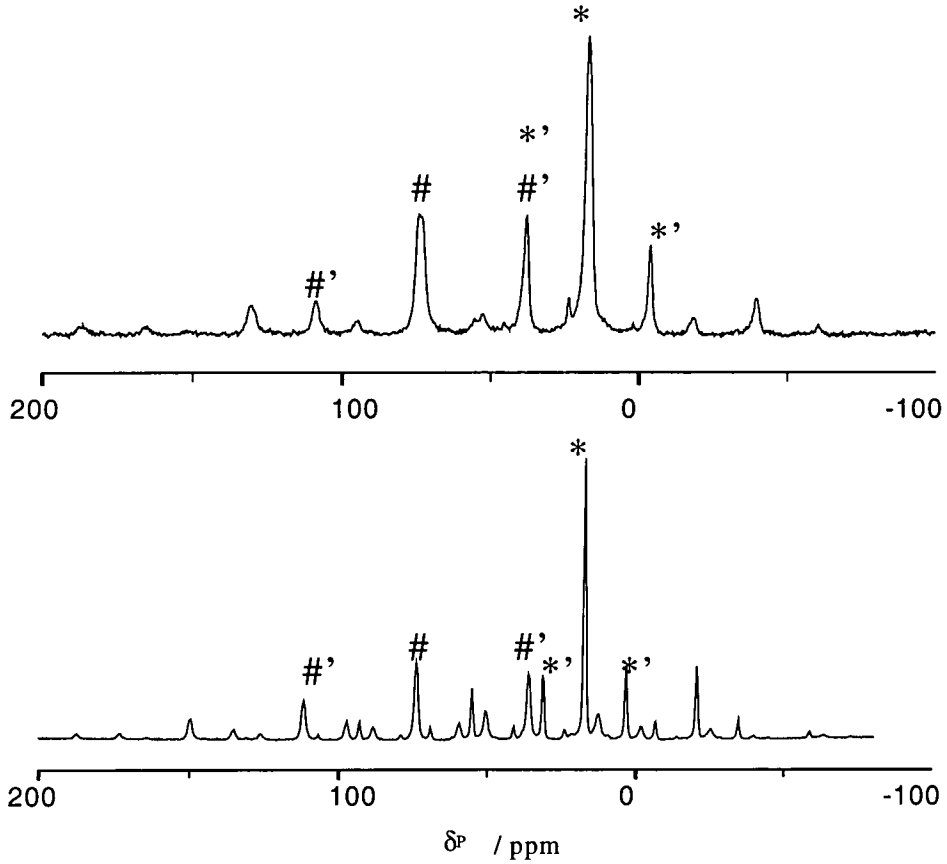

*Figure 12. ^{31}P spectra of compound II showing platinum satellites. Cross polarisation from protons, contact time 9 ms, recycle delay 5 s, 400 acquisitions, spin rate 4600 Hz. Top spectrum shows overlap of satellites from the two peaks (run on 200 MHz spectrometer). Lower spectrum has no overlap (300 MHz spectrometer). Isotropic shifts marked # and *, satellites marked #' and *' with the remaining peaks being spinning sidebands of isotropic and satellite peaks.*

The solution-state data describe the existence of two possible isomers, as isomerisation (Ar' or Ar") is possible. This occurs as there are two possible lithiation sites on $C_6H_4(CF_3)_2$ (meta substituents) to produce the species that is then reacted with PCl_3. Conversion from the trans to the stable cis isomer occurs after completion of the synthesis. This is true for this sample as the significant splitting from trans P-P coupling (680 Hz) is not observed. Due to re-crystallisation and the cis/trans isomer

conversion, it is highly probably that the powder sample studied is a single isomer. The solution-state data are compared with the solid-state results from this work in Table 3.

	δ_P	$^1J_{PPt}$	δ_P	$^1J_{PPt}$
solid	73.6	5720	16.9	3410
solution[1] Ar'PCl_2	94.50	5260.0	20.14	2916.0
solution[1] Ar"PCl_2	97.90	5488.1	19.54	3444.7

Table 3. Comparison of solution- and solid-state phosphorus data.

Although at first inspection, the coupling constants from the solid-state data appear to be closer to those of the Ar" compound in solution, the high-frequency phosphorus shift is very different for both isomers. This suggests that a direct comparison of the isomers between the solid and solution states is not possible. We will also see that the fluorine spectrum at room temperature is consistent with a single species with a single fluorine environment (suggesting Ar' and not Ar"). It is highly possible that, due to the different configuration, interactions, lack of random molecular reorientation and crystal-packing effects in the solid-state, the coupling constants are significantly modified. The impurity peaks at 11.9 and 23.6 ppm are too low in intensity to see any possible satellite peaks, which if they exist are lost in the noise, and there is no other high-frequency peak which could be due to the presence of an isomer. The isomer present has been assigned as the cis form from solution-state experiments, which can also be confirmed by the absence of any observable splitting from ^{31}P-^{31}P coupling. A trans isomer would have a very strong ^{31}P-^{31}P coupling constant of around 500 Hz, which would easily be resolved, given the linewidths in these solid-state spectra. Such an effect is not seen. It can therefore be concluded that this re-crystallised powder sample gives an NMR spectrum consisted with a single isomer.

Magic-angle Turning.

Following some of the work on the PHORMAT experiments that involved initial investigation of the applicability of such a pulse sequence to a simple phosphorus system, it was decided to run the experiment with some 'real' systems, containing more than one phosphorus site. Once a satisfactory brushite spectrum had been obtained (clear spectra were observed from the single phosphorus site), the experiment was

attempted for this multiple-site system, and the resulting two-dimensional plot is illustrated in Figure 13.

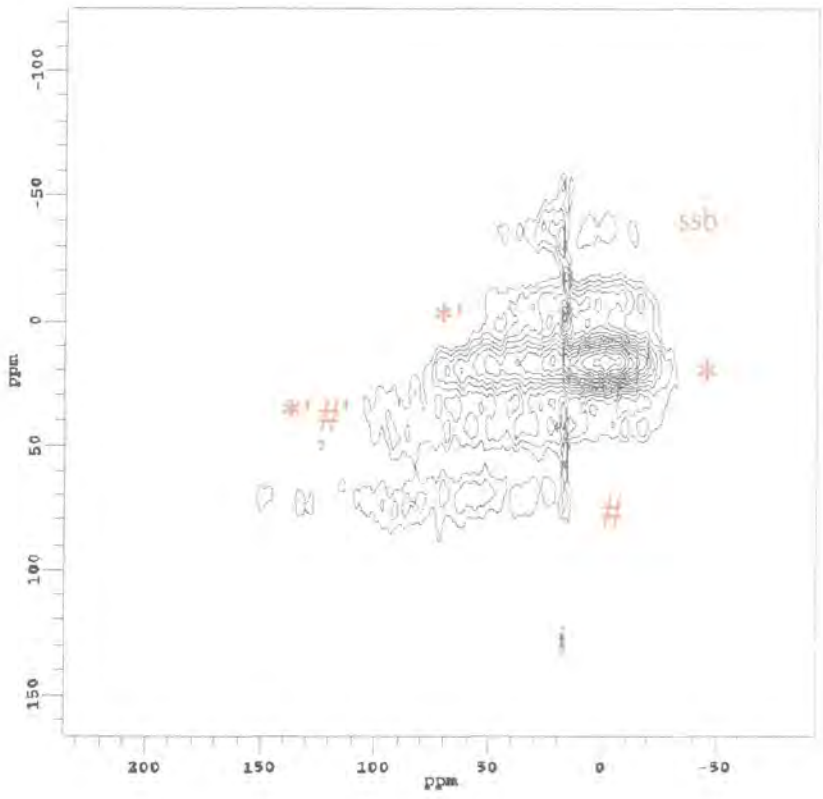

Figure 13. MAT spectrum of Ar'PPt dimer. 81 MHz phosphorus frequency, number of acquisitions 1000, no. of increments 28, spinning speed 38 Hz, contact time 2.5 μs, recycle delay 3 s.

In order to cut out the noise in 'baseline' of the contour plot above, the isotropic # is poorly represented in this view. However, it is seen later that the anisotropic powder pattern for this peak can clearly be seen in slices through the two-dimensional plot.

Despite the overlap of satellite peaks observed in the phosphorus spectrum of this compound on the 200 MHz instrument, a PHORMAT experiment was attempted at this field (Figure 13) as the initial work was done on the Chemagnetics system. It is known that the P-P distance is sufficiently large (at 3.3 Å) to avoid problems of a significant homonuclear dipolar interaction. This experiment should give the isotropic shifts and powder pattern separated into the two dimensions. The anisotropy patterns for the singlet isotropic peaks are visible (* and #) and the satellite powder shapes still show overlap as expected (*' and #'). The resolution is not as good as could have been hoped

for, but the individual sites are still seen. A longer experimental time would be desirable to reduce the noise level, but the drift in spinning speed at this time makes this impossible. Perhaps a better calibration of pulse duration would help to reduce the artefact (seen vertically through the centre of the two-dimensional spectrum), although checks were made in this case that would lead to pulse widths being accurate to at least 0.1 μs.

Figure 14 shows a comparison of the anisotropic patterns obtained from different experiments. It can be seen from the top spectra that an overlay of the 4 pseudo-static lineshapes from slices of the two-dimensional experiment is in good agreement with the one-dimensional, static powder pattern. This means that the shapes from PHORMAT have similar accuracy, in terms of the anisotropic pattern produced, as a simple one-dimensional static. The advantage here is that the individual lines have also been separated in a similar way to the sideband manifolds in an MAS spectrum.

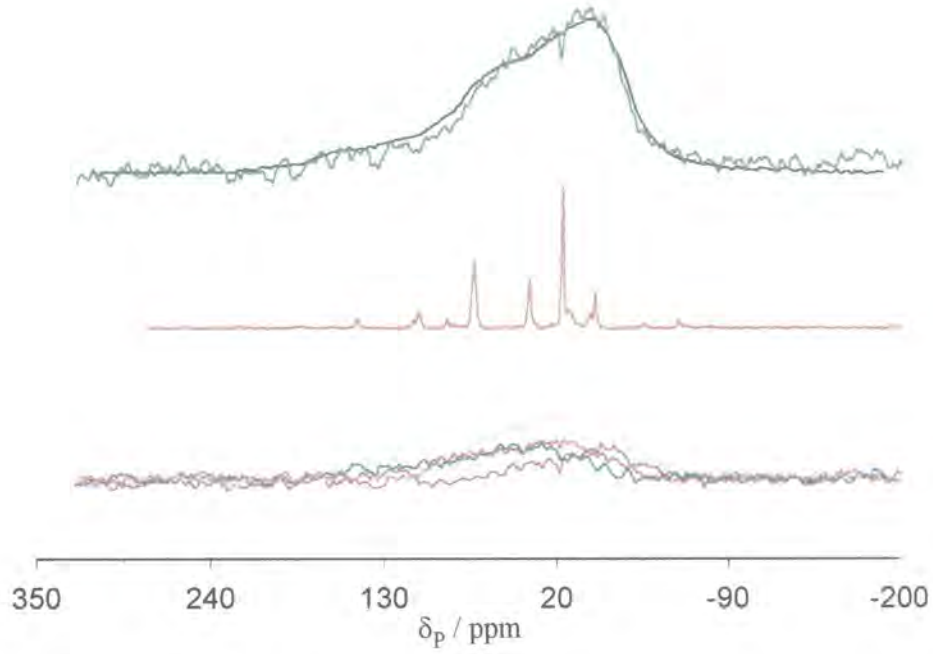

Figure 14. Comparison of lineshapes from different experiments, observing ^{31}P (81.02 MHz), for compound II. Lower: Maximum intensity slices in PHORMAT experiment; Middle: MAS spectrum; Top: Static spectrum (blue) and sum of slices through PHORMAT experiment (green).

Figure 15 shows an iterative (simplex) fit of the pseudo-static lineshapes that represent the isotropic shifts in the PHORMAT experiment. The programme for this simulation

was provided by P. Hodgkinson.[9] The data extracted from this fit are as follows: ζ = -60 ppm, η = 0 (upper spectrum) and ζ = -97 ppm, η = 0.5 (lower spectrum). These anisotropy values are in excellent agreement with the data from spinning sideband analysis, considering the noise level of these spectra and it can be seen by the overlay that the experimental and calculated lineshapes are very similar. There is some discrepancy between the asymmetry values, though it has been commented before that the accuracy of determination of η is highly dependent on the method of calculation (MAS vs. static simulations). It can therefore be concluded that this PHORMAT experiment accurately represents the individual powder patterns of a multiple site system, and that the 3.3 Å separation between the phosphorus centres is sufficient to avoid the problems caused by homonuclear dipolar interactions.

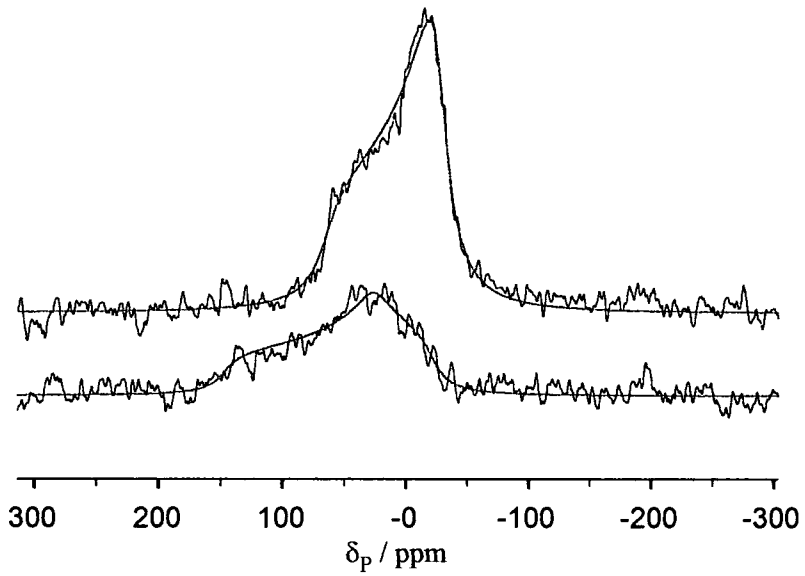

Figure 15. Slices through the maximum intensity of the PHORMAT experiment representing the two isotropic shifts. The overlaid lines (red) represent the fit of the pseudo-static lineshape.

Carbon-13 NMR.

The phenyl region is crowded and poorly resolved, so distinction of shifts in cross-polarisation experiments with and without dipolar dephasing (non-quaternary suppression) is difficult. A contact time of 7 ms gave the highest signal intensity. Approximate individual shifts (in ppm) observed are 8 (Me), 16 (CH), 125, 128 (aromatic CH) and 134 (quaternary aromatic).

Fluorine-19 spectra and motion.

An isotropic shift of -51.6 ppm with a linewidth (full width half height) of 800 Hz is recorded by observing the fluorine spectrum at 27°C with a restricted sample volume confined to the centre of the rotor (see top spectrum of Figure 16). A single fluorine shift would suggest less than one molecule in the asymmetric unit. Even though the crystal structure shows approximate symmetry, it is difficult to conclude that this would make all fluorines equivalent in the solid state if all atoms are in these static positions. It is suggested that molecular motion is occurring. A recycle delay of 4 s was used for the CP experiment; a similar value of 5 s was also appropriate for direct polarisation. T_2 was measured using a 90-τ-180-τ pulse sequence[10] with proton decoupling applied during the variable delay, τ and acquisition. The measured linewidth can be compared to that of 500 Hz calculated from a T_2 of 0.6 ms.

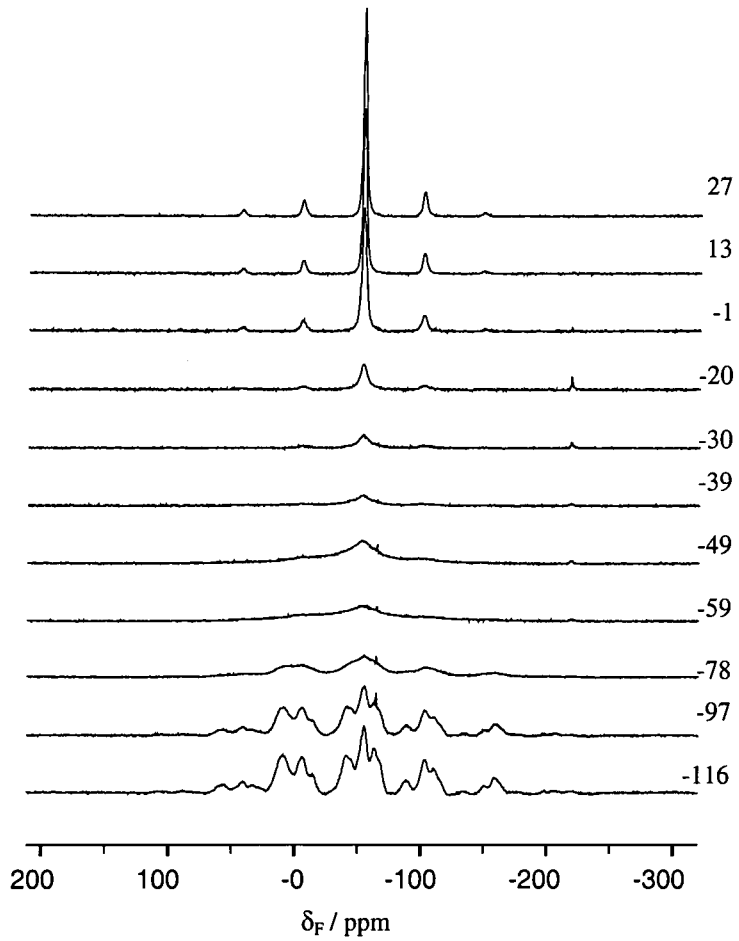

Figure 16. Variable temperature ^{19}F spectrum (188.3 MHz). Temperatures given in °C. Cross polarisation from protons, contact time 6 ms, recycle delay 4 s, 300 acquisitions, spin rate 9 kHz.

Variable-temperature experiments show an initial broadening of the signal as the sample is cooled, followed by a splitting into a more complex bandshape with a spinning sideband manifold as the CF_3 motion is slowed sufficiently. This change was observed to be reversible and reproducible whether acquiring spectra during increase or decrease of sample temperature. Clearly, at low temperature it is possible to slow down some of the motion in the molecule. Both the rotation of the whole Ar' group and of the individual CF_3 groups can presumably occur to create the single resonance observed at ambient probe temperature (~25-27 °C under normal spinning conditions).

An initial energy minimisation was carried out for the structure of compound II using CAChe (3.0) molecular modelling software (as above for the EFG calculations in compound I), with the crystal structure data as the input. The optimised structure produced by the programme (MM/AM1) produces a different minimum energy structure (Figure 17) than the known crystal structure,[1] in terms of the orientation of the Cl atoms on platinum being parallel or perpendicular to the Pt-P-Ph bonds, the most likely cause of this being the simplification of modelling a single molecule. The interactions between molecules in the crystal may well modify the structure and minimum energy configuration. This study was continued by producing energy maps for the possible re-orientations within the Ar' group in the energy optimised structure. Using these simulation results for energy barriers to rotation, the origin of the exchange process can be investigated. There are several possibilities for motion which would cause averaging of the CF_3 groups. Two different orientations of the Ar' [$Ph(CF_3)_2$] group in or out of plane of the molecule (rotation of Ar' as a whole) will give two types or one type of CF_3 group, which can then, themselves, rotate to average the three fluorines on each. The energy barrier to Ar' rotation is likely to be a lot higher than that of the simple CF_3 rotation, and it can be shown by the energy calculations using CAChe molecular modelling (MM/AM1) that this is in fact the case. Rotation of the whole Ar' group requires around 60 kJ mol^{-1}, and that of the CF_3 groups, only 12 kJ mol^{-1}. These can be compared with the estimated energy barriers from the relaxation time study of the molecular dynamics.

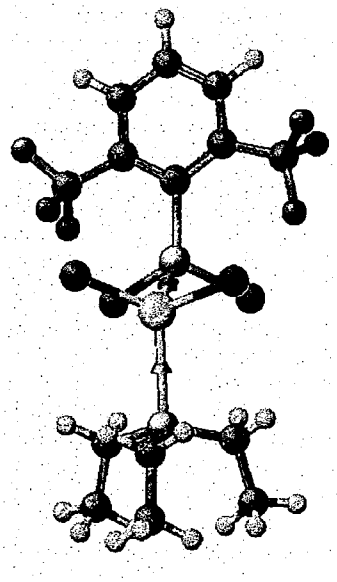

Figure 17. CAChe optimization.

The higher the energy barrier to rotation, the higher the temperature needed to see averaging on the NMR timescale. In this case, observing the ^{19}F spectrum at temperature in the range -116 to 27 °C, the change from six peaks to one peak is observed as the temperature is raised. This would require both the rotations described above to change rate over the temperature range observed. The three resolved bands at low temperature do not each consist of single lines. Deconvolution using the Spinsight software[2] clearly gives six resonances, in three close pairs. As there are six different fluorine resonances at low temperature, it is not possible to cause complete averaging by simple CF_3 rotation (which would lead to two resonances at high temperature), assuming that a static Ar' orientation would be the same as in both the crystal structure and minimum energy simulation. Another possible explanation, that is, that $^4J_{PF}$ (measured in solution-state spectra of compound I as approximately 30-60 Hz) or $^2J_{FF}$ coupling (which can be as large as 170-220 Hz)[11] is causing three peaks at low temperature to split into doublets. Deconvolution of the splitting was carried out. It is observed that the possible 'doublets' have a lot larger splitting (~600 Hz) than the estimated J values.

As the two rotation processes postulated have different energies, it is expected that two different coalescence points will be seen over the temperature range. At first inspection there appears to be only one coalescence, but in the range where the signal is broad (-30 to -80 °C) there is no resolution, and, due to the poorer signal-to-noise in this region, as

the linewidth increases dramatically, it is difficult to see if two changes are occurring at different coalescence temperatures. On 'deconvolution' of these spectra to produce an estimated linewidth at these central temperatures, it is possible to postulate that at -49 °C we have a slightly narrower line and are therefore between the two coalescence temperatures. Estimates of temperatures at which the broadest lines (coalescence points) occur then become -35 and -70 °C.

Spinning sideband analysis was carried out from these spectra at the two temperature extremes. Because the low-temperature spectrum is not resolved, the three distinguishable peak heights (which actually consist of two overlapping lines) were extracted and three different shielding anisotropy values calculated.

Temperature / °C	27	-116	-116	-116
Isotropic shift / ppm	-52.2	-40.8	-53.9	-63.6
anisotropy (± 4 ppm)[a]	-55	128	103	-110
asymmetry (± 0.1)	0.0	0.0	1.0	0.75

[a] $\zeta = \sigma_{33} - \sigma_{iso}$ / ppm

errors are estimated from the statistical uncertainty given in the fitting of sidebands (error analysis, according to the method of Olivieri, is incorporated into the sideband fitting programme, as described earlier)

Table 4. Spinning sideband analysis results.

This indicates that the anisotropy is larger at the low temperature and also that the system deviates from zero asymmetry. As the temperature is decreased and the averaging motion within each molecule is reduced, the orientation dependence of the shielding tensors at each fluorine lead to these observed effects. This effect was not observed in the case of the phosphorus signals in the TPPO-phenol study, as in that case the phosphorus atoms are in fixed positions and we are seeing an averaged and individual effects of the motion of a hydrogen bonded molecule (see chapter 7).

Relaxation times.

Relaxation times have been measured at different temperatures. As it is the motion of the CF_3 groups that is of dynamic interest, the fluorine spin-lattice relaxation and spin-lattice relaxation in the rotating frame were measured from ambient probe temperature down to the limits of the probe specifications (-140 °C set temperature) and up to +50

°C. These parameters were both measured by the direct observation of the fluorine signal, T_1 via the inversion recovery method (with direct observation of the fluorine signal without cross polarisation),[12] and $T_{1\rho}$ measurements were obtained from a single-channel variable spin-lock time array. The fitting of intensity was done within Chemagnetics Spinsight software.[2] That for T_1 used a three-parameter fit taking into account the efficiency of the inversion. 15-20 data points were recorded at each temperature and proton decoupling was not applied during relaxation.

Minima are observed in both the T_1 (Figure 18) and $T_{1\rho}$ (Figure 19) measurements over the temperature range -130 to +50 °C. The two minima suggest that two different motional processes are occurring, with very different rates.

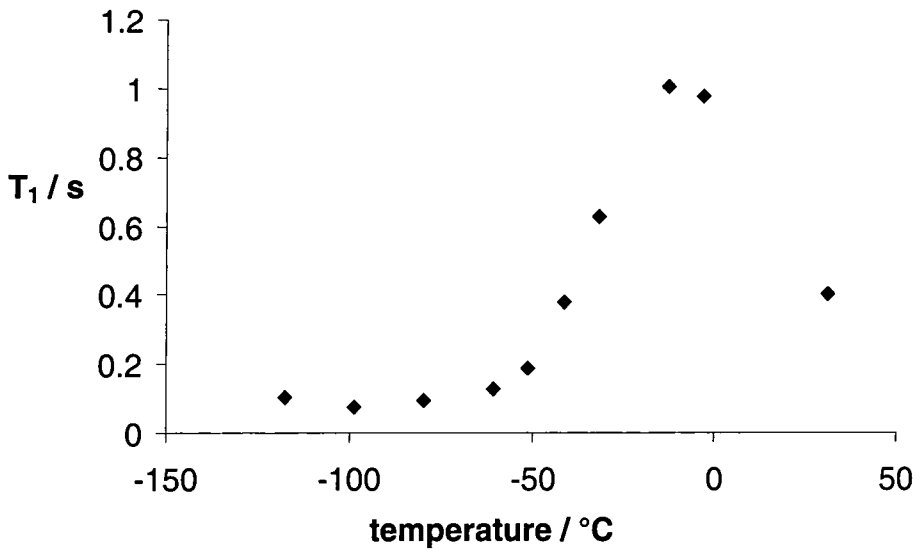

Figure 18. Variable temperature T_1 measurements.

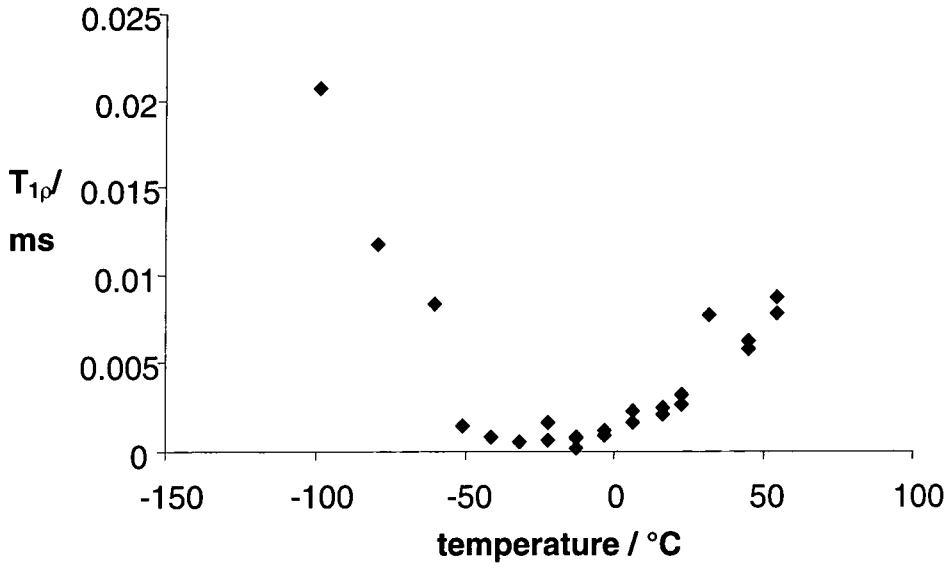

Figure 19. Variable temperature $T_{1\rho}$ measurements.

The T_1 minimum of 0.07 s occurs at -100 °C, and could represent the change to 6 peaks in the spectrum and therefore the energy barrier for Ar' group rotation. T_1 is sensitive to motions of the order of hundreds of MHz, and at the minimum $\tau_c = \omega_o^{-1}$ is defined by the spectrometer operating frequency, whereas $T_{1\rho}$ interference depends on Ω_1, the spin-lock field, which is of the order of tens of kHz. At the temperature where there is a minimum in $T_{1\rho}$, the spin-lock field can be related to the correlation time for motion and therefore, to a value of the exchange rate constant.[13] The correlation time for 360 ° motion is equal to the reciprocal of the spin-lock field at the temperature where the minimum $T_{1\rho}$ is reached. The theory used for this correlation time is based on the equation given by Deverell et al[14]. An expression of the form

$$\frac{1}{T_{1\rho}} = C\frac{\tau_c}{1+\omega_1^{\,2}\tau_c^{\,2}},$$

where C is a constant and $\omega_1 = \gamma_F B_{1F}$, is applicable and can be differentiated to give a minimum in $T_{1\rho}$ when $\omega_1\tau_c = 1$. Further terms in $\omega_o\tau_c$ concern motions influencing T_1 and, in this case, should be considered as there is also a variation of T_1 with temperature. At the temperature of the minimum $T_{1\rho}$ the corresponding T_1 is at its maximum value of 1 s. However, for motions on the order of kHz the system can normally be considered rigid on the T_1 scale. The ^{19}F 90 ° pulse duration was measured as being 3 μs, representing a field equivalent to 83 kHz. For $T_{1\rho}$ the minimum (0.8 ms)

is at the much higher temperature of -26 °C. In the simple case where T_1 is assumed long, and therefore related terms can be neglected, the correlation time obtained from the $T_{1\rho}$ minimum for 360 ° re-orientation is 3 μs, corresponding to a rate of 83 kHz. The corresponding rate constant for the process producing the T_1 minimum is 188 MHz. It can also be seen that there appears to be a second minimum above room temperature for the T_1 measurements. However, at these temperatures it was not possible to continue experiments to define a clear minimum. It should be noted that these rate constants apply to the motion at the particular temperature of the minimum in relaxation which is not the same for the two different motions. The process that is apparent at the higher temperature has a slow rate and a correspondingly higher activation energy, as can be derived from the slopes of the logarithmic relationship away from the minimum. The slope of the $\ln T_{1\rho}$ vs. 1/T plot at high temperature is -2500. This leads to an activation energy of 21 kJ/mol. Similarly, for T_1 at high temperature (covering the range of the $\ln T_{1\rho}$ minimum) the slope, -1600, leads to E_a = 14 kJ/mol. These are of the same order of magnitude as the calculated values, considering that the optimised, not actual, structure for an isolated molecule is used for the energy map calculations.

The trifluoromethyl group has been reported as having an energy barrier to hindered rotation, in solution, about the single bond of 36-46 kJ/mol in N,N-dialkyl amide and chloride derivatives of 2-methoxy-2-phenyl-3,3,3-trifluoropropanoic acid where the coalescence temperature is high. Barriers to CCF_3 bond rotation are generally in the range 16-35 kJ/mol.[15] These results relate to motion in the solution-state and it is also known that activation energy barriers of solid-state dynamic processes are generally about 30% higher than the analogous barriers in solution,[16] suggesting that the energy barriers to rotation in the system studied here are unusually low. From a space-filling point of view CF_3 rotation is clearly less hindered than rotation of the Ar' group.

The phosphorus and proton relaxation times (Table 5, Figure 20 and Figure 21) were measured by the methods given in the table. Spectra were acquired with phosphorus-observe experiments, proton decoupling being applied during acquisition, but not relaxation. The time constants, derived from intensity measurements, have an accuracy of 2-8 %, depending on the level of noise. For all T_1 and $T_{1\rho}$ measurements 12 data points were recorded, the maximum spin-lock time (an instrumental restriction) for

the latter being 20 ms, which obviously limits the accuracy of measurement of long rotating frame relaxation times.

Experiment		Phosphorus shift	
		74 ppm	17 ppm
T_1^H	(Torchia CP method)	0.4 s	0.4 s (+ small component 3.5 s)
T_1^P	(Torchia CP method)	9.8 s	9.5 s (+ small component 3.5 s)
$T_{1\rho}^H$	(variable spin lock)	23 ms	22 ms
$T_{1\rho}^P$	(variable spin lock)	500 ms	130 ms
T_{HP}	(variable contact time, [a])	1 ms	0.4 ms

[a] Standard equation used. As $T_{1\rho}^P$ is long, the classic equation, fitting the exponential rise of the variable contact time is applicable. This is discussed in detail in Chapter 3. A $T_{1\rho}$ value was not derived from this experiment due to the limits on contact time.

Table 5. Relaxation data.

It is clear from all the measurements of T_1 that the relaxation times are the same throughout the molecule. For example, even though non-equivalent protons exist in the molecule, spin-diffusion is averaging T_1^H throughout the molecule. It is perhaps surprising that the two phosphorus environments have so similar relaxation times. However, if you consider that ^{31}P is 100 % natural abundance and the two positions are fairly close (~3.3 Å), it is possible that interaction is causing relaxation phenomena to be averaged. However, at this distance the dipolar interaction can be calculated as 550 Hz and was said to be low enough to avoid problems in the PHORMAT experiment. The $T_{1\rho}^P$ measurement shows distinct values, but this may be because in principle spin diffusion is less effective for $T_{1\rho}$. The similarity in $T_{1\rho}^H$ is most likely due to spin-diffusion effects. It is noticeable that the cross-polarisation efficiency is greater for the low-frequency peak because of the proximity of the ethyl groups and possibly also due to rapid internal rotation of the aromatic group.

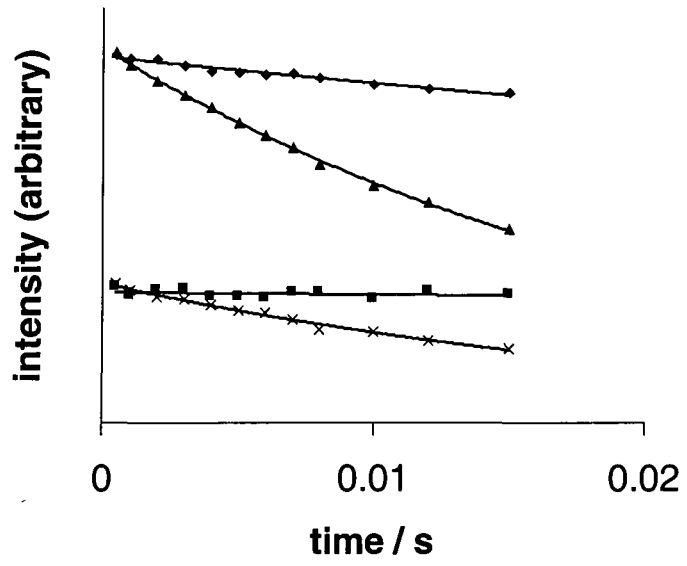

Figure 20. Exponential decay plots from measurement of $T_{1\rho}$ relaxation times. ♦$T_{1\rho}^{P}$ (17 ppm), ■$T_{1\rho}^{P}$ (74 ppm), ▲$T_{1\rho}^{H}$ (17 ppm), × $T_{1\rho}^{H}$ (74 ppm)

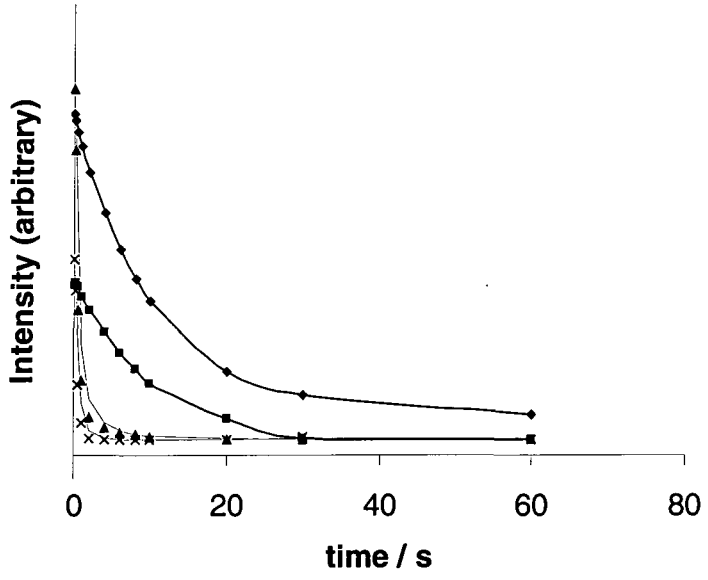

Figure 21. Exponential decay plots from measurement of T_1 relaxation times. ♦$T_{1\rho}^{P}$ (17 ppm), ■$T_{1\rho}^{P}$ (74 ppm), ▲$T_{1\rho}^{H}$ (17 ppm), × $T_{1\rho}^{H}$ (74 ppm)

In conclusion, this compound has been used to explore some of the techniques available to characterise motion in the solid-state, and to investigate the phosphorus sites in terms of coupling and anisotropy, including application of the two-dimensional PHORMAT experiment. Relaxation times have also been investigated for the three 'abundant'

nuclei, ^{1}H, ^{31}P and ^{19}F, for characterisation and variable temperature studies. We have seen that there is extensive motional averaging in the molecule and that it is likely that the sample consists of a single isomer, with no more than one molecule in the asymmetric unit distinguishable by these NMR experiments.

Compound III. Carbonyl(dihydrido)tris(triphenylphosphine)ruthenium(II)

Before beginning the discussion of this compound, it is worth considering some previous results on similar systems in order to bring this data into context. The effects of cis/trans phosphorus coupling in an ABX spin system have been described in the literature for the transition metal complex (Wilkinson's catalyst), $RhCl(PPh_3)_3$.[17] The splitting from J_{PP}(trans) is 365 Hz, and that for the cis coupling is so small so as to be unresolved. Although there was also the additional effect of J_{PRh} coupling in $RhCl(PPh_3)_3$, the pattern produced can still be compared with that from the triphenylphosphine ligands of the ruthenium complex described here.

Phosphorus-31 NMR spectroscopy of metal carbonyl derivatives[18] shows a large effect on chemical shift anisotropy of ^{31}P resonances caused by the bonding mode of the P donor atoms. Data from this compound can be compared with other ruthenium complexes to give confirmation of the 'terminal' mode of bonding. Figure 22 gives examples of anisotropy values, defined as (σ_{33} - σ_{11}), for several Ru, CO, PPh_3 clusters. The differences in anisotropy are due to bridging / terminal differences and bond angle differences for bridging phosphorus groups.

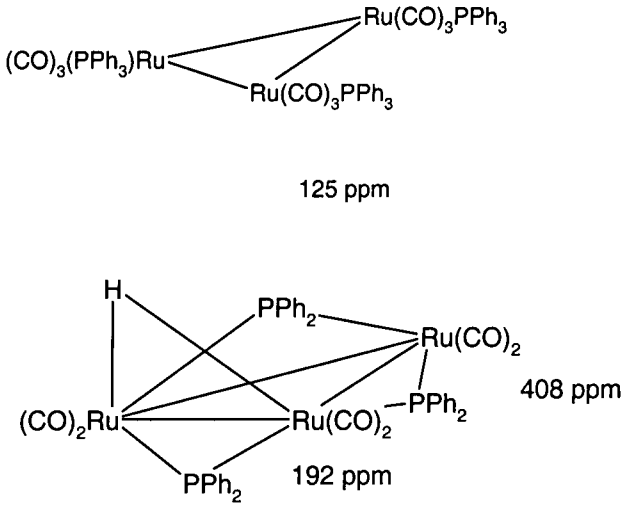

Figure 22. Phosphorus anisotropies in ruthenium complexes.

Phosphorus, carbon and proton MAS spectra of compound III have been recorded. For both carbon and phosphorus, MAS rates of up to 6 kHz were used.

Phosphorus-31 spectra.

For the phosphorus spectrum a 30 s recycle delay and a 2 ms contact time for cross polarisation from protons were found to give optimum signal intensity. The spectrum consists of three bands, a single resonance from one phosphorus and a pair of roofed doublets of an AB spin system from two strongly-coupled phosphorus centres (Figure 23). The five centreband peaks are those around 50 ppm, the remaining signals being identified as spinning sidebands and a low intensity impurity (~30 to 40 ppm).

The roofing suggests that two of the phosphorus centres are trans to each other, as this gives much stronger coupling than the cis arrangement. The intensity ratio is consistent with the singlet representing one phosphorus and each of the trans-coupled doublets having a similar intensity. This is in agreement with a postulated structure of an octahedral complex with mer-isomer phosphine ligands with hydrides. Such a structure, a transition metal centre with possible variable oxidation state and this particular arrangement of ligands, is ideally set up as a possible catalyst for hydrogenation and isomerisation processes.

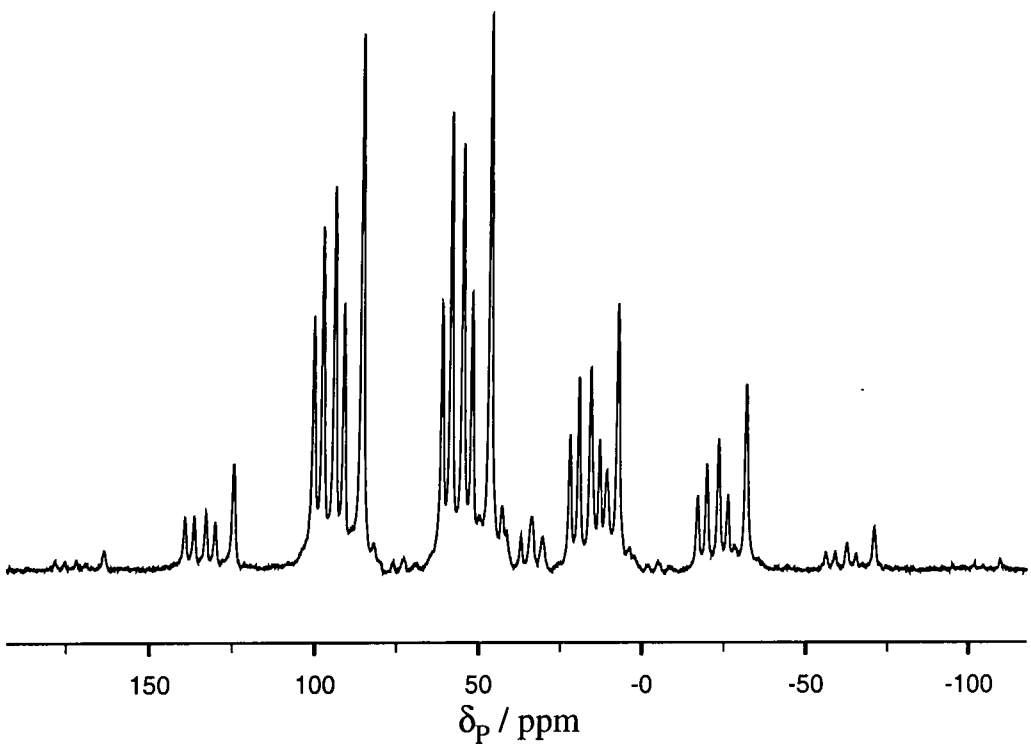

Figure 23. ^{31}P spectrum of Carbonyl(dihydrido)tris(triphenylphosphine)ruthenium (II). 30 s recycle delay, 2 ms contact time (cross-polarisation from protons, with high-power proton decoupling), spin rate 3 kHz, frequency 81 MHz.

Phosphorus shifts of 61, 58, 54 and 52 ppm for the roofed doublets are observed with splittings of 230 Hz for $|J_{PP}|$. This leads to an average chemical shift of 56 ppm. Calculation from the splittings, where $\Delta\nu = \sqrt{(xy)}$, where x and y are the separations between the outer most and innermost lines of the band, gives individual shifts for the AB system of 53 and 59 ppm. Spinning sidebands also exhibit 230 Hz splittings for the roofed doublets. These values are governed by the accuracy of measurement of peak positions. The single resonance from the cis phosphine is at 46 ppm. It will only be weakly coupled to the other phosphine ligands, therefore, so that splittings are not observed.

The coupling is lower than that for the published rhodium compound (Wilkinson's catalyst), and, interestingly, in contrast to the situation observed in this work, the chemical shift of the cis triphenylphosphine is to higher frequency of the trans doublets. As Wilkinson's catalyst is only a 4 co-ordinate species, the actually geometry will be very different, even though it has the same ABX spin system of 3 trans/cis triphenylphosphine ligands.

The change of the roofing pattern, with different resolution, has been observed by running spectra at higher fields. At a 600 MHz (proton) field, the average shift is measured as 56.7 ppm, giving the individual shifts as 59.8 and 53.7 ppm. These are consistently 0.7 ppm higher than at 200 MHz, suggesting the difference is purely from referencing error (sample replacement was used). At this higher field the |J| value is 220 Hz, which agrees with the original spectra, to within the experimental limits of accurate measurement of splittings. The conditions used for the spectrum on the 600 spectrometer were; spectral frequency 242.8 MHz, 3 μs duration for the proton 90° pulse, variable amplitude CP with a 8 ms total contact time in ten increments. Variable-amplitude CP was used to avoid any possible decrease in CP efficiency with a single amplitude Hartmann-Hahn match, as can often be the case with high-speed spinning (~16 kHz). The recycle delay was 30 s and 52 acquisitions were recorded.

The individual lineshapes, as initially observed for a CMX200 spectrum, are asymmetric in the centreband, with each peak of the multiplets having a high frequency shoulder. Deconvolution of the 'singlet' shows two peaks, each with full width at half height 100 Hz, a separation of the same order of magnitude, and an intensity ratio of

approximately 1:2. The quartet shows a similar pattern. Ruthenium has two spin 5/2 isotopes, at 13 and 17 % natural abundance, with quadrupole moments of the order of, and one order of magnitude higher than, that of nitrogen-14, respectively, for which residual dipolar coupling to carbon is commonly seen. However, this is unlikely to be the case here, and the effect would not be so simple as to cause 1:2 doublets. Also, the spinning sideband peaks do not show this asymmetry of the individual lineshapes. In order to elucidate the source of this effect, the experiment was repeated. Immediately before running the spectrum, the magic angle was checked and set accurately by observing the ^{31}P spectrum of zinc (II) bis(O,O'-diethyldithiophosphate (ZDP).[19] The distorted lineshapes were removed and it can be concluded that the phosphorus spectrum of the ruthenium complex is highly sensitive to the accuracy of the magic angle. This is often the case when samples have a large shielding anisotropy. Suitable samples for setting the magic-angle will have a large shielding anisotropy, and, to enable fast repetition of single acquisitions as the angle is being adjusted, a short T_1^H (e.g through spin diffusion effects). Although this sample is proved to be highly sensitive to magic angle, the 30 s pulse delay with CP from protons limits its use as a standard sample.

Spinning sidebands are evident from 200 to -100 ppm. By the use of the programme ssb97, the shielding anisotropy values have been calculated to be 106, 97, 105 and 106 ppm (asymmetry 0.4 to 0.5) for the trans phosphorus centres (values for highest frequency peak given first) and 108 (0.5) for the manifold of the lowest-frequency resonance (cis phosphine ligand). There is a slight variation in the relative intensities, within the coupled doublets, over the sideband manifold. This suggests that the sideband pattern is affected by both the shielding and dipolar interactions (effective anisotropy is observed).

The anisotropy for ZDP (described in the experimental chapter) is approximately half this magnitude (i.e. around 45 ppm). Another sample commonly used for checking the magic angle, dimethylphenylphosphine oxide, has an axially symmetric shielding tensor with an anisotropy of 226 ppm.[20]

Carbon-13 NMR.

Carbon-13 (Figure 24) spectra were acquired under conditions of cross polarisation from protons using an echo sequence with and without a delay time (50 μs) for dipolar dephasing to separate quaternary and protonated carbons. Here a short contact time of 1.5 ms was appropriate. This is consistent with the nature of the PPh_3 groups.

The carbon -13 chemical shifts are as follows:

Protonated: 124.8, 127.3, 128.6, 132.6 ppm (plus a broad underlying peak).

Quaternary: 134.6, 136.4, 140.2, 143.4 ppm (low intensity peaks).

A spectrum with better signal to noise ratio has been obtained, but because of shimming problems does not contain the same resolution. As there are three triphenylphosphine ligands, and from the phosphorus NMR it is known that these are in three distinct environments, it is possible that there are up to 9 different quaternary carbons. However, they will be in very close proximity, especially within one PPh_3 ligand, and molecular motion (rotation of each phenyl ring) may cause further averaging of the carbon-13 shifts. In the case of the protonated aromatic carbons there will be signals from ortho, meta and para positions on each of the PPh_3 phenyl rings. All this means that definite individual assignments within the band, for all possible phenyl carbons, are impossible.

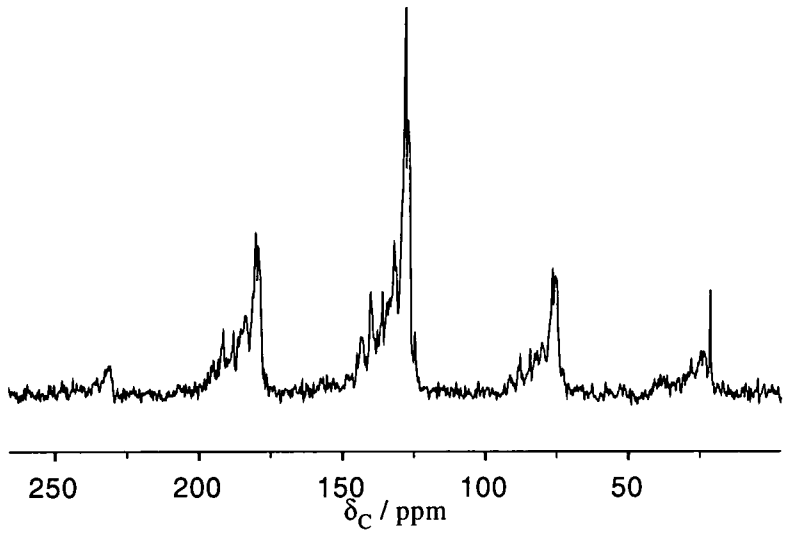

Figure 24. Carbon-13 (50.3 MHz) spectrum of compound III. Spin rate 2.6 kHz (spinning sidebands are observed at either side of the main, highest intensity, centreband), 1000 acquisitions, 30 s recycle delay, 1.5 ms contact time.

From predictions[21] considering only the effect of the phosphorus (i.e. an isolated PPh_3 group), the chemical shifts (Figure 25) are as follows:

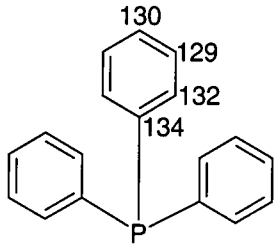

Figure 25. P substituent effects on ^{13}C aromatic shifts.

The quaternary carbon prediction is low compared to those observed experimentally, but the proton carbon shifts are of the correct approximate values considering the simplifications made in the predictions (the prediction will only use the fragment illustrated).

From known data, a shift around 190 ppm would be expected for the carbonyl ligand,[22] with a trend of lower carbon frequency with increasing force constant (C=O stretching frequency). A very low intensity peak at 205 ppm is observed in the ^{13}C spectrum, which can be assigned to the single CO group (it is not visible with the expansion of the spectrum shown above). The shape of this peak is certainly complex.

Proton MAS NMR.

A broad proton resonance is observed, from direct polarisation with MAS at 7 kHz, covering 0 to 15 ppm, with sharper resonances at 1.6 and 6.4 ppm. These two are most likely an impurity and the aromatic protons (PPh_3), respectively. The hydrides were not observed, but would be expected to be to much lower frequency (~ -10 to -20 ppm). As the solid-state MAS proton spectra are broad it is not possible to resolve the difference between the different aromatic positions. For this type of structure it will be expected that the phenyl and hydride protons are well separated in space. It is often the case that a solid-state MAS proton spectrum is a single, broad, featureless band due to strong homonuclear interactions.

Conclusions

The combined information from the solid-state NMR experiments has led to structure predictions which can be used as a starting point for powder X-ray diffraction data. The

success of this technique relies on the accuracy of any initial estimate of the geometry, and so the more information that can be obtained from other sources the more accurate the final structure will be. It was seen from these NMR results that there is one molecule in the asymmetric unit. Phosphorus-31 NMR was the obvious choice for sensitivity reasons and easy distinction of cis and trans groups. This gave detailed information on the environments and NMR properties of the phosphine centres, and therefore the whole molecule. Carbon-13 spectra were obtained to help with structural assignments, and it was hoped that, because of the hydride ligands, a proton spectrum may contain some structure and therefore it was attempted to try and complete the picture.

REFERENCES

[1] M Roden PhD Thesis, Durham University, UK. 1998.

[2] Chemagnetics Spinsight. Version 3.5.2. © Otsuka Electronics (U.S.A.) Inc.

[3] Encyclopædia of NMR, Ed. R.K. Harris, D.M. Grant (Phosphorus-31 NMR)

[4] R.K Harris, A.C. Olivieri, *Progress in Nuclear Magnetic Resonance Spectroscopy*, 1992, **24**, 435.

[5] S. Carss, PhD Thesis, Durham University, UK. 1995.

[6] Gaussian 94 (Revision D.1), M.J. Frisch, G.W. Treucks, H.B. Schelegel, P.M.W. Gill, B.G. Johnson, M.A. Robb, J.R. Cheeseman, T.A.Kieth, G.A. Petersson, J.A. Montgomery, K. Raghavachari, M..A. Al-Laham, V.G. Zakrzewski, J.V. Ortiz, J.B. Foresman, J. Cioslowski, B.B. Stefanov, A. Nanayakkara, M. Challacombe, C.Y. Peng, P.Y. Ayalla, W. Chen, M.W. Wong, J.L.Andres, E.S. Replogle, R. Gomperts, R.L. Martin, D.J. Fox, J.S. Binkley, D.J. Defrees, J.Baker, J.P. Stewart, M. Head-Gordon, C. Gonzalez, and J.A. Pople, Gaussian, Inc., Pittsburgh PA, 1995.

[7] A.C. Olivieri, University of Rosario, Argentina. Personal Communication.

[8] K.B. Dillon, University of Durham. Personal Communication.

[9] P. Hodgkinson, University of Durham. Personal Communication.

[10] E.L. Hahn, *Phys. Rev.*, 1950, **80**, 580.

[11] Encyclopædia of NMR, Ed. R.K. Harris, D.M. Grant (Fluorine-19 NMR)

[12] E.L. Hahn, *Phys. Rev.*, 1949, **76**, 145.

[13] D.C. Douglass, G.P. Jones, *J. Chem. Phys.*, 1966, **45**, 956.

[14] C.Deverell, R.E.Morgan, J.H.Strange, Mol.Phys., 1970, **18**, 553.

[15] M.A. Khan, D.F. Tavares, A. Rauk, *Can. J. Chem*, 1982, **60**, 2451.

[16] W. Domalewski, F.G.Riddell, L. Stefaniak, *Bulletin of the Polish Academy of Sciences.*, 1998, **46**, 35.

[17] J.W. Diesveld, E.M. Menger, H.T. Edzes, W.S. Veeman, *J. Am. Chem. Soc.*, 1980, **102,**, 7936.

[18] M. Gielen, R. Willem, B. Wrackmeyer, *Advanced Applications of NMR to Organometallic Chemistry,* Wiley, Chichester. 1996.

[19] A. Kubo, C.A. McDowell, *J. Magn. Reson.*, 1991, **92**, 409.

[20] R.C. Crosby, J.F. Haw, *J. Magn. Reson,* 1989, **82**, 367.

[21] Daresbury database. Spec Info Version 3.2.3, Jan 1999, Chemical Concepts GmbH, Weinheim.

[22] J. Mason, *Multinuclear NMR.* Pleneum, New York, London. 1987.

Conclusions and Further Work.

Within this work, various effects have been discussed: motion in the solid state, NMR properties, structural studies and characterisation not possible by other techniques. Differences between physical states, solution and solid, (which can constitute significant and vital knowledge for any potential applications) have been investigated.

Application of techniques to these diverse phosphorus system has been successful and important structural and dynamic information, qualitative and quantitative, has been obtained. In addition to this, a deeper understanding of some of the fundamental NMR properties of phosphorus-containing compounds has been developed. In many cases, information has been obtained that would not be possible to extract from solution-state NMR or other solid-state characterisation techniques alone. Although solid-state NMR has been the major concentration in this work, in some instances information from other methods, such as single-crystal and powder X-ray diffraction, have been called upon to complete the picture.

Within this work, there are a number of achievements worth noting in conclusion:

- The fundamental aspects of $^{1}H \rightarrow ^{31}P$ cross-polarisation have been examined for a series of phosphates and other simple compounds.
- Shielding tensor and coupling interactions have been defined in various phosphorus systems.
- The effects of tensor interplay in NMR spectra of PF_n systems have been explored.
- Characterisation of insoluble calix[4]resorcinols has been possible, along with comparison of NMR data within a series of compounds.
- Two-dimensional correlation experiments have lead to structural conclusions about some of the calix[4]resorcinols.
- Molecular motion in fluorinated diazadiphosphetidines has been studied in the solid-state.
- Distinction of axial and equatorial fluorine sites has been possible by observation of fluorine chemical shifts and $^{1}J_{PF}$ coupling constants.

- Some unusual triple-channel spectra have been recorded: phosphorus, fluorine and carbon combinations with proton as the third nucleus.
- Chlorinated diazadiphosphetidines were compared with the fluorinated systems and, again, variable temperature studies were used to investigate efficiency of self-decoupling.
- A complete dynamic characterisation has been carried out for a complex of TPPO-Phenol. Several techniques were used to extend the study over a wide temperature range.
- Single crystal work to determine tensor orientation was also possible in the case of TPPO-Phenol.
- The two-dimensional PHORMAT experiment has been applied to multiple-site phosphorus systems with successful fitting of the resulting pseudo-static lineshapes.
- Interesting NMR properties have been explored for two fluoroaromatic phosphorus compounds and a triphenylphosphine ruthenium compound. Motional properties and structural information have been obtained from solid, powder samples.

Information available from some of the systems has been limited by experimental and computer simulation feasibility. For example, in the CP dynamics study it was necessary to make modifications to the language used in the original computer programme to enable it to be used with the software available. However, when systems start to get complicated (for example tensor component determination for multiple spin systems), any computer simulation would have required a large amount of computational time and advanced programming to achieve meaningful results.

For the determination of ΔJ, a parameter not easily obtained by any other means, there are still problems. An accurate full crystal structure is essential as the absolute value of D (and its value relative to the experimentally determined D') can be severely altered by a small change in internuclear distance. Due to the method of determination of D' from anisotropy, requiring very high accuracy spinning sideband analysis, very small uncertainties can be compounded to give a large scatter in possible values of ΔJ.

There are, of course, more avenues to be explored in future work on the topics included here, another limitation being the equipment presently available. More sophisticated

instrumentation could help with triple-channel fluorine experiments. In particular, overcoming the problems of insufficient ^{1}H-^{19}F isolation encountered in ^{19}F-{^{31}P} experiments meant that proton decoupling, and therefore good resolution, were not possible in this particular case. A fluorine background on the HFX probe could have been removed in theory by CP. Proton-to-fluorine CP was not a sensible option with the isolation issue, but if sensitivity had been high enough phosphorus-to-fluorine CP could have been used. Both proton decoupling and background suppression by CP together could have led to a more in-depth study of the spinning sidebands in the PF systems. This could include further use of the multiple-fitting programmes which have only been applicable to ^{31}P (^{19}F coupled and decoupled) spectra in this work.

Some variable temperature work that would have been useful for some of the PF systems is also limited due to the coil platform design in the HFX probe, which will currently only allow temperatures above -10 °C. At lower temperatures, the coil platform will move, damaging the MAS system. Most of the work would have required spectra at temperatures a lot lower than -10 °C to observe the change from the slow-motion regime to that in which intramolecular motion tends to average NMR parameters.

It was planned to do more work on the HXY probe, particularly with respect to direct carbon-phosphorus correlation and further investigation of decoupling. However, limitations on the maximum length of experimental time not allowing for extensive 2-dimensional experiments with low sensitivity and/or inefficient cross-polarisation, and an intermittent problem with the probe tuning circuit meant that this has not been possible.

Despite the limitations, significant progress was made in expanding work on the possible 'observe' and 'decouple' nuclei for both the HFX and HXY probes. Although not exactly related to the work reported here, I have had collaborative involvement in several projects with experiments and equipment in Durham. These include testing a new 'home-built' 250 MHz system and trials of tuning combinations for the HXY probe, as well as general maintenance work.

The recent acquisition of a share of time on the 600 MHz system in the Physics Department at Warwick University has also shown promising results for some systems. There have been several 'teething problems' with this new spectrometer and specifications have only just been met. Many initial tests have been run and therefore time so far to obtain actual results has been limited.

With regard to improvement of the data reported, further re-measurement of CP dynamics with a longer spin-lock time may be advantageous. This will be particularly appropriate in the case where the optimisation of $T_{1\rho}^{P}$ is not successful.

Simpler systems may help with the diazadiphosphetidine spinning sideband work - unsymmetrical systems, with for example C=O replacing one P, would remove cross-ring effects, which are undoubtedly causing some of the complications. Attempts, by the Inorganic Chemistry group in Braunschweig, to synthesise such compounds proved unsuccessful at this time.

Appendix

Meetings/Research conferences attended:

- Solid-state NMR Summer School, Durham University, UK.
  16th-20th September 1996.

- NMR Discussion Group - NMR of Inclusion and Recognition Phenomena in Solids and Liquids, University of Birmingham, UK.
  15th April 1997.

- RSC Annual Congress, Young Researcher's Meeting, Durham University, UK. 6th-9th April 1998.

- 40th ENC, Orlando, Florida, USA.
  28th February - 4th March 1999.

Work presented:

Seminars/oral presentations:

- Braunschweig University, Germany. 27th November 1997.
  'Solid-state NMR of Phosphorus Compounds'

- Durham University Chemistry Department Research Symposia. 23rd June 1999.
  'Solid-state NMR of Phosphorus Compounds'

Posters presented:

- RSC Annual Congress, Young Researcher's Meeting, Durham University, UK. 6th-9th April 1998.
  'Solid-state NMR of Diazadiphosphetidines'

- ICI / Durham University Chemistry Department Christmas Poster Competition. 21st December 1998. (Highly Commended)
  'Solid-State NMR of Calix[4]resorcinols'

- 40th ENC, Orlando, 28th February - 4th March 1999.
  'Dynamics of Phenol within a Framework of Triphenylphosphine oxide studied by Solid-state NMR'.
  Lindsey A Crowe,* Robin K Harris, David C Apperley, Claudia M Lagier.

- TPPO-Phenol work (presented by R.K. Harris)

  - Edinburgh Conference, 27th June-2nd July 1999.

  - Alpine Solid-State NMR Conference, 12th -16th September 1999.

Papers published / prepared:

- 'Synthesis, structure, and reactivity of tetrakis(O,O-phosphorus)-bridged calix[4]resorcinols and their derivatives.'
  A. Vollbrecht, I. Neda, H. Thönnessen, P.G. Jones, R.K. Harris, L.A. Crowe, R. Schmutzler.
  Chemische Berichte-Recueil, 1997, **130**, 1715.

- 'Solid-state NMR studies of Fluorinated Diazadiphosphetidines.'
  R. K. Harris and L. A. Crowe.
  Accepted for publication in *J. Chem. Soc. Dalton.*

- 'Diffraction and NMR Studies of the Dynamically Disordered 3:2 Phenol-Triphenylphosphine Oxide Complex.'
  D. C. Apperley, P. A. Chaloner, L. A. Crowe, R. K. Harris, R. M. Harrison, P. B. Hitchcock, C. M. Lagier.
  In final stages of preparation.

Work outside the Department:

- Discussion/observation of synthetic work at the Inorganic Chemistry Department, Braunschweig University, Germany. Visiting group of Prof. R. Schmutzler. 22-30th November 1997.

- Academic year 1998/1999, several 3 day visits to use 600 MHz Chemagnetics spectrometer in the Physics Department, Warwick University, UK.

Post Graduate Colloquia, Lectures and Seminars from Invited Speakers

(‡ denotes lectures attended)

1996

October 9	Professor G. Bowmaker, University Auckland, New Zealand. Coordination and Materials Chemistry of the Group 11 and Group 12 Metals : Some Recent Vibrational and Solid State NMR Studies.‡
October 14	Professor A. R. Katritzky, University of Gainesville, University of Florida, USA. Recent Advances in Benzotriazole Mediated Synthetic Methodology.
October 16	Professor Ojima, Guggenheim Fellow, State University of New York at Stony Brook. Silylformylation and Silylcarbocyclisations in Organic Synthesis.
October 22	Professor Lutz Gade, Univ. Wurzburg, Germany. Organic transformations with Early-Late Heterobimetallics: Synergism and Selectivity.
October 22	Professor B. J. Tighe, Department of Molecular Sciences and Chemistry, University of Aston. Making Polymers for Biomedical Application - can we meet Nature's Challenge? Joint lecture with the Institute of Materials.‡
October 23	Professor H. Ringsdorf (Perkin Centenary Lecture), Johannes Gutenberg-Universitat, Mainz, Germany. Function Based on Organisation.‡
October 29	Professor D. M. Knight, Department of Philosophy, University of Durham. The Purpose of Experiment - A Look at Davy and Faraday.‡
October 30	Dr Phillip Mountford, Nottingham University. Recent Developments in Group IV Imido Chemistry.
November 6	Dr Melinda Duer, Chemistry Department, Cambridge. Solid-state NMR Studies of Organic Solid to Liquid-crystalline Phase Transitions.‡
November 12	Professor R. J. Young, Manchester Materials Centre, UMIST. New Materials - Fact or Fantasy? Joint Lecture with Zeneca & RSC.‡
November 13	Dr G. Resnati, Milan. Perfluorinated Oxaziridines: Mild Yet Powerful Oxidising Agents.
November 18	Professor G. A. Olah, University of Southern California, USA. Crossing Conventional Lines in my Chemistry of the Elements.‡
November 19	Professor R. E. Grigg, University of Leeds. Assembly of Complex Molecules by Palladium-Catalysed Queuing Processes.
November 20	Professor J. Earnshaw, Department of Physics, Belfast. Surface Light Scattering: Ripples and Relaxation.‡
November 27	Dr Richard Templer, Imperial College, London. Molecular Tubes and Sponges.‡
December 3	Professor D. Phillips, Imperial College, London. "A Little Light Relief".

December 4 — Professor K. Muller-Dethlefs, York University.
Chemical Applications of Very High Resolution ZEKE Photoelectron Spectroscopy.‡

December 11 — Dr Chris Richards, Cardiff University.
Stereochemical Games with Metallocenes.‡

1997

January 15 — Dr V. K. Aggarwal, University of Sheffield.
Sulphur Mediated Asymmetric Synthesis.

January 16 — Dr Sally Brooker, University of Otago, New Zealand.
Macrocycles: Exciting yet Controlled Thiolate Co-ordination Chemistry.

January 21 — Mr D. Rudge, Zeneca Pharmaceuticals.
High Speed Automation of Chemical Reactions.‡

January 22 — Dr Neil Cooley, BP Chemicals, Sunbury.
Synthesis and Properties of Alternating Polyketones.

January 29 — Dr Julian Clarke, UMIST.
What can we learn about polymers and biopolymers from computer-generated nanosecond movie-clips? ‡

February 4 — Dr A. J. Banister, University of Durham.
From Runways to Non-metallic Metals - A New Chemistry Based on Sulphur.‡

February 5 — Dr A. Haynes, University of Sheffield.
Mechanism in Homogeneous Catalytic Carbonylation.‡

February 12 — Dr Geert-Jan Boons, University of Birmingham.
New Developments in Carbohydrate Chemistry.

February 18 — Professor Sir James Black, Foundation/King's College London.
My Dialogues with Medicinal Chemists.‡

February 19 — Professor Brian Hayden, University of Southampton.
The Dynamics of Dissociation at Surfaces and Fuel Cell Catalysts.‡

February 25 — Professor A. G. Sykes, University of Newcastle.
The Synthesis, Structures and Properties of Blue Copper Proteins.

February 26 — Dr Tony Ryan, UMIST.
Making Hairpins from Rings and Chains.

March 4 — Professor C. W. Rees, Imperial College.
Some Very Heterocyclic Chemistry.

March 5 — Dr J. Staunton FRS, Cambridge University.
Tinkering with biosynthesis: towards a new generation of antibiotics.

March 11 — Dr A. D. Taylor, ISIS Facility, Rutherford Appleton Laboratory.
Expanding the Frontiers of Neutron Scattering.

March 19 — Dr Katharine Reid, University of Nottingham.
Probing Dynamical Processes with Photoelectrons.‡

October 8	Professor E Atkins, Department of Physics, University of Bristol. Advances in the control of architecture for polyamides: from nylons to genetically engineered silks to monodisperse oligoamides.‡
October 15	Dr R M Ormerod, Department of Chemistry, Keele University. Studying catalysts in action.‡
October 21	Professor A F Johnson, IRC, Leeds. Reactive processing of polymers: science and technology.
October 22	Professor R J Puddephatt, University of Western Ontario, USA. Organoplatinum chemistry and catalysis. RSC Endowed Lecture.
October 23	Professor M R Bryce, University of Durham, Inaugural Lecture. New Tetrathiafulvalene Derivatives in Molecular, Supramolecular and Macromolecular Chemistry: controlling the electronic properties of organic solids.
October 28	Professor A P de Silva, The Queen's University, Belfast. Luminescent signalling systems.‡
October 29	Professor R Peacock, University of Glasgow. Probing chirality with circular dichroism.
November 5	Dr M Hii, Oxford University. Studies of the Heck reaction.
November 11	Professor V Gibson, Imperial College, London. Metallocene polymerisation.
November 12	Dr J Frey, Department of Chemistry, Southampton University. Spectroscopy of liquid interfaces: from bio-organic chemistry to atmospheric chemistry.‡
November 19	Dr G Morris, Department of Chemistry, Manchester Univ. Pulsed field gradient NMR techniques: Good news for the Lazy and DOSY.‡
November 20	Dr L Spiccia, Monash University, Melbourne, Australia. Polynuclear metal complexes.
November 25	Dr R Withnall, University of Greenwich. Illuminated molecules and manuscripts.
November 26	Professor R W Richards, University of Durham, Inaugural Lecture. A random walk in polymer science.
December 2	Dr C J Ludman, University of Durham. Explosions.‡
December 3	Professor A P Davis, Department. of Chemistry, Trinity College Dublin. Steroid-based frameworks for supramolecular chemistry.
December 10	Sir G Higginson, former Professor of Engineering in Durham and retired Vice-Chancellor of Southampton Univ. 1981 and all that.‡
December 10	Professor M Page, Department of Chemistry, University of Huddersfield The mechanism and inhibition of beta-lactamases.

1998

January 14	Professor D Andrews, University of East Anglia. Energy transfer and optical harmonics in molecular systems.‡
January 20	Professor J Brooke, University of Lancaster. What's in a formula? Some chemical controversies of the 19th century.
January 21	Professor D Cardin, University of Reading. No title given.
January 27	Professor R Jordan, Dept. of Chemistry, Univ. of Iowa, USA. Cationic transition metal and main group metal alkyl complexes in olefin polymerisation.
January 28	Dr S Rannard, Courtaulds Coatings (Coventry). The synthesis of dendrimers using highly selective chemical reactions.‡
February 3	Dr J Beacham, ICI Technology. The chemical industry in the 21st century.‡
February 4	Professor P Fowler, Department of Chemistry, Exeter University. Classical and non-classical fullerenes.
February 11	Professor J Murphy, Dept of Chemistry, Strathclyde University.
February 17	Dr S Topham, ICI Chemicals and Polymers. Perception of environmental risk; The River Tees, two different rivers.‡
February 18	Professor G Hancock, Oxford University. Surprises in the photochemistry of tropospheric ozone.
February 24	Professor R Ramage, University of Edinburgh. The synthesis and folding of proteins.
February 25	Dr C Jones, Swansea University. Low co-ordination arsenic and antimony chemistry.
March 4	Professor T C B McLeish, IRC of Polymer Science Technology, Leeds University. The polymer physics of pyjama bottoms (or the novel rheological characterisation of long branching in entangled macromolecules).
March 11	Professor M J Cook, Dept of Chemistry, UEA. How to make phthalocyanine films and what to do with them.
March 17	Professor V Rotello, University of Massachusetts, Amherst, USA. The interplay of recognition & redox processes - from flavoenzymes to devices.
March 18	Dr J Evans, Oxford University. Materials which contract on heating (from shrinking ceramics to bullet proof vests).
October 7	Dr S Rimmer, Ctr Polymer, University of Lancaster. New Polymer Colloids.‡
October 9	Professor M F Hawthorne, Department Chemistry & Biochemistry, UCLA, USA. RSC Endowed Lecture.
October 21	Professor P Unwin, Department of Chemistry, Warwick University. Dynamic Electrochemistry: Small is Beautiful.‡

October 23 — Professor J C Scaiano, Department of Chemistry, University of Ottawa, Canada.
In Search of Hypervalent Free Radicals.
RSC Endowed Lecture.

October 26 — Dr W Peirs, University of Calgary, Alberta, Canada.
Reactions of the Highly Electrophilic Boranes HB(C6F5)2 and B(C6F5)3 with Zirconium and Tantalum Based Metallocenes.

October 27 — Professor A Unsworth, University of Durham.
What's a joint like this doing in a nice girl like you?
In association with The North East Polymer Association.

October 28 — Professor J P S Badyal, Department of Chemistry, University of Durham.
Tailoring Solid Surfaces.
Inaugural Lecture.‡

November 4 — Dr N Kaltscoyannis, Department of Chemistry, UCL, London.
Computational Adventures in d & f Element Chemistry.

November 3 — Dr C J Ludman, Chemistry Department, University of Durham.
Bonfire night Lecture.

November 10 — Dr J S O Evans, Chemistry Department, University of Durham.
Shrinking Materials.

November 11 — Dr M Wills, Department of Chemistry, University of Warwick.
New Methodology for the Asymmetric Transfer Hydrogen of Ketones.

November 12 — Professor S Loeb, University of Windsor, Ontario, Canada.
From Macrocycles to Metallo-Supramolecular Chemistry.

November 17 — Dr J McFarlane.
Nothing but Sex and Sudden Death! ‡

November 18 — Dr R Cameron, Department of Materials Science & Metallurgy, Cambridge University.
Biodegradable Polymers.

November 24 — Dr B G Davis, Department of Chemistry, University of Durham.
Sugars and Enzymes.

December 1 — Professor N Billingham, University of Sussex.
Plastics in the Environment - Boon or Bane.
In association with The North East Polymer Association.‡

December 2 — Dr M Jaspers, Department of Chemistry, University of Aberdeen.
Bioactive Compounds Isolated from Marine Invertebrates and Cyanobacteria.

December 9 — Dr M Smith, Department of Chemistry, Warwick University.
Multinuclear solid-state magnetic resonance studies of nanocrystalline oxides and glasses.‡

1999

January 19 — Dr J Mann, University of Reading.
The Elusive Magic Bullet and Attempts to find it?

January 20 — Dr A Jones, Department of Chemistry, University of Edinburgh.
Luminescence of Large Molecules: from Conducting Polymers to Coral Reefs.‡

January 27	Professor K Wade, Department of Chemistry, University of Durham. Foresight or Hindsight? Some Borane Lessons and Loose Ends.‡
February 3	Dr C Schofield, University of Oxford. Studies on the Stereoelectronics of Enzyme Catalysis.
February 9	Professor D J Cole-Hamilton, St. Andrews University. Chemistry and the Future of life on Earth.
February 10	Dr C Bain, University of Oxford. Surfactant Adsorption and Marangoni Flow at Expanding Liquid Surfaces.‡
February 17	Dr B Horrocks, Department of Chemistry, Newcastle University. Microelectrode techniques for the Study of Enzymes and Nucleic Acids at Interfaces.
February 23	Dr C Viney, Heriot-Watt. Spiders, Slugs And Mutant Bugs.
February 24	Dr. A-K Duhme, University of York. Bioinorganic Aspects of Molybdenum Transport in Nitrogen-Fixing Bacteria.
March 3	Professor B Gilbert, Department of Chemistry, University of York. Biomolecular Damage by Free Radicals: New Insights through ESR Spectroscopy.
March 9	Dr Michael Warhurst, Chemical Policy issues, Friends of the Earth. Is the Chemical Industry Sustainable?
March 10	Dr A Harrison, Department of Chemistry, University of Edinburgh. Designing model magnetic materials.
March 17	Dr J Robertson, University of Oxford. Recent Developments in the Synthesis of Heterocyclic Natural Products.
May 11	Dr John Sodeau, University of East Anglia. Ozone Holes and Ozone Hills.
May 12	Dr Duncan Bruce, Exeter University. The Synthesis and Characterisation of Liquid-Crystalline Transition Metal Complexes.‡
May 14	Professor Yoshifuji, Tohoku University, Japan. New Chemistry of organophosphorus compounds.‡
July 20	Professor K Müeller, Stuttgart University. Guest Dynamics in Inclusion Compounds as Studied by Solid NMR Techniques.‡